UNIVERSITA' DEGLI STUDI DI NAPOLI

FEDERICO II

FACOLTA' DI INGEGNERIA

Tesi di Dottorato di Ricerca in Ingegneria dei Sistemi Meccanici

XXIV Ciclo

EXPERIMENTAL AND SIMULATIVE ANALYSIS OF A MICROTRIGENERATION SYSTEM BASED ON AN AIR HANDLING UNIT WITH DESICCANT WHEEL

Coordinatore del Corso:

Ch. mo Prof. Ing.

FABIO BOZZA

Relatore:

Ch. mo Prof. Ing.

MAURIZIO SASSO

Candidato:

Ing. GIOVANNI ANGRISANI

Acknowledgements

I must foremost thank Prof. Maurizio Sasso, for providing me the opportunity to pursue my Ph.D. in Mechanical Systems Engineering, and the guidance and support necessary to attain it.

My sincere gratitude goes also to Dr. Carlo Roselli, who have provided invaluable support and wisdom.

Thanks to Professors, colleagues and friends of the DING at University of Sannio, too numerous to thank by name, from whom I have learned a great deal about engineering, life and the world around me.

Thanks also to Professors and Researchers of University of Naples Federico II and Second University of Naples.

INDEX

LIST OF PERSONAL PUBLICATIONS

I. "Experimental analysis of small scale polygeneration system based on a natural gas fired micro-CHP and a hybrid HVAC system equipped with a desiccant wheel", 22nd International Conference on Efficiency, Cost, Optimization Simulation and Environmental Impact of Energy Systems, August 31 – Settembre 3, 2009, Foz do Iguaçu, Paraná, Brasile, (G. Angrisani, F. Minichiello, C. Roselli, M. Sasso, G.P. Vanoli), ISSN 2175-5426;

II. "Desiccant HVAC system driven by a micro-CHP: experimental analysis", *Energy and Building* 42 (2010) 2028-2035, (G. Angrisani, F. Minichiello, C. Roselli, M. Sasso);

III. "Numerical analysis of a Small Scale Polygeneration Plant with a Desiccant-Based Air Handling Unit", 23rd International Conference on Efficiency, Cost, Optimization Simulation and Environmental Impact of Energy Systems, Losanna, Svizzera, 14 – 17 Giugno 2010, (G. Angrisani, C. Roselli, M. Sasso) ISBN/EAN13 1456303201 / 9781456303204;

IV. "Experimental investigation to optimise a desiccant HVAC system coupled to a small size cogenerator", *Applied Thermal Engineering* 31 (2011) 506-512, (G. Angrisani, F. Minichiello, C. Roselli, M. Sasso);

V. "Desiccant wheel regenerated by thermal energy from a microcogenerator: experimental assessment of the performances", *Applied Energy* 88 (2011) 1354-1365, (G. Angrisani, A. Capozzoli, F. Minichiello, C. Roselli, M. Sasso);

VI. "Analisi sperimentale di impianti di poligenerazione di piccola taglia basati su un motore a combustione interna alimentato a gas naturale", 65° Congresso Nazionale ATI – Domus de Maria (CA), 13 – 17 settembre 2010 (G. Angrisani, C. Roselli, M. Sasso, S. Sibilio);

VII. "Creazione di un database di sistemi di microcogenerazione", Report RSE/2009/118, ENEA – MSE, 2009 (G. Angrisani, M. Sasso, C. Roselli, M. Citterio), http://old.enea.it/attivita_ricerca/energia/sistema_elettrico/Governance/RSE118.pdf;

VIII. "Experimental validation of constant efficiency models for the subsystems of an unconventional desiccant-based Air Handling Unit and investigation of its performance", *Applied Thermal Engineering* 33-34 (2012) 100-108, (G. Angrisani, C. Roselli, M. Sasso);

IX. "Experimental tests on a polygeneration system with a desiccant-based AHU", 2nd International Conference on Microgeneration and Related Technologies, University of Strathclyde, Glasgow, UK, 4 – 6 April 2011, (G. Angrisani, C. Roselli, M. Sasso);

X. "Trial results of domestic CHP & thermally driven cooling technologies use in an office application", 2nd International Conference on Microgeneration and Related Technologies,

University of Strathclyde, Glasgow, UK, 4 – 6 April 2011, (G. Angrisani, A. Rosato, C. Roselli, M. Sasso, S. Sibilio);

XI. "Experimental analysis on the performances of a desiccant wheel regenerated by low grade thermal energy", International Sorption Heat Pump Conference, Padova, Italia, 6 – 8 Aprile 2011, (G. Angrisani, F. Minichiello, C. Roselli, M. Sasso) ISBN 978-1-61782-952-9;

XII. "Design and simulation of a solar assisted desiccant-based air handling unit", HEFAT 2011, 8th International Conference on Heat Transfer, Fluid Mechanics and Thermodynamics, 11 – 13 July 2011, Pointe Aux Piments, Mauritius, (G. Angrisani, C. Roselli, M. Sasso, C. Stellato), ISBN 978-1-86854-948-1;

XIII. "Analisi sperimentale di un sistema di microcogenerazione per utenze residenziali", 66° Congresso Nazionale ATI – Università della Calabria, Rende (CS), 5 – 9 settembre 2011 (G. Angrisani, C. Roselli, M. Sasso, S. Sibilio, A. Rosato);

XIV. "Distributed microtrigeneration systems", sottomesso alla rivista internazionale *Progress in Energy and Combustion Sciences*, 2011 (G. Angrisani, C. Roselli, M. Sasso, S. Sibilio);

XV. "Experimental analysis on the dehumidification and thermal performances of a desiccant wheel", accettato per la pubblicazione nella rivista internazionale *Applied Energy*, 2011 (G. Angrisani, C. Roselli, M. Sasso, F. Minichiello);

XVI. "Experimental results of a micro-trigeneration installation", sottomesso alla rivista internazionale *Applied Thermal Engineering*, 2011 (G. Angrisani, C. Roselli, M. Sasso, S. Sibilio, A. Rosato);

XVII. "Sviluppo di un ambiente di monitoraggio, controllo e gestione remota di una rete di micro_poligeneratori distribuiti", Report RdS/2011/131, ENEA – MSE, 2011 (G. Angrisani, C. Roselli, M. Sasso, in collaborazione con A. Rosato, S. Sibilio), http://editors.enea.it/it/Ricerca_sviluppo/documenti/ricerca-di-sistema-elettrico/efficienza-energetica-servizi/rds-131.pdf;

XVIII. "Risultati dell'attività sperimentale su sistemi distribuiti di micro_poligenerazione", Report RdS/2011/130, ENEA – MSE, 2011 (G. Angrisani, C. Roselli, M. Sasso, in collaborazione con A. Rosato, S. Sibilio), http://editors.enea.it/it/Ricerca_sviluppo/documenti/ricerca-di-sistema-elettrico/efficienza-energetica-servizi/rds-130.pdf;

XIX. "Review of existing Micro-Generation performance assessments studies and experimental activity", a draft report of Subtask B of IEA/ECBCS Annex 54, Integration of Micro-Generation and Related Energy Technologies in Buildings, 2011 (G. Angrisani, C. Roselli, M. Sasso);

XX. “Methodologies for the Performance Assessment of Micro Hybrid Poligeneration Systems”, a draft report of Subtask B of IEA/ECBCS Annex 54, Integration of Micro-Generation and Related Energy Technologies in Buildings, 2011 (G. Angrisani, C. Roselli, M. Sasso).

INTRODUCTION

During last years, air conditioning demand is spreading, both in the commercial (shops, warehouses, offices, schools…) and in the residential sector. This caused a sensible increase in primary energy consumption in these sectors, especially in industrialized countries, where people spend the major part of the day in confined environments, therefore it is very important to guarantee a high Indoor Air Quality (IAQ) and thermal comfort. In fact, individuals perform more effectively in conditioned than in untreated indoor air environments.

The operation of a Heating, Ventilation and Air-Conditioning (HVAC) system is usually required to achieve comfortable indoor conditions. It has to provide a sufficient amount of fresh air to the occupied zone, remove indoor generated contaminants and maintain suitable indoor air temperature and humidity; moreover, it has to supply or remove heat and/or moisture to or from the occupied space. However, HVAC systems often consume large amounts of energy. Therefore, it is very important to investigate the possibility of efficiently attaining improved indoor environmental quality, without increasing energy consumption or even reducing it.

Different types of HVAC systems have different energy consumption for the same IAQ and thermal comfort. Therefore, it is highly desirable to provide each building with an optimal HVAC system, which would provide the best IAQ and thermal comfort for the occupants with minimum energy consumption.

The increase of the ventilation air flow rate, favouring the dilution of pathogenic agents, is the commonly used strategy to guarantee a hygienic and comforting environment for the occupants. Unfortunately, the increase of ventilation flow rate determines higher air conditioning energy requirements; in fact, ventilation air represents the main source of latent load, especially in humid areas as in Mediterranean countries. Moreover, the demand for summer cooling in domestic and commercial sectors is usually satisfied by electrically driven units; this involves high electric peak loads and black-outs.

Furthermore, during last years, great attention was focused on the transition from centralized to decentralized energy “production” systems (Decentralized or Distributed Generation, DG), to reduce T&D (Transmission and Distribution) energy losses: a miniaturization process (“size” effect) is in progress.

The boost towards the reduction of electrical loads for air conditioning and the decentralization of energy conversion devices is determining increasing interest in small scale

trigeneration systems fuelled by natural gas ("gas cooling"), able to shift energy demand in summer from electricity to gas, at the same time allowing the exploitation of natural gas surplus during the warm season.

Finally, the increasingly need to drastically reduce the use of HCFC and HFC refrigerants, because of their direct greenhouse contribution and ozone depletion potential, should be taken into account.

A particularly interesting technology that meets these requirements is represented by desiccant-based dehumidification systems, eventually integrated with conventional air conditioning devices. In the most common configuration, these systems use a desiccant wheel, that consists of a rotor, filled with a desiccant material (i.e. silica gel), in which humid air is dehumidified by the desiccant material, to balance latent loads of the ambient. To guarantee continuous operation, the wheel has to be regenerated by a hot air stream.

Desiccant dehumidification is not a new technology (the first patent by the American engineer Pennington goes back to '30s), but the recent developments in desiccant materials and cycles make it a viable alternative or integration to conventional air conditioning systems. In fact, the traditional niche markets (special areas like electronics, food and arms storage, pharmaceutical industry, hospitals…) are greatly expanding towards application characterized by high latent loads, such as supermarkets, ice arenas, restaurants, theaters, cinemas, school and museums.

Moreover, during last years, thanks to its benefits, this technology is also spreading in residential and tertiary sectors and office buildings; this is not the case for European countries, in particular in Mediterranean areas, like Italy, where this technique, that allow to separately control temperature and humidity, is still rarely implemented, due to several obstacles, such as high investment costs, low familiarity, lack of knowledge about performances and cost/benefit ratio and high thermal energy requirements to regenerate the desiccant material.

As regards the last topic, it is possible to use a "free" thermal energy source to regenerate the desiccant material, in particular waste heat recovered from a microcogenerator (MCHP – Micro Combined Heating and Power), eventually integrated with a conventional fossil fuelled heating system (e.g. a boiler). In this case it is possible to design a microtrigeneration system (MCCHP – Micro Combined Cooling, Heating and Power), that allows to significantly increase the operating hours of the MCHP, hence improving the energy, environmental and economic performances of the whole system. Small scale cogeneration devices are nowadays widely available on both national

and international markets; a database of commercially available or prototype microcogenerators were developed.

It is also possible to regenerate the desiccant wheel by means of solar energy; in particular, the use of solar energy for space cooling requirements ("solar cooling") is highly desirable, because its availability coincides with the need for cooling, therefore the summer peak demand of electricity due to extensive use of electric air conditioners, that matches with the peak solar irradiance, can be lowered.

The aim of this thesis, starting from experimental tests carried out at "Università degli Studi del Sannio", in Benevento, is to demonstrate the technical feasibility of a MCCHP system, consisting of a hybrid desiccant-based Air Handling Unit (AHU) and a microcogenerator.

First of all, an experimental analysis on dehumidification and thermal performances of the silica-gel desiccant wheel, contained in the Air Handling Unit, is presented. Useful performance curves were obtained, as a function of five operating parameters: outdoor air temperature and humidity ratio, regeneration temperature, the ratio between regeneration and process air flow rates and desiccant wheel rotational speed. Experimental results were also compared with data provided by the manufacturer.

Furthermore, experimental tests allowed to evaluate energy, environmental and economic performances of the decentralized MCCHP system, compared to a conventional one based on cooling dehumidification and separate electric, thermal and cooling "production".

In order to deepen the benefits of distributed generation systems, an experimental analysis of a MCHP, carried out at Technical University of Munich, is presented. Experimental tests were conducted in a test facility, that allows to simulate the space heating and domestic hot water requirements of a residential user. In this case also, the microcogeneration plant was compared, in terms of energy and environmental analysis, with a conventional reference system based on separate "production".

In distributed energy systems, a central management unit, with the aims of operating costs minimization, primary energy saving and reduction of climate-changing emissions, coordinates the operation of numerous distributed devices, according to a Virtual Power Plant approach. "Università degli Studi del Sannio" and "Seconda Università di Napoli" cooperated with ENEA to the development of the software *POLILAB*, aimed at the experimental analysis and the centralized

remote control and thermo-economic optimization of the small scale polygeneration systems installed in the test facilities of the two mentioned universities.

Experimental data were also used to calibrate and validate models of the main components and energy conversion devices, in order to analyze the effect of various operating parameters, namely, regeneration temperature, outdoor air temperature and humidity ratio, etc.

Finally, these models were used to simulate the current MCCHP system and a solar desiccant-based Air Handling Unit, in which a solar collectors system provides a part of the required regeneration thermal energy. The systems were simulated by means of the TRNSYS software, in order to evaluate operational data and performance parameters.

Such modeling and simulating activities fit in the framework of the International Energy Agency Energy Conservation in Buildings and Community Systems Programme (IEA/ECBCS) Annex 54, Integration of Micro-Generation & Related Energy Technologies in Buildings. It is an international research project, involving both industrial and academic partners, in which an in depth analysis of micro-generation and associated other energy technologies is in progress[1].

[1] http://www.iea-annex54.org/

CHAPTER 1: DEHUMIDIFICATION

1.1 Cooling and desiccant dehumidification

In a conventional air conditioning system, in order to dehumidify air, it is usually cooled below the dew point by a coil interacting with an electric compression chiller and, subsequently, it is heated up to the desired supply temperature (Fig. 1. 1, an ideal unitary bypass factor has been assumed for the cooling coil). That is the so-called *"cooling dehumidification"* or *"mechanical dehumidification"*.

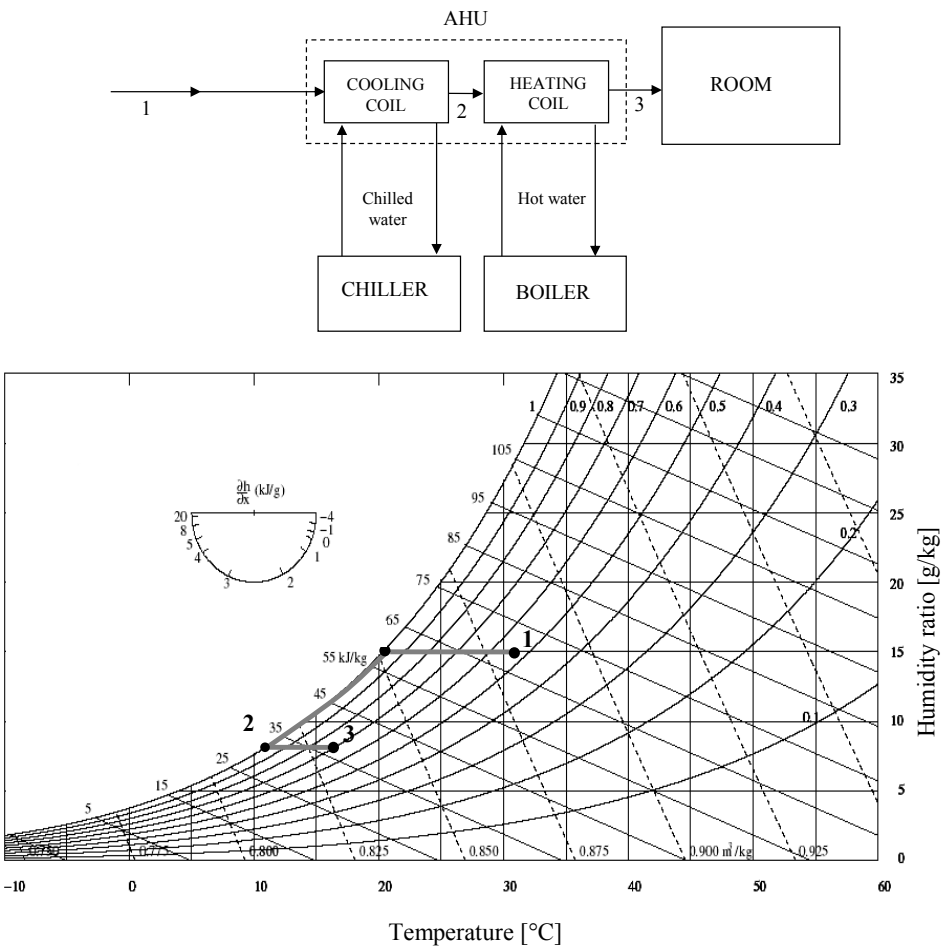

Fig. 1. 1: Air conditioning in a conventional air handling unit

Desiccant cooling is based on air dehumidification by means of a desiccant material (solid or liquid), and its subsequent cooling. The process is called absorption if a liquid material is used, or adsorption if the desiccant material is solid.

The desiccant dehumidification process is exothermic and determines a sensible heating of the air flow being dehumidified; hence it has to be cooled down to the thermal-hygrometric conditions required to handle the thermal loads, [1, 2].

To obtain a continuous operation of this system, the desiccant material has to be periodically regenerated by means of a hot air flow, in order to evaporate the absorbed/adsorbed water vapour. The required regeneration temperature depends on the desiccant material; for the last generation of desiccants, however, it can be low enough (60-70 °C are often sufficient) to allow the use of waste heat from cogeneration devices or energy recovered from a solar collector.

Therefore, a desiccant cooling system comprises three main components (Fig. 1. 2): the dehumidifier, the regeneration heat source and the cooling device.

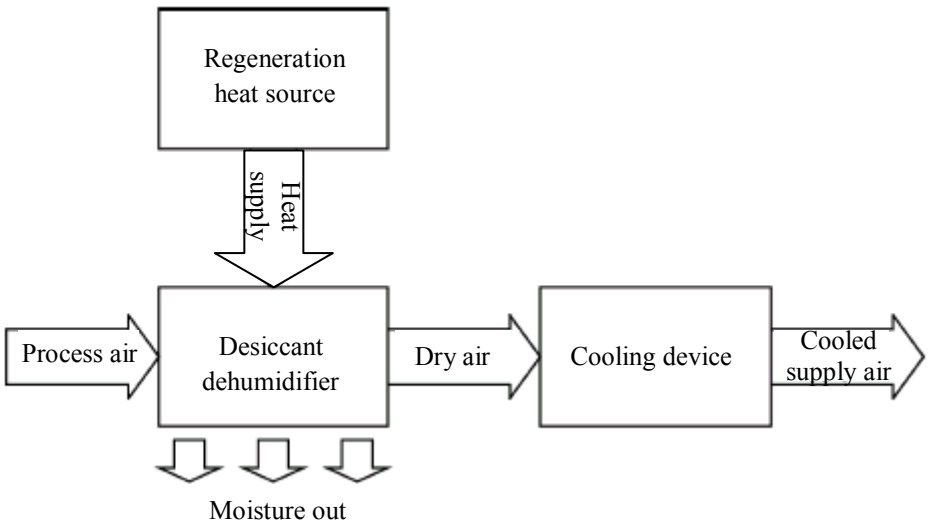

Fig. 1. 2: Simplified scheme of a desiccant cooling system

As regards the dehumidifier, one of the most common configurations is the Desiccant Wheel (DW) that is a rotor, filled with a solid desiccant material, which slowly rotates between the process air to be dehumidified and the regeneration air, [3]. With reference to the thermal energy source for regeneration, the desiccant wheel can be regenerated in several ways, such as by a gas-fired boiler, an electric resistance, or even through microwave heating, [4].

However, the energy saving and the reduction of the environmental impact that these systems can achieve are higher when the desiccant material is regenerated by means of “free” thermal energy, for example from cogenerators, [5], or solar collectors [6]; in these cases, a

desiccant material that can be effectively regenerated with low-temperature thermal energy is obviously needed.

As regards the cooling device, it can be a direct or indirect evaporative cooler, an air-to-air heat pump (in cooling mode), or an air-cooled water chiller. If the cooling device is an inverse machine, the whole air conditioning system is defined hybrid HVAC system, where the term hybrid refers to the contemporary presence of the desiccant system and the conventional cooling device.

1.2 Hybrid Air Handling Units

The process air stream flows through the desiccant material (such as silica gel, activated alumina, lithium chloride salt, or molecular sieves) that retains the moisture of the air; the desiccant capacity of this material can be restored through its regeneration via a hot air stream, usually heated by a gas-fired boiler. The process air stream exiting the wheel is then cooled down to desired supply temperature, e.g. by the cooling coil of an electric chiller (hybrid air handling units, Fig. 1. 3).

A hybrid air handling unit (either with a solid or a liquid desiccant) offers an effective means of controlling space humidity while providing an energy-efficient air temperature control. Such hybrid systems combine an electric vapor compression cycle with a desiccant dehumidification system. The desiccant material can be partially regenerated by thermal wastes rejected at the condenser of the vapor compression cycle.

Desiccant systems in HVAC applications, as an alternative or a supplement to traditional air conditioning systems, are primarily used where the latent load is high or where independent control of temperature and humidity is a very important factor, [1].

The main advantages of this system, in comparison with the conventional one, are [7, 8]:

- sensible and latent loads can be controlled separately, [8];
- lower humidity levels in occupied spaces provide equivalent comfort levels at higher space temperatures;
- they can reach very low dew point temperatures of process air, lower than -6.0 °C, while conventional systems usually do not reach dew point temperatures lower than about 4.0 °C. Hence, the desiccant dehumidification technology is particularly used when very dry air is needed for specific operating processes, such as in the chemical, pharmaceutical and food

industries, or when a very low indoor humidity ratio is needed in order to preserve or manipulate hygroscopic or humidity sensitive materials;

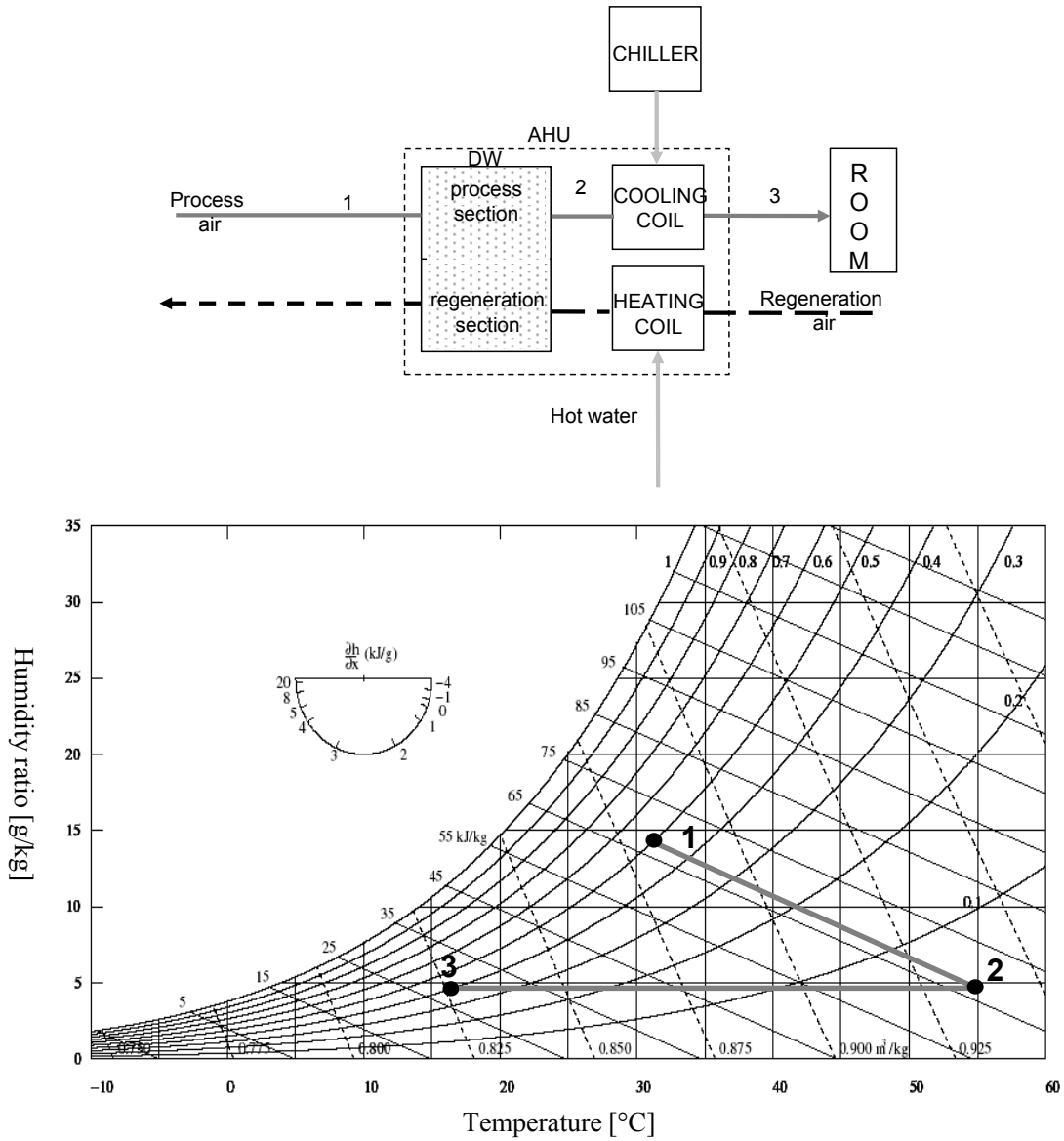

Fig. 1. 3: Air conditioning in the hybrid desiccant air handling unit

- the cooling machine only has to cool the process air (without dehumidifying it); therefore, it can operate with a higher chilled water temperature compared to a cooling machine coupled to a conventional cooling and dehumidification system, where the process air has to be cooled below the dew point temperature to obtain the desired humidity ratio. Hence, the cooling machine interacting with the hybrid HVAC system has a higher COP (Coefficient Of Performance);

- due to the higher value of the COP, electric energy requirement of the cooling machine is reduced;
- consistent energy savings can be obtained, thanks to the increase in the overall energy efficiency, by avoiding overcooling air and reheating;
- as the cooling machine only has to cool the process air, a reduction of its size and the refrigerant fluid mass is obtained; this consequently determines a lower environmental impact, both in terms of direct impact (ozone layer reduction and greenhouse effect due to refrigerant fluids) and indirect one (the reduced electric energy use determines lower equivalent CO_2 emissions of the power plants);
- a better Indoor Air Quality (IAQ) can be obtained, due to sanitizing effects of desiccant [9-11]. Furthermore, desiccant systems avoid the formation of condensed water; this strongly reduces the presence of microorganisms as bacteria, viruses and fungi. Therefore these systems are particularly recommended in applications in which severe hygienic conditions must be maintained, such as medical facilities and laboratories.

Thanks to these advantages, the use of desiccant technology is also spreading for tertiary and residential buildings.

The drawbacks of this technology are the low familiarity, the lack of knowledge about performances and cost/benefit ratio and the high thermal energy requirements to regenerate the desiccant wheel; however the major drawback is the high investment costs of the desiccant rotor.

In Fig. 1. 4, the average specific cost of dehumidification systems, comprising both the desiccant wheel and a heat recovery wheel (tipycally used to recover the adsorption heat for the regeneration process), is shown as a function of the process air volumetric flow rate, for both industrial and commercial applications, [8]. The target price for commercial dehumidifiers, that should be reached in order to obtain a widespread use of the technology, is also shown.

Some commercial applications of hybrid systems include schools, auditoriums, hospitals, office buildings, supermarkets, restaurants, etc.

For example, Lazzarin and Castellotti, [12], studied how a desiccant heat pump hybrid system performed when employed in a supermarket. A self-regenerating liquid desiccant cooling system was integrated to an electric heat pump. Their work demonstrated the possible energy savings of this system, compared to a traditional system based on mechanical dehumidification.

Aynur et al., [13], conducted field performance tests on a novel hybrid system by the integration of the variable refrigerant flow and heat pump desiccant systems. Their results demonstrated that this novel system allows significant energy savings while providing the best indoor thermal comfort and air quality conditions.

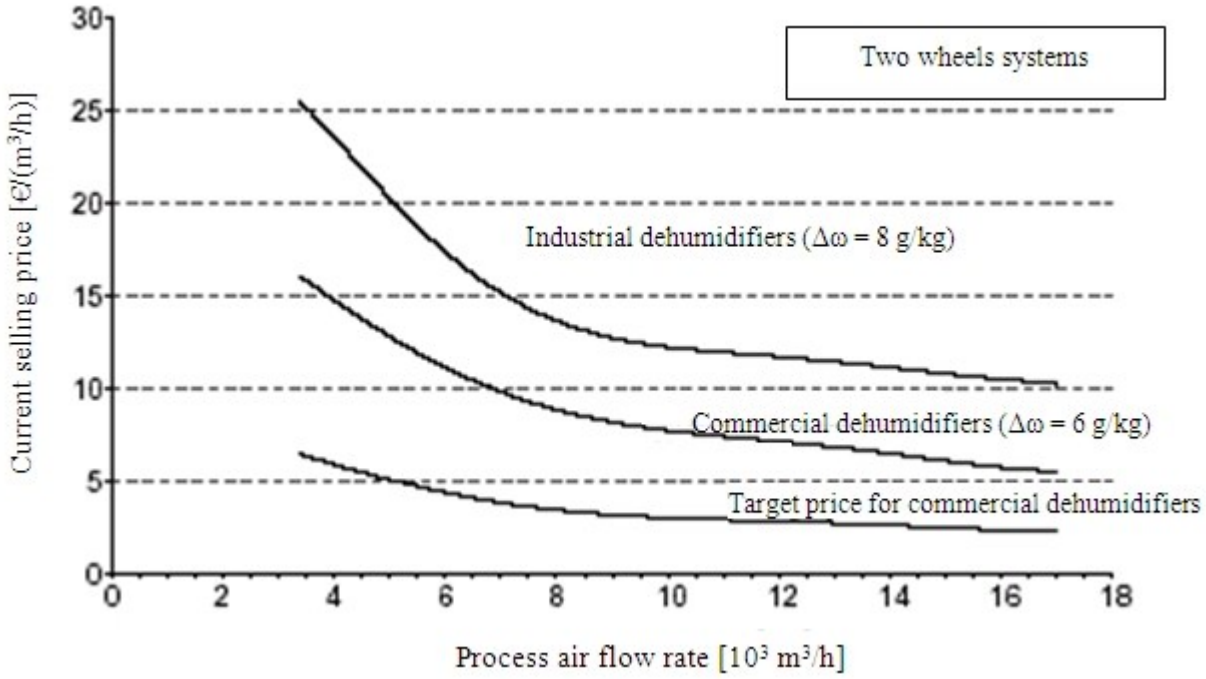

Fig. 1. 4: Average specific cost of dehumidification systems as a function of the process air volumetric flow rate

CHAPTER 2: EXPERIMENTAL PERFORMANCES OF THE DESICCANT WHEEL

2.1 The test facility

At "Università degli Studi del Sannio", in Benevento (Southern Italy), a desiccant Air Handling Unit coupled to a natural gas-fired reciprocating internal combustion engine cogenerator, an electric chiller and a natural gas-fired boiler, has been experimentally analyzed. The experimental plant can be conveniently used for the evaluation of the performances, in Mediterranean climate, of both the main components of the HVAC system and the complete plant.

In Fig. 2. 1, temperature and humidity ratio of outdoor air during the tests are shown, [14]; the summer reference conditions of outdoor air in Benevento are: temperature = 32 °C, humidity ratio = 15 g/kg.

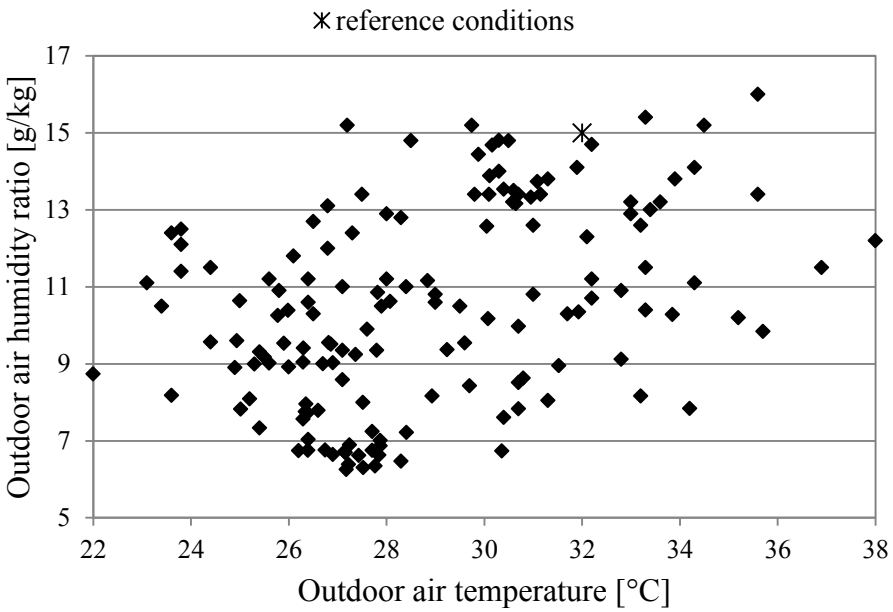

Fig. 2. 1: Temperature and humidity ratio of outdoor air during the tests

The maximum values of outdoor air temperature and humidity ratio during the tests were 38 °C and 16 g/kg, respectively. Therefore, Benevento is characterized by a quite warm and humid climate.

The hybrid HVAC system is based on the dehumidification of outdoor air by a desiccant wheel and its subsequent cooling by an electric chiller. The desiccant wheel is described in section 2.1.1.

In Fig. 2. 2, the layout of the test facility is shown [14, 15].

Nominal characteristics of the devices are the following:

- cogenerator: P_{el} = 6.00 kW (0.200 kW for the auxiliaries electric load), Q_{th} = 11.7 kW, η_{el} = 28.8%, η_{th} = 56.2%; the MCHP supplies thermal power for the regeneration of the desiccant wheel by recovering heat from the exhaust gas and from the engine jacket. More features are provided in section 3.3.1;
- air-cooled water chiller: Q_{cool} = 8.50 kW, COP = 3.00;
- boiler: Q_{th} = 24.1 kW, η_b = 90.2%. The boiler can be used to supply thermal energy when the hybrid HVAC system is powered by separate "production" systems, or to integrate the thermal power available from the MCHP. In fact, the maximum regeneration air temperature that can be reached with the thermal recovery of the MCHP (65 °C) could be insufficient to reach the desired supply air humidity ratio in hot and humid climates; hence thermal power is supplied also by the boiler, allowing to reach a higher regeneration temperature;
- heat storage: capacity = 1000 dm^3 (855 dm^3 net volume); it is manufactured with carbon steel and insulated with 100 mm flexible polyurethane layer. It can be fed by three different thermal energy sources.

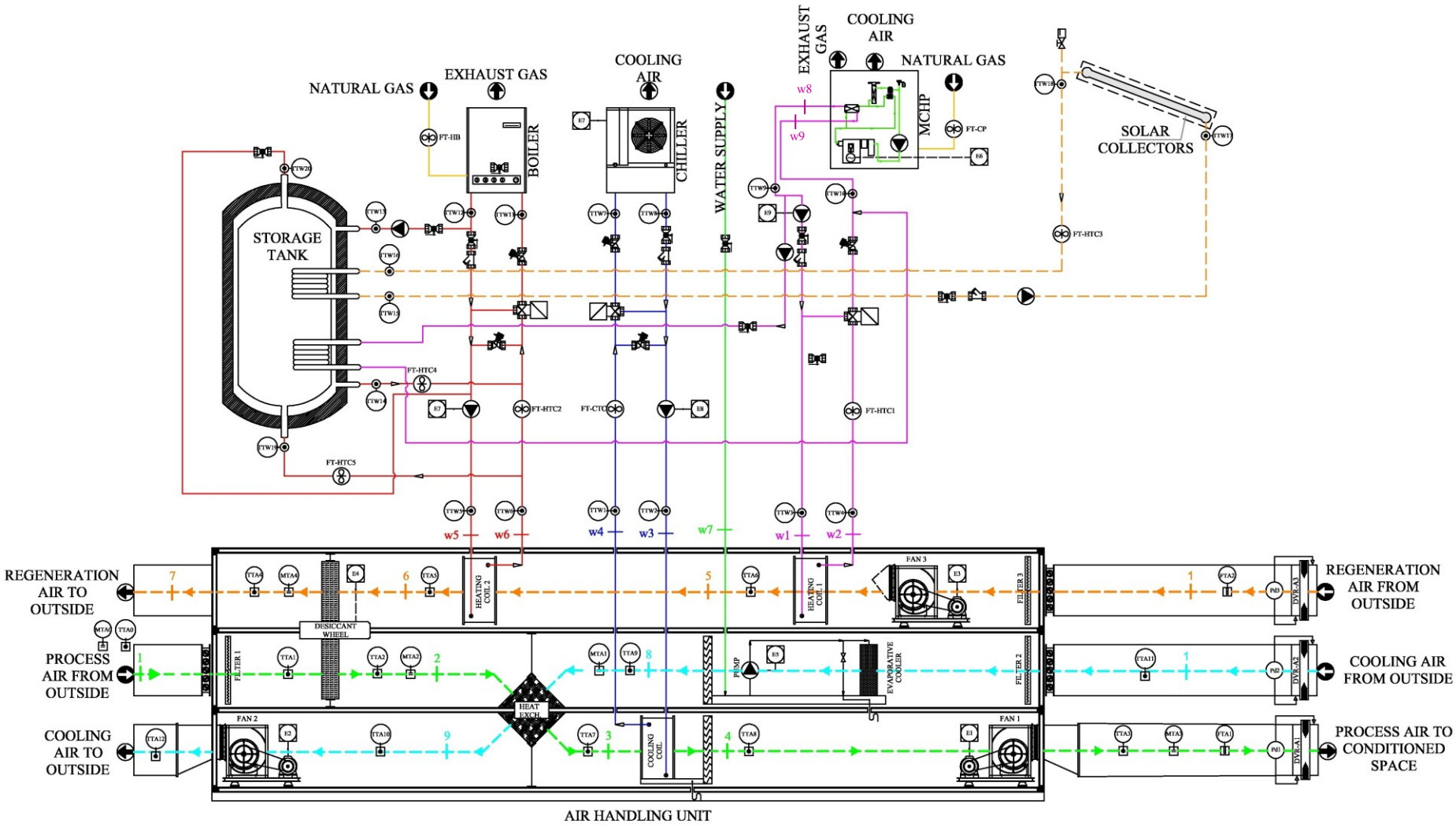

Fig. 2. 2: The layout of the test facility

The symbols used in Fig. 2. 2 as well as the characteristics of the sensors (the measured parameter, the measuring range and the accuracy) are reported in Tab. 2. 1.

LEGEND

	GATE VALVE
	BALANCE VALVE
	FILTER
	THREE-WAY VALVE
	PUMP
	ELECTRIC ENERGY METER

SENSORS

NAME AND SYMBOL		MEASURED PARAMETER	MEASURING RANGE	ACCURACY
TTA0,1,3,7...12		AIR TEMPERATURE	-50 / +50 °C	± 0.5 °C
TTA2,4...6		AIR TEMPERATURE	-10 / +90 °C	± 0.15 °C
MTA0		AMBIENT RELATIVE HUMIDITY	0 - 99%	± 2% RH (5-90% RH) ± 2.5% RH (0-5% and 90-100% RH)
MTA2, ... 5		RELATIVE HUMIDITY	0 - 99%	± 2% RH (5-90% RH) ± 2.5% RH (0-5% and 90-100% RH)
FTA1,2		AIR VELOCITY	0 - 10 m/s	± 0.2 m/s + 3% of measured value
FT-HTC1...5 FT-CTC		VOLUMETRIC FLOW RATE	2 - 60 L/min	± 2% FS
Pd1, ... 3		DIFFERENTIAL PRESSURE	0 - 500 Pa	± 14 Pa
FT-HB FT-CP		MASS FLOW RATE	0 - 2.5 Nm3/h	± 0.2% FS
TTW1, ... 20		WATER TEMPERATURE	-10 / +120 °C	± 1.4 °C

Tab. 2. 1: Legend and sensors for Fig. 2. 2

To determine air thermal-hygrometric properties, temperature and Relative Humidity (RH) sensors are installed. Therefore, the relative humidity method is used to evaluate air humidity ratio, [16]. It is calculated, in g/kg, by means of the following equation:

$$\omega = \frac{0.622 \; {}^{RH}\!/_{100} \; p_{v,sat}}{p - {}^{RH}\!/_{100} \; p_{v,sat}} \cdot 1000 \tag{2.1}$$

where RH is expressed in percentage and $p_{v,sat}$ is the vapour partial pressure in saturated condition, [17].

Air enthalpy is a function of humidity ratio and temperature and can be calculated with the following equation:

$$h = \frac{(2500.5 + 1.805t)\omega}{1000} + 1.005t \tag{2.2}$$

Concerning the AHU, it treats 800 m^3/h of air that achieves the summer supply conditions required by the room (t_s = 13-19 °C, ω_s = 7-11 g/kg).

There are three outdoor air streams:

- process air, dehumidified by the desiccant wheel (1-2), pre-cooled by the cooling air stream in an air-to-air cross flow heat exchanger (2-3), finally cooled to the supply temperature by a cooling coil interacting with the chiller (3-4); it is used to maintain thermal and humidity comfort values in the conditioned space;
- regeneration air, heated by the heating coil interacting with the MCHP (1-5) and/or by the heating coil interacting with the boiler (5-6); it is used to regenerate the desiccant wheel (6-7);
- cooling air, cooled by a direct evaporative cooler (1-8) and then used to pre-cool the process air exiting the desiccant wheel (8-9).

The volumetric flow rates of the three air streams can be controlled by means of manual shutters. When these are at their maximum opening, the air flow rates get their nominal values (800 m^3/h).

In Fig. 2. 3, the transformations of process, regeneration and cooling air flows are reported in a psychrometric chart.

The three air streams are entirely drawn from the outdoor (state 1, common to the three airflows), therefore no recirculation is carried out.

Desiccant-based AHUs normally use two air flows (process and regeneration) and a recuperative heat exchanger between them to pre-cool the process air flow and pre-heat the regeneration one; to this aim, regeneration air, drawn from outside or indoor ambient, is usually cooled in a direct evaporative cooler, in order to reduce its temperature and enhance the heat exchange in the recuperator, [18]. But the evaporative cooling process increases regeneration air humidity, hence reducing its desorption capacity; this could determine an insufficient capability of the desiccant cooling system to balance ventilation and internal latent loads, in particular in Mediterranean climates, such as in Benevento.

Therefore, in this work a new layout of the desiccant-based AHU is investigated: it uses an air-to-air heat exchanger between the process air flow and a cooling air flow.

Fig. 2. 4 presents a photograph of the air handling unit, highlighting the desiccant wheel, the hydraulic pipes which connect the cogenerator, the boiler and the chiller with the corresponding coils inside the AHU, and the aeraulic ducts which intake and discharge process, regeneration and cooling air.

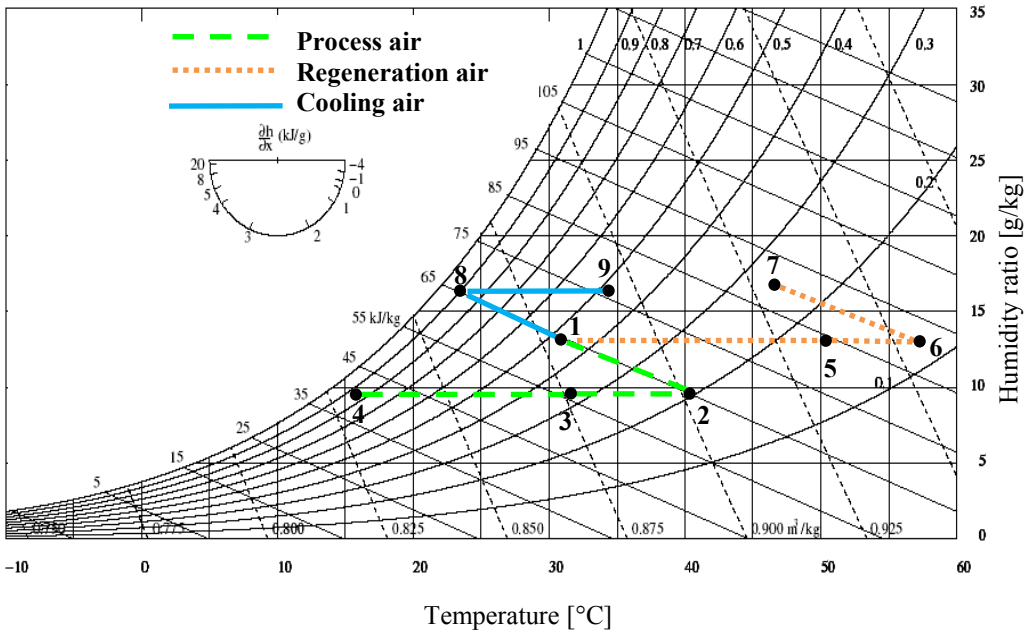

Fig. 2. 3: Air transformations in the psychrometric chart

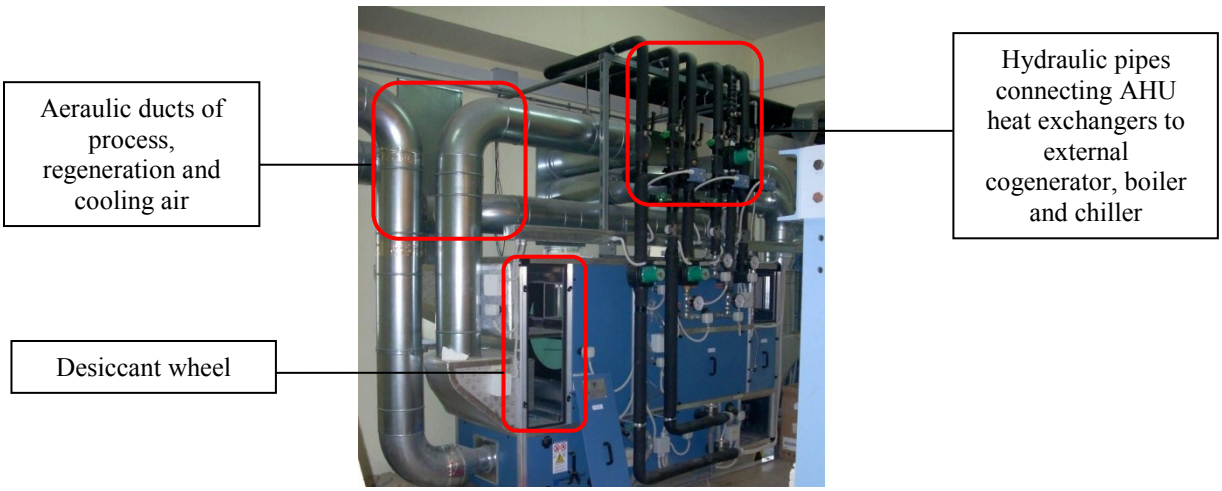

Fig. 2. 4: The air handling unit equipped with the desiccant wheel.

2.1.1 The desiccant wheel

The desiccant wheel (Fig. 2. 5) is filled with silica-gel; it has a weight of 50 kg and its dimensions are 700 mm x 200 mm (diameter x thickness). In reality, the frontal area of the rotor exposed to process and regeneration air flows is relative to a diameter of about 600 mm, since a circular crown of the total area is obstructed by the metallic frame of the desiccant wheel cassette in the AHU.

The rotor has the following configuration: 60% of the rotor area is crossed by the process air, while the remaining 40% by the regeneration air. This layout is often used when low temperature regeneration thermal energy is available. In fact, the DW is filled with silica-gel, a desiccant material that can be effectively regenerated at temperatures as low as 60-70 °C; these values can be achieved with the thermal recovery from the MCHP and, only when necessary, the natural gas boiler.

The rotor matrix is composed of alternate layers (smooth and wavy) of silica-gel sheets and metallic silicate, chemically bound into an inorganic fiber frame. The so realized “honeycomb” frame has several advantages, such as the maximization of the superficial contact area, low pressure drops (154 Pa), low weight and high structural durability. The nominal rotational speed of the DW is 12 RPH (Revolutions Per Hour).

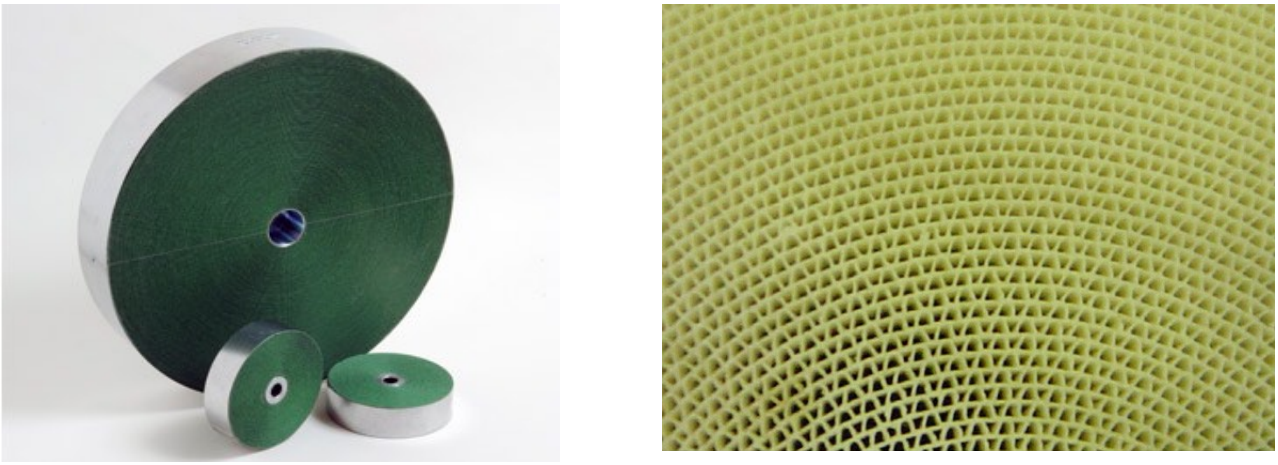

Fig. 2. 5: The desiccant wheel and the rotor matrix

2.2 Performance of the desiccant wheel

Performances of the desiccant wheel, in terms of humidity reduction, moisture removal, process air outlet temperature and effectiveness, depend on several operational parameters.

As a result of the importance of the desiccant wheel in desiccant cooling systems, many investigations have been performed on its design, modeling and optimization, considering different operating variables and evaluating several types of performance parameters.

A mathematical model of desiccant wheel, that uses a commercial software for solving mass and heat transfer equations, was developed by Esfandiari Nia et al., [19]. The model is used to obtain simple correlations for calculating humidity and temperature of the air exiting the wheel as a function of some physically measurable input variables; furthermore, it also allows to determine the optimal rotational speed.

Stabat et al., [20], developed and validated a mathematical model in order to evaluate the desiccant wheel performance; then, it was utilized to calculate some figures of merit as a function of different variables, such as rotational speed of the wheel, inlet process air temperature, humidity ratio and flow rate, regeneration temperature.

Jia et al., [21, 22], worked out a mathematical model to predict the performance of a rotary solid desiccant cooling system using a novel compound adsorbent material; this model was then validated by means of experimental tests.

Ge et al., [23], developed mathematical models, validated by means of experimental data, for predicting the performances of a desiccant wheel; then they used these models to calculate the values of some performance parameters of the component, such as the dehumidification effectiveness and the Dehumidification Coefficient Of Performance (DCOP), as a function of various operating variables (inlet temperature and humidity ratio of the process air, regeneration temperature, wheel rotational speed, process air flow rate…).

Similar parametric studies were carried out by other authors through experimental investigations, [24-26]; other desiccant wheel performance parameters, such as Moisture Removal Capacity (MRC), were evaluated too.

Stabat et al., [27], implemented a desiccant wheel model to be adapted to building simulation code, which was in good agreement with experimental and manufacturer data.

Hamed et al., [28], developed a mathematical model to evaluate the effect of the operating conditions on the performance of a rotating dehumidification system using a liquid desiccant. The effects of regeneration air temperature, process air and regeneration air inlet humidity ratio, rotational speed, process and regeneration air velocity on the amount of water absorbed were investigated.

Xiong et al., [29], investigated a novel two-stage liquid desiccant dehumidification system using an exergy analysis method. The proposed system is characterized by higher COP and exergy efficiency compared to a basic liquid desiccant dehumidification system.

The transient and steady state transport phenomena in the DW were analyzed by Z. Gao et al., [30], who developed a mathematical model based on the one-dimensional Navier-Stokes equations. The model evaluates the humidity ratio and temperature in the air flow channels as a function of time. The predicted results were validated by means of data taken from experimental results.

Beccali et al., [31, 32], presented some models to evaluate the performance of dehumidification rotors with different solid desiccant materials. The models were derived from the interpolation of experimental data obtained from the industry. Some correlations were developed for predicting outlet temperature and humidity ratio.

Mandegari and Pahlavanzadeh, [33], presented an experimental study considering different climates (hot dry and hot humid) and various operating conditions, in terms of regeneration temperature and wheel speed. The desiccant wheel effectiveness values in each operating condition were calculated and a new definition for effectiveness was introduced.

Yao et al., [34], investigated a new regeneration method using power ultrasound. The experimental study proved that the proposed method can help to improve the regeneration efficiency and reduce regeneration energy requirement.

Panaras et al., [35], carried out the validation of a desiccant wheel model by means of experimental data taken in a test facility, as well as a satisfactory comparison between experimental results and manufacturer data.

Concerning the thermal energy source to regenerate the DW, in the literature great attention is taken to solar energy. The evaluation and optimization of the performance of a solar assisted desiccant wheel was carried out by Ahmed et al., [36]. They developed a numerical model to study

the effect of several parameters, such as wheel thickness, speed and porosity, regeneration to adsorption area ratio, process air flow rate and humidity ratio as well as regeneration air temperature. A solar air collector is used as thermal energy source to regenerate the desiccant material.

Vitte et al., [37], showed that a correctly controlled solar desiccant cooling system can allow interesting energy savings in building air conditioning. The influence of indoor and outdoor air conditions is analyzed using numerical simulations, by means of a validated model of the desiccant wheel.

A numerical and experimental study of a solar assisted desiccant cooling system for air conditioning applications in Pakistan was presented by Khalid et al., [38]. Tests were conducted on a gas-fired hybrid desiccant cooling test rig. Using sets of measured data, a validation of a numerical model of the cooling system, in which the gas-fired heater is substituted by a solar air collector, was undertaken.

Enteria et al., [39, 40], analysed a solar thermal desiccant cooling system incorporating hot water preparation. It has several operation procedures to optimize its performance based on weather, cooling requirements or comfort conditions in the indoor ambient and the time of operation. The desiccant cooling subsystem was tested to evaluate its dehumidification performance, in terms of COP.

Eicker et al., [41], experimentally evaluated the performance of a solar air collector driven desiccant cooling system, focusing on two types of dehumidification efficiency.

On the other hand, few research investigations were carried out to experimentally evaluate the performance of a desiccant wheel regenerated by means of low temperature thermal energy recovered from a cogenerator, [42-46].

In particular, the influence of the regeneration air temperature ($t_{reg} = t_6$), the temperature ($t_{out} = t_1$) and humidity ratio ($\omega_{out} = \omega_1$) of the outdoor air entering the desiccant wheel, the desiccant wheel rotational speed and the ratio between regeneration and process air flow rates, is analyzed[2], [47, 48, 49].

---

[2] Numeric subscripts, starting from this section and through all the thesis, refer to Fig. 2. 2.

As regards this last parameter, some research activities, [19, 23, 26, 33, 35], investigated the desiccant wheel performance as a function of process and/or regeneration air flow rates, but these works have not satisfactorily clarified if the highest influence on the dehumidification process is due to the regeneration air flow rate or the regeneration temperature, especially as regards the quantitative effect of both variables. Therefore, this research topic has been particularly analyzed in this work. Both the cases of fixed regeneration temperature (t_{reg}) and fixed regeneration thermal power ($Q_{th,reg}$) have been examined; in fact, when a fixed $Q_{th,reg}$ is available, it can be exploited either increasing the regeneration air flow rate and reducing the regeneration temperature or vice versa. To this aim, some tests have been carried out in order to clarify if the highest influence on the dehumidification process is due to the regeneration air flow rate or temperature.

There are other parameters that affect desiccant wheel performances, e.g. the regeneration air humidity or structural parameters, such as the rotor thickness, the type of desiccant material, process and regeneration angles. However, with the current configuration of the test facility, regeneration air has the same humidity of process air, while the influence of structural parameters cannot be investigated.

Some definitions of desiccant wheel effectiveness are used [33, 50-52]:

- the *thermal effectiveness*, the conventional effectiveness definition for a heat exchanger:

$$\eta_{th} = \left(t_2 - t_1\right) \Big/ \left(t_6 - t_1\right) \tag{2.3}$$

- the *regeneration effectiveness*, that expresses, for unitary mass flow rate, the latent load handled by the DW with respect to the regeneration thermal power required for the regeneration process:

$$\eta_{reg} = \left(\omega_1 - \omega_2\right)\Delta h_{vs} \Big/ \left(h_6 - h_1\right) \tag{2.4}$$

- the *dehumidification effectiveness*:

$$\eta_{deh} = \left(\omega_1 - \omega_2\right) \Big/ \left(\omega_1 - \omega_{2,ideal}\right) \tag{2.5}$$

where $\omega_{2,ideal}$ is the ideal humidity ratio of process air stream at the desiccant wheel outlet. If its value is zero, the process in the DW is ideal and the process air is completely dehumidified. Hence, η_{deh} expresses the comparison between the real dehumidification capability and the ideal one.

- the *adiabatic effectiveness*:

$$\eta_{ad} = 1 - \left(h_2 - h_1\right) / h_1 \tag{2.6}$$

The real adsorption process is not isoenthalpic (air enthalpy increases), so the comparison between the real adsorption process and the isoenthalpic one becomes significant.

The followings performance parameters are also evaluated:

- the Moisture Removal Capacity, which represents the flow rate of moisture removed by the wheel, [16]:

$$MRC = \rho_1 \dot{V}_{proc} \left(\omega_1 - \omega_2\right) \tag{2.7}$$

- the Dehumidification Coefficient Of Performance, [23], which represents the ratio between the thermal power related to the dehumidification process and the regeneration thermal power:

$$DCOP = \frac{\rho_1 \dot{V}_{proc} \Delta h_{vs} \left(\omega_1 - \omega_2\right)}{\rho_1 \dot{V}_{reg} \left(h_6 - h_1\right)} = \frac{\dot{V}_{proc} \Delta h_{vs} \left(\omega_1 - \omega_2\right)}{\dot{V}_{reg} \left(h_6 - h_1\right)} \tag{2.8}$$

The latent heat of vaporization of water, Δh_{vs}, is approximated by the following empirical cubic function, [53]:

$$\Delta h_{vs} = -0.614342 \cdot 10^{-4}\, t_1^3 + 0.158927 \cdot 10^{-2}\, t_1^2 - 0.236418 \cdot 10\, t_1 + 0.250079 \cdot 10^4 \tag{2.9}$$

- the Sensible Energy Ratio, SER, which represents the ratio between the thermal power related to the air heating through the wheel on the process side and the thermal power supplied for the regeneration process, [40]:

$$SER = \frac{\rho_1 \dot{V}_{proc}\, c_p \left(t_2 - t_1\right)}{\rho_1 \dot{V}_{reg}\, c_p \left(t_4 - t_1\right)} = \frac{\dot{V}_{proc} \left(t_2 - t_1\right)}{\dot{V}_{reg} \left(t_4 - t_1\right)} \tag{2.10}$$

In equations 2.8 and 2.10, the ideal gas model with constant specific heat has been assumed for both process and regeneration air.

Both the experimental results and the data provided by the manufacturer have been used to calculate η_{deh}, MRC, DCOP and SER, and a comparison of the results is presented. Experimental

and manufacturer results for these four parameters are shown as trend lines; the reason for using trend lines, instead of points, for the experimental data, is related to author's ongoing modelling activity in the framework of IEA Annex 54 project, that will lead, in future works, to the use of trend lines equations to develop a performance map model of the component.

Moreover, for the experimental results, the absolute value of the determination coefficient, R^2, is reported; this parameter is defined as:

$$R^2 = \frac{\sum_{j=1}^{N} \left(\hat{v}_{j,e} - \overline{v_e}\right)^2}{\sum_{j=1}^{N} \left(v_{j,e} - \overline{v_e}\right)^2} \tag{2.11}$$

where $\hat{v}_{j,e}$ are the values estimated by the trend line, $v_{j,e}$ are the experimental values, $\overline{v_e}$ is the average of experimental values and N denotes the number of measurements. R^2 varies between 0 and 1 and expresses how well the trend line fits the data (0 means no fit, 1 means perfect fit).

Except where otherwise indicated, all the experimental results refer to the nominal value of the process and regeneration volumetric air flow rates (800 m^3/h) and desiccant wheel rotational speed (12 RPH). All the fixed boundary conditions to derive the results are reported in each figure caption.

Finally, little attention has been paid in the literature on the capability of the desiccant wheel in handling ventilation and internal latent loads. Therefore, fixing the regeneration temperature at the maximum value achievable with the thermal recovery from the MCHP (65 °C), ventilation and internal latent loads that the DW can handle are evaluated and compared to the required values, considering both a set of cities all over the world and the entire range of climatic conditions occurred in the experimental tests.

2.2.1 Uncertainty analysis

Uncertainty analysis is the tipycally used procedure to assess the uncertainty in a result calculated from measured variables with known values of uncertainties.

The uncertainty analysis carried out in this work is based on the root sum square method reported by Kline and McClintock, [54], and it allows the evaluation of the uncertainty in results obtained by calculation from measured variables. Rather than sum the individual contributions of each measurement, the method argues that, as the errors are statistically independent, they will

partially counteract each other most of the time, such that the square root of the sum of the squares of the individual uncertainties is a more representative value of the overall random uncertainty. The method uses the following equation to evaluate the absolute uncertainty:

$$\Delta y = \left[\left(\frac{\partial f}{\partial x_1} \right)^2 (\Delta x_1)^2 + \left(\frac{\partial f}{\partial x_2} \right)^2 (\Delta x_2)^2 + \ldots + \left(\frac{\partial f}{\partial x_n} \right)^2 (\Delta x_n)^2 \right]^{1/2} \tag{2.12}$$

where f is a function of the independent variable x_i , Δx_i is the absolute uncertainty associated with the variable x_i, y is the dependent variable and Δy is its absolute uncertainty. The relative uncertainty is therefore:

$$\frac{\Delta y}{y} = \left[\left(\frac{\partial f}{\partial x_1} \right)^2 \left(\frac{\Delta x_1}{y} \right)^2 + \left(\frac{\partial f}{\partial x_2} \right)^2 \left(\frac{\Delta x_2}{y} \right)^2 + \ldots + \left(\frac{\partial f}{\partial x_n} \right)^2 \left(\frac{\Delta x_n}{y} \right)^2 \right]^{1/2} \tag{2.13}$$

The performance parameters described in the previous section are obtained by calculation from measured variables (temperature, relative humidity and velocity of the air); each of these measured variable is characterized by a known value of uncertainty, that depends on the accuracy of the sensors (see Tab. 2. 1).

In particular, the air humidity ratio has been calculated considering the measured values of temperature and relative humidity, but a relevant attention is required for the RH measurement at the outlet of the desiccant wheel on the process side. In fact, the uncertainty of the measured RH value strongly rises when very low values of this property are attained, [55], and it would be very high if the RH measurements were taken at the outlet of the DW, (state 2 of Fig. 2. 2), where it can be lower than 5%. For this reason, the RH and temperature measurements have been carried out just after a dry cooling coil (i.e., a coil that only cools, but does not dehumidify, the air), installed behind the wheel to obtain higher relative humidity values, more suitable for the RH measurement (state 3 in Fig. 2. 2). Then, the air humidity ratio, which remains constant throughout the dry cooling coil, has been calculated.

In Fig. 2. 6, the percentage uncertainty in humidity ratio measurements, as a function of humidity ratio and for different relative humidity, is shown.

Concerning the previously defined performance parameters, the uncertainty analysis has been carried out for η_{deh}, MRC, DCOP and SER; the overall obtained uncertainty values obtained are: 10.8 % for η_{deh}, 12.7 % for MRC, 15.2 % for DCOP and 3.64 % for SER. The very low value

of uncertainty in the Sensible Energy Ratio parameter can be explained by noting that the relative humidity sensors are not involved in its evaluation.

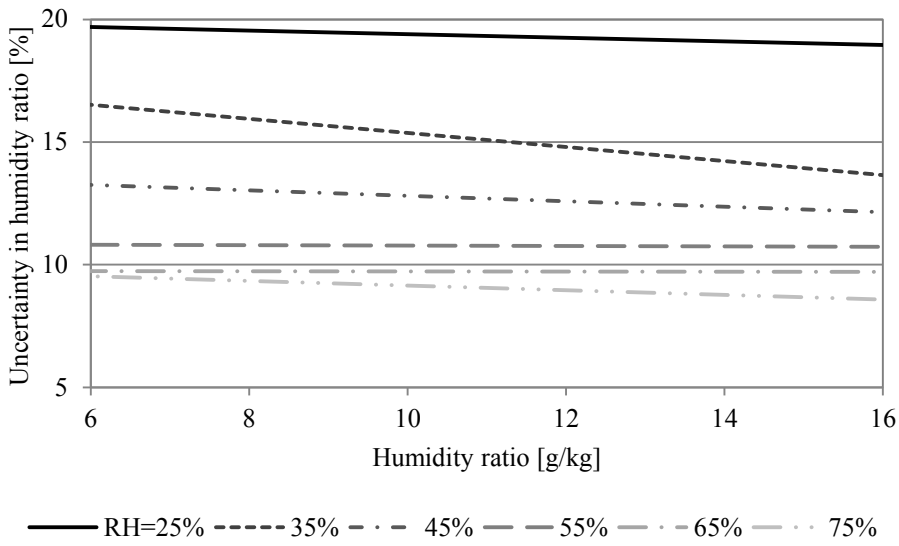

Fig. 2. 6: Uncertainty in humidity ratio calculation as a function of humidity ratio and for different relative humidity values

2.2.2 Effect of regeneration temperature

Increasing the regeneration air temperature, $t_{reg} = t_6$, with fixed outdoor humidity ratio, the dehumidification capability ($\Delta\omega = \omega_1 - \omega_2$), that is the difference in process air humidity ratio between upstream and downstream of the DW, increases, Fig. 2. 7. In fact, the moisture desorption process from the desiccant matrix (on the regeneration side) is endothermic, thus favored by high temperatures. Increasing the regeneration temperature, the section of the DW being regenerated is subjected to a deeper drying process. As a consequence, the desiccant matrix can attract more moisture from process air during the successive dehumidification process.

In Fig. 2. 7, it can be also noted that the best performance, in terms of $\Delta\omega$, is obviously obtained considering the isoenthalpic process (the ideal adsorption process).

Among the three real tests considered, with the same regeneration temperature, the best performance is obtained in test #3, during which ω_{out} attains its maximum value, and hence the capability of the desiccant material to catch water vapour droplets on its surface is maximized. In fact, the higher the water vapour content in outdoor air, the higher the difference in terms of vapour

partial pressure between outdoor air and desiccant material surface. Accordingly, diffusion of the water vapor droplets from the former to the latter is higher.

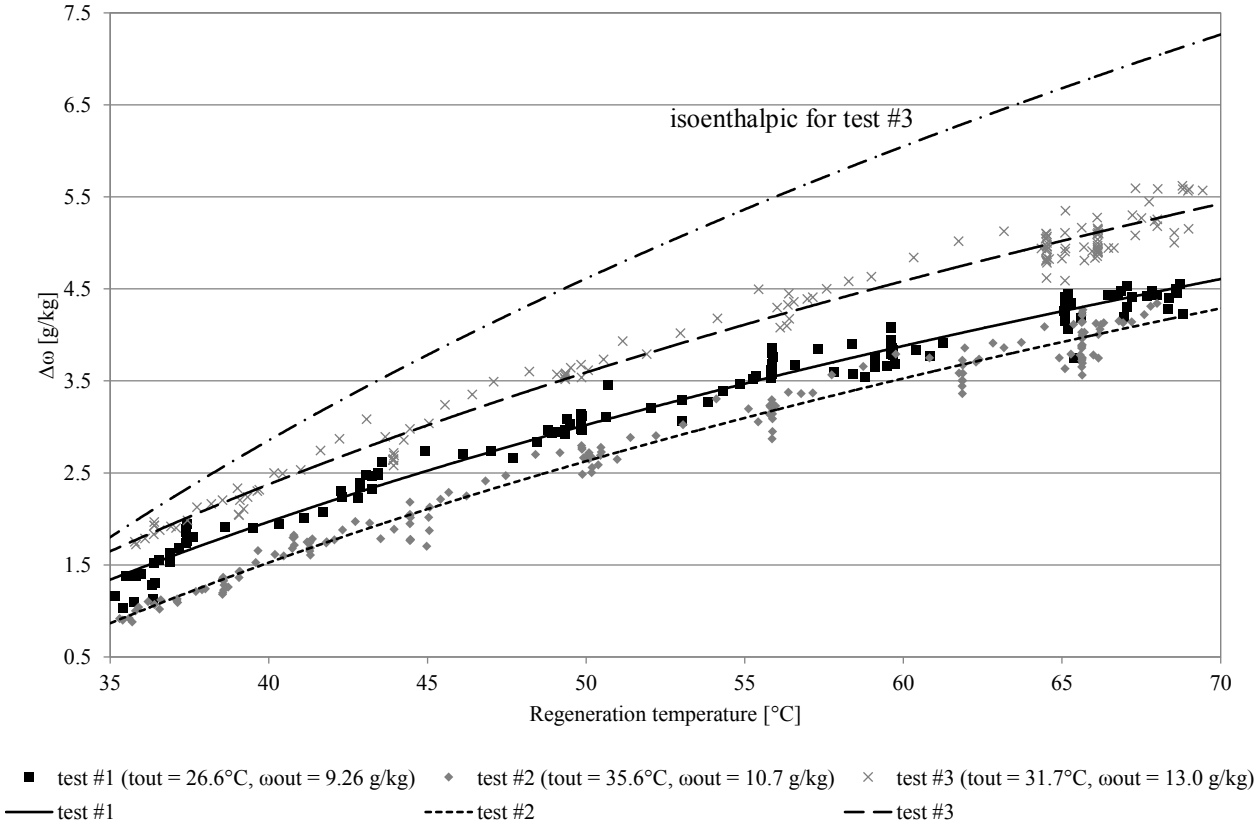

Fig. 2. 7: Difference between process air humidity ratio at inlet and outlet of the desiccant wheel as a function of regeneration temperature

When comparing tests #1 and #2, characterized by similar values of ω_{out}, the dehumidification capability is higher for test #1, due to the lower outdoor air temperature. In fact the adsorption process is exothermic, hence favored by low temperatures.

In Fig. 2. 8, Δt, the process air temperature difference between downstream and upstream of the DW, is reported as a function of t_{reg}, for three tests characterized by different values of t_{out} and ω_{out}. Evidently, Δt increases with t_{reg}, because of the heating of the desiccant matrix on the regeneration side and, as a consequence of the rotation of the wheel, on the process side. Obviously, the increase in Δt is only due to the rise in t_2, t_1 being constant. Moreover, the lowest values of Δt occur in test #1, due to the lowest values of t_{out} and ω_{out}. As regards the remaining tests, test #3 is characterized by a lower t_{out} but a higher ω_{out} compared to test #2. This last condition is predominant

such that the highest Δt occurs for test #3. In fact, Δt increases with process air inlet humidity ratio as the wheel removes a greater quantity of water vapour when ω_{out} grows. Therefore, Δt rises due to the increase in the adsorption heat released during the process. Furthermore, Δt is lower in the case of isoenthalpic process.

In Fig. 2. 9, the values of the above-mentioned effectiveness as a function of t_{reg} are shown, for fixed values of t_{out} and ω_{out}.

The rise in t_{reg} causes an increase in the heat losses from the hot side of the DW (regeneration section) to both the cold side (process section) and the outdoor environment, due to enhanced convective – conductive heat transfer mechanisms, and a stronger heating of the matrix and the desiccant material is also caused. Thus, the regeneration effectiveness decreases (the augmentation of the latent load handled by the DW does not balance the increase in the regeneration thermal power).

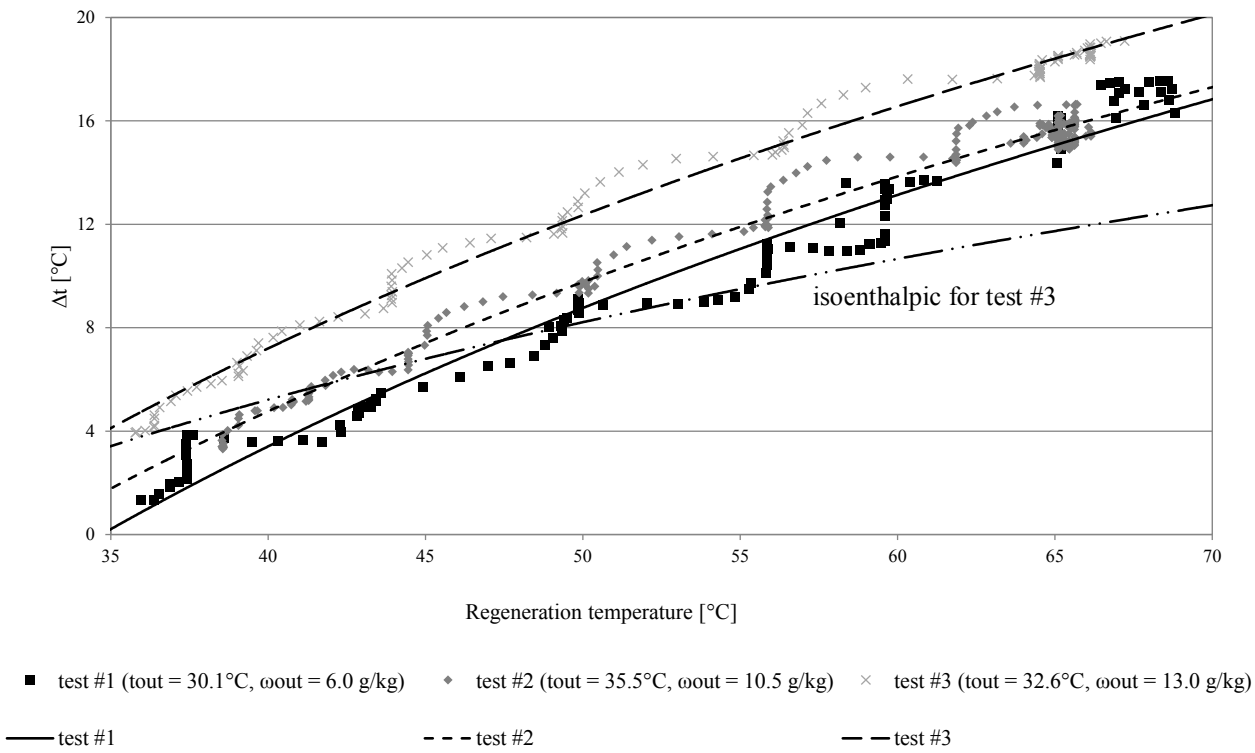

Fig. 2. 8: Difference between process air temperatures at outlet and inlet of the desiccant wheel as a function of regeneration temperature

Furthermore, the enthalpy h_2 increases, causing a light fall of the adiabatic effectiveness. Finally, the consequent augmentation in t_2 is lower than the increase in the regeneration temperature, so the thermal effectiveness has a descending behavior.

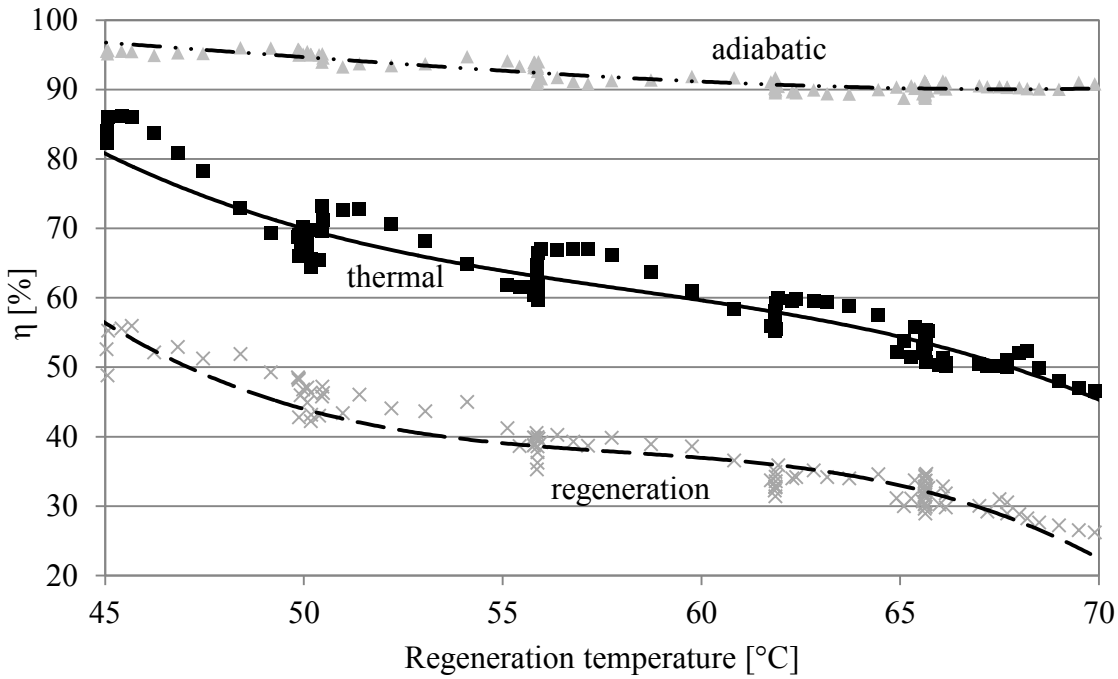

Fig. 2. 9: Various types of desiccant wheel effectiveness as a function of regeneration temperature (t_{out} = 32.7 °C – ω_{out} = 13.0 g/kg)

In Fig. 2. 10, the MRC is reported as a function of the regeneration temperature. It is well known that when increasing t_{reg}, the dehumidification capability of the desiccant rotor rises, and thus MRC. In this case, experimental results and manufacturer's data are almost coincident for regeneration temperatures lower than about 53 °C, while manufacturer's data show slightly better performances for higher t_{reg}.

In Fig. 2. 11, the effect of t_{reg} on η_{deh} is shown. Obviously, the increase in t_{reg} causes a rise in η_{deh}, in agreement with [23].

As regards DCOP (Fig. 2. 12), the increase of the dehumidification capability, $\Delta\omega$, with t_{reg} does not balance the rise in the specific regeneration thermal power (h_{reg}-h_{out} = h_6-h_1), so DCOP decreases. In particular, the reduction is more significant in the range 37-47 °C. Moreover, the very good agreement between experimental results and manufacturer's data should be underlined.

The effect of regeneration temperature on the Sensible Energy Ratio is shown in Fig. 2. 13.

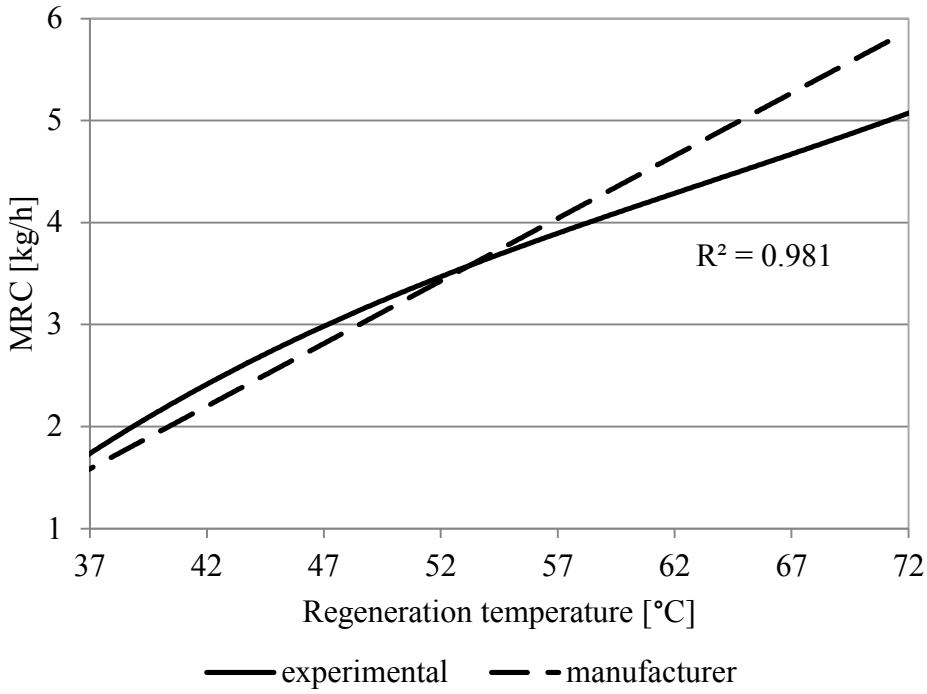

Fig. 2. 10: MRC as a function of t_{reg} (t_{out} = 31.6°C – ω_{out} = 13.2 g/kg)

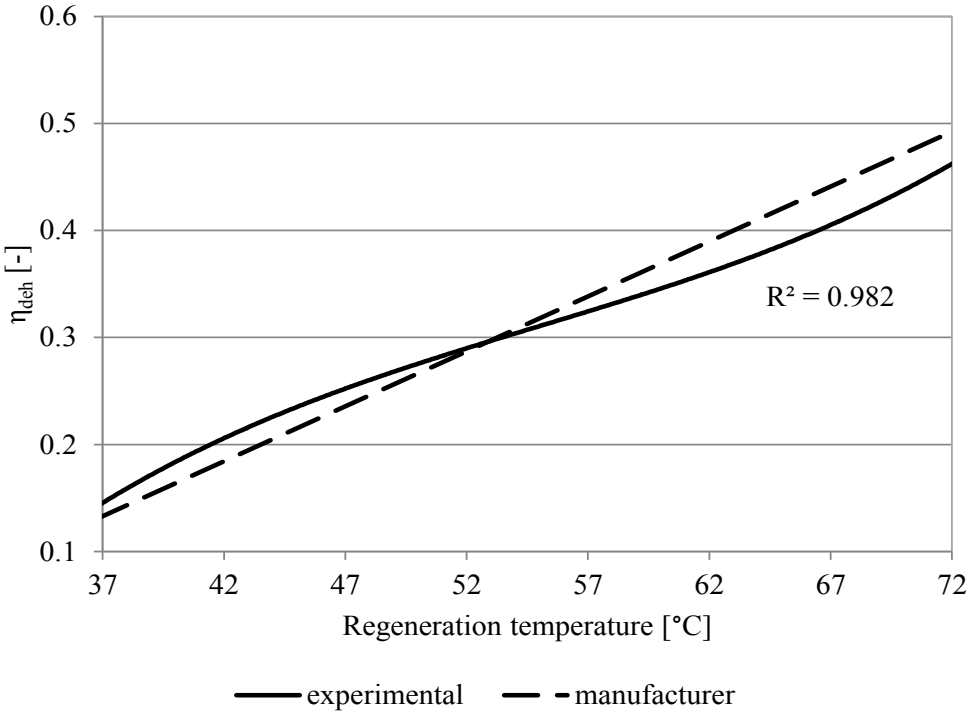

Fig. 2. 11: η_{deh} as a function of t_{reg} (t_{out} = 31.6 °C – ω_{out} = 13.2 g/kg)

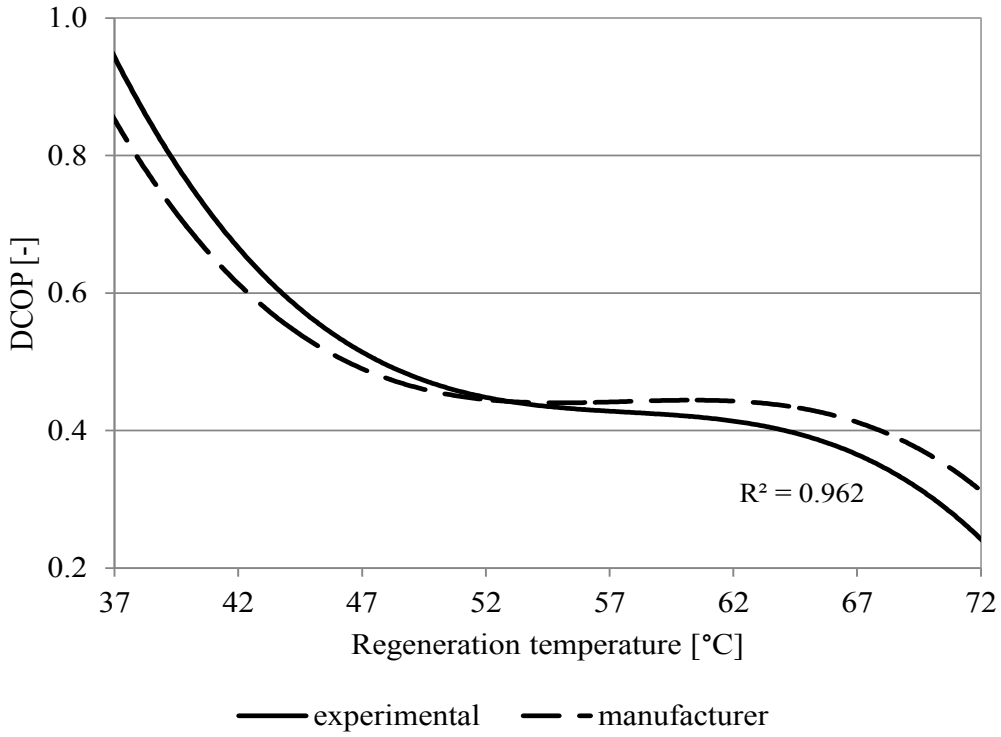

Fig. 2. 12: DCOP as a function of t_{reg} (t_{out} = 31.6 °C – ω_{out} = 13.2 g/kg)

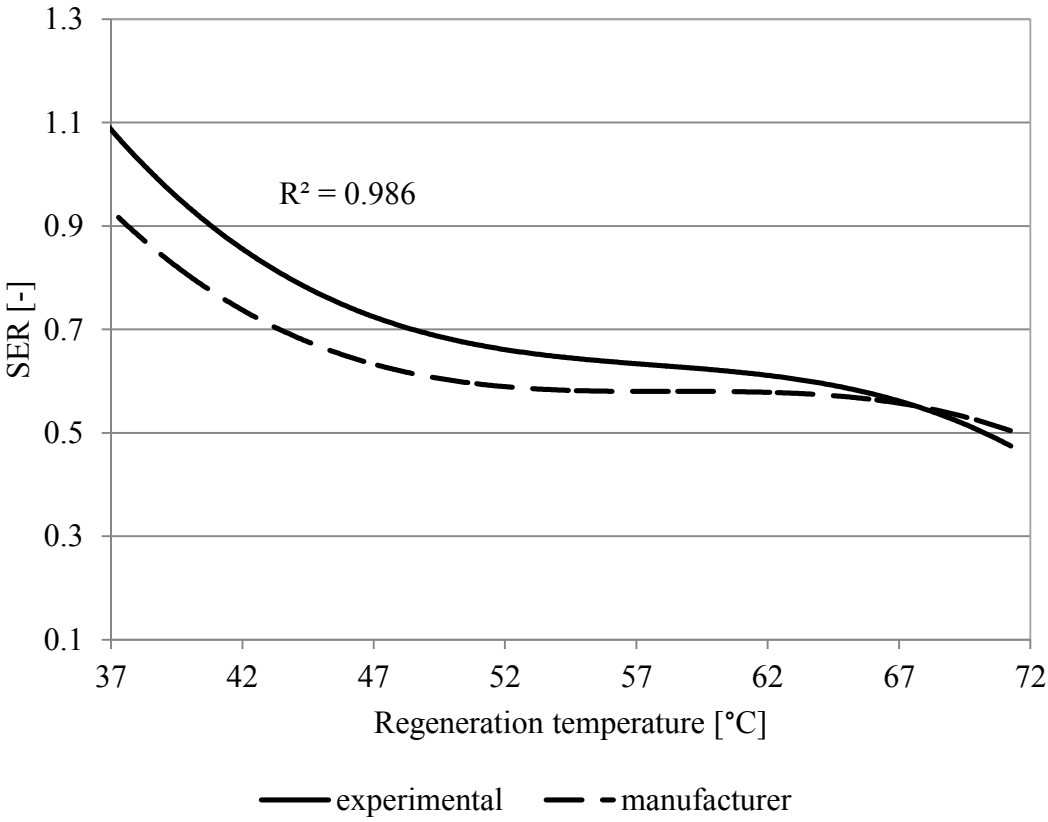

Fig. 2. 13: SER as a function of t_{reg} (t_{out} = 31.6 °C – ω_{out} = 13.2 g/kg)

Note that, contrariwise to the other performance parameters herein considered, better performances of the DW correspond to lower values of SER (that means a lower increase of the process air temperature through the wheel). t_2 rises with t_{reg}, because of the increased heating of the desiccant matrix on the regeneration side and, as a consequence of the rotation of the wheel, on the process side; but the increase in t_{reg} itself causes an overall reduction of SER, as expected on the basis of equation 2.10.

The results of Fig. 2. 13 are also confirmed by [33], in which thermal performances of the DW are evaluated by means of thermal effectiveness, instead of SER. However, the two parameters coincide for balanced flows, in which process and regeneration air flow rates are equal.

2.2.3 Effect of process air humidity ratio

In Fig. 2. 14, $\Delta\omega$ as a function of ω_{out} is reported, for different t_{out} and for t_{reg} = 65.0 °C. It monotonically increases with ω_{out}, while, for fixed values of ω_{out}, it decreases when t_{out} rises. These results are in good agreement with data supplied by the manufacturer: the experimental $\Delta\omega$ is lower than the indicated one by about 15%.

In Fig. 2. 15, Δt as a function of ω_{out} is reported, for different values of t_{out}. It can be seen that Δt increases when ω_{out} rises and/or t_{out} decreases, because in these cases the adsorption process is enhanced and therefore the adsorption heat rises.

In Fig. 2. 16 the effectiveness values are reported as a function of outdoor air humidity ratio, for fixed values of t_{reg} and t_{out}. As regards η_{reg}, the increase in $\omega_{out} = \omega_1$ causes an augmentation in the dehumidification capability, ω_1-ω_2, while t_{reg} is fixed; hence η_{reg} grows. With reference to η_{th}, the growth in the dehumidification capability determines a rise in the released heat of adsorption, therefore both t_2 and η_{th} rise.

Finally, at higher outdoor humidity ratio, adiabatic effectiveness improves, according to data supplied by the manufacturer of the desiccant wheel.

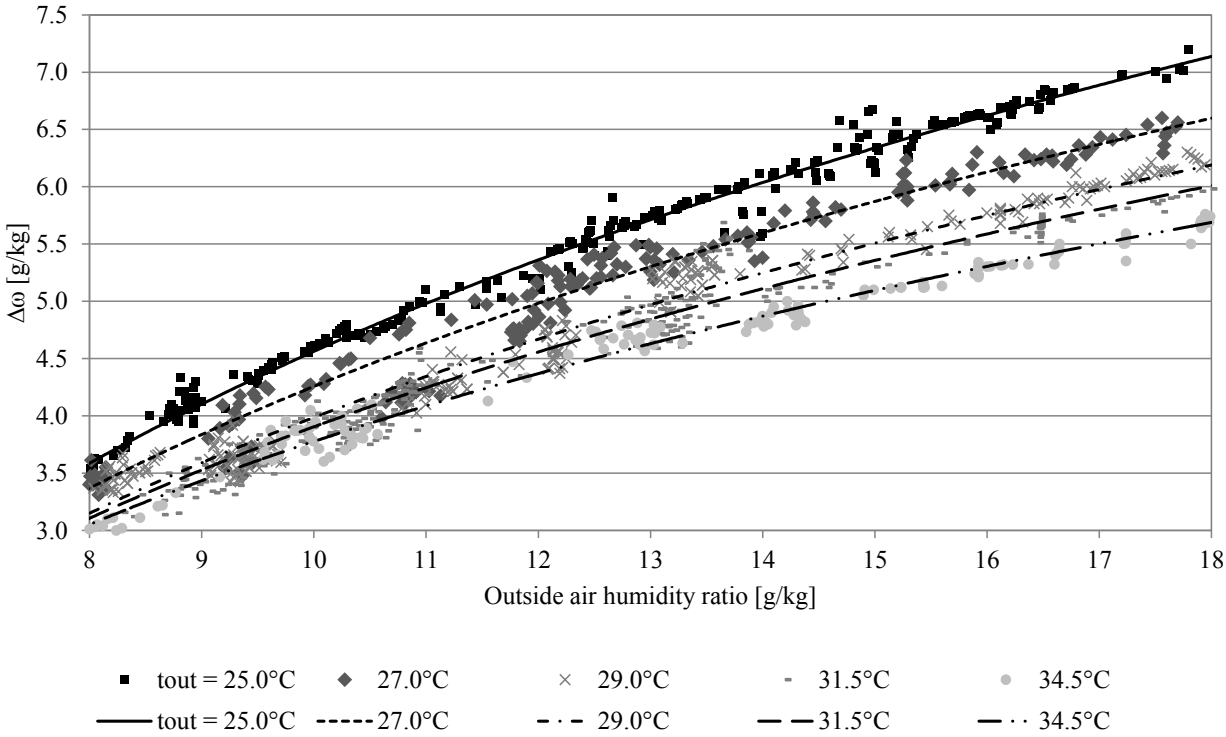

Fig. 2. 14: Difference between process air humidity ratio at inlet and outlet of the desiccant wheel as a function of outside air humidity ratio (t_{reg} = 65.0 °C)

In Fig. 2. 17, the moisture removal capacity is reported as a function of outdoor air humidity ratio ($\omega_{out} = \omega_1$). The rise in ω_{out} causes an increase in the dehumidification capability of the DW, and hence in the MRC. In fact, in presence of higher water vapour content in the process air, there is a major difference of vapour partial pressure between process air and desiccant material surface, and this determines a higher diffusion of the water vapour droplets from the air to the surface.

In Fig. 2. 18, the effect of ω_{out} on η_{deh} is shown. Experimental and manufacturer data show that, even if the increase in $\omega_{out} = \omega_1$ determines a rise of the dehumidification capability, η_{deh} reduces due to the increase of outdoor humidity itself (see equation 2.5), [19, 23]. Both experimental and manufacturer data show a linear decreasing trend.

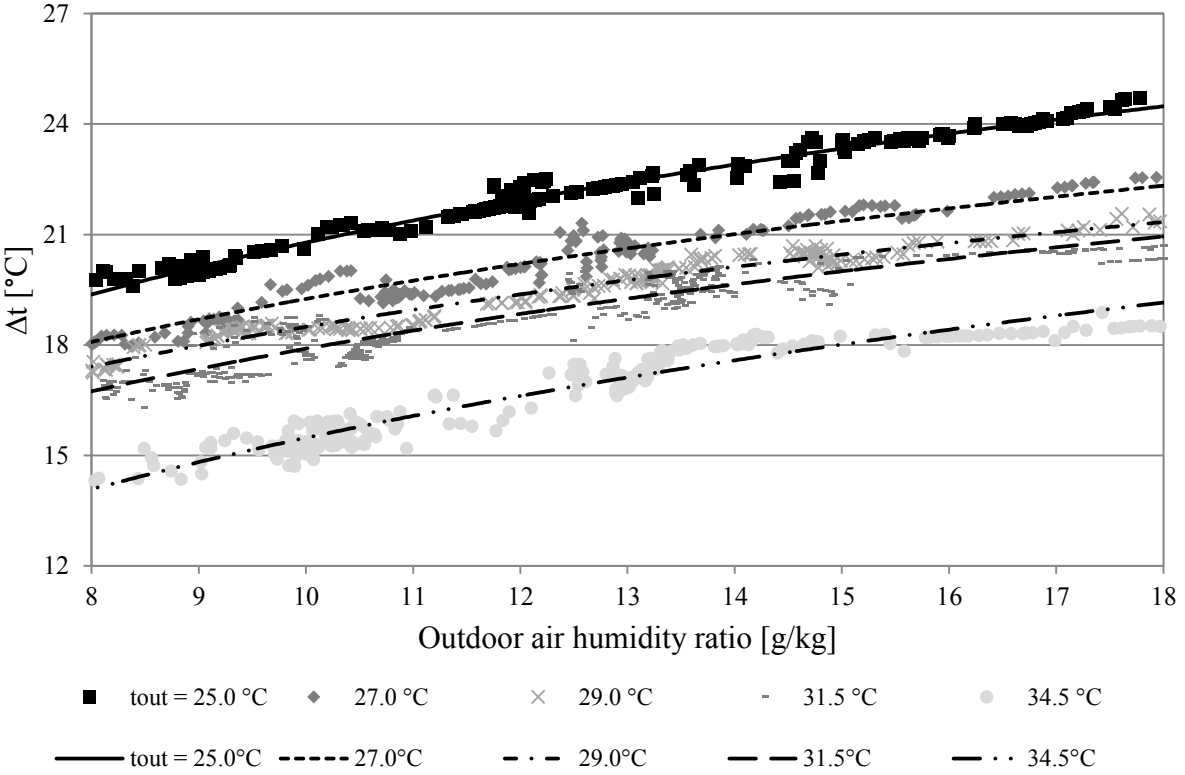

Fig. 2. 15: Difference between process air temperatures at outlet and inlet of the desiccant wheel as a function of ω_{out} (t_{reg} = 65.0 °C)

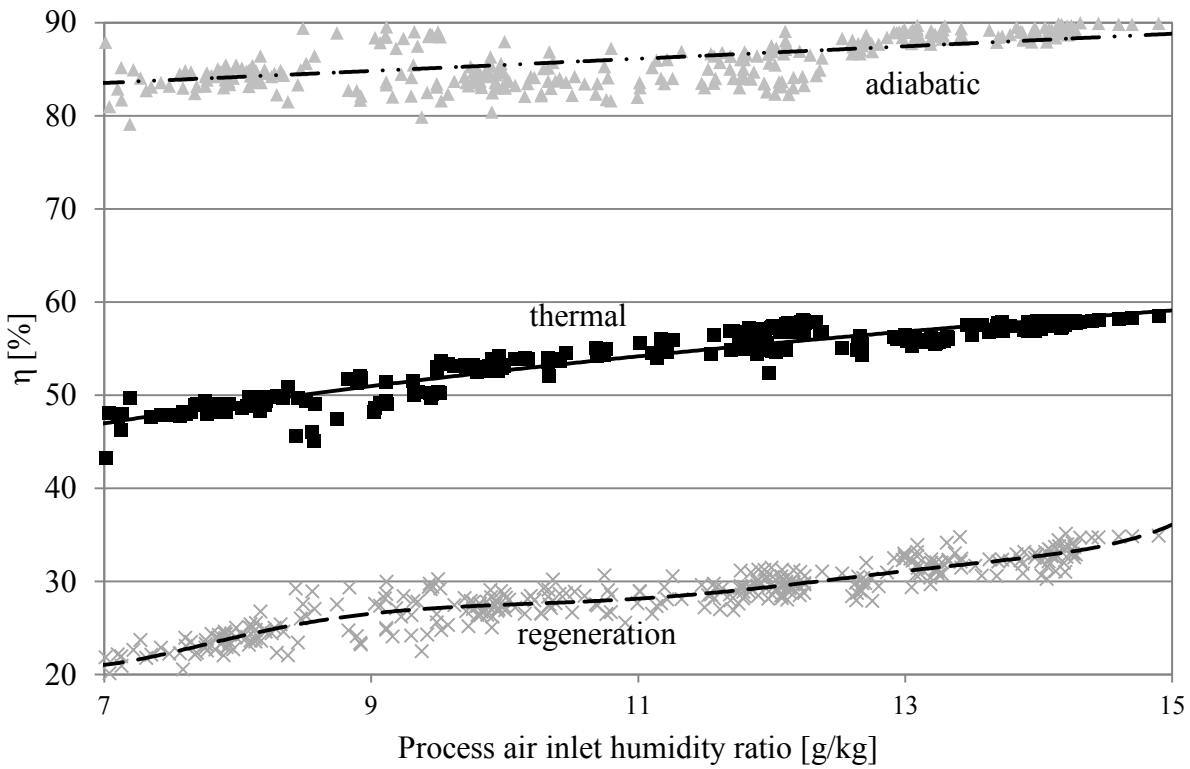

Fig. 2. 16: Various types of desiccant wheel effectiveness as a function of process air humidity ratio (t_{out} = 31.6 °C – t_{reg} = 66.2 °C)

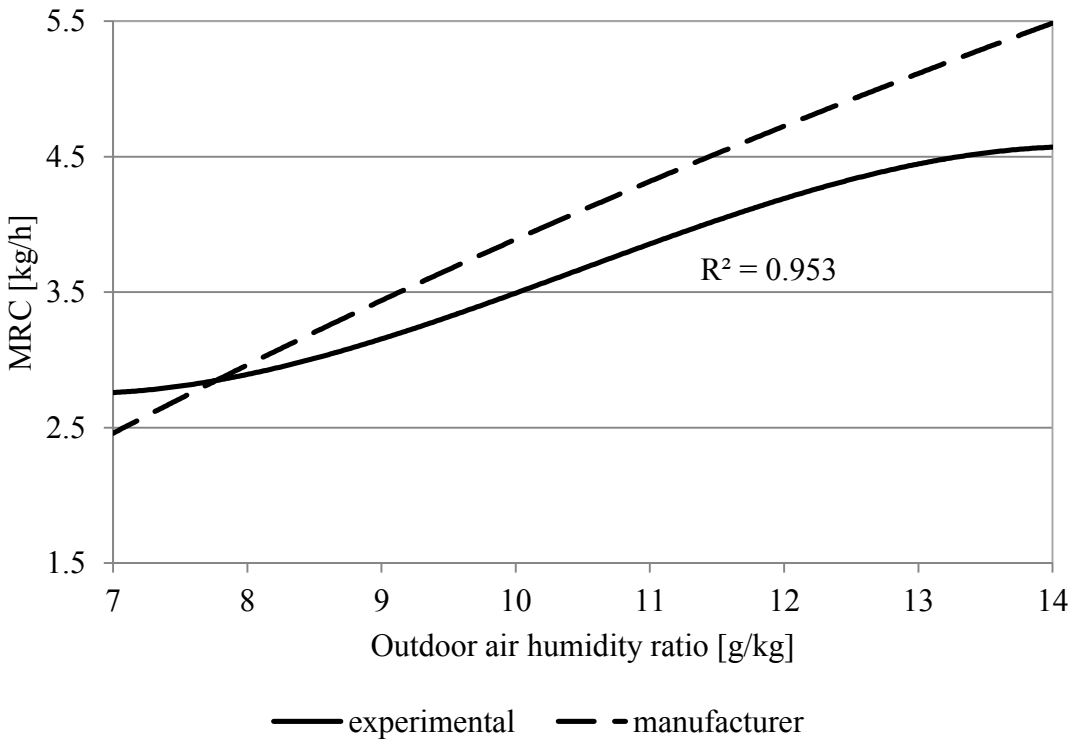

Fig. 2. 17: MRC as a function of ω_{out} (t_{out} = 31.6 °C – t_{reg} = 65.0 °C)

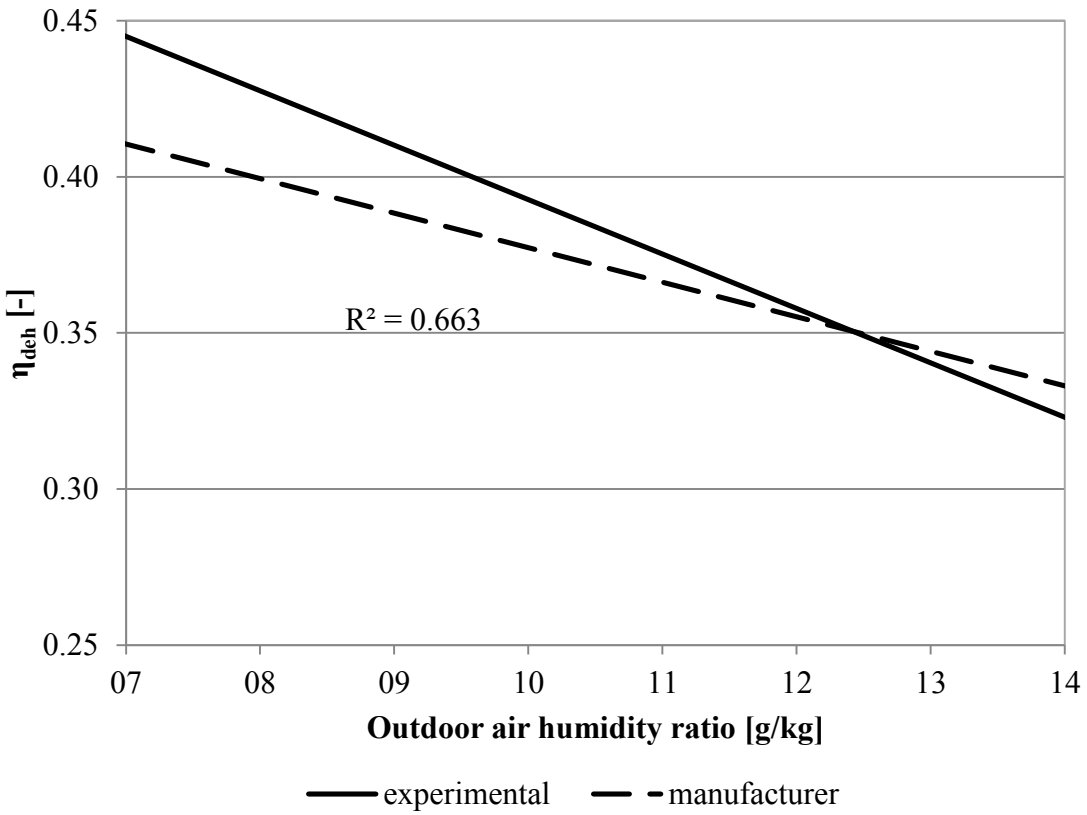

Fig. 2. 18: η_{deh} as a function of ω_{out} (t_{out} = 31.6 °C – t_{reg} = 65.0 °C)

DCOP increases with the rise in ω_{out}, Fig. 2. 19, as confirmed in [23]; in fact, the rise in ω_{out} causes an increase of the dehumidification capability of the desiccant rotor, while the regeneration thermal power remains constant.

The effect of outdoor air humidity ratio on SER is shown in Fig. 2. 20. t_2 increases significantly with process air inlet humidity ratio, as the wheel removes a greater quantity of water vapour. Therefore, Δt on the process air rises due to the increase in the released adsorption heat, while Δt on the regeneration side remains constant: thus, SER increases.

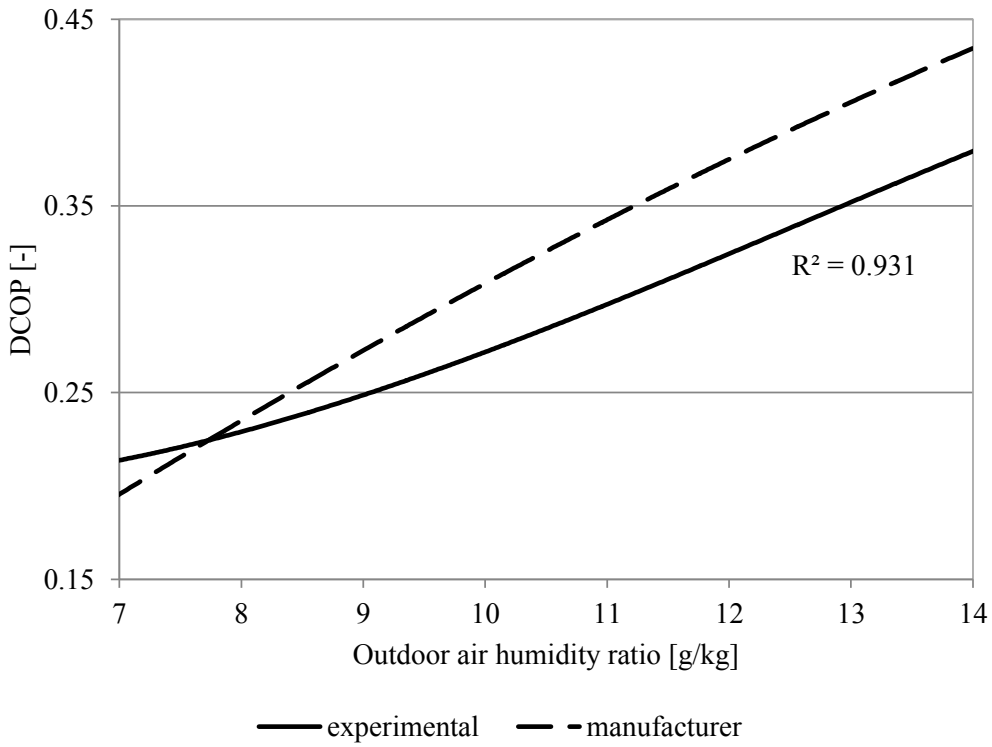

Fig. 2. 19: DCOP as a function of ω_{out} (t_{out} = 31.6 °C – t_{reg} = 65.0 °C)

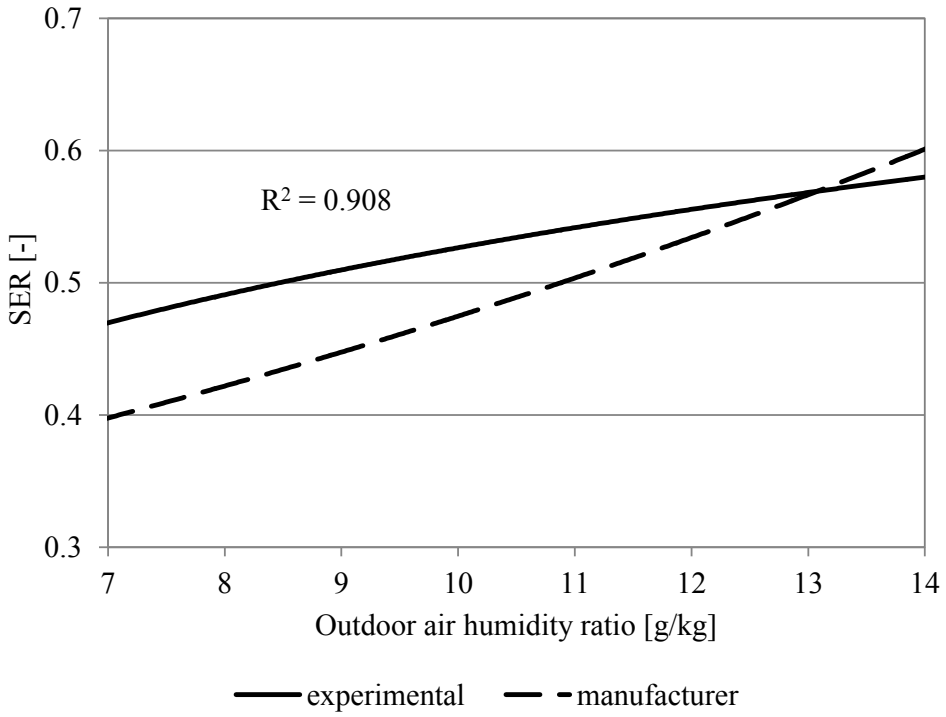

Fig. 2. 20: SER as a function of ω_{out} (t_{out} = 31.6 °C – t_{reg} = 65.0 °C)

2.2.4 Effect of process air temperature

In Fig. 2. 21, the effectiveness trends are reported as a function of the outdoor air temperature, for fixed values of t_{reg} and ω_{out}. The growth in t_{out} leads to a reduction in the dehumidification wheel capability, thus to a decrease in regeneration effectiveness.

With higher air temperatures at the DW inlet, t_1, the adsorption process is penalized. As a consequence, the reduction in the released heat of adsorption leads to the enhancement of the adiabatic efficiency.

As regards η_{th}, at constant regeneration temperature, process air temperatures at the inlet and the outlet of the rotor both increase. The thermal effectiveness passes through a declining trend, in accordance with the manufacturer's data.

The effectiveness trends shown in Fig. 2. 16 and Fig. 2. 21 are also in good agreement with the trends reported in [33].

In Fig. 2. 22, the MRC is reported as a function of outdoor air temperature ($t_{out} = t_1$). MRC trends are in agreement with the physical behaviours: the adsorption process is exothermic, so

favoured by low temperatures [3]; therefore, the rise in the process air temperature t_{out} causes a decrease in $\Delta\omega$, [23], and MRC; furthermore, the manufacturer's data show better performances compared to the experimental results.

In Fig. 2. 23, the effect of t_{out} on η_{deh} is shown. The increase in outdoor air temperature causes a lowering in ω_1-ω_2; therefore, $\omega_{out} = \omega_1$ being constant, the dehumidification effectiveness reduces, as confirmed by [19, 23, 33].

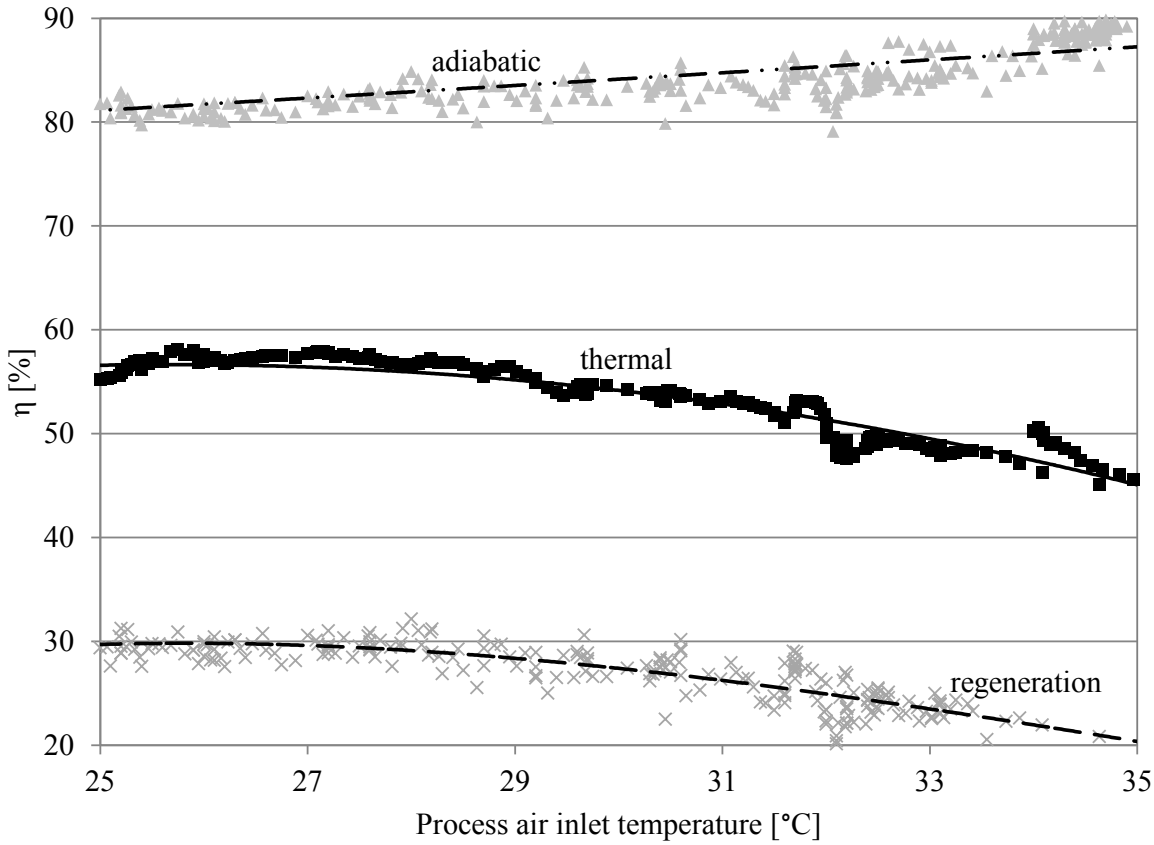

Fig. 2. 21: Desiccant wheel effectiveness as a function of process air inlet temperature (ω_{out} = 11.2 g/kg – t_{reg} = 66.4 °C)

Concerning DCOP, the rise in $t_{out} = t_1$ determines a reduction in both Δh_{vs} and, above all, in the dehumidification capability, but also an increase in $h_{out} = h_1$. Consequently, there are opposing factors in equation 2.8, and DCOP shows a nearly constant value for both experimental results and manufacturer's data (Fig. 2. 24).

The effect of the outdoor air temperature on the Sensible Energy Ratio is shown in Fig. 2. 25. The increase in t_{out} does not determine a significant variation of SER, and the experimental results and manufacturer data are very close.

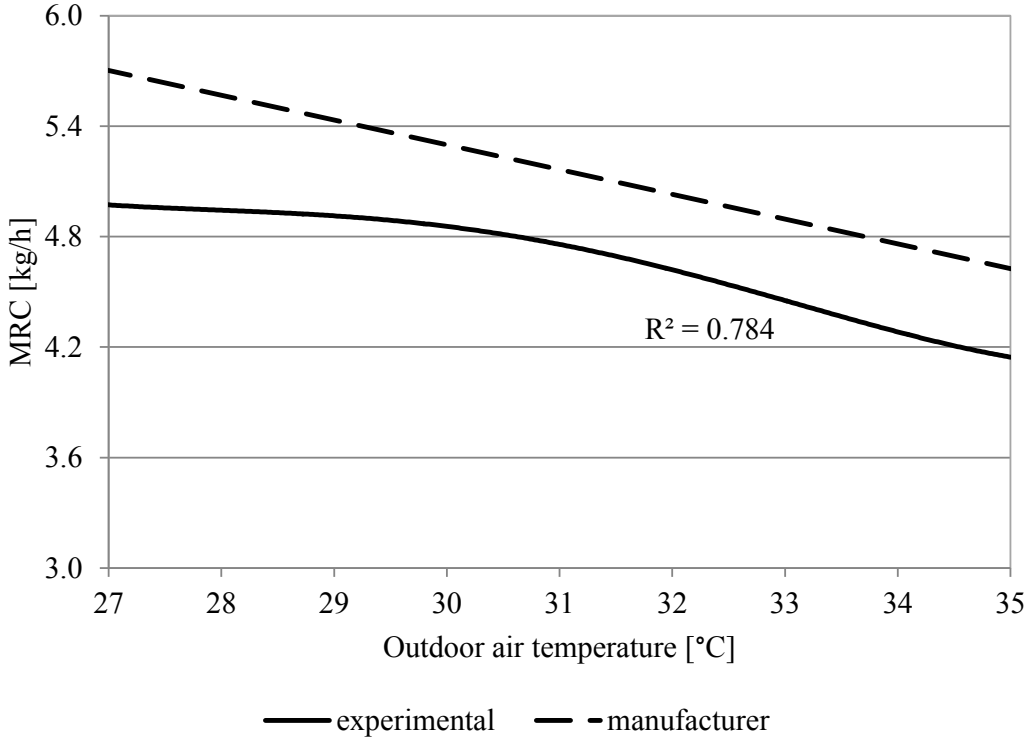

Fig. 2. 22: MRC as a function of t_{out} (ω_{out} = 13.2 g/kg – t_{reg} = 65.0 °C)

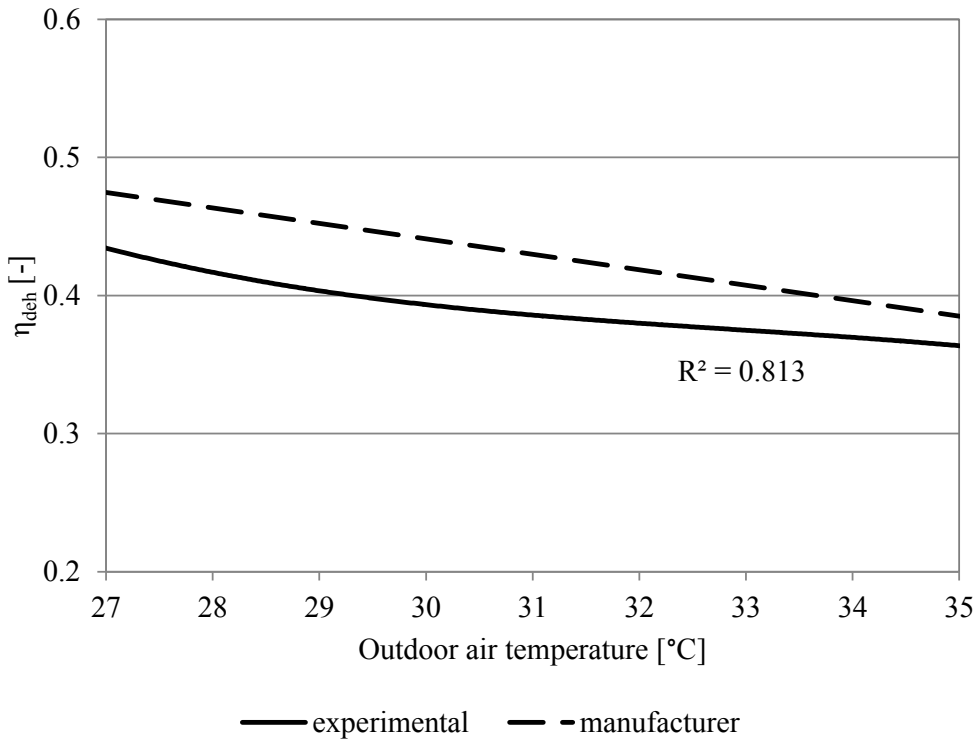

Fig. 2. 23: η_{deh} as a function of t_{out} (ω_{out} = 13.2 g/kg – t_{reg} = 65.0 °C)

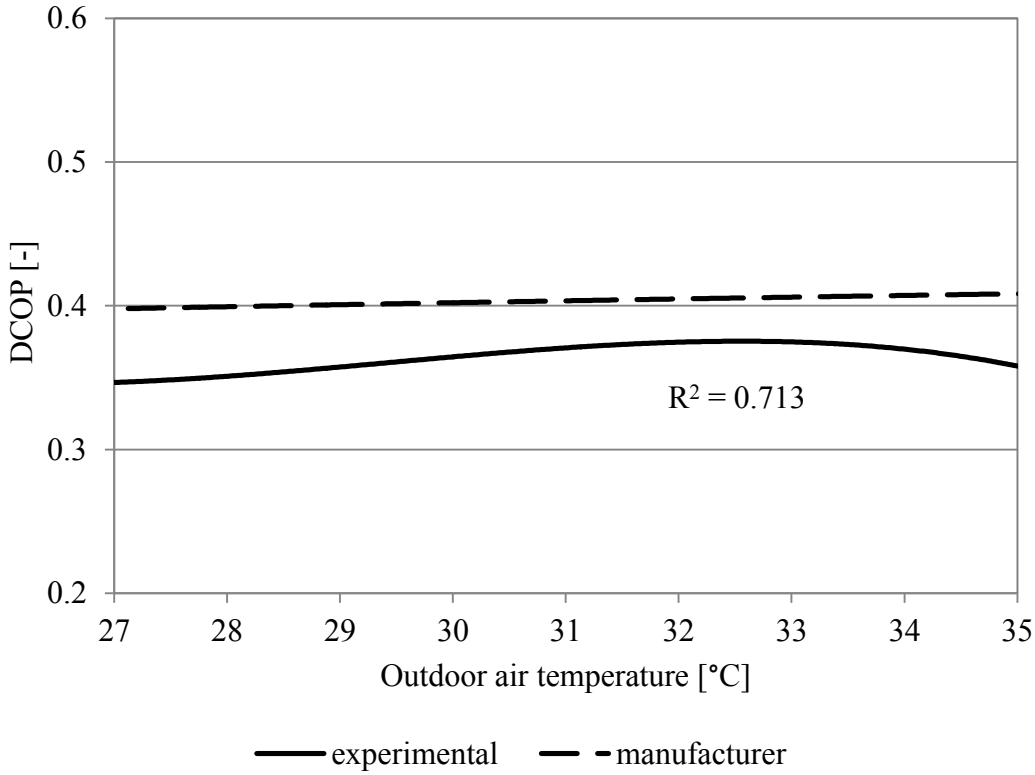

Fig. 2. 24: DCOP as a function of t_{out} (ω_{out} = 13.2 g/kg – t_{reg} = 65.0 °C)

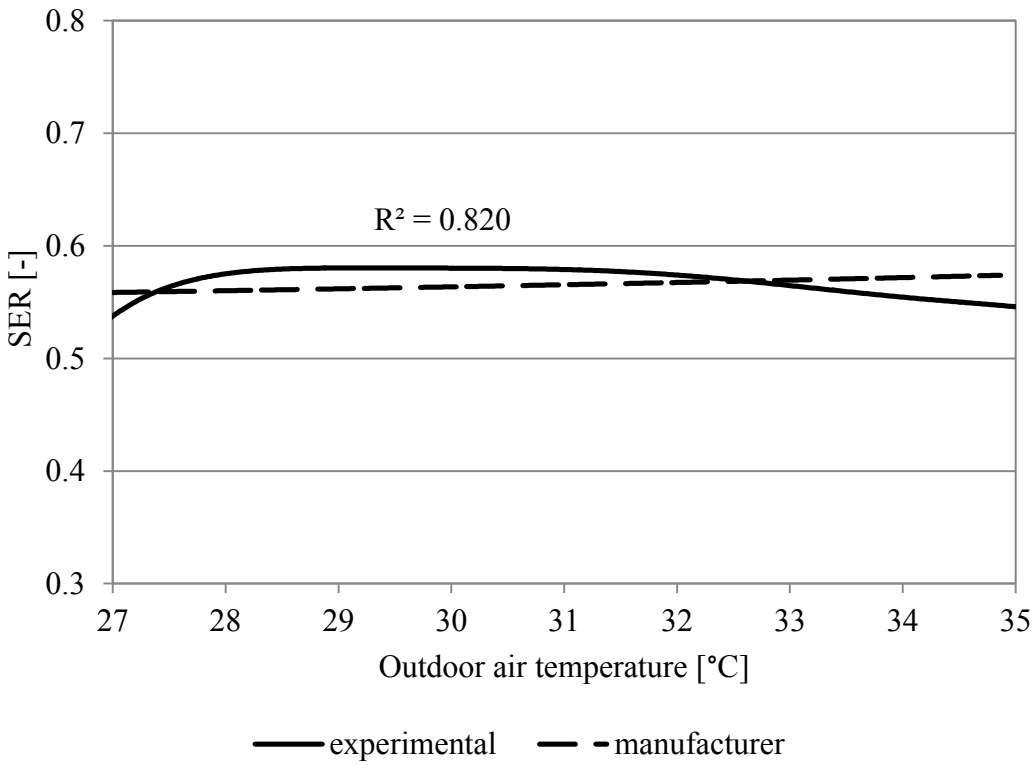

Fig. 2. 25: SER as a function of t_{out} (ω_{out} = 13.2 g/kg – t_{reg} = 65.0 °C)

The results of Fig. 2. 25 are also confirmed by [33].

2.2.5 Effect of the ratio between regeneration and process air flow rates

From Fig. 2. 26 to Fig. 2. 33, the influence of the parameter $\dot{V}_{reg}/\dot{V}_{proc}$, that is the ratio between the regeneration and the process air flow rates, is analysed: during the tests, the process air flow rate was kept constant, while varying the regeneration air flow rate.

Fig. 2. 26 to Fig. 2. 29 are relative to a constant regeneration temperature, t_{reg} = 65.0 °C; the increase in regeneration air flow rate involves an increase in $Q_{th,reg}$ (from 4.92 kW for $\dot{V}_{reg}/\dot{V}_{proc}$ = 0.5 to 9.84 kW for $\dot{V}_{reg}/\dot{V}_{proc}$ = 1.0).

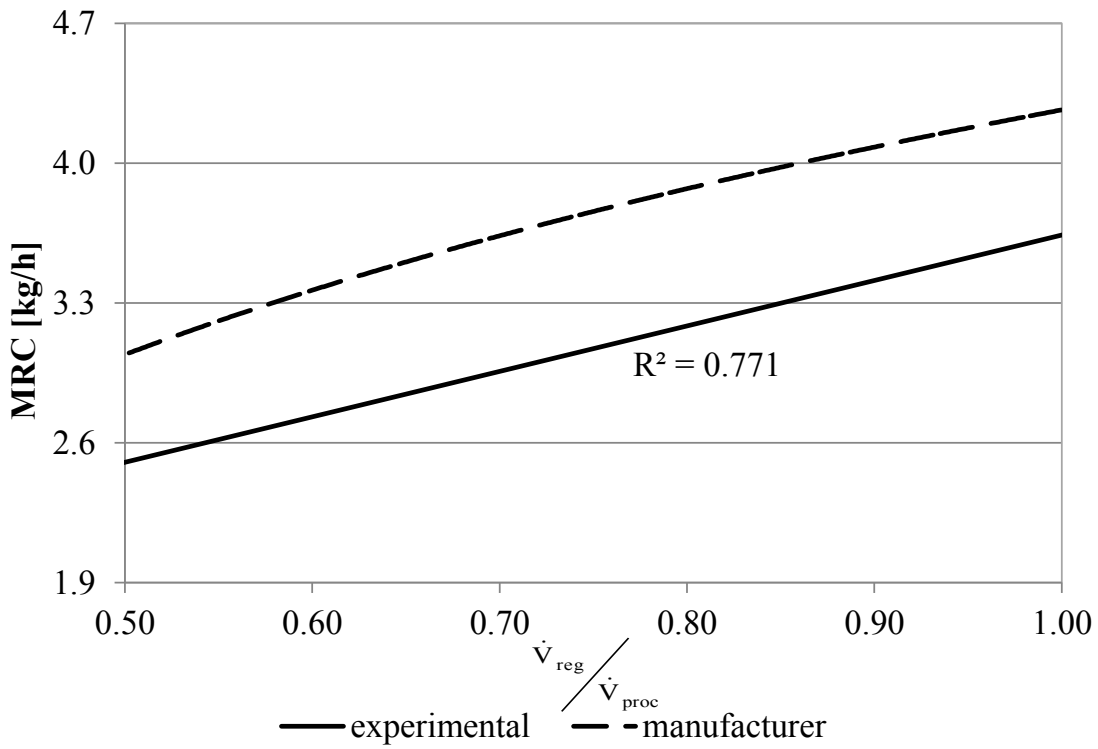

Fig. 2. 26: MRC as a function of the ratio between regeneration and process air volumetric flow rate for fixed regeneration temperature (t_{out} = 29.4 °C – ω_{out} = 6.73 g/kg – t_{reg} = 62.7 °C)

Fig. 2. 26 shows that MRC increases with $\dot{V}_{reg}$: in fact, the increase in regeneration air flow rate, with a fixed t_{reg}, determines a rise in the available regeneration thermal power, so the desiccant material in the regeneration side is subjected to a deeper drying process, [23, 56]; the same trend of the experimental results is observed for the manufacturer's data, even if with fairly higher values.

Similar considerations can be made with reference to Fig. 2. 27.

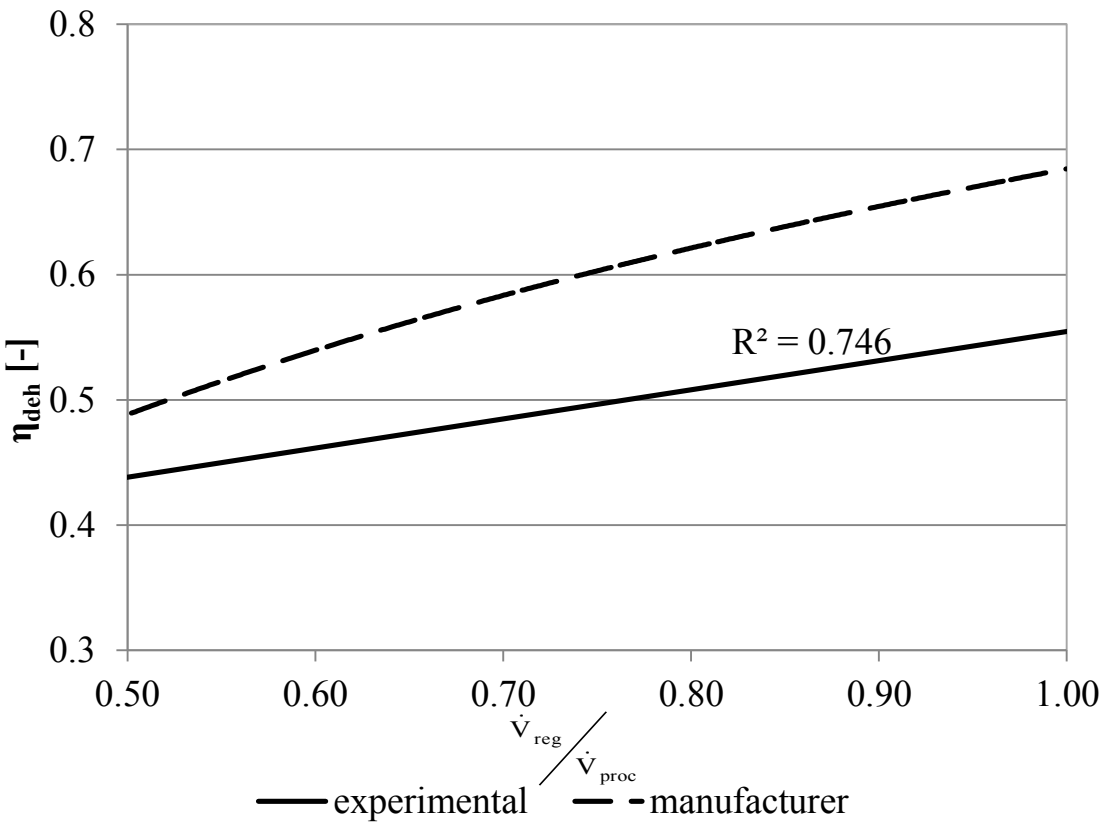

Fig. 2. 27: η_{deh} as a function of the ratio between regeneration and process air volumetric flow rate for fixed regeneration temperature (t_{out} = 29.4 °C – ω_{out} = 6.73 g/kg – t_{reg} = 62.7 °C)

Contrariwise, the increase of $\dot{V}_{reg}/\dot{V}_{proc}$ (or, which is the same, the reduction of $\dot{V}_{proc}/\dot{V}_{reg}$) determines a decreasing monotonic trend of both experimental and manufacturer results for DCOP (Fig. 2. 28); in fact, even if $\Delta\omega$ rises (see Fig. 2. 26 and Fig. 2. 27), on the other side the increase in $\dot{V}_{reg}$ causes a proportional rise in regeneration thermal power, so DCOP reduces, as follows from equation 2.8.

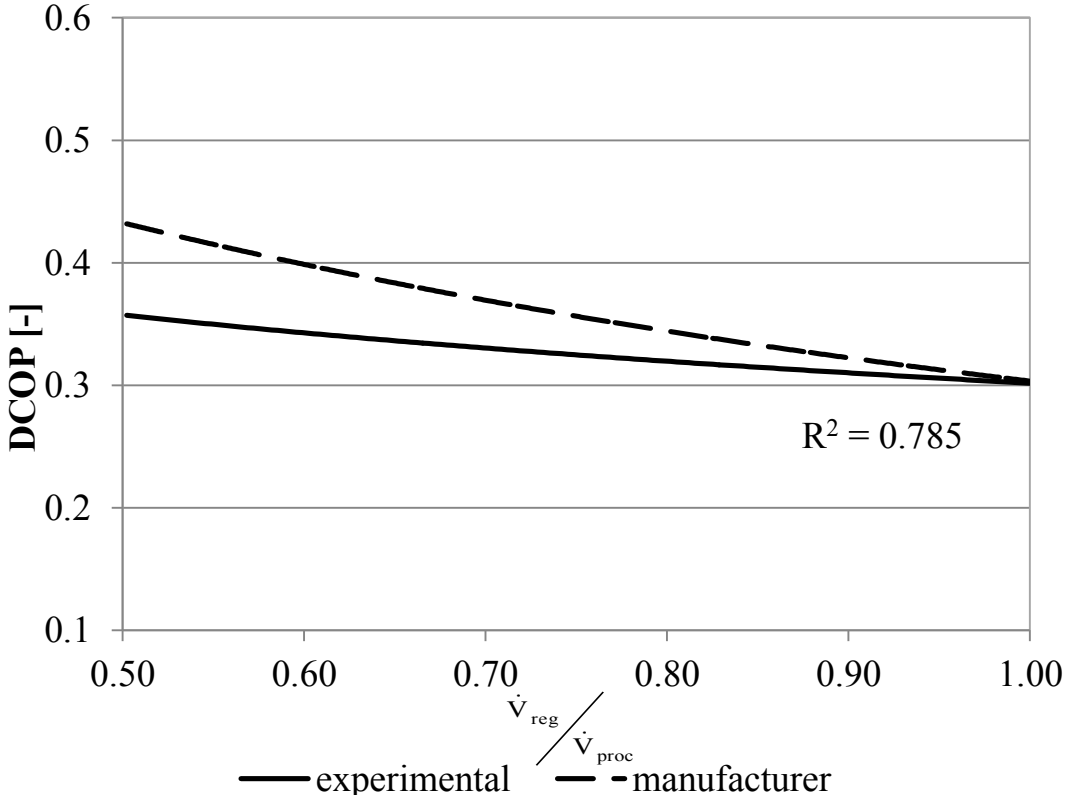

Fig. 2. 28: DCOP as a function of the ratio between regeneration and process air volumetric flow rate for fixed regeneration temperature (t_{out} = 29.4 °C – ω_{out} = 6.73 g/kg – t_{reg} = 62.7 °C)

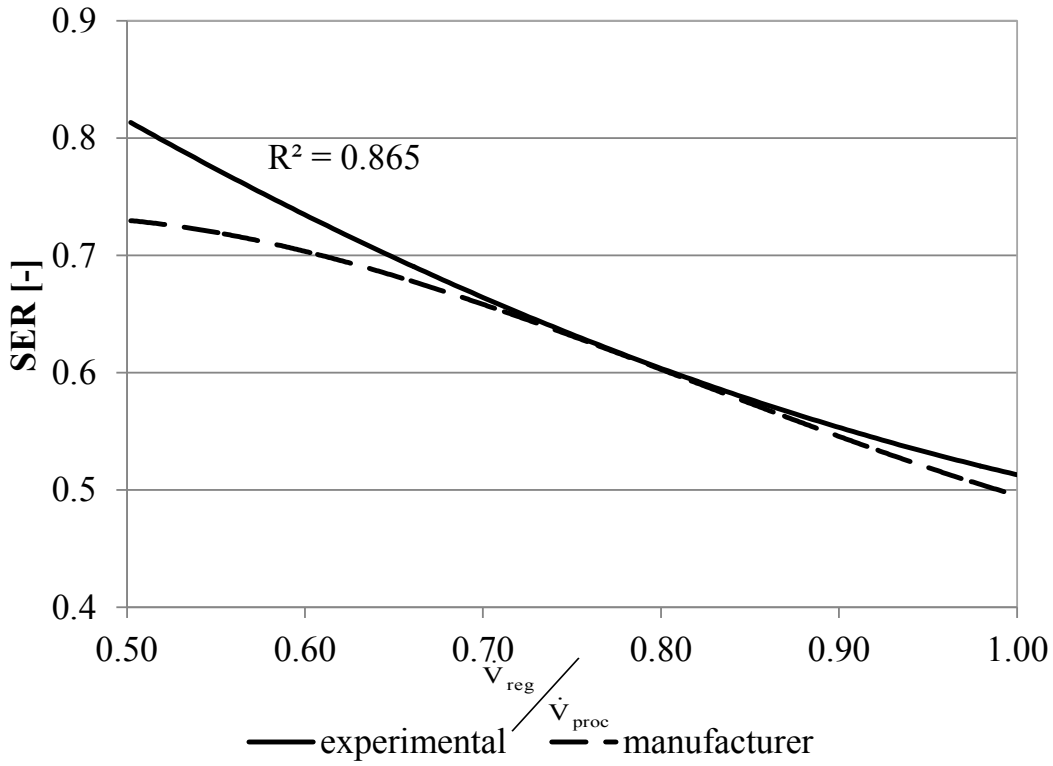

Fig. 2. 29: SER as a function of the ratio between regeneration and process air volumetric flow rate for fixed regeneration temperature (t_{out} = 29.4 °C – ω_{out} = 6.73 g/kg – t_{reg} = 62.7 °C)

In Fig. 2. 29 the effect of the ratio between regeneration and process air flow rates on SER is shown. As seen for the previous figures, the increase in $\dot{V}_{reg}$ determines a rise in the water vapour adsorbed by the silica gel, therefore an increase in the adsorption heat and t_2, [56]; nevertheless, the increase in $\dot{V}_{reg}/\dot{V}_{proc}$ prevails and causes the fall of SER, with very similar trends for experimental and manufacturer's data.

Fig. 2. 30 to Fig. 2. 33 are relative to a constant regeneration thermal power, $Q_{th,reg}$ = 4.30 kW; the increase in regeneration air flow rate involves a reduction in t_{reg} (from 65.0 °C for $\dot{V}_{reg}/\dot{V}_{proc}$ = 0.5 to 46.7 °C for $\dot{V}_{reg}/\dot{V}_{proc}$ = 1.3, with a process air flow rate of 590 m^3/h).

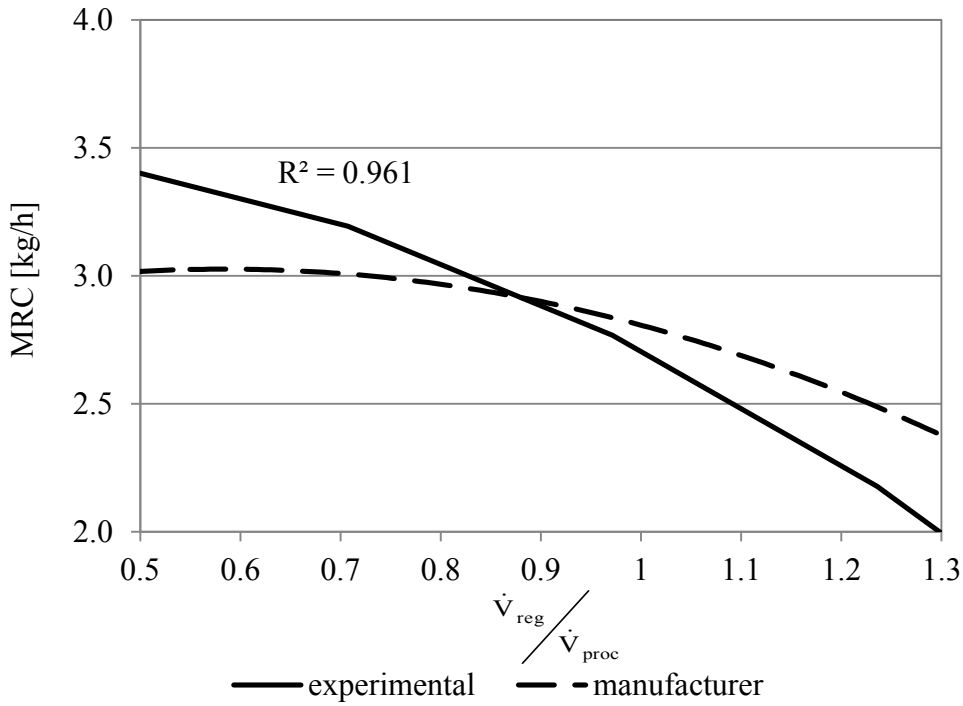

Fig. 2. 30: MRC as a function of the ratio between regeneration and process air volumetric flow rate for fixed regeneration thermal power (t_{out} = 25.6 °C – ω_{out} = 9.02 g/kg – $\dot{V}_{proc}$ = 590 m^3/h – $Q_{th,reg}$ = 4.30 kW)

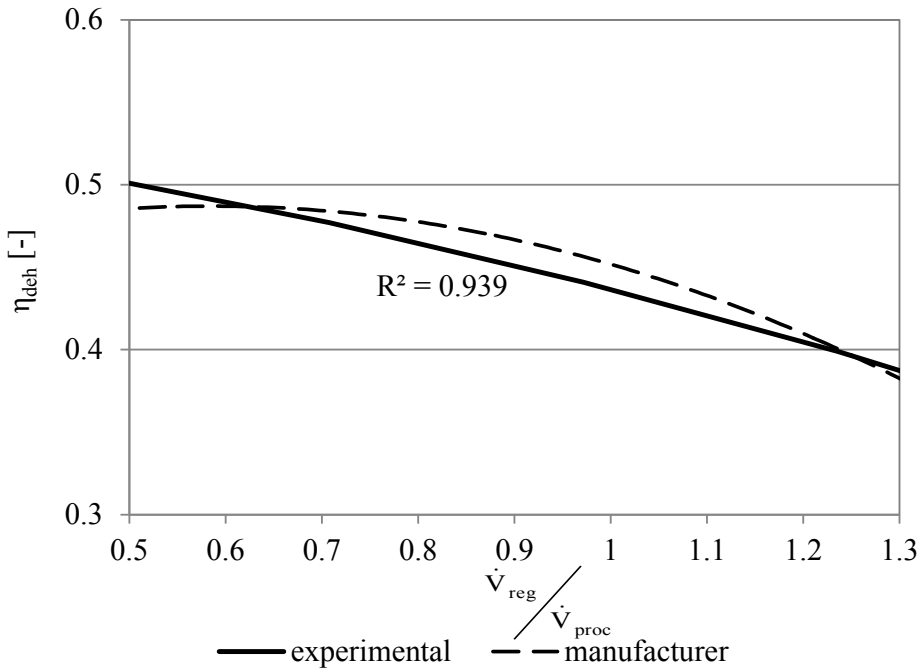

Fig. 2. 31: η_{deh} as a function of the ratio between regeneration and process air volumetric flow rate for fixed regeneration thermal power (t_{out} = 25.6 °C – ω_{out} = 9.02 g/kg – $\dot{V}_{proc}$ = 590 m^3/h – $Q_{th,reg}$ = 4.30 kW)

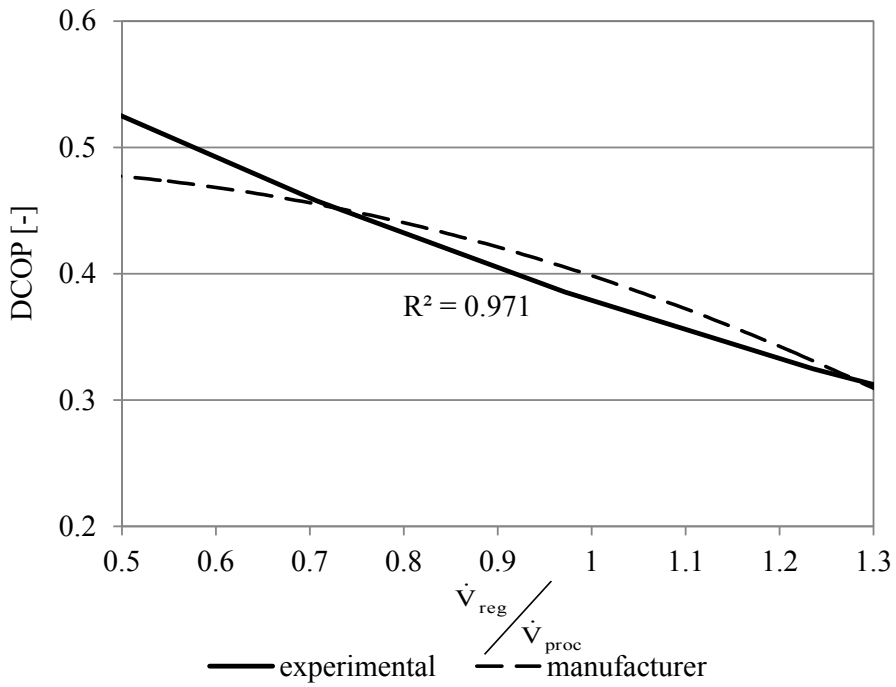

Fig. 2. 32: DCOP as a function of the ratio between regeneration and process air volumetric flow rate for fixed regeneration thermal power (t_{out} = 25.6 °C – ω_{out} = 9.02 g/kg – $\dot{V}_{proc}$ = 590 m^3/h – $Q_{th,reg}$ = 4.30 kW)

Experimental results show a reduction in MRC and η_{deh} (Fig. 2. 30 and Fig. 2. 31); this means that the best results in terms of dehumidification capability are obtained with a low regeneration air flow rate but a high regeneration temperature rather than with a high $\dot{V}_{reg}$ and a low t_{reg}. The same result is also valid considering the curves obtained by using manufacturer's data.

The same considerations can be made for Fig. 2. 32: in this case also, it is preferable to exploit a fixed regeneration thermal power by increasing the regeneration temperature rather than the regeneration air flow rate.

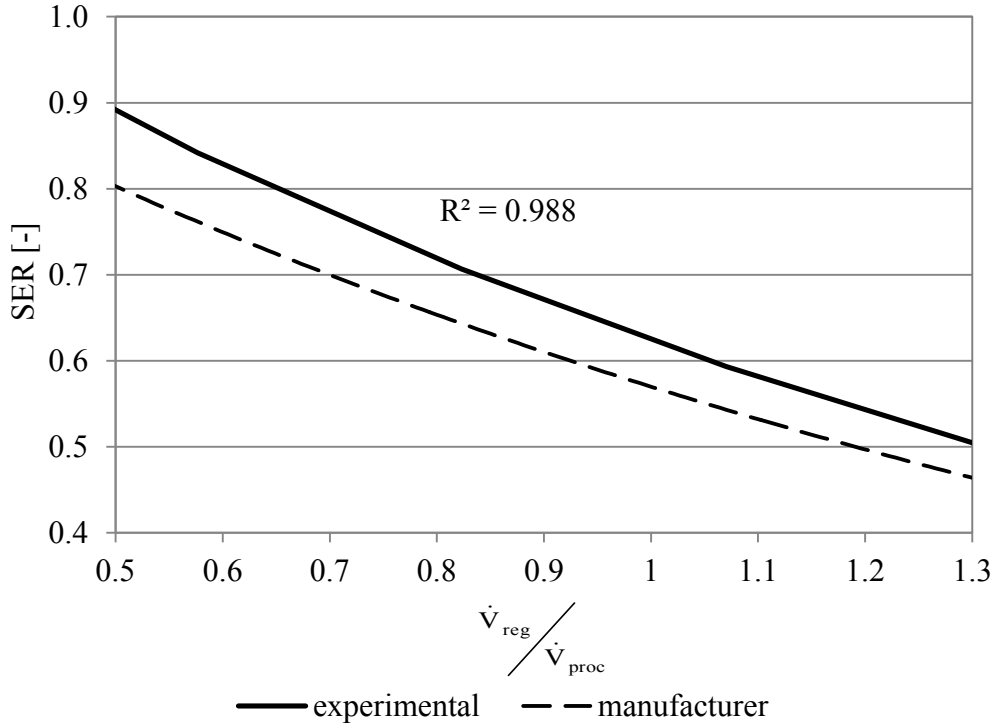

Fig. 2. 33: SER as a function of the ratio between regeneration and process air volumetric flow rate for fixed regeneration thermal power (t_{out} = 25.6 °C – ω_{out} = 9.02 g/kg – $\dot{V}_{proc}$ = 590 m^3/h – $Q_{th,reg}$ = 4.30 kW)

As seen for Fig. 2. 29, the increase in $\dot{V}_{reg}/\dot{V}_{proc}$ causes the fall of SER also in the case of constant $Q_{th,reg}$ (Fig. 2. 33).

With respect to the comparison between experimental data and trend lines, very high values of the determination coefficient R^2 have been obtained in almost all cases.

2.2.6 Effect of desiccant wheel rotational speed

The rotational speed of the desiccant wheel is widely recognized as a crucial parameter: in fact, if the wheel rotates too fast, the desiccant material in the process side does not have enough time to remove the moisture. Likewise, the moisture contained in the desiccant material cannot be completely desorbed in the regeneration side. On the other hand, if the wheel rotates too slowly, equilibrium is reached while the desiccant material is still in the process section, therefore saturation occurs. As a result, there must exist an optimal rotational speed, depending on the operating conditions, that guarantees the best dehumidification performance, [23, 57].

The performance of the desiccant wheel has been experimentally evaluated by varying the rotational speed, Φ, from 2 to 33 RPH.

In Fig. 2. 34, η_{deh} as a function of Φ for different regeneration temperature is shown. Optimal rotational speed, Φ_{opt}, rises with t_{reg}, from 6 RPH for t_{reg} = 45.0 °C, to 10 RPH for t_{reg} = 65.0 °C; in fact, with higher regeneration temperatures, the moisture adsorbed in the desiccant is much easier to be desorbed, therefore the rotational speed should be increased to make the well desorbed desiccant rotate out of the regeneration section in time. This result is also confirmed in [23] and [58-60].

In [58], for example, it is shown that, regardless of the outdoor conditions, as the regeneration temperature becomes higher, the optimum time required per one wheel revolution (the inverse of the rotational speed) decreases and then approaches a constant value.

In [59], the existence of an optimal value of Φ, that minimizes the ratio between outlet and inlet process air humidity ratio, is shown; furthermore, Φ_{opt} rises with t_{reg}.

In [60], experimental data derived from the literature were used to formulate correlations for the adiabatic and dehumidification effectiveness of a desiccant wheel. These correlations were then used to evaluate the effect of the rotational speed of the DW, expressed as sorption cycle duration, on process air temperature and humidity ratio at the outlet of the rotor. A comparison with experimental data was also carried out. Both predicted and experimental data show a minimum value of outlet ω for a given value of the sorption cycle duration; furthermore, this value decreases, hence Φ_{opt} increases, when t_{reg} rises.

In Fig. 2. 35, η_{deh} as a function of the rotational speed for different outdoor air humidity ratio is shown. Φ_{opt} slightly increases from 6 RPH to 9 RPH when ω_{out} increases from 9.03 g/kg to 10.3

g/kg. The mass transfer capacity on the process side is improved with higher outdoor air humidity ratio, as the adsorption rate increases. Hence, the time for achieving equilibrium state is shortened, which results in higher optimal rotational speed. The agreement with [23] should be highlighted in this case too. However, this aspect should be further investigated, as for the test with ω_{out} = 11.1 g/kg, the optimal Φ has nearly the same value obtained for the test with outdoor humidity ratio of 9.03 g/kg.

In Fig. 2. 36, η_{deh} as a function of the rotational speed for different outdoor air temperature is shown. Φ_{opt} decreases from about 8 RPH to about 6 RPH when t_{out} changes from 25.6 °C to 34.3 °C. In fact, the adsorption rate of the desiccant wheel is higher at a lower process air inlet temperature, therefore the optimal rotation speed increases to lead the desiccant material away from the equilibrium state. In other words, with higher t_{out}, the adsorption process is thwarted, hence a longer adsorption time is required.

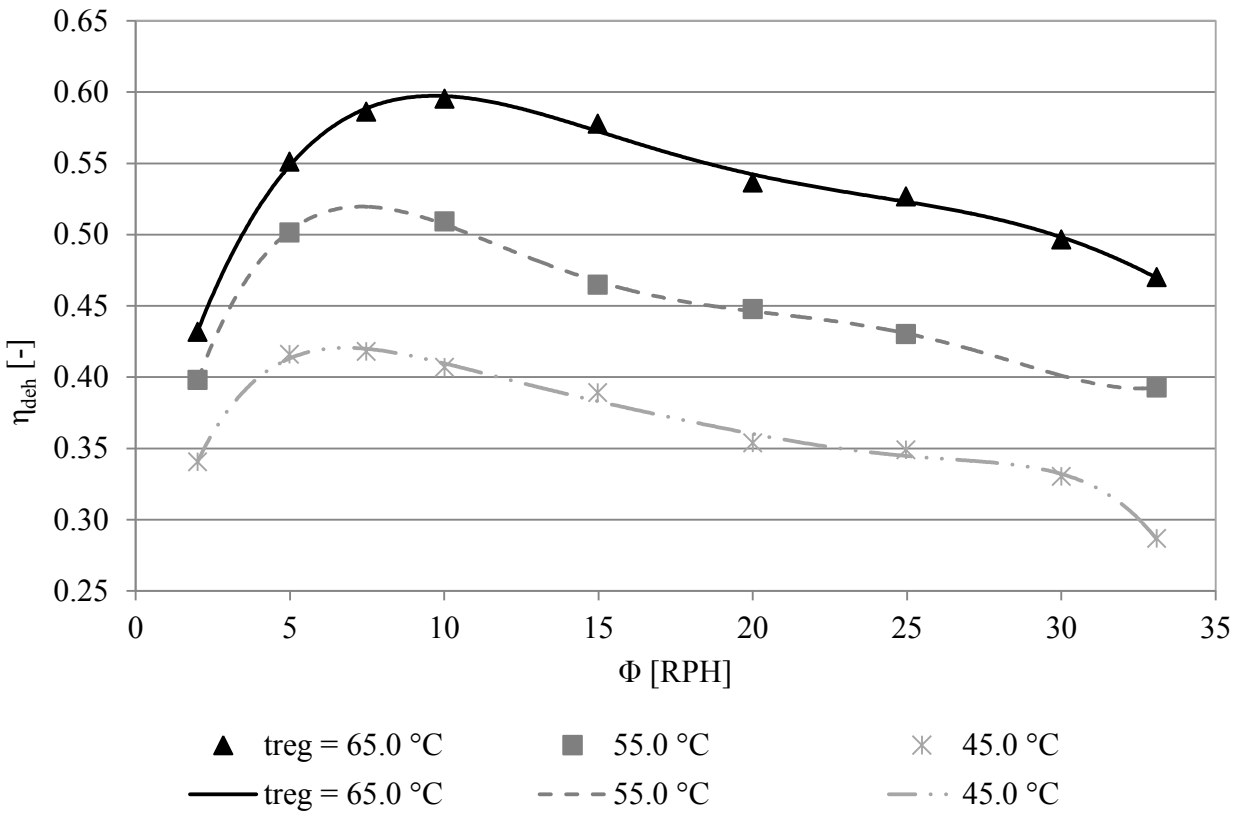

Fig. 2. 34: η_{deh} as a function of the rotational speed for different regeneration temperature (t_{out} = 25.6 °C – ω_{out} = 10.9 g/kg)

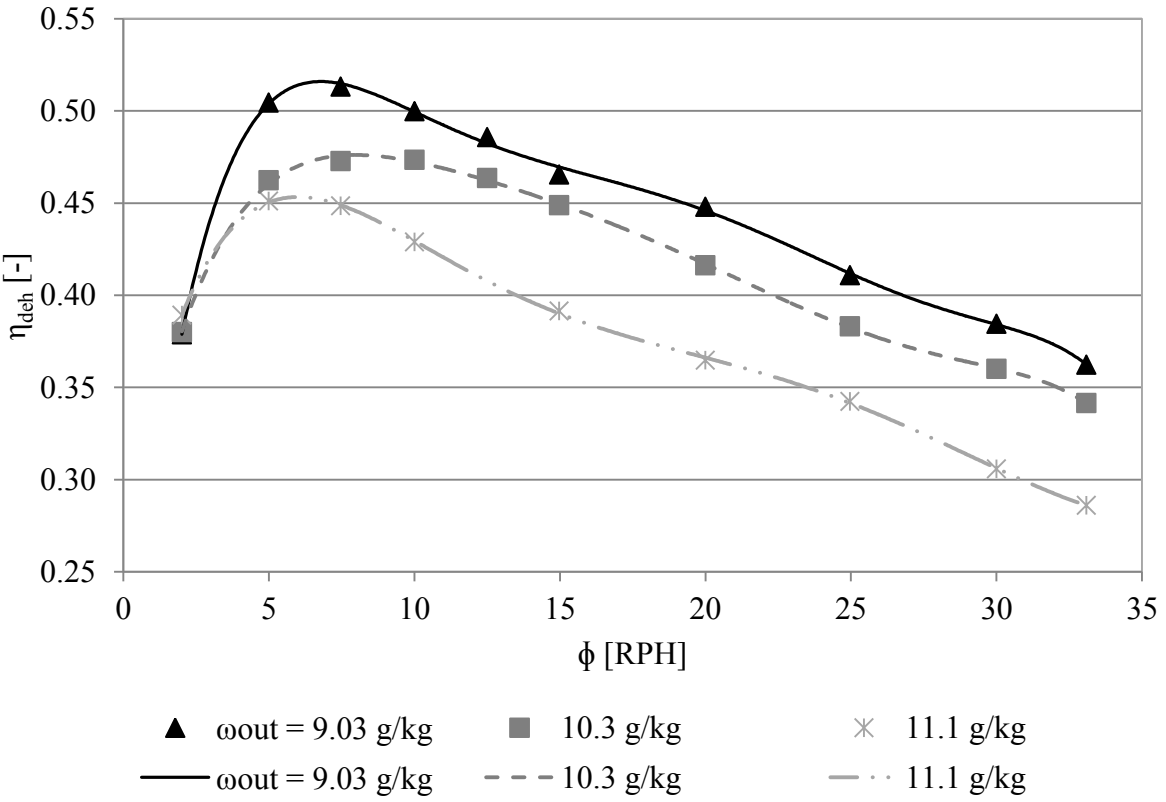

Fig. 2. 35: η_{deh} as a function of the rotational speed for different outdoor air humidity ratio (t_{out} = 29.2 °C – t_{reg} = 55.0 °C)

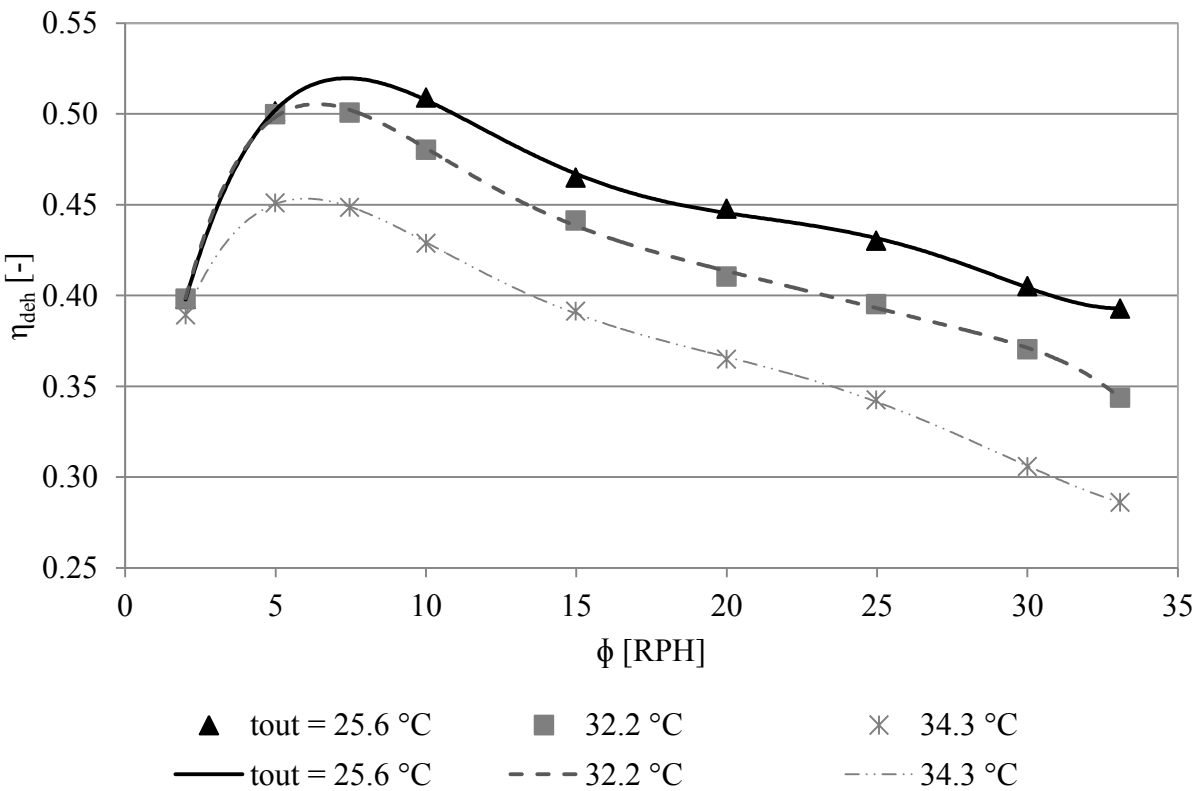

Fig. 2. 36: η_{deh} as a function of Φ for different outdoor air temperature (ω_{out} = 11.2 g/kg – t_{reg} = 55.0°C)

In Fig. 2. 37, η_{deh} as a function of the rotational speed for different $\dot{V}_{reg}/\dot{V}_{proc}$ is shown. Φ_{opt} increases from 5 RPH to 9 RPH when the ratio between regeneration and process air flow rates increases from 0.5 to 1.11. In fact, with higher regeneration flow rates, the moisture adsorbed in the desiccant is much easier to be desorbed, therefore the rotational speed should be increased to avoid that the well desorbed desiccant material remains too much time in the regeneration section.

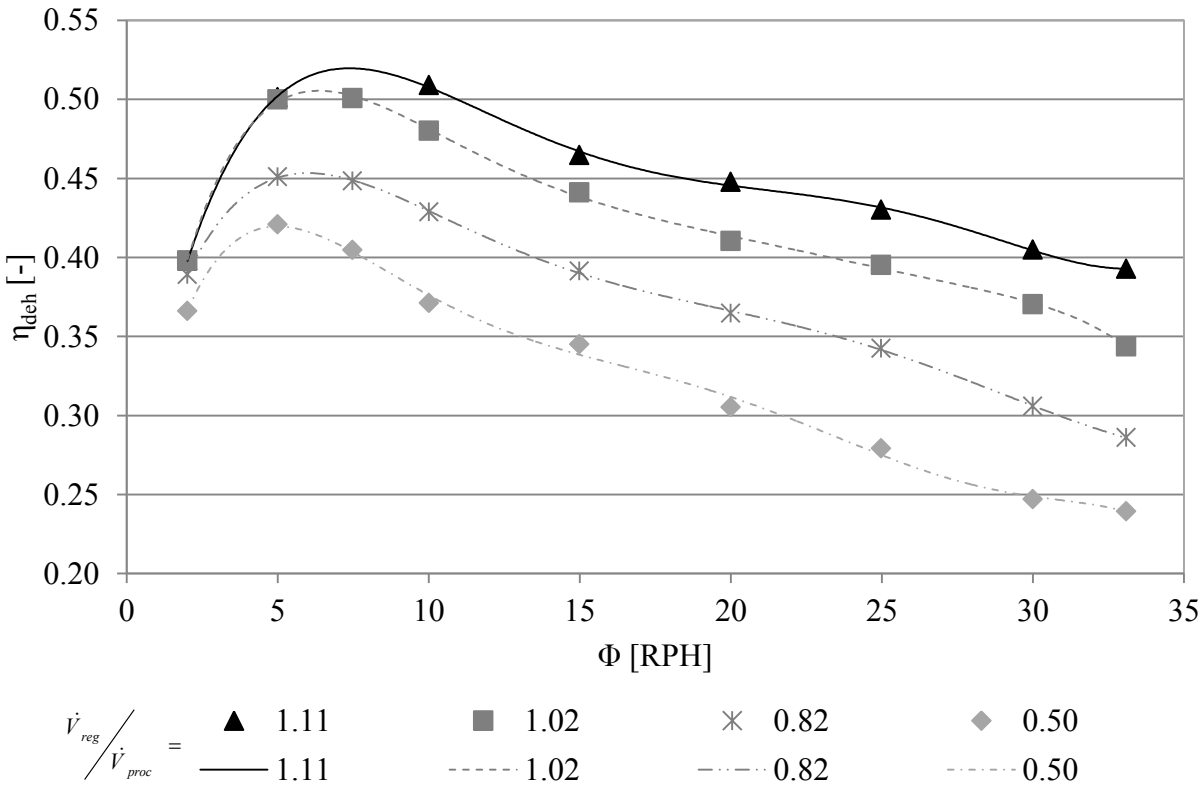

Fig. 2. 37: η_{deh} as a function of Φ for different $\dot{V}_{reg}/\dot{V}_{proc}$ (ω_{out} = 11.4 g/kg – t_{out} = 32.5 °C – t_{reg} = 55.0 °C – $\dot{V}_{proc}$ = 721 m^3/h)

2.2.7 Comparison between experimental and manufacturer data

As seen, the agreement between experimental and manufacturer's data is quite good in most cases, even if, generally, the latter provide better performances of the DW, i.e. a higher dehumidification capability and a lower increase of the process air temperature.

As regards a possible reason for this deviation, it should be noted that the tests were performed on a real system; hence, some negative influence (e.g. air leakages or infiltrations) on the performance of the wheel is expected, despite the care taken in the experimental set-up.

To provide a more accurate comparison between experimental and manufacturer's data, for each performance parameter and each operating variable, the average and maximum difference and the Root Mean Square Error, RMSE, have been evaluated and reported in Tab. 2. 2, [49].

They have been calculated by means of the following equations:

$$Difference_{j} = \frac{\left| v_{j,m} - v_{j,e} \right|}{v_{j,m}} \tag{2.14}$$

$$RMSE = \sqrt{\frac{\sum_{j=1}^{N} \left(v_{j,m} - v_{j,e} \right)^{2}}{n}} \tag{2.15}$$

where $v_{j,m}$ is the manufacturer's value, $v_{j,e}$ is the experimental one and n is the number of values.

As can be seen from Tab. 2. 2, the average difference is always lower than 17% (anyway, in most cases the value is lower than 10%). Moreover, the maximum difference is always not higher than 19%. Finally, low values of the RMSE have been also achieved. According to that, the good agreement between experimental and manufacturer's data should be highlighted.

2.2.8 Desiccant saturation

The quantity and quality (temperature) of the regeneration thermal power strongly influence the dehumidification process. Some tests have been realized in order to study the saturation process of the desiccant material, silica gel, contained in the rotor, keeping the desiccant wheel in rotation without regeneration air, while process air continuously crosses the rotor. The difference in humidity ratio, $\Delta\omega = \omega_1 - \omega_2$, quickly decreases, Fig. 2. 38.

The graph shows the time trend of $\Delta\omega$ for two different tests, characterized by similar temperatures, but different moisture contents of outdoor air entering the DW. The two curves start from the same initial value of $\Delta\omega$, and then continue differently. Particularly, in the test #2, characterized by a higher value of ω_{out}, the saturation process is more rapid.

Performance parameter	*Operating variable*	*Average difference [%]*	*Maximum difference [%]*	*RMSE*
MRC	t_{out}	9.52	13.4	$5.07 \cdot 10^{-1}$
	ω_{out}	10.5	15.0	$4.83 \cdot 10^{-1}$
	t_{reg}	8.70	13.0	$4.09 \cdot 10^{-1}$
	$\dot{V}_{reg} / \dot{V}_{proc} \big\|_{t_{reg} = cos\ t}$	17.1	18.9	$6.43 \cdot 10^{-1}$
	$\dot{V}_{reg} / \dot{V}_{proc} \big\|_{Q_{th,reg} = cos\ t}$	7.35	13.1	$2.30 \cdot 10^{-1}$
η_{deh}	t_{out}	9.33	10.9	$4.12 \cdot 10^{-2}$
	ω_{out}	3.56	9.26	$1.74 \cdot 10^{-2}$
	t_{reg}	7.76	12.3	$2.68 \cdot 10^{-2}$
	$\dot{V}_{reg} / \dot{V}_{proc} \big\|_{t_{reg} = cos\ t}$	16.7	18.9	$10.6 \cdot 10^{-1}$
	$\dot{V}_{reg} / \dot{V}_{proc} \big\|_{Q_{th,reg} = cos\ t}$	2.06	3.17	$1.04 \cdot 10^{-2}$
DCOP	t_{out}	9.59	13.0	$3.91 \cdot 10^{-2}$
	ω_{out}	11.5	13.5	$4.11 \cdot 10^{-2}$
	t_{reg}	8.40	17.2	$4.89 \cdot 10^{-2}$
	$\dot{V}_{reg} / \dot{V}_{proc} \big\|_{t_{reg} = cos\ t}$	7.97	17.4	$3.95 \cdot 10^{-2}$
	$\dot{V}_{reg} / \dot{V}_{proc} \big\|_{Q_{th,reg} = cos\ t}$	4.21	6.74	$1.89 \cdot 10^{-2}$
SER	t_{out}	3.44	12.0	$2.14 \cdot 10^{-2}$
	ω_{out}	8.48	18.2	$4.56 \cdot 10^{-2}$
	t_{reg}	8.24	16.8	$7.88 \cdot 10^{-2}$
	$\dot{V}_{reg} / \dot{V}_{proc} \big\|_{t_{reg} = cos\ t}$	3.36	11.4	$3.18 \cdot 10^{-2}$
	$\dot{V}_{reg} / \dot{V}_{proc} \big\|_{Q_{th,reg} = cos\ t}$	9.60	10.5	$6.05 \cdot 10^{-2}$

Tab. 2. 2: Comparison between experimental and manufacturer's data for each performance parameter and each operating variable, by means of average and maximum difference and root mean square error

In fact, after a same amount of time, the residual Δω is less than in the test #1; this is due to the higher quantity of water vapour in the air in the test #2, which tends to more rapidly saturate the surface of the desiccant.

After about 76 minutes during which the wheel dries the process air without being regenerated, the saturation process may be considered almost entirely completed, as the residual Δω at the end of the test, compared to the initial value, is about 1/4 and 1/8, for test #1 and test #2 respectively.

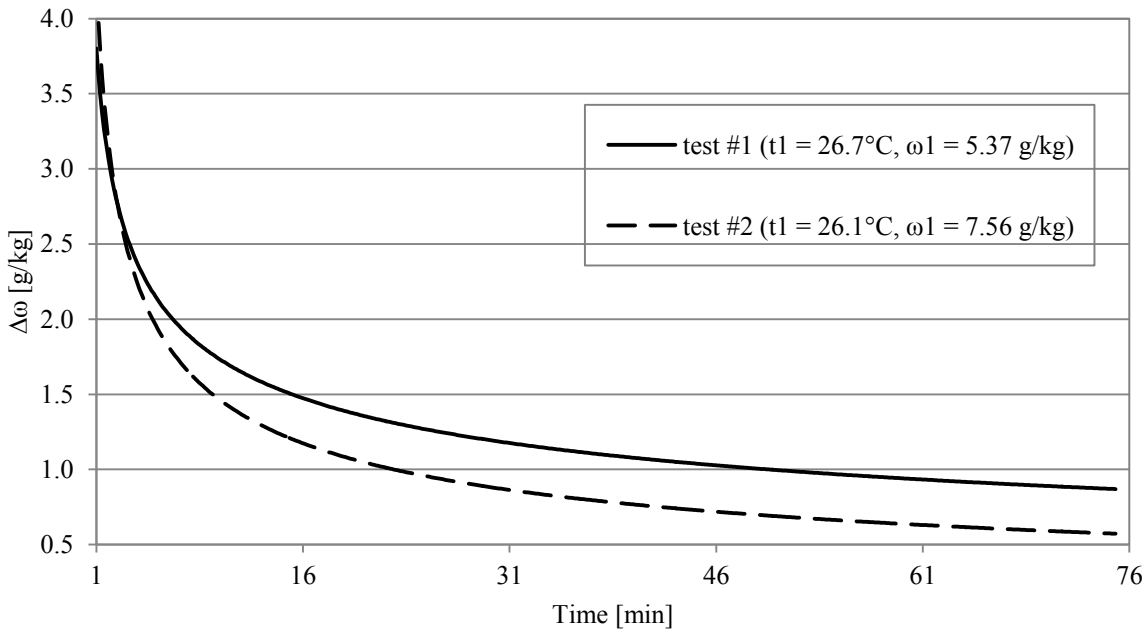

Fig. 2. 38: Difference between process air humidity ratio at inlet and outlet of the desiccant wheel as a function of the time, in absence of regeneration thermal energy

It should be noted that all the previously reported tests, carried out to evaluate the performance of the desiccant wheel, have been conducted in stationary conditions. This occurred when the temperature of hot water supplied by the MCHP and/or boiler reached and maintained a stable value, that depends on the electric power delivered by the cogenerator. In real operation, however, stationary regime is reached in a certain time, which depends on boundary operating conditions (outdoor air, electric power supplied by the cogenerator…). During this time, which can last longer than 30 minutes, or when regeneration air temperature is low, the desiccant material could saturate somewhat.

2.3 Latent load handled by the desiccant wheel

On the basis of the previously reported experimental data, an analysis on the silica-gel rotor has been carried out to estimate the performance of the AHU in handling ventilation and internal latent loads of a conditioned space. To this aim, experimental tests showed that the process air volumetric flow rate has a negligible influence on the desiccant wheel performance (in terms of dehumidification capability, i.e. $\Delta\omega$) if the following conditions are satisfied:

a) the face velocity of the process air at the inlet of the DW remains constant;

b) the ratio between process and regeneration air flow rate is equal to 1. Therefore, for the following analysis, only the experimental tests in balanced flow conditions have been used.

In this case, the dehumidification performance of the DW is substantially independent of volumetric flow rates. In the following analysis, the ventilation and internal latent loads are expressed per unitary volumetric air flow rate, considering indoor thermal-hygrometric conditions characterized by t_r = 25 °C and ω_r = 10.5 g/kg (relative humidity = 54%), and supply air temperature equal to 17 °C; t_{reg} is fixed to 65 °C (maximum value obtainable by using the selected MCHP).

The outdoor design conditions herein considered are based on the following ASHRAE data, [61]:

- design for cooling: 0.4% DB-MCWB (Dry Bulb - Mean Coincident Wet Bulb), 1.0% DB-MCWB and 2.0% DB-MCWB;

- design for dehumidification: 0.4% DP-MCDB (Dew Point – Mean Coincident Dry Bulb) and 1.0% DP-MCDB.

It is helpful to use an example for understanding these design data. For Istanbul, 0.4% DB = 31.1 °C and MCWB = 21.4 °C: as regards DB temperature, this means that the value 31.1 °C is exceeded on average by the indicated percentage (0.4%) of the total number of hours in a year (8760), i.e. by 35 hours per year, for the period of record; as regards MCWB temperature, the value 21.4 °C defines the average wet bulb temperature that was observed when the air was at the extreme high dry bulb temperature (31.1 °C). In other words, the value 21.4 °C is not the average wet bulb temperature during the entire warm season, but just its average value when the air is very hot, [62].

The designer has to choose the set of conditions and probability of occurrence that can be conveniently applied to the specific situation. The DB-MCWB data represent outdoor conditions of hot, mostly sunny days. They are therefore commonly used in sizing cooling equipment, such as chillers and cooling coils. On the contrary, design conditions based on dew point temperatures (DP-MCDB) are directly related to the highest values of humidity ratio, which represent peak moisture loads from the weather. These values are especially useful for humidity control applications, hence in desiccant cooling and dehumidification, cooling-based dehumidification and ventilation system design.

In Fig. 2. 39, the specific ventilation latent load that can be handled by the desiccant wheel for different cities around the world is reported. The cities selected for the analysis are characterized by values of the outdoor humidity ratio (derived from DB-MCWB and DP-MCDB data) included within the range of experimental data available for the desiccant wheel performance.

Fig. 2. 39a refers to DB-MCWB data (for cooling purposes), while Fig. 2. 39b refers to DP-MCDB data (for dehumidification purposes). For those cities where the DW is able to handle the entire required specific ventilation latent load (L, proportional to ω_1 - ω_r), it is reported on the ordinate. This occurs for all the cities in Fig. 2. 39a and only for some of them in Fig. 2. 39b. On the contrary, for those cities where the DW cannot entirely balance L, only the fraction of it covered by the DW (proportional to ω_1 - ω_s, with ω_s experimentally evaluated) is shown on the ordinate and reported in percentage too. This occurs for some cities (such as Athinai, Bologna, etc.) in Fig. 2. 39b. This result strictly depends on the above-mentioned difference between DB-MCWB and DP-MCDB data. Moreover, note that for some cities and for certain percentiles (Athinai, Beograd, Sarajevo, Sydney), the ordinate is equal to zero (Fig. 2. 39a) because the assumed indoor humidity ratio is higher than outdoor one (i.e., there is no ventilation latent load).

As regards the experimental evaluation of ω_s (the supply air humidity ratio, equal to the process air humidity ratio after the desiccant wheel), it is obtained for each city by the experimental knowledge of the maximum desiccant wheel dehumidification capability ($\Delta\omega$) relative to a regeneration temperature of 65 °C, i.e. $\omega_s = \omega_2 = \omega_1 - \Delta\omega$.

In Fig. 2. 40a and b, the maximum specific internal latent load that could be handled by the desiccant wheel (independently of the type of internal latent load) is presented, considering the ASHRAE cooling and dehumidification design data, respectively. This load is proportional to ω_r - ω_s, with ω_s experimentally evaluated as reported above.

In Fig. 2. 40b, note that for the cities in which the ventilation latent load cannot be completely handled by the desiccant wheel (because $\omega_s > \omega_r$, as occurs, for example, in Bologna), no internal latent load can be balanced by the wheel, such that negative values are shown. In these cases, the lower the ventilation latent load covered by the DW with respect to the required value (Fig. 2. 39b), the higher the absolute value of the internal latent load reported in Fig. 2. 40b.

Thus, in these cases, a higher t_{reg} is necessary and the only waste heat from MCHP is not sufficient for the regeneration process.

The results reported in Fig. 2. 40, for given cities, can be generalized for any climatic condition, which is the main purpose of Fig. 2. 41, where the following parameters have been reported as a function of outdoor air humidity ratio:

- the specific latent load that can be globally handled by the desiccant wheel, for different outdoor temperatures (Fig. 2. 41a, dotted lines). This is proportional to $\omega_1 - \omega_s$;
- the required specific ventilation latent load (Fig. 2. 41a, continuous line). This is proportional to $\omega_1 - \omega_r$. Therefore, for fixed indoor conditions, it depends only on the climatic conditions;
- the specific internal latent load that can be balanced by the desiccant wheel, for different outdoor air temperatures (Fig. 2. 41b). This is proportional to $\omega_r - \omega_s$.

Analysing Fig. 2. 41a, it can be noted that, for values of outdoor humidity ratio lower than about 15.5 g/kg, the specific latent load that can be handled by the desiccant wheel is higher than the specific ventilation latent load required by the outdoor air humidity ratio. This means that in these conditions the desiccant wheel is always able to balance at least the ventilation latent load. On the contrary, for outdoor humidity ratio higher than 15.5 g/kg, the desiccant wheel can handle the required ventilation latent load only for low outdoor air temperatures. This confirms that the process air inlet temperature also strongly affects the dehumidification capability of the DW.

As a consequence, in Fig. 2. 41b, only for outdoor humidity ratio lower than about 15.5 g/kg, the desiccant wheel can also balance a part or all the internal latent load, such that positive values occur.

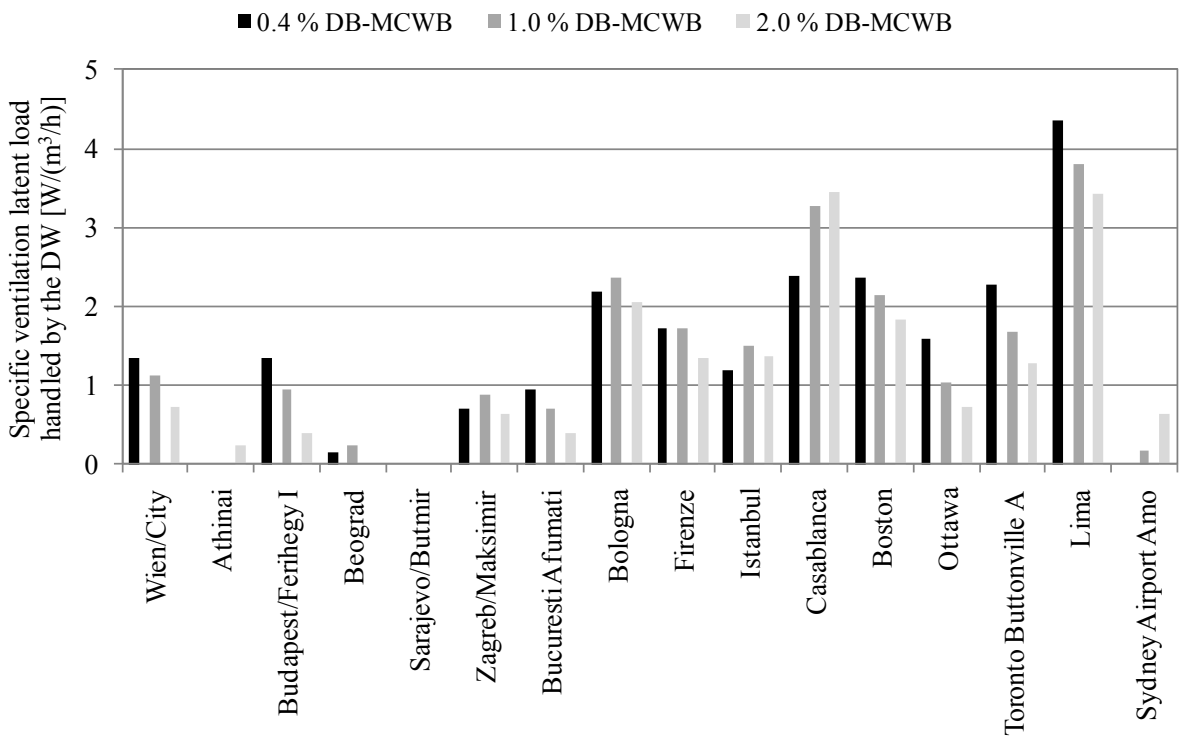

(a)

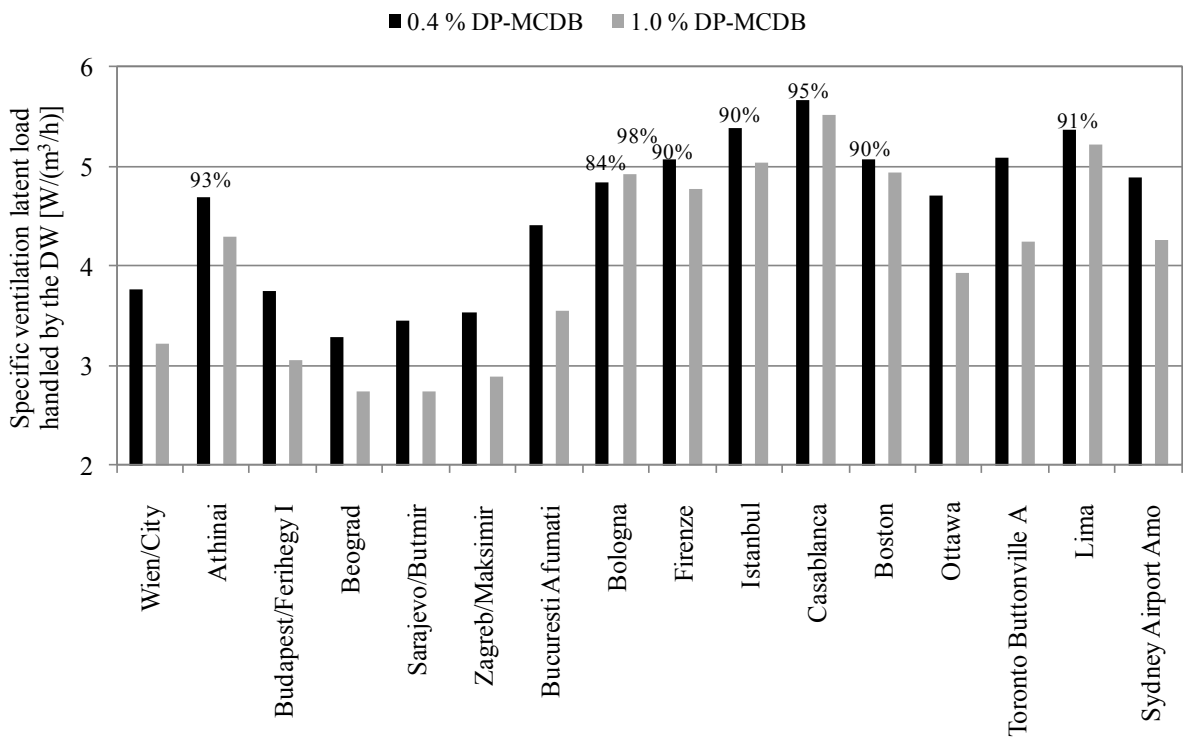

(b)

Fig. 2. 39: Specific ventilation latent load handled by the desiccant wheel for various cities and for different outdoor design thermal-hygrometric conditions (t_{reg} = 65 °C)

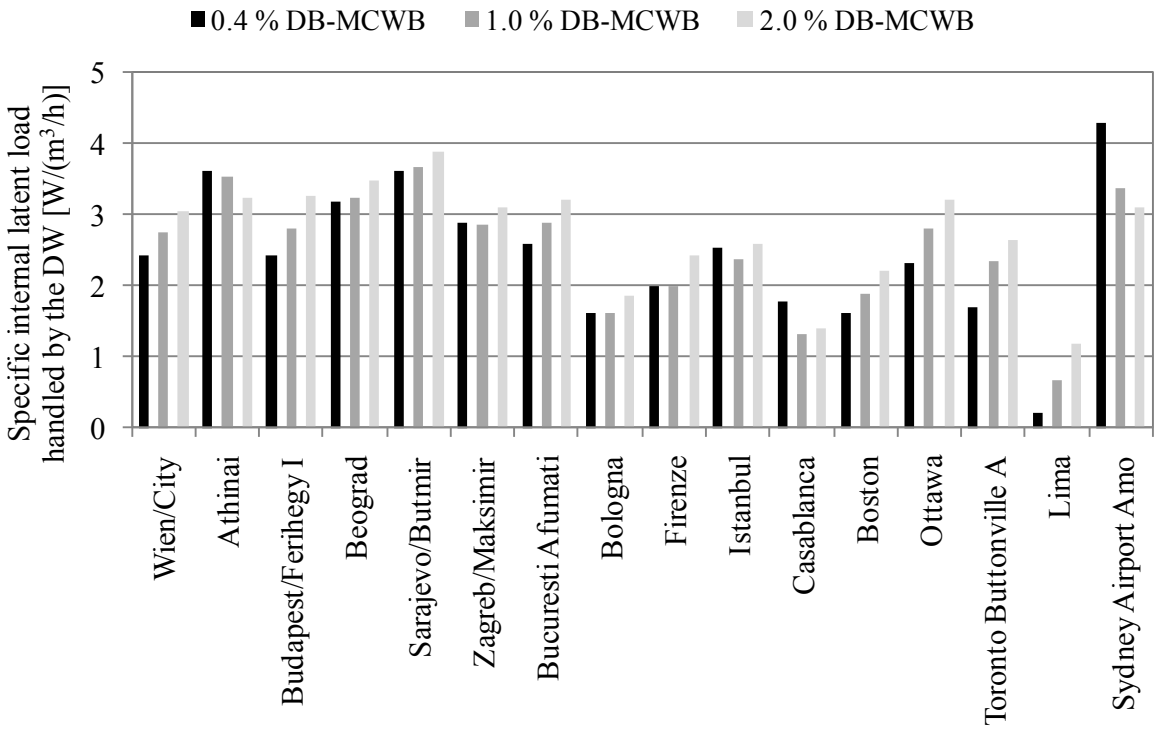

(a)

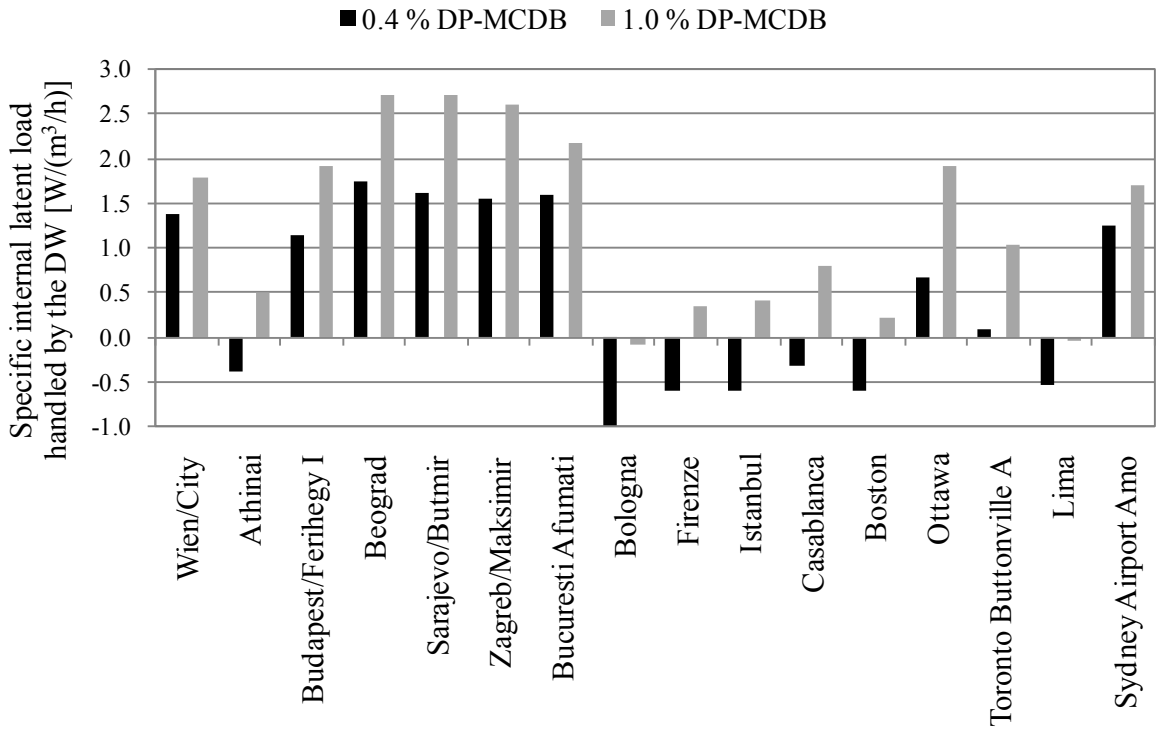

(b)

Fig. 2. 40: Specific internal latent load handled by the desiccant wheel for various cities and for different outdoor design thermal-hygrometric conditions (t_{reg} = 65 °C)

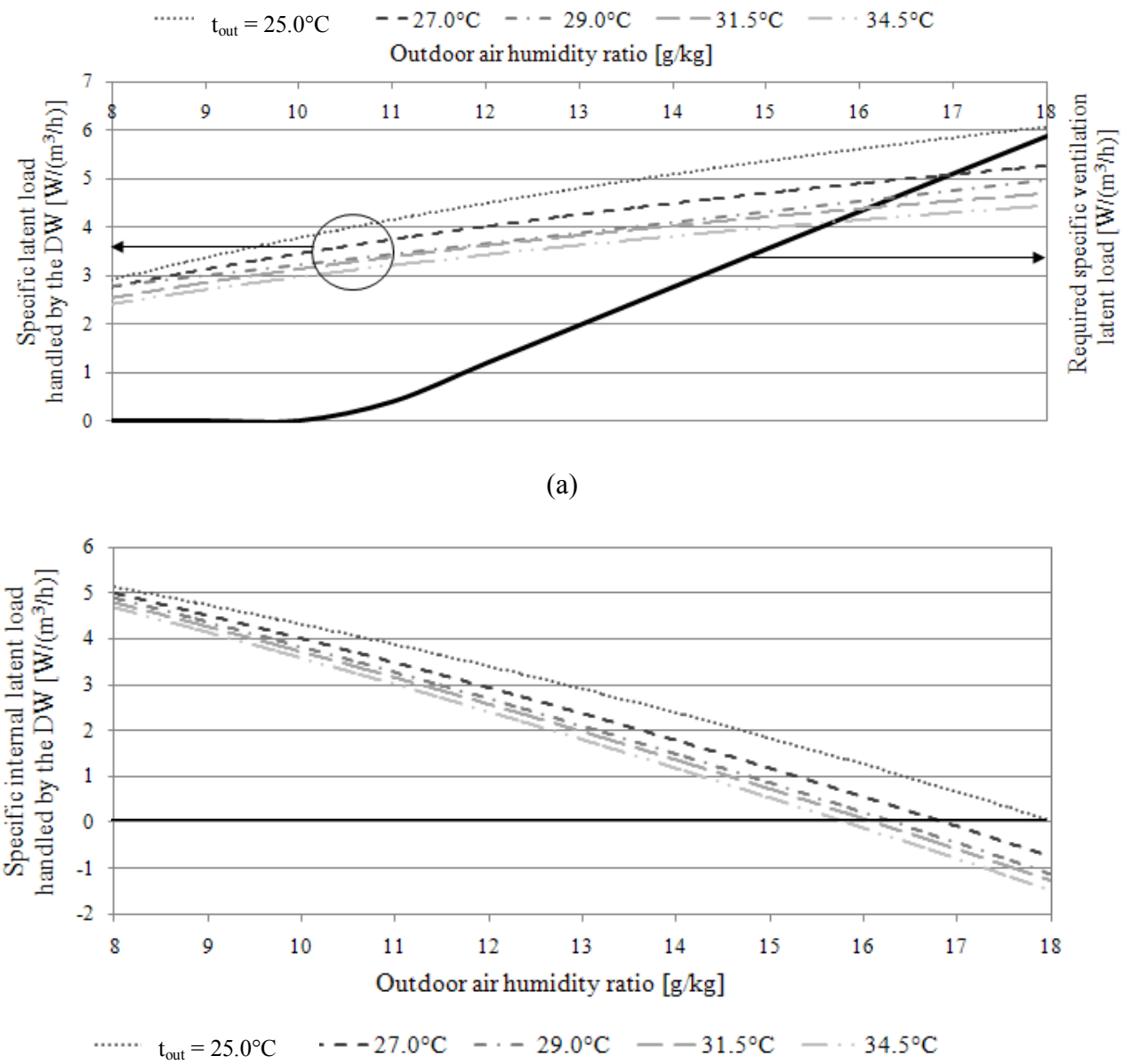

Fig. 2. 41: Specific latent load handled by the DW (a), required specific ventilation latent load (a) and specific internal latent load handled by the DW (b), as a function of outdoor humidity ratio (t_{reg} = 65 °C)

In order to check if the wheel is able to entirely cover the internal latent load for a given application, Fig. 2. 42 (coupled to Fig. 2. 41b) can be useful. In Fig. 2. 42, the specific internal latent load required by a given application is presented as a function of the room SHR (Sensible Heat Ratio, i.e. the ratio between the sensible and total thermal load). This allows to identify the value of the specific internal latent load to be balanced (Fig. 2. 42) through the knowledge of both the sensible and latent load of the considered indoor ambient. Successively, by the diagram of Fig.

2. 41b, the user can check if the desiccant wheel is able to balance the required internal latent load for certain outdoor design conditions.

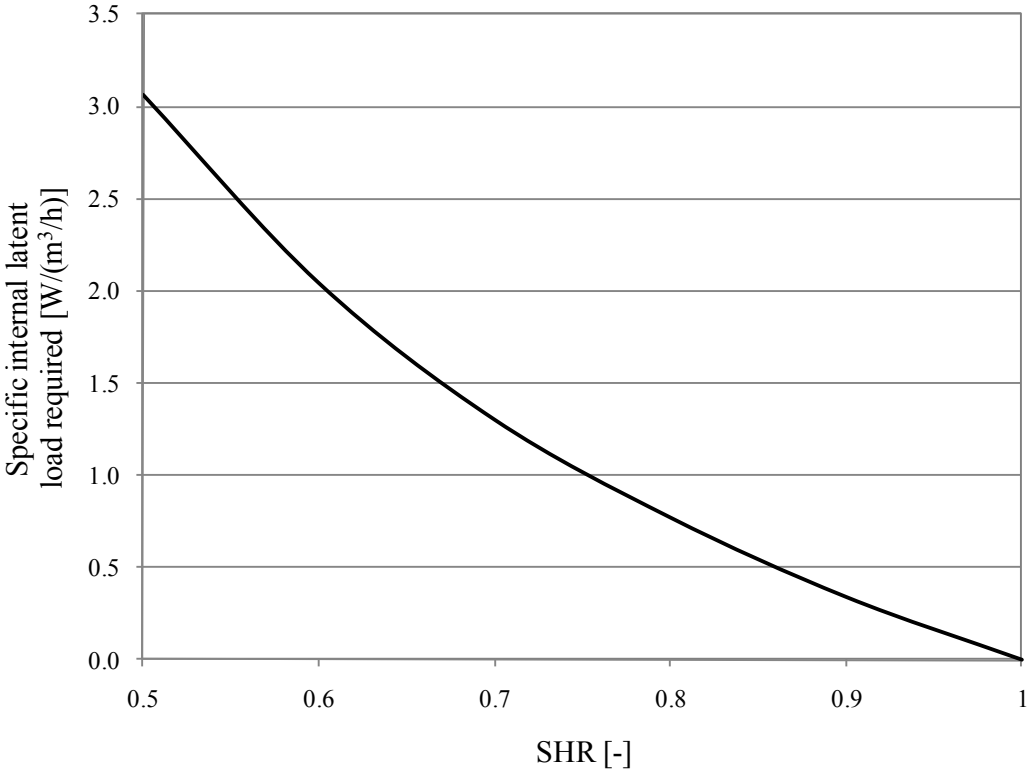

Fig. 2. 42: Specific internal latent load required as a function of Sensible Heat Ratio

With reference to both Fig. 2. 41 and Fig. 2. 42, in all the cases in which the desiccant wheel cannot balance the required latent load, a higher t_{reg} is necessary.

CHAPTER 3: 3-E ANALYSIS OF MCHP AND MCCHP SYSTEMS

3.1 Distributed Polygeneration: CHP and CCHP

During last years, great attention was focused on the transition from centralized to decentralized energy "production" systems, to reduce T&D energy losses: a miniaturization process ("size" effect) is in progress.

The bulk of electric power used in the world is delivered by centralized power plants, most of them utilizing large, fossil-fuel combustion or nuclear power plant to produce steam that drives steam turbine generators. Distributed Generation includes the application of small scale generators, located on the utility system, at the site of a utility customer, or an isolated site not connected to the grid, to provide electrical power needed by electrical consumers. By avoiding or reducing transmission and distribution costs, DG can provide lower operating costs in many cases.

Furthermore, small, modern generators can be more efficient and less costly to operate than large and old generators. These circumstances have led some people to conclude that there is no longer an economy of scale in power generation. But a large modern power generation unit has higher electric efficiency and lower operating cost per kWh delivered than a small modern DG unit based on the same technology.

In [63], the exergy efficiency for electricity generation of the main energy conversion systems in use today, has been evaluated as a function of the electric power of the plant ("size") in the range 0.01-1,000 MW. All the systems, based on renewable energies (photovoltaic, solar thermal, wind and hydroelectric) and non-renewable ones (reciprocating internal combustion engines, steam and gas turbines, combined cycles, nuclear power plants and fuel cells,) exhibit an exergetic performance index decreasing with the "size".

In [64], the comparison between the centralized power system, based on plants of an average age of over 20 years, and that of the distributed one is analyzed.

Since the "size" effect does not always lead to energy savings and pollutant emissions reduction, there is the need to support the diffusion of on-site small complex energy conversion devices, Distributed Polygeneration, DP, which are able to supply, with high performance, two or

more energy outputs (electric, cooling and heating) to the end-user, rather than the simple single-output equipments.

A widespread use of DP systems could allow energetic, economic and environmental benefits: the benefits and drawbacks of DP are analysed in [65].

In order to evaluate if the miniaturization process will provide energy and environmental benefits, special attention must be paid in finding the optimal tradeoff between the advantages, due to the reduction of duct and cycle losses, and the disadvantages due to the negative influence of the size on the system performance [66, 67].

Microcogenerators are most common systems for DP. Cogeneration, or Combined Heating and Power (CHP), represents the combined "production" of electric (and/or mechanical) and thermal energy (heating), starting from a single primary energy source, [68]. It is a well-established technology, which has important benefits and has been noted by the European Community as one of the first strategy to save primary energy, reduce greenhouse gas emissions with respect to the reference separate "production" by large thermal power stations and avoid network losses, [69].

Different definitions of small size cogeneration system (microcogeneration, MCHP) are available on technical and scientific literature, generally, on the basis of maximum electric power output of the unit, suitable, above all, for residential and light commercial users, [70]. Dentice et al. refer to residential and light commercial applications to characterize MCHP and Domestic CHP (DCHP) system considering the maximum power output of 15 kW_{el}, [71]; this is the reference size for microcogeneration used in this work.

Technical characteristics of MHCPs based on different prime movers (PM) are reported in [72]. It is the final report of a project in which ENEA (the Italian National Agency for new technologies, energy and sustainable economic development) and Università degli Studi del Sannio cooperated to the development of a database of commercially available or prototype microcogenerators. The database has a main menu, Fig. 3. 1, from which it is possible to see the complete list of models or to perform a search and visualize the models with specific characteristics (type of prime mover or fuel, range of electric power…).

For each model, a mask containing the main technical and energy characteristics, as well as related bibliography and websites, has been realized, Fig. 3. 2.

Furthermore, in many applications in the tertiary (hotels, hospitals, commercial buildings) and residential sectors, distributed trigeneration systems (Combined Cooling, Heating and Power, CCHP) allow the simultaneous satisfaction of different energy requirements (electricity, cooling and heating), [73, 74], allowing energy, economic and environmental benefits.

The "heart" of these energy conversion systems is a Prime Mover, based on different technologies (Stirling, Reciprocating Internal Combustion – RIC, Fuel Cell, Gas Turbine, and so on), especially designed to operate in stationary conditions for a long time with high efficiency and very low pollutant emissions. At the moment, the most mature technology available on the market, which is gas-fired RIC engines, achieves small installation space, high thermal efficiency, low noise, vibrations and maintenance requirement as well as long life service, [75, 76].

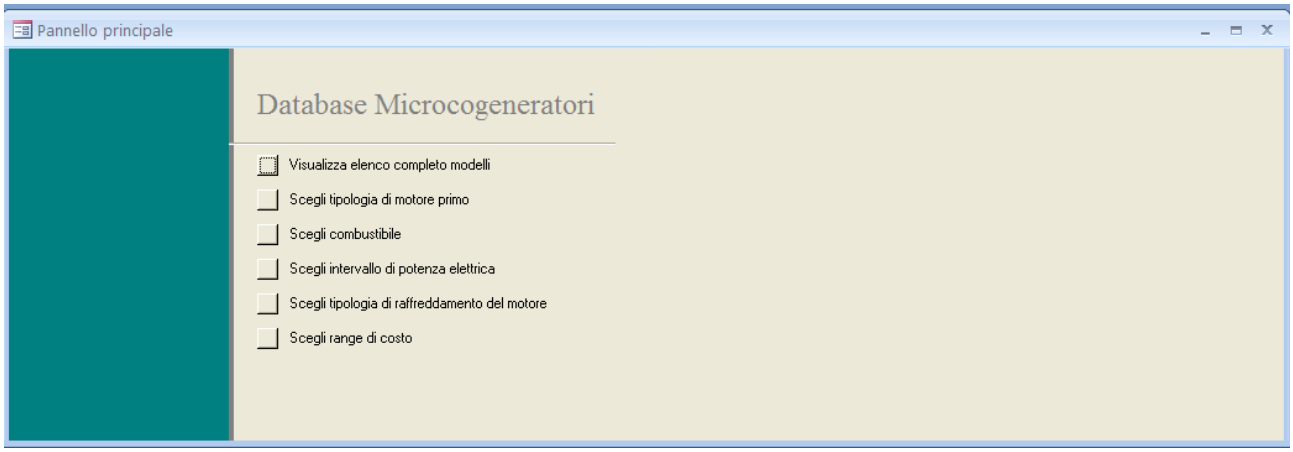

Fig. 3. 1: database main menu

Typical CCHP operating modes are:

- "separate": the system provides heating during cold season, cooling during hot period and power all year round ("seasonal trigeneration"). This strategy is usually adopted in residential and tertiary sector;
- "simultaneous": the CCHP, in addition to supply electric energy, simultaneously satisfies cooling and heating requirements, to meet typical industrial loads.

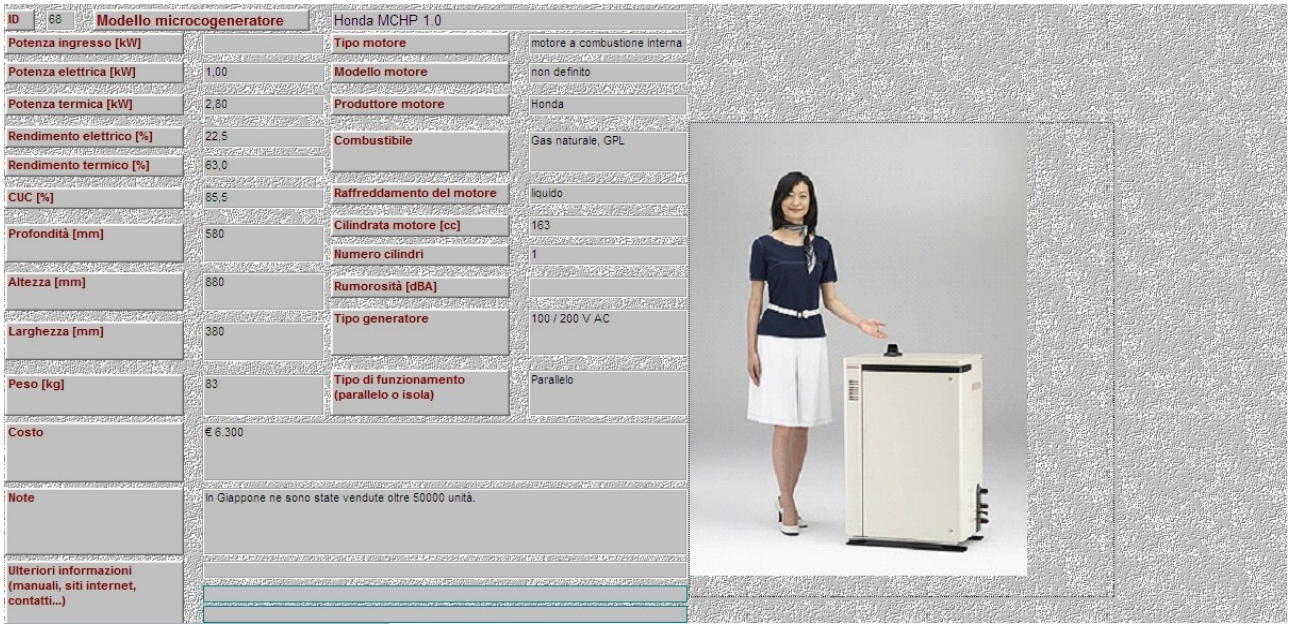

ID 68	Modello microcogeneratore	Honda MCHP 1.0	
Potenza ingresso [kW]		Tipo motore	motore a combustione interna
Potenza elettrica [kW]	1,00	Modello motore	non definito
Potenza termica [kW]	2,80	Produttore motore	Honda
Rendimento elettrico [%]	22,5	Combustibile	Gas naturale, GPL
Rendimento termico [%]	63,0		
CUC [%]	85,5	Raffreddamento del motore	liquido
Profondità [mm]	580	Cilindrata motore [cc]	163
		Numero cilindri	1
Altezza [mm]	880	Rumorosità [dBA]	
Larghezza [mm]	380	Tipo generatore	100 / 200 V AC
Peso [kg]	83	Tipo di funzionamento (parallelo o isola)	Parallelo
Costo	€ 6.300		
Note	In Giappone ne sono state vendute oltre 50000 unità.		
Ulteriori informazioni (manuali, siti internet, contatti...)			

Fig. 3. 2: mask for a MCHP model

A CCHP system, CHP/THP (Thermally activated Heat Pump), which is usually adopted, is composed of four main components, Fig. 3. 3:

- a prime mover, PM;
- an electricity generator, G;
- a thermal recovery system (typically from exhaust gas and engine cooling liquid);
- a cooling energy "production" system which is usually adopted as a THP, fuelled by thermal energy instead of mechanical energy. This energy system, interacting only with external thermal reservoirs, operates as a heat transformer.

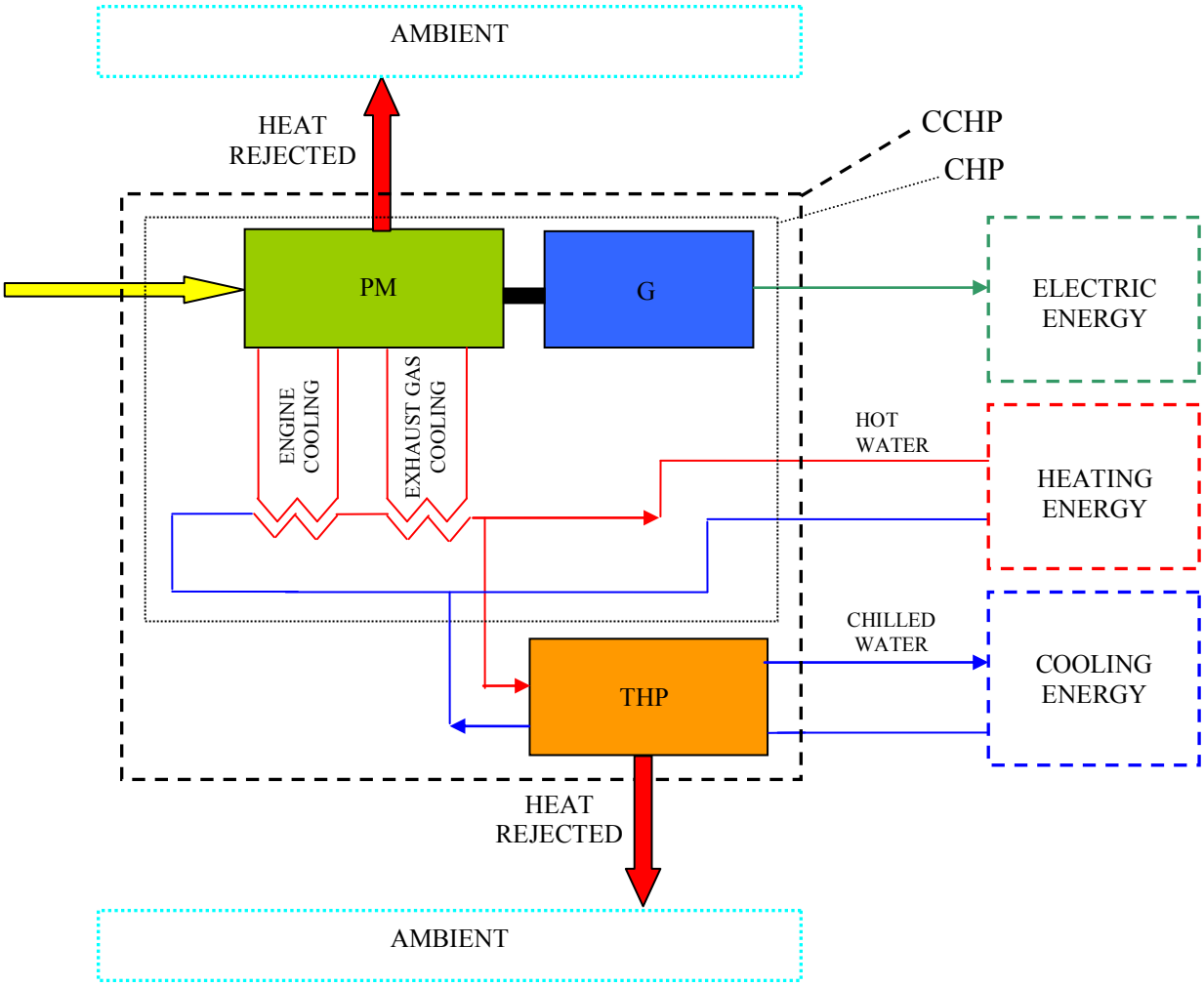

Fig. 3. 3: A CCHP system.

Moreover, it is common knowledge that both CCHP and CHP systems usually interacts with the external electric grid, to optimize the system operating modes with respect to technical, energy and economic restraints.

Prime movers can drive (mechanically, electrically, thermally) electric generators and/or electric heat pumps, absorption heat pumps, desiccant wheels and so on, in different ways, allowing a wide range of operating conditions to match thermal (heating and cooling) and electric end-user requirements, [77-79], and achieving significant primary energy and emissions savings, if all energy outputs are correctly exploited.

For example, in Fig. 3. 4, the PES and the ΔCO_2 (see next section for the definition of these parameters), that a MCHP/EHP system (the MCHP electrically drives an EHP, Electric Heat Pump) can obtain with respect to a conventional system, based on the separate "production" of the same

quantities of useful energies, are shown as a function of the percentage of the recovered thermal energy effectively used by the final user during the summer season, for instance for domestic hot water purposes, [74].

The lower limit value of thermal energy used is 60% to achieve a primary energy saving and 40% to obtain an equivalent CO_2 emissions reduction.

A MCHP/ABHP system (the MCHP thermally drives an ABHP, Absorption Heat Pump) is also considered in [74]. A numerical analysis has been carried out, assuming that the cogenerator works at full load for 6 hours during summer and provides electric energy to the final user and thermal energy to feed the ABHP, for which a COP of 0.65 has been assumed. Thermal energy provided by the MCHP is not enough, both in terms of quantity and quality (temperature) to feed the generator of the heat pump, therefore an integration from an auxiliary boiler is needed.

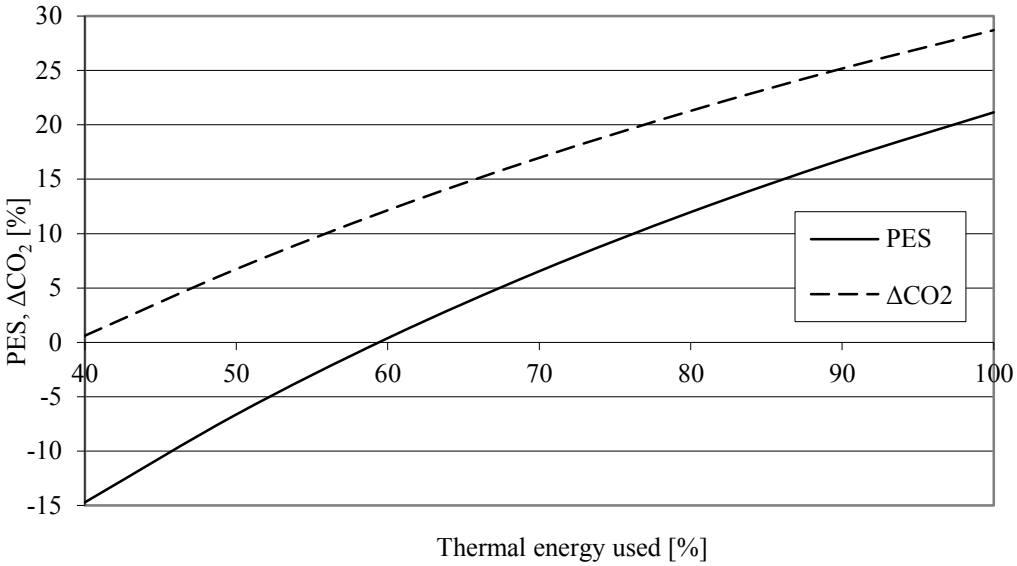

Fig. 3. 4: PES and ΔCO_2 for the MCHP/EHP system as a function of the percentage of thermal energy used

The MCHP/ABHP system can achieve a PES of about 9% and a ΔCO_2 of about 21% with respect to the separate "production" of thermal, cooling and electric energy.

This numerical analysis have been deepened in [79], in which experimental results for the MCHP/ABHP system have been reported. They show that the thermally activated absorption system has a quite low COP, lower than the value stated by the manufacturer (0.70). This determines very low energy performance of the whole trigeneration system.

In Fig. 3. 5, the PER for the MCCHP, the conventional separate "production" system (CS) and the separate "production" one based on the Best Available Technology (BAT) are reported as a function of time for a typical test day. The figure shows that, in the investigated operating conditions, the microtrigeneration system is always less efficient than both the CS and the BAT: the minimum percentage difference is 24% if compared to the Conventional System and 42% when the comparison is with the Best Available Technology.

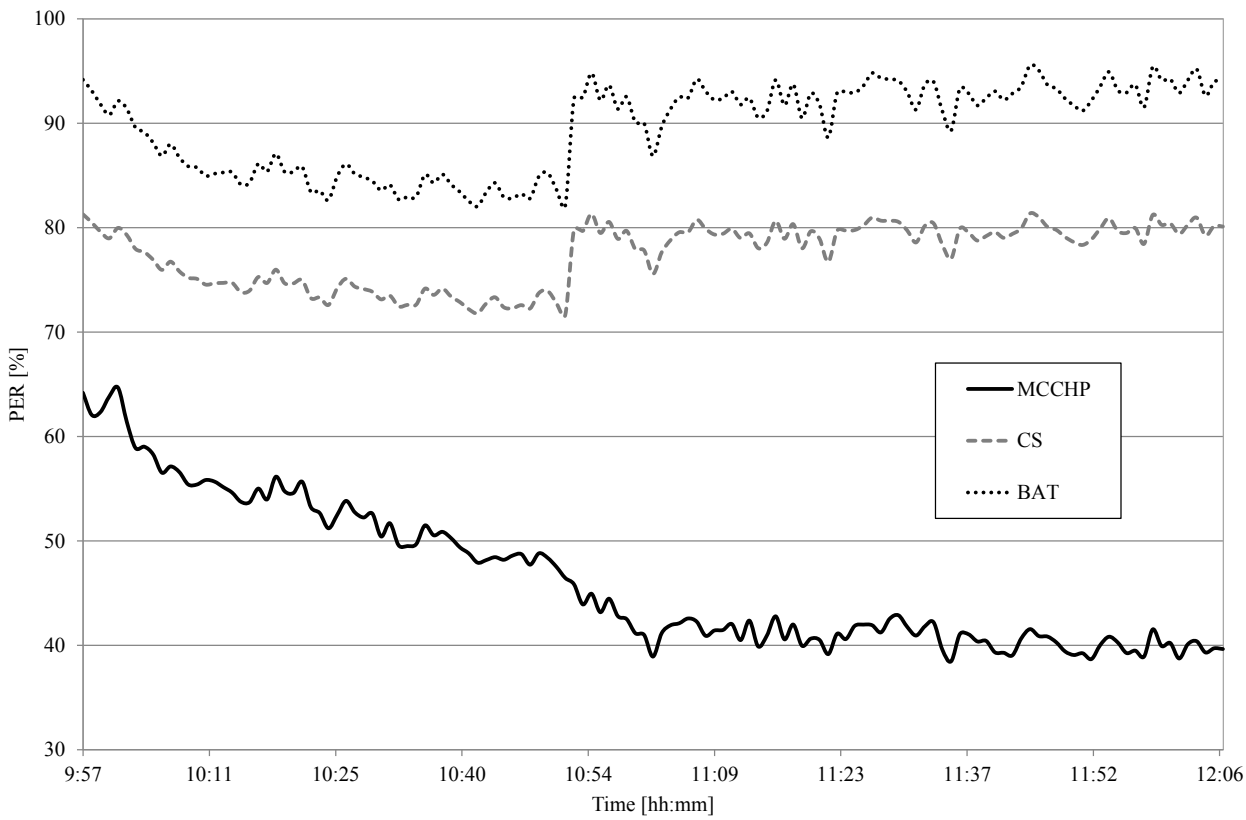

Fig. 3. 5: Primary Energy Ratio as a function of time in summer mode

MCHPs and MCCHPs can represent the base of the shift from centralized to decentralized energy "production" systems. This transition is already partially being carried out; the benefits and drawbacks that DG will provide to the end-user and the community have been widely analyzed in the technical and scientific literature. Furthermore, there are worldwide a significant number of R&D projects on trigeneration systems based on thermally activated equipments, [80].

In [81], an overview of available performance assessment studies and a description of the experimental activity (field test, laboratory), performed by both research groups involved in IEA

Annex 54 and other researchers on DP systems, is presented. The analysis is focused on multi-source microcogeneration systems, polygeneration systems (i.e. integrated heating/cooling/power generation systems) and renewable hybrid systems (collectively termed Micro-Generation, MG). The aim of this report is the evaluation of MG systems in terms of energy, environmental and economic criteria, as well as in terms of technical criteria, including control and operation.

Furthermore, in the framework of the Annex 54 project, a report aimed at defining the methodologies for the performance assessment of micro hybrid poligeneration systems is in progress, with a special focus on complex energy conversion systems, i.e. trigeneration systems interacting, in a bidirectional way, with electric and thermal networks and renewable energy based technologies, [82].

As seen, CCHP is an upgrade of cogeneration unit, where thermal, mechanical or electric energy is utilized to provide space or process cooling capacity. In this way, energy efficiency increases and the economic pay back decreases due to the large amount of operating hours per year.

CCHP systems, besides being generally more efficient than separate "production" systems, have another outstanding advantage as they are tipycally fuelled with natural gas. In fact, especially in Mediterranean areas, there is an increasing demand of summer cooling energy in domestic sector, usually satisfied by electrically-driven units; this involves electric load peaks and black-outs. Hence, an increasing interest occurs in small scale polygeneration systems fuelled by natural gas. In fact, the HVAC market is largely dominated by electrically-driven units, which determine an increased power generation capacity of electric utilities and a summer peak of electric energy consumption, with the related problem of electric black-out. Japan and USA were involved in this problem 20 years ago and it is currently very pressing in Mediterranean areas. Gas Cooling Technologies (GCT) can shift energy demand in summer from electricity to gas, at the same time allowing the utilization of the natural gas surplus during the warm season.

The main benefits of gas fuelled CCHP, with respect to the reference separate energy "production" system, typically based on a centralized power plant, a boiler and an electric chiller, are:

- energy independence of the user;
- primary energy saving;

- low pollutant emissions;
- reduction of fuel costs;
- a widespread use of GCT, to shift from electricity to gas, due to the high energy demands during warm seasons, caused by the large diffusion of electrically-driven HVAC systems, especially in residential applications.

As regards environmental impact, on the other side, the introduction of MCCHP systems within urban areas, where the problem of air quality standards is very important, forces to take into account the effects of local emissions, that depends, above all, on the fuel and technology used, [83]; hazardous air pollutants such as NO_X, CO, SO_X, particulate matter, unburned hydrocarbons and so on, lead to expand the environmental analysis, considering not only the global effects, for example through the evaluation of equivalent CO_2 emissions, but also the local ones. The concentration of these pollutants is also affected by the morphology of the territory and climatic conditions and could happen that DG systems lead to an increase in local emissions, [84, 85]. Furthermore, specific emissions of MCHP and MCCHP systems at partial load are greater than those at rated load: this aspects lead to the introduction of a further element of variability in the analysis of the local environmental impact, [86].

3.2 3-E analysis

According to a typical 3-E (Energetic, Environmental and Economic) simplified approach, the performances of the Alternative System, AS≡MCCHP or MCHP, are usually compared to those of a reference system (in the following defined as the Conventional System, CS) based on separate electric, thermal and cooling "production". Both the alternative and conventional systems have to satisfy the electric and thermal (space heating and cooling, domestic hot water) user's requirements. A very common CS, that characterizes European countries is based on the electric grid (transmission and distribution from a centralized power plant), a natural gas-fired boiler (for domestic hot water and space heating requirements) and an electric chiller (for space cooling requirements).

The energy efficiency of both AS and CS is evaluated by means of the Primary Energy Ratio (PER) performance factor, defined as the ratio of the useful energy output supplied to the end-user to the primary energy consumption:

$$PER = \frac{E_{el} + E_{th} + E_{cool}}{E_p} \tag{3. 1}$$

Useful cooling energy, E_{cool}, is obviously present if MCCHP systems are analyzed.

According to scientific literature [87, 88], and European directive, [69, 89], in order to compare the ability of energy conversion systems to satisfy the same user, it is important to evaluate the Primary Energy Savings, PES, which is defined as:

$$PES = \frac{E_p^{CS} - E_p^{AS}}{E_p^{CS}} * 100 \tag{3.2}$$

Furthermore, the environmental impact is a key factor in selecting the proper energy system. A simplified approach is based on the evaluation of carbon dioxide equivalent emissions of the analyzed energy systems. The comparison is then based on the equivalent CO_2 avoided emissions, ΔCO_2, defined as, [90]:

$$\Delta CO_2 = \frac{CO_2^{CS} - CO_2^{AS}}{CO_2^{CS}} * 100 \tag{3.3}$$

where CO_2^{CS} and CO_2^{AS} are carbon dioxide equivalent emissions of the conventional system and the alternative one.

PER, PES and ΔCO_2 are strongly influenced by energy performance parameters (η, COP, ...) and fuel used by both alternative and conventional systems. For instance, the power plant efficiency and emission factor can be characterized with respect to a specific country mix (e.g. Italy), the Best Available Technology (Gas Turbine Combined Cycle) or through other different approaches, [91].

Finally, to complete the analysis, the evaluation of proper economic performance indices is necessary. In fact, aiming at a large diffusion of MCCHP technology, characterized by energy and environmental benefits, a reasonable short payback period should be obtained. However, the external factors that affect the market access of these technologies vary with country; furthermore, there is a large number of parameters (initial and operating costs, tax rates, economic contributions, ...), involving both government and private operators (gas utilities, manufacturers, ...), to take into account. For example, the possibility of obtaining funds or the convenience in selling the electric

surplus to the grid could strongly influence the economic availability of these new equipments. However, for a simplified estimation, the Simple Pay-Back period, SPB, is usually evaluated, by means of the following equation:

$$SPB = \Delta IC \Big/ \left(AOC^{CS} - AOC^{AS} \right) \tag{3.4}$$

where ΔIC is the Investment Cost difference between the alternative and conventional system, while AOC^{CS} and AOC^{AS} are the Annual Operating Costs of CS and AS, respectively.

3.2.1 3-E parameters for the reference separate "production" system

The aim of this section is to provide an overview of the available methodologies to define the energy, environmental and economic performance of the separate "production" reference system, in particular as regards the following parameters, [82]:

- $\eta_{el,ref}$: energy performance factor of reference system for electricity supply (ratio of electric energy output to primary energy input, [kWh_{el}/kWh_p]);
- $CO_{2,el,ref}$: carbon dioxide emission factors of reference system for electricity supply (ratio of CO_2 emissions to electric energy output, [kg_{CO2}/kWh_{el}]);
- $\eta_{th,ref}$: energy performance factor of reference system for heating supply (ratio of thermal energy output to primary energy input, [kWh_{th}/kWh_p]);
- $CO_{2,th,ref}$: carbon dioxide emission factor of reference system for heating supply (ratio of CO_2 emissions to primary energy input, [kg_{CO2}/kWh_p]);
- $COP_{cool,ref}$: Coefficient Of Performance of reference system for cooling supply (ratio of cooling energy output to electric energy input, [kWh_{co}/kWh_{el}]);
- $SC_{el,ref}$: specific cost of reference system for electricity supply (ratio of electric energy cost to electric energy output, [€/kWh_{el}]);
- SC_{NG}: specific cost of natural gas (ratio of natural gas cost to its normal volume, [€/Nm^3]); this parameter is used for the natural gas consumption of both the reference gas boiler and the microcogenerator; even so, different values of SC_{NG} can

be used for the two equipments, as the MCHP can, for example, benefit from a discounted price for natural gas.

On estimating the energy and environmental performance of the reference system based on separate "production", three different approaches can be used.

The first one is to use energy performance and CO_2 factors of the separate "production" reference systems based on a national or regional technological mix. In this case, different time references can be adopted, e.g. average annual, monthly or even hourly values (the last approach is especially used when renewable energy sources, that are very random, significantly contribute to separate energy "production").

The second one is to use the Best Available and economically justifiable Technology, e.g. Gas Turbine Combined Cycle power plant for electricity supply and condensing gas boiler for heating supply.

The third one is to use values provided by some national or international directive, e.g. European Directive 2004/8/CE on the promotion of cogeneration based on a useful heat demand, that defines reference values for separate electricity "production"; these values depend on the year of construction of the cogeneration plant, the type of fuel, the average national temperature, etc…

Concerning the emission factors, they are coefficients that quantify the emission of a specific pollutant per unit of energy consumed and/or supplied. The emissions of a device are then estimated by multiplying the emission factor with the corresponding energy consumptions data. Two different approaches may be followed when selecting the emission factors:

- using 'Standard' emission factors, in line with the IPCC (International Panel on Climate Change) principles, which cover all the CO_2 emissions that occur due to energy consumption, either directly due to fuel combustion or indirectly via fuel combustion associated with electricity and heat/cold usage. The standard emission factors are solely based on the carbon content of each fuel, like in the context of the UNFCCC (United Nations Framework Convention on Climate Change) and the Kyoto protocol.

  In this approach, CO_2 is the most important greenhouse gas, and the emissions of CH_4 and N_2O do not need to be calculated. However, also other greenhouse gases can be included in the analysis if standard emission factors are chosen. The

emissions of other greenhouse gases than CO_2 are converted to CO_2-equivalents by using the Global Warming Potential (GWP) values. In this case, emissions are expressed as 'CO_2 equivalent emissions'. This is the approach used by equation 3.3.

Furthermore, the CO_2 emissions from the sustainable use of biomass/biofuels, as well as emissions from certified green electricity, are considered to be zero.

- using LCA (Life Cycle Assessment) emission factors, which take into consideration the overall life cycle of the energy carrier, [92]. This approach includes not only the emissions of the final combustion, but also all emissions of the supply chain. It includes emissions from exploitation, transport and processing (e.g. refinery) steps in addition to the final combustion. This hence includes also emissions that take place outside the location where the fuel is used.

  In this approach, the GHG emissions from the use of biomass/biofuels, as well as emissions from certified green electricity, are higher than zero. If this approach is used, other greenhouse gases than CO_2 may play an important role. Therefore, emissions should be reported as CO_2-equivalent.

The standard approach, although it does not reflects the total environmental impact related to the use of an energy carrier, has several advantages with respect to the LCA approach, [93]; in particular, it is compatible with the monitoring of progress towards EU's 20-20-20 target and, especially, all the needful emission factors are easily available. In fact, the standard emission factors depend solely on the carbon content of the fuels; therefore they do not vary significantly from case to case. But for the LCA approach, obtaining information on the emissions upstream in the production process may be challenging and considerable differences may occur even for the same type of fuel. This is especially the case of biomass and biofuels. Therefore, in this work, the standard emission factors approach is used.

As regards electric energy separate "production" system, micro-generation systems generate electricity near the point of use, so they allow a reduction of the transmission and distribution losses from not using or minimizing the use of the electric network, in comparison to larger and centralized electricity "production" systems. Typically, a large CHP plant connected at the high voltage network would avoid nearly 2.5% losses, whilst a MCHP plant in a house connected at the low voltage network would avoid losses of at least 10%.

Both transmission and distribution electric networks show considerable losses variation across each country, hence it would be useful to define a simple and workable method to correct the central power plants energy performance to take into account national circumstances. A simple approach to this issue defines standard grid losses, for each voltage level of the network system. Therefore, depending on the voltage level a CHP unit is connected to, it is easy to determine the total avoided grid losses of the unit.

As regards the thermal energy separate "production" system, the real-life operational efficiencies of boilers can differ significantly from their nominal values, as they depend on load conditions and supply/return water temperature. For instance, the nominal operation efficiency of a condensing gas boiler can increase of more than 8% if the return temperature decreases from 60 °C to 30°C.

Also for the cooling energy separate "production" system, the real-life operational efficiencies of electric vapour compression cooling devices can differ significantly from their nominal values, as they depend on climatic and load conditions, supply and return water temperature. For instance, the COP of a small size air-cooled vapour compression chiller can reduce of more than 30% when air temperature at the condenser increases from 30 °C to 40 °C.

Furthermore, different efficiency values can be used depending on whether the auxiliaries electric consumption of the vapour compression cooling device are accounted for; for example manufacturers define the COP as the ratio of cooling power output to the electric power input to the motor driving the compressor, and the EER (Energy Efficiency Ratio) as the ratio of cooling power output to total electric power input (motor and auxiliaries).

Finally, the efficiency of vapour compression cooling devices strongly depends on their load condition. In fact, during real-life operation, the cooling unit works at full load only for a limited number of hours, while during the remaining time it works at partial load with a reduced efficiency. For example, the Eurovent Standard introduces the European Seasonal Energy Efficiency Ratio (ESEER), to take into account this effect. It is a parameter that considers the operation of the cooling device with four different Partial Load Ratio – PLR: 25%, 50%, 75% and 100%.

In the framework of Annex 54, the parameters used by the participating research groups to characterize the reference separate "production" system have been collected. In Tab. 3. 1, some of them are reported.

			TUM (Germany)	NIST (USA)	UNISANNIO (Italy)	SUN (Italy)	JAPAN
Reference Separate "Production" System	Heating	*Type of device*	SB – CB	Natural gas furnace (NC) A/A Heat Pump (SC)[1]	SB CB	SB CB	
		$\eta_{th,ref}$	SB=80% CB=95%	AFUE = 94% (NC) HSPF = 8.5 (SC)	SB = 85% CB = 102%	SB = 85% CB = 95%	73.5%
		$CO_{2,th,ref}$ $[g_{CO2}/kWh_p]$	205		200	200	205
	Storage water heater	*Type of device*		Natural gas (NC) Electric (SC)			
		$\eta_{th,wh,ref}$		EF = 0.7 (NC) EF = 0.92 (SC)			
	Cooling	*Type of device*		Air conditioner	Air cooled electric chiller	Air cooled electric chiller	
		$COP_{cool,ref}$		SEER = 13	COP = 3.0	COP=2.0 (average) COP=3.5 (BAT)	
	Electricity	$\eta_{el,ref}$	38.5%	Vary by region	46%[3] (Italian mix) 54.3%[3] (BAT)	46%[3] (Italian mix) 52.0%[3] (BAT)	36.1%[4] (daytime) 38.8%[4] (nighttime)
		$CO_{2,el,ref}$ $[g_{CO2}/kWh_{el}]$	580	Vary by region (both marginal and overall)	531 (Italian mix) 400 (BAT)	531 (Italian mix)	360
		T&D losses		7 % (US average)	6.5% (average)		
		$SC_{el,ref}$ $[€/kWh_{el}]$			0.18	0.18	0.1 (industrial) 0.2 (domestic)
	Natural gas	*PEF*	1.1		-	-	
		SC_{NG} $[€/Nm^3]$			0.80[2]	0.80[2]	0.5 (industrial) 1.2 (domestic)

Tab. 3. 1: Energy, environmental and economic parameters for the reference separate "production" system used by some Annex 54 research groups

[1]NC = Northern Climate; SC = Southern Climate
[2]a lower value is assumed for MCHP use
[3]including T&D losses
[4]based on HHV

3.3 The MCHP/HVAC-DW system

In the most common configuration of a MCCHP system, in which a THP is present, the MCHP provides thermal energy to an AHP, which provides cooling energy to the final user.

In a less diffuse layout, thermal energy recovered by the microcogenerator is used to regenerate a desiccant wheel contained in an hybrid Air Handling Unit (MCCHP=MCHP/HVAC-DW). In fact, the waste heat of a small cogeneration plant can be effectively used to regenerate the desiccant material (both solid and liquid), while the cogenerated electricity can drive a chiller or an Electric Heat Pump to meet the room sensible load.

In [42], the results of a simulation model, carried out to design an experimental hybrid HVAC system, were reported. The test facility is placed in the South of Italy, in a humid town. A microcogenerator supplies electric energy to an EHP and other electric devices. Waste heat recovered from the MCHP is utilized to regenerate the DW. Possible excess of thermal energy can be used to produce domestic hot water.

In [43, 44] a hybrid HVAC system coupled with a MCHP was analyzed. The test facility is placed in Hamburg, Germany. The system is characterized by a radiant floor cooling which interacts with borehole heat exchangers and balances the sensible load of the room. Thermal energy recovered from the MCHP, at a temperature between 55 °C and 65 °C, is used to heat the regeneration air, while electric energy supplied by the MCHP powers the electric devices of the office. This system is energetically compared with other systems, such as a hybrid HVAC system without the microcogenerator and a conventional HVAC system.

In [45], a hybrid air conditioning system, incorporating an engine-driven chiller and a desiccant dehumidification system, was experimentally tested to measure the performance of the engine-driven chiller and the dehumidification capacity. A comparison between theoretically predicted and measured values was presented. The waste heat recovered from engine-cooling system and exhaust gases was experimentally determined. Also the performance improvement of chiller, due to higher temperatures of chilled water (only sensible cooling is needed), was measured. Economic benefits of the hybrid air conditioning system over the conventional electric chiller were calculated for a reference building; the results revealed that more than 30% savings on operation costs can be achieved.

In [46], the performance of a desiccant cooling system, regenerated by means of heat recovery from a gas-fired reciprocating internal combustion engine, was evaluated. The system offers sufficient sensible and latent cooling capacities for a wide range of climatic conditions. Energy efficiency and water consumption of the desiccant cooling system were also evaluated and compared with those of a conventional system.

Air dehumidification can also be achieved by means of a liquid desiccant system: typically a LiCl-water solution is sprayed in a conditioning chamber (the absorber) and comes in contact with the air to be dehumidified. The solution concentration is restored by spraying part of it in a regeneration section, while the remainder is recirculated. Also for liquid desiccant systems, regeneration thermal energy can be derived from cogenerator thermal wastes, [94-97].

Both in the case of solid and liquid desiccant systems, thermal energy for regeneration can be also obtained by a solar collector system, typically integrated with an auxiliary fossil-fuelled heater [37, 98-100].

From the literature review above reported, few investigations have been carried out on solid desiccant hybrid systems coupled to small scale combined cooling, heat and power systems; particularly, little attention has been paid on both energy and environmental performances, [43-46].

Therefore, this work experimentally analyses a desiccant-based MCCHP system based on a hybrid Air Handling Unit (as already said, the term hybrid refers to the contemporary presence of a desiccant wheel and an electric chiller, that, in succession, dehumidify and cool the air to be introduced in the conditioned space), especially suitable for residential and small commercial users; a 3-E analysis, considering different operating modes, is carried out.

The system performances are evaluated as a function of various operating conditions (outdoor and supply air thermal-hygrometric conditions, partial load operation of the MCHP), in order to establish its effectiveness, compared to a conventional HVAC system based on separate electric, thermal and cooling “production”. Finally, the influence of the electric grid efficiency is considered to analyse the polygeneration system in different electricity mix scenarios.

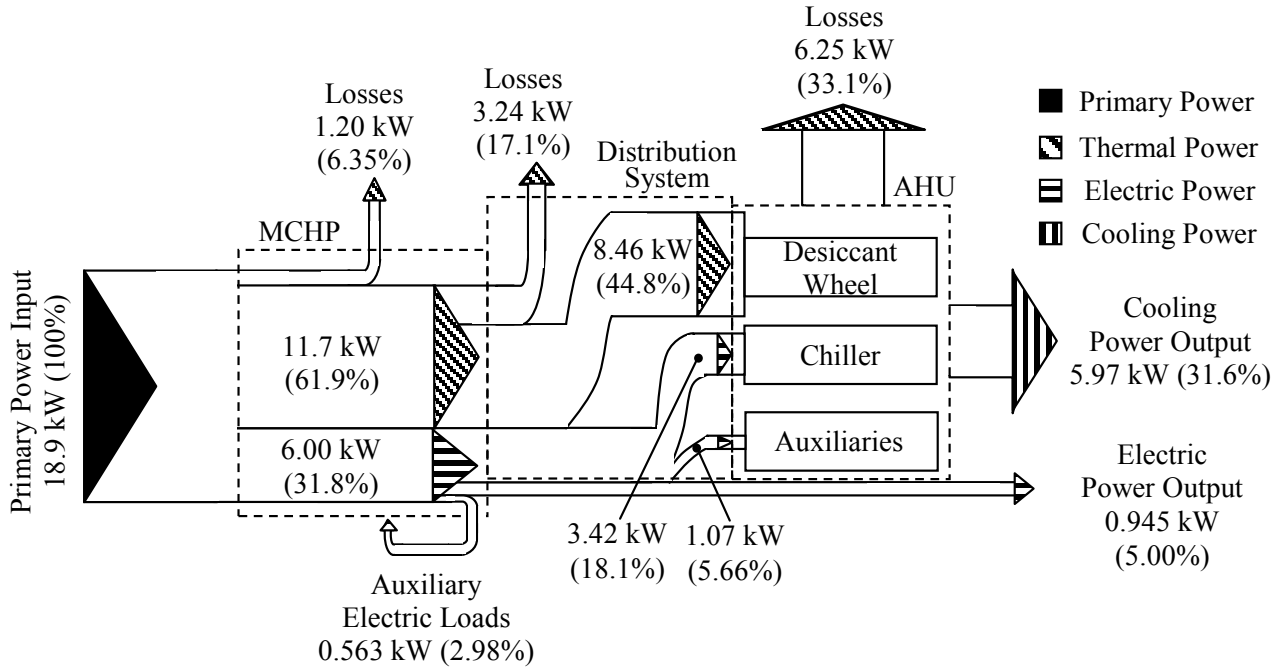

Fig. 3. 6: Sankey diagram of the polygeneration system

In Fig. 3. 6 the Sankey diagram of the polygeneration system is shown, to highlight the main power flows (electric, thermal and cooling) and losses. For the global system and for its main subsystems, power inputs and outputs are reported, also considering MCHP auxiliary electric loads (including circulation electric power absorption) and electric power supplied to AHU auxiliaries.

In Fig. 3. 7, the energy flows of the MCCHP ≡ MCHP/HVAC-DW system are reported, [101]. Electric energy can be splitted between the chiller and the direct use (lights, appliances, …): by means of r_e parameter (0÷1), which represents the electric energy share provided to the chiller, different operating modes can be considered. Thermal energy can also be splitted between the regeneration of desiccant wheel and the direct use (heating, hot water,…), by varying r_t parameter (0÷1), which represents the thermal energy share provided to the DW.

E_p is the primary energy input to the MCHP, η_{th} and η_{el} are its thermal and electric efficiency, respectively.

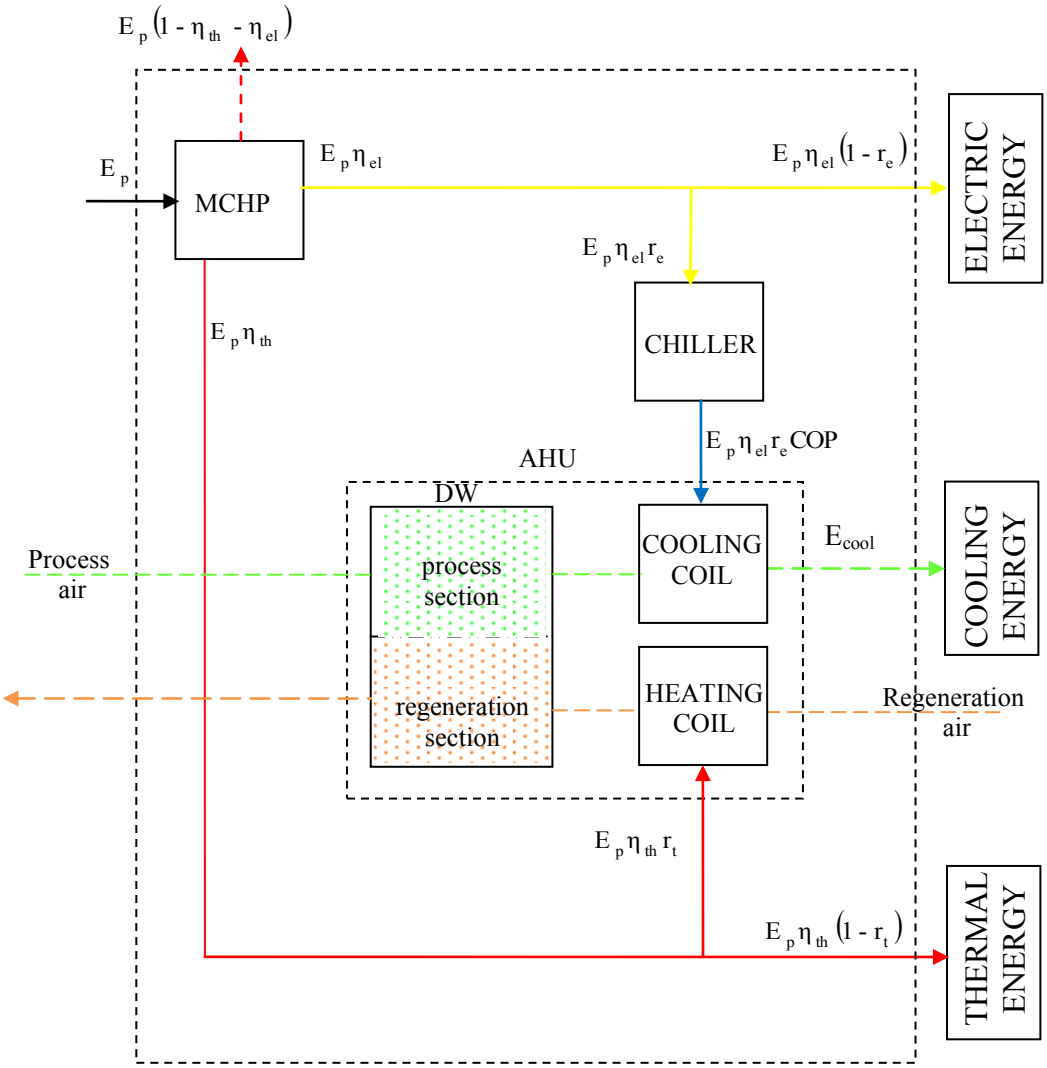

Fig. 3. 7: Energy flows of MCHP/HVAC-DW system

The MCHP/HVAC-DW system can operate in different modes, [102]:

- MCHP mode ($r_t = r_e = 0$): the cogenerator directly supplies electricity and thermal energy to the end-user. The HVAC system does not operate. This is the typical winter operating mode.

- HVAC-DW mode ($r_t = r_e = 1$): the electric and thermal energy delivered by the MCHP are totally used to activate the hybrid HVAC system based on the desiccant wheel; cooling energy is the only useful output;

- MCHP/HVAC-DW mode ($0 < r_t < 1$, $0 < r_e < 1$): this trigeneration configuration allows to satisfy electric, heating and cooling energy end-user's requirements.

3.3.1 The AISIN TOYOTA Microcogenerator

The analyzed MCHP is manufactured by AISIN-SEIKI, [103], a Japanese Toyota group company, model GECC60A2N (Fig. 3. 8), distributed by TECNOCASA CLIMATIZZAZIONE (Loreto – AN) for the European market, [104, 105]. The prime mover, which has already been used in widely tested GHPs (Gas engine driven Heat Pumps), is a 6.0 kW_{el} modulating unit. The system works in parallel with the electrical network, both in single and in three phase installations.

As it is possible to see in Tab. 3. 2, the rated characteristics show a thermal power of 11.7 kW with a water flow rate of 33.5 l/min and an output temperature of 60 – 65 °C. The actual flow rate during the tests (17.0 l/min) is lower than the nominal one; as a consequence, hot water is available at a higher temperature (72.5 °C). However, due to thermal losses in the distribution pipes and in the air-to-water heat exchanger (heating coil 1 in Fig. 2. 2), the maximum achievable regeneration air temperature (state 5 in Fig. 2. 2) is 65 °C; furthermore, the MCHP supplies electric energy for the electric loads of the AHU (fans, pumps, desiccant wheel, etc…), the chiller and further external electric devices (computers, lights, etc…).

The MCHP heat production system recovers heat by flowing the engine coolant (45% glycol-ethylene mixture) through a pipe heat exchanger, where the exhaust gas is cooled down, and through the engine walls. No invasive measurements equipments have been introduced inside the MCHP casing, therefore it was not possible to separately evaluate the share of thermal power recovered from the exhaust gas and the engine jacket.

The coolant circulation is achieved by means of a magnet pump that sets a constant volumetric flow rate through the exhaust gas heat exchanger and the engine. The heat is then transferred to water in a brazed plate heat exchanger.

The engine coolant circuit is managed during the operation by two thermostatic valves, Fig. 3. 9. In fact, once the solution has carried out the thermal recovery, it passes through the plate heat exchanger or, depending on the temperature of the solution near the double thermostatic valve, a part (or in some cases the whole) of it can cross the by-pass circuit or go to the radiator, that can eventually disperse the exceeding heat.

For example, at the start up, the whole thermal energy is used to warm the engine up in the shortest time; hence the solution flow rate completely bypasses the plate heat exchanger and recirculates through the engine.

Fig. 3. 8: The AISIN microcogenerator

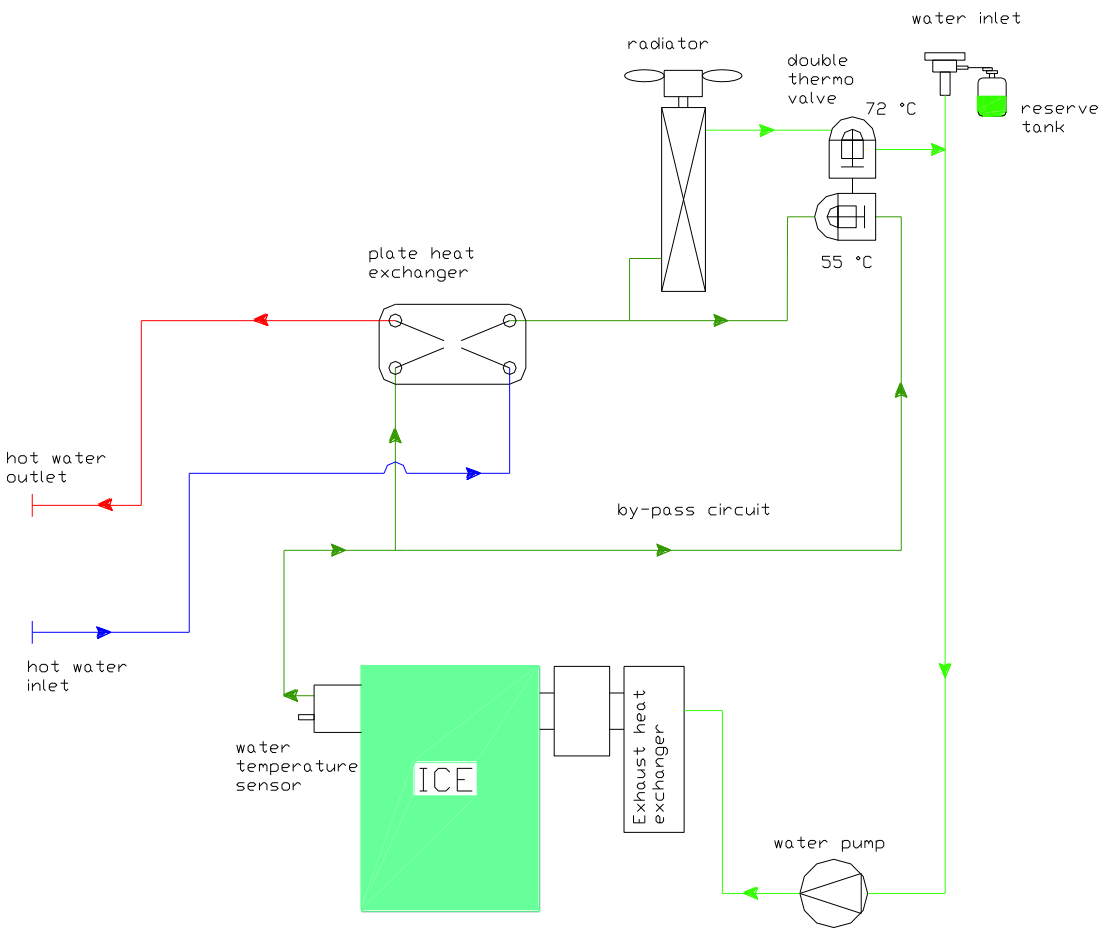

Fig. 3. 9: Thermal recovery circuit of the AISIN MCHP

Electrical power [kW]	0.3 – 6
Output voltage [V]	200
Thermal power [kW]	11.7
In/Out water temperature [°C]	60 – 65
Water flow rate [l/min]	33.5
Fuel	Natural gas
Power input [kW]	20.8
Engine type	Water cooled, 3 cylinder, 4 strokes
Engine displacement [cm^3]	952
Rated engine speed [rpm]	1600 – 1800
Generator type	Permanent magnet type, 16 pole synchronous generator
Depth [cm]	66
Width [cm]	110
Height [cm]	150
Weight [kg]	465
Electrical efficiency [%]	28.8
Thermal efficiency [%]	56.2
Overall efficiency [%]	85.0
Operating sound at 1 m distance [dB(A)]	54

Tab. 3. 2: Aisin microcogenerator characteristics

The MCHP has an auxiliary electric consumption that ranges from 200W (fan radiator off) to 350 W (fan radiator on).

3.3.2 Numerical 3-E analysis

In this section, a numerical analysis, based on design operating conditions and nominal characteristics of the devices, is carried out in order to compare the performance, in terms of primary energy consumptions, greenhouse gas emissions and annual operating costs, of the MCHP/HVAC-DW system with respect to conventional cooling dehumidification HVAC systems powered by separate electric, thermal and cooling "production", [106].

A simplified numerical analysis of the MCCHP plant is conducted, considering nominal outdoor and indoor air thermal-hygrometric conditions, nominal devices characteristics and assuming that the MCHP always works at full load, [107]. This is obviously a simplified approach and a more detailed analysis, based on experimental results, considering part load performance and the influence of thermal-hygrometric conditions, will be described in next section.

The energy, environmental and economic comparison is carried out on equal useful energy delivered to final user. In particular, it is supposed that thermal, cooling and electric energy is fully supplied to an office building, for space heating and cooling, for domestic hot water purposes and to power electric appliances (lights, computers, AHU auxiliaries,…).

Winter season

During the winter season, the polygeneration system works in cogeneration mode: in fact, the desiccant-based AHU does not work and only electrical and thermal energy are available, for direct electric use (computer, lights…) and for space heating and domestic hot water purposes, respectively. As the MCHP works at full load, its primary power input is P_p = 20.8 kW.

The reference separate "production" system (based on a natural gas-fired boiler and electric grid), has to supply the same electric and thermal power of the MCHP; so its primary power input is:

$$P_{p,ref,win} = P_{el}^{*} / \eta_{el,ref} + Q_{th} / \eta_{th,ref} = 25.8 \ kW \tag{3.5}$$

where $P_{el}^{*} = 5.78$ kW is the net electric power production of the microcogenerator, assuming a value of 220 W for its auxiliary electric consumption. This value correspond to a situation in which the radiator fan is off; in fact, the operation of the MCHP with this fan on should be strictly avoided, as it represents a condition in which thermal load is too low. Hence the cogenerated thermal energy would not be effectively used, and this often undermines the benefits of combined electrical and thermal "production".

The energy efficiency of both electric grid ($\eta_{el,ref}$) and boiler ($\eta_{th,ref}$) have been evaluated, with respect to Italy, in accordance with the European Directive 2004/8/EC and its associated Commission Decision [69, 89, 107]:

- electric grid: $\eta_{el,ref}$ = 45.2%, equivalent CO_2 emission = 0.531 $kgCO_2/kWh_{el}$, [108];
- boiler: $\eta_{th,ref}$ = 90%, CO_2 equivalent emission = 0.200 $kgCO_2/kWh_p$; natural gas lower heating value = 9.59 kWh/Nm^3.

Summer season

To evaluate the performance during summer season, outside air thermal-hygrometric conditions were assumed equal to the design values for Benevento: t = 32 °C, ω = 15 g/kg, relative humidity = 50%, [109].

During summer, the hybrid AHU is switched-on, therefore cooling energy is also supplied to the final user. The following parameters for some AHU components were used:

- evaporative cooler saturation efficiency

$$\eta_{dec} = \frac{(t_1 - t_8)}{(t_1 - t_{wb,1})} \tag{3.6}$$

where $t_{wb,1}$ is wet bulb temperature at point 1;

- cross flow heat exchanger effectiveness

$$\varepsilon_{cf} = \frac{(t_2 - t_3)}{(t_2 - t_8)} \tag{3.7}$$

The following typical values were used for the two aforementioned parameters: η_{dec} = 0.6; ε_{cf} = 0.5.

Finally, a by-pass factor of 17% for the cooling coil, [110], and a temperature increase of 10% for process air flowing through the supply fan, [111], were assumed. These two values were also used for the cooling coil and the supply fan in the AHU of the reference system.

The nominal temperature and humidity ratio values that occur in different sections of the desiccant-based AHU are listed in Tab. 3. 3.

The temperature decrease in the regeneration air passing through the boiler heating coil, that is switched-off, was neglected. Process air thermal-hygrometric conditions exiting the desiccant wheel were provided by a simulation software of the rotor, considering outdoor air temperature and humidity ratio at the inlet of the DW, regeneration air temperature and volumetric flow rate of process and regeneration air (800 m^3/h).

		t [°C]	ω [g/kg]
Outdoor air	1	32.0	15.0
Process air at desiccant wheel outlet	2	49.8	9.35
Process air at cross-flow heat exchanger outlet	3	38.0	9.35
Process air at cooling coil outlet	4	17.3	9.35
Regeneration air at MCHP heating coil outlet	5	65.0	15.0
Regeneration air at desiccant wheel inlet	6	65.0	15.0
Cooling air at humidifier outlet	8	27.0	17.0
Process air at the fan outlet	10	19.0	9.35

Tab. 3. 3: Thermal-hygrometric air conditions in the hybrid AHU

The cooling power provided by the cooling coil in the desiccant-based AHU can be evaluated as:

$$Q_{cool,cc} = \dot{m} \cdot (h_3 - h_4) = 5.30 \text{ kW} \tag{3.8}$$

where $\dot{m}$ is the rated supply air flow rate (0.251 kg/s), equal to the regeneration one.

To evaluate the net electric power supplied by the MCCHP system to the external electric appliances, the electric requirements of both the chiller and the auxiliaries of the AHU (fans, pumps…) must be accounted too. Electric requirement of the desiccant wheel motor can be neglected because it is smaller than 10 W.

The electric requirements of the chiller can be estimated with the following equation:

$$P_{el}^{CH} = Q_{cool,cc} / COP_M = 1.60 \text{ kW} \tag{3.9}$$

where COP_M is the Coefficient Of Performance of the electric chiller interacting with the desiccant-based AHU, equal to 3.31.

AHUs based on desiccant dehumidification have the advantage of reducing cooling energy demand, for the lack of cooling dehumidification, on which conventional air conditioning systems are instead based. In fact, the refrigeration unit is allowed to produce chilled water at higher temperatures, and to consequently operate with a higher COP. For these reasons, attention was paid to the evaluation of the performance of the electric chiller in both the MCCHP system and the reference one: a detailed model, based on well-known simulation softwares of inverse machines, allows to evaluate the performance of the air-cooled water chiller interacting with external secondary fluids, air and water [112, 113].

The AHU auxiliaries electric consumption, $P_{el,aux}$, due to the presence of three fans and two circulation pumps, is approximately 1.05 kW, so the net electric power supplied to external electric appliances is:

$$P_{el,n} = P_{el}^{*} - P_{el}^{CH} - P_{el,aux} = 3.13 \text{ kW} \tag{3.10}$$

where $P_{el}^{*} = 5.78 \text{ kW}$ is the effective electric power "production" of the MCHP, as 0.22 kW is used for the cogenerator self-consumptions.

Thermal power to regenerate the desiccant wheel is fully supplied by the cogenerator and can be evaluated with the following expression:

$$Q_{th,reg} = \dot{m} \cdot (h_5 - h_1) = 8.56 \text{ kW} \tag{3.11}$$

The thermal power that can be used for domestic hot water preparation, $Q_{th,dhw}$, is:

$$Q_{th,dhw} = Q_{th} - Q_{th,reg} = 3.14 \text{ kW} \tag{3.12}$$

MCHP primary power input is 20.8 kW during summer too, as a full load operation was assumed.

The hybrid AHU can also be driven by separate electric and thermal "production": in that case the cogenerator is replaced by the electric grid, that powers the chiller, the auxiliaries and external electric devices (computers, lights…), and by a natural gas-fired boiler, that supply thermal power to regenerate the desiccant wheel and to produce domestic hot water. Electric grid and natural gas boiler efficiencies are as previously defined.

The primary power input of the hybrid AHU powered by separate "production" can be evaluated with the following relation:

$$P_p^{SP} = P_{el}^{*} / \eta_{el,ref} + \left(Q_{th,reg} + Q_{th,dhw}\right) / \eta_{th,ref} = 25.8 \ kW \tag{3. 13}$$

The desiccant-based AHU powered by separate "production" has a larger primary power consumption than the same AHU powered by the MCHP. Therefore, in the remaining of the analysis, only the latter is considered for comparison with the HVAC reference system.

The reference system is an AHU based on conventional cooling dehumidification and post-cooling of air; it is supposed to reach the same inlet conditions of the hybrid Air Handling Unit and process the same air mass flow rate. The chiller, the AHU self-consumptions and electric appliances are powered by the electric grid, while the post-cooling of air and domestic hot water are obtained with a natural gas-fired boiler; their efficiencies are as previously defined. The nominal values of temperature and humidity ratio that occur in different sections of the reference AHU are listed in Tab. 3. 4.

The cooling power supplied by the cooling coil can be calculated with the following relation:

$$Q_{cool,cc,ref} = \dot{m} \cdot \left(h_1 - h_{2'}\right) = 7.77 \ kW \tag{3.14}$$

		t [°C]	ω [g/kg]
Outdoor air	1	32.0	15.0
Process air at cooling coil outlet	2'	15.9	9.35
Process air at heating coil outlet	3'	17.3	9.35
Process air at fan outlet	4'	19.0	9.35

Tab. 3. 4: Thermal-hygrometric air conditions in AHU of the reference system.

The thermal power supplied by the heating coil can be evaluated as:

$$Q_{th,\,hc,\,ref} = \dot{m} \cdot \left(h_{3'} - h_{2'}\right) = 0.39 \;\; kW \tag{3.15}$$

The auxiliaries electric power consumption in the reference system, $P_{el,aux,ref}$, is about 0.59 kW, due to the presence of both chiller and boiler circulation pump and the supply air fan.

Hence, the primary power input to the system can be evaluated with the following relation:

$$P_{p,\,ref,\,sum} = \frac{Q_{cool,\,cc,\,ref} \big/ COP_{ref} + P_{el,\,n} + P_{el,\,aux,\,ref}}{\eta_{el,\,ref}} + \frac{\left(Q_{th,\,hc,\,ref} + Q_{th,\,dhw}\right)}{\eta_{th,\,ref}} = 17.9 \;\; kW \tag{3.16}$$

where COP_{ref}, equal to 3.0, is lower than COP_M because the chiller interacting with the reference system has to dehumidify and cool the process air, hence it works with a lower chilled water temperature.

The primary power input to the reference system, at nominal outdoor conditions, is lower than the MCCHP one: this result seems to discourage the employ of the trigeneration plant during the summer season. Nevertheless, there are operating conditions, in terms of outdoor and supply air thermal-hygrometric conditions, partial load ratio of the MCHP and electric grid efficiency, in which the hybrid AHU energetically matched with a MCHP can obtain a lower primary power input with respect to a conventional cooling AHU based on separate "production", as will be experimentally shown in section 3.3.3.

Annual energy performance

The heating period for Benevento is from 15 November to 31 March, [109], 10 hours a day, 5 days a week (an office application is assumed); therefore, the winter operating hours for an office are about N_{win}=1,000 h. For the summer period, a value of N_{sum}=650 h is assumed (from 1 June to 7 August and from 24 August to 15 September, 5 days a week, 10 hours a day).

The annual Primary Energy Saving, PES, of the MCCHP system with respect to the reference one is:

$$PES = 1 - \frac{P_p \cdot \left(N_{win} + N_{sum}\right)}{P_{p,\,ref,\,win} \cdot N_{win} + P_{p,\,ref,\,sum} \cdot N_{sum}} = 8.30 \;\; \% \tag{3.17}$$

As the annual PES is positive, winter operation has a higher effect on it than summer operation, for the higher number of winter operating hours, [114].

The environmental performances of the MCCHP and reference systems were also compared in terms of carbon dioxide equivalent emissions. To this aim, the equivalent CO_2 avoided emissions, on an annual basis, was evaluated as follows:

$$\Delta CO_2 = 1 - \frac{CO_{2,M,win} \cdot N_{win} + CO_{2,M,sum} \cdot N_{sum}}{CO_{2,ref,win} \cdot N_{win} + CO_{2,ref,sum} \cdot N_{sum}} = 17.8\% \tag{3.18}$$

where $CO_{2,M,win}$ (4.16 kg/h) and $CO_{2,ref,win}$ (5.66 kg/h) are MCCHP and reference system winter carbon dioxide equivalent emissions, respectively, while $CO_{2,M,sum}$ (4.16 kg/h) and $CO_{2,ref,sum}$ (4.13 kg/h) are the respective values during summer.

The two system have almost the same greenhouse-gas emissions during summer, while in winter the MCCHP can obtain a significant greenhouse-gas emissions reduction with respect to the reference one.

An economic analysis, even though simplified, of an innovative system, which usually requires high initial capital costs, plays a very important role in the assessment of its viability. In this feasibility study, the following assumptions were considered:

- unitary cost of electric energy equal to 0.17 €/kWh$_{el}$;
- unitary cost of natural gas equal to 0.50 €/Nm^3 for the cogenerator and 0.65 €/Nm^3 for the boiler in the reference system (natural gas employed in cogenerative applications may be subject to a lower taxation).

A simplified approach was used, evaluating the Simple Pay Back:

$$SPB = \Delta IC \Big/ \left(AOC_{ref} - AOC_M \right) \tag{3.19}$$

where ΔIC is the Investment Cost difference between the MCCHP system with respect to the reference one, 20 k€, while AOC_{ref} (2.67 k€/y) and AOC_M (1.79 k€/y) are the Annual Operating Costs of reference and MCCHP systems.

At the moment, the investment cost of both the cogenerator and the desiccant wheel is very high to allow an acceptable economic return. However there are a great number of private and public subjects (gas utilities, manufacturers,…) involved in the definition of the economic variables concerning this type of system. For example, government grants along with attractive rates for electricity export to the grid may significantly encourage MCHP and desiccant dehumidification market penetration.

3.3.3 Experimental energetic and environmental analysis

Several tests were carried out to analyze the MCHP/HVAC-DW system. Firstly, the experimental tests had the goal to verify the correct running of the desiccant dehumidification based AHU, interacting with a gas fuelled microcogenerator, and the effectiveness of such a system with respect to a "cooling dehumidification" based conventional AHU.

Considering the experimental results obtained in different operating modes, an energetic and environmental analysis was carried out, comparing the hybrid polygeneration system with a conventional HVAC system.

In each energetic and environmental comparison, two systems are involved: an Alternative System, characterized by the presence of the desiccant based AHU, and a reference system, usually the conventional system or another alternative system.

The following systems were analyzed:

- AS I (Desiccant based AHU powered by the MCHP): the MCHP supplies electric energy for AHU electric loads (fans, pumps, desiccant wheel…) and thermal energy for regeneration of the desiccant wheel;
- AS II (Desiccant based AHU powered by the MCHP with additional external devices): this system is altogether similar to the previous one. The only difference is that MCHP electric power output is increased up to the nominal value to supply external electric devices, obtaining higher values of thermal and mechanical efficiency of the MCHP;
- AS III (Desiccant based AHU powered by the electric grid and a natural gas-fired boiler): thermal power for regeneration of the wheel is supplied by a natural gas-fired boiler, while

electric power is supplied by the electric grid. In particular, two different AS III are defined: in system IIIa the grid powers AHU electric loads and the chiller, while in system IIIb it powers external electric devices too (computers, lights…);

- AS IV (Desiccant based AHU powered by the MCHP and a natural gas-fired boiler): thermal power for regeneration of the wheel is supplied by both the natural gas-fired boiler and the MCHP, which obviously drives the chiller and the AHU electric self-consumptions too;

- AS V (Desiccant based AHU powered by the MCHP, with additional external loads, and by a gas-fired boiler): this system is altogether similar to the previous one. The only difference is that MCHP electric power output has been increased until the nominal value to supply external electric devices;

- CS (Conventional System): it is the usually adopted HVAC system, based on "cooling dehumidification". External air is cooled below dew point temperature and consequently dehumidified in a cooling coil interacting with an electric chiller powered by the electric grid; then, it is reheated to the desired temperature in a heating coil interacting with a natural gas-fired boiler.

Energy and environmental reference values for separate electric and thermal "production" are the same as in section 3.3.2.

The COP of the air to water chiller in the CS has been estimated on the basis of the secondary fluid temperatures. Considering that the chiller interacting with the desiccant AHU has to balance only the sensible load of the room, while the chiller interacting with the conventional AHU has to balance the latent load too, the last one operates at a higher temperature lift with a smaller COP than the first one.

The energy and environmental comparison is carried out on equal useful energy (thermal, electric and cooling) delivered to final users: in particular, in each test, equal supply air condition and volumetric flow rate (800 m^3/h) for both the alternative and the conventional system have been assumed. As an example, in Fig. 3. 10, the energy flows of AS II and CS are shown. In all tests, thermal energy recovered from the MCHP was fully used to regenerate the DW; therefore, $r_t = 1$. E_{el}^{US} and E_{cool}^{US} are electric and cooling energy delivered to the final user, respectively. E_p^B is

boiler primary energy input, E_{th}^{B} is thermal energy supplied by the boiler, E_p^{EG} is electric grid primary energy input and E_{el}^{CH} is electric energy supplied to the chiller. E_p^{CS} and E_p^{AS} are primary energy inputs required by the conventional system and the alternative one.

In the following analysis, the two parameters PES and ΔCO_2, defined in equations 3.2 and 3.3, are based on power values and are characterized by two subscripts, which refer to the systems involved in the comparison: the first subscript refers to the alternative system, the second one refers to the reference system (the conventional system or another alternative system).

Starting from these tests, an energy and environmental analysis was carried out in order to compare the performance of the different described systems.

For each test, with fixed outdoor and supply air thermal-hygrometric properties, the energy consumption and equivalent CO_2 emissions of AS I, II, IV and V were evaluated on the basis of the experimental results, while for AS III and CS they are based on a numerical analysis.

In Fig. 3. 11, the performances of AS I and AS III are compared to establish if the matching of the hybrid HVAC system with a microcogeneration system is effective, [74]. The results of 43 tests are reported: AS I has always a higher PER than AS III (about 23% higher, on average). Furthermore, AS I has lower equivalent CO_2 emissions than AS III (about 35% lower, on average), because AS I requires less primary energy and uses only natural gas, a relatively clean fuel, as primary energy source.

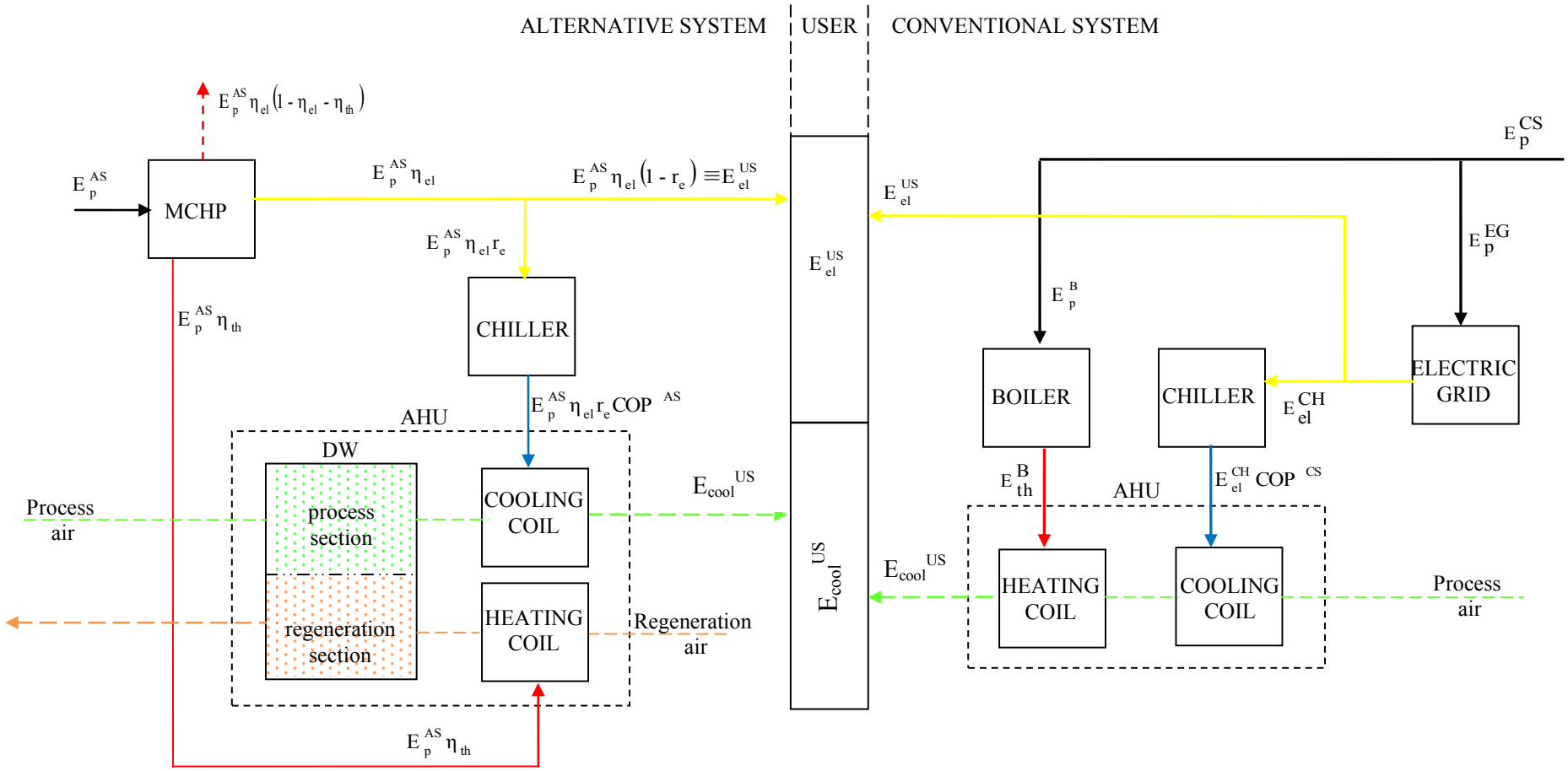

Fig. 3. 10: Energy flows of alternative system II and conventional system.

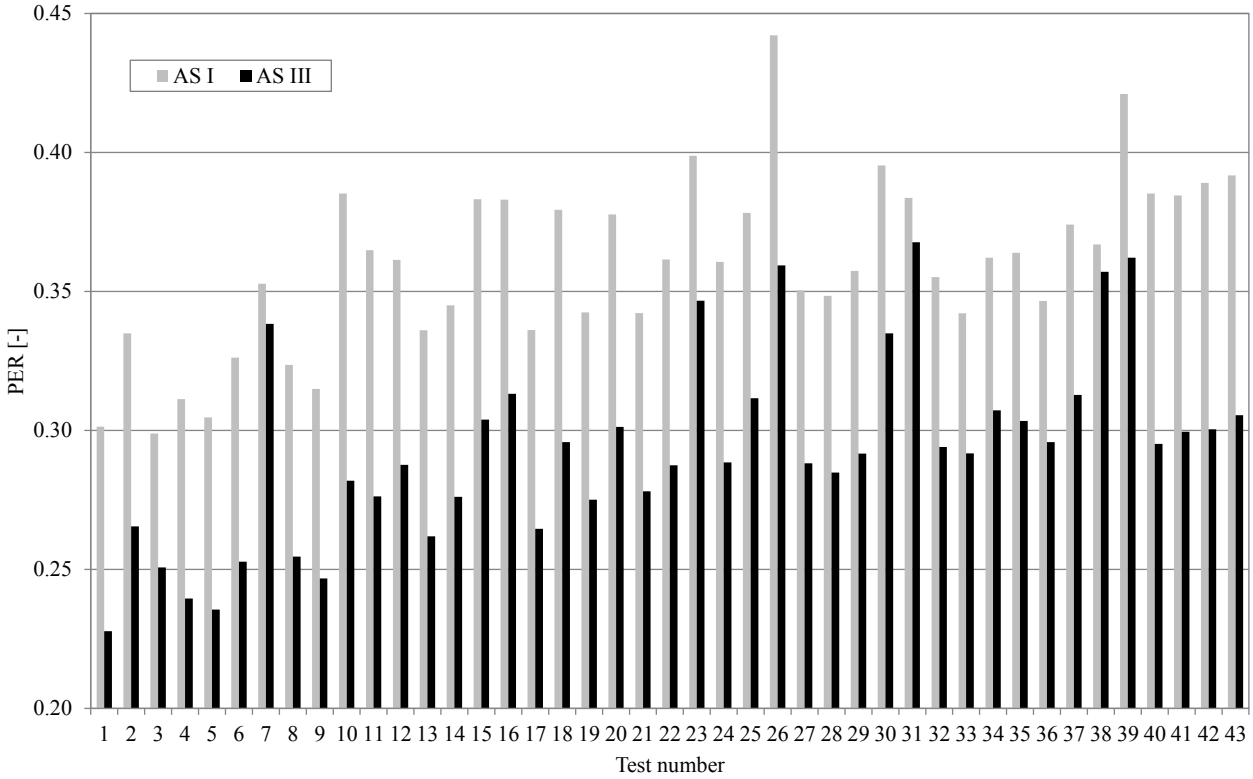

Fig. 3. 11: PER of AS I and AS III for different tests

In Fig. 3. 12 the average results of the energy comparison between alternative systems and conventional one are reported, while in Fig. 3. 13 the average results of environmental comparison among the same systems are shown.

It is possible to note that AS I, AS II and AS III, which are characterized by the presence of the desiccant based HVAC, can assure energy savings, in comparison with CS, greater than 6.5% and greenhouse gas avoided emissions, with respect to the usually adopted HVAC system, greater than 14.6%.

The desiccant based AHUs powered by the boiler and the grid, AS IIIa and AS IIIb, without and with external electric devices, respectively, perform better than the conventional system.

Therefore, the desiccant dehumidification technology, matched with an electric chiller for sensible cooling only, can autonomously guarantee significant energy (6.5 and 11.7%) and CO_2 emissions (14.6 and 20.2%) reductions with respect to the traditional HVAC based on cooling dehumidification, even when powered by separate “production” systems.

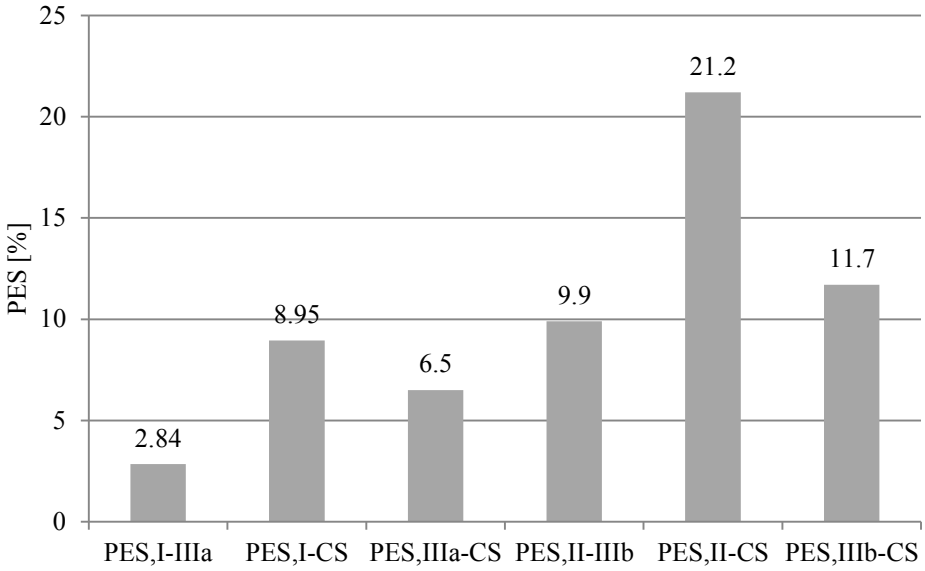

Fig. 3. 12: Average results of energy comparison between alternative and conventional systems

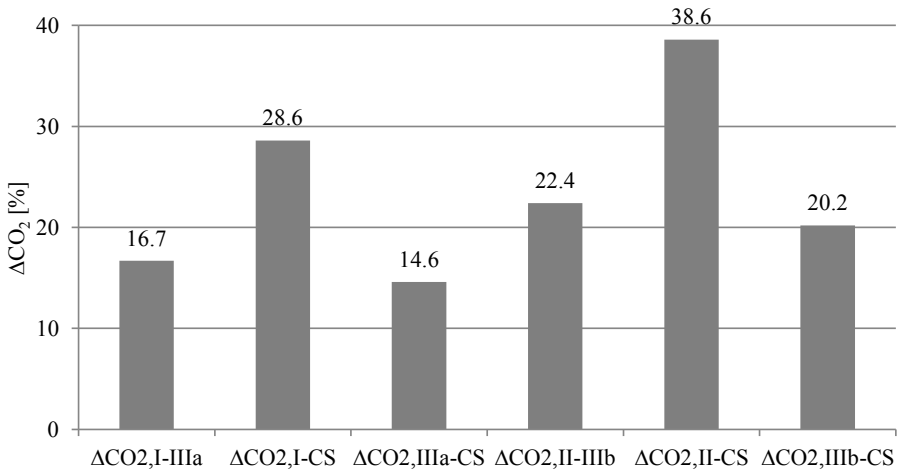

Fig. 3. 13: Average results of environmental comparison between alternative and conventional systems

These benefits increase when the desiccant based AHU is powered by the MCHP, as in AS I and AS II, which perform always better than the desiccant-based AHUs powered by separate "production", AS IIIa and AS IIIb. In fact $PES_{,I\text{-}IIIa}$ and $PES_{,II\text{-}IIIb}$ are 2.8 and 9.9% respectively, while $\Delta CO_{2,I\text{-}IIIa}$ and $\Delta CO_{2,II\text{-}IIIb}$ are 16.7 and 22.4%, respectively.

Furthermore, PES and ΔCO_2 reach their maximum values when the electric power supplied by the MCHP is increased until its nominal value (6 kW) for the presence of the external electric devices, as in AS II. This system has the best energy and environmental performance, with respect

to both the desiccant based HVAC system without MCHP and the conventional system ($PES_{,II-CS}$ and $\Delta CO_{2,II-CS}$ are 21.2 and 38.6% respectively).

It is well known that the dehumidification performances of the DW are affected by the available regeneration thermal power. To increase it, a natural gas boiler can operate, with the MCHP at partial load (AS IV) or at full load (AS V: electric chiller ON + AHU self-consumptions + external electric devices). Experimental results show that the polygeneration system can obtain moderate energy and environmental benefits in its best configuration only (AS V).

Obviously, the energy and environmental performances of the desiccant based HVAC systems analyzed in this work vary not only with the type of system, as previously described, but also with other operating variables, such as, for example, outdoor air and supply air thermal-hygrometric conditions, MCHP partial load conditions and electric grid efficiency, [115, 116].

3.3.3.1 Effect of supply air thermal-hygrometric conditions

In order to highlight the influence of supply air thermal-hygrometric conditions, in Fig. 3. 14, PES_{I-SC} and $\Delta CO_{2,I-CS}$ as a function of supply air humidity ratio are shown. Both parameters increase when supply air humidity ratio decreases. In fact, the reduction in ω_s determines a decrease in the supply air dew point temperature; this involves a decrease in the chilled water temperature, produced by the electric chiller to dehumidify the air in the conventional system; therefore its COP strongly reduces.

As a consequence, energy consumptions and emissions increase with respect to the system based on adsorption dehumidification: the desiccant dehumidification technology is therefore particularly indicated when a very low supply humidity ratio is needed.

In Fig. 3. 15, PES_{II-CS} and $\Delta CO_{2,II-CS}$ as a function of supply air humidity ratio are shown. It is possible to repeat the same considerations as for Fig. 3. 14, but it should be noted that in this case PES_{II-CS} remains always positive.

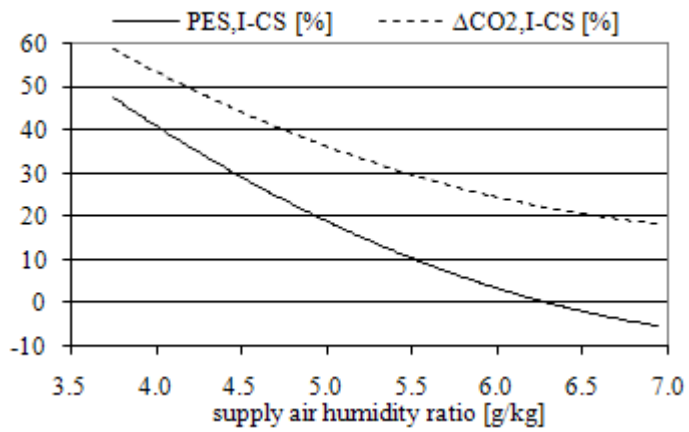

Fig. 3. 14: $PES_{I\text{-}CS}$ and $\Delta CO_{2,I\text{-}CS}$ versus supply air humidity ratio

For both Fig. 3. 14 and Fig. 3. 15, slightly different reference values of energy and environmental indices for separate electric and thermal "production" were used:

- electric grid: $\eta_{el,ref}$ = 39.1%, equivalent CO_2 emission = 0.700 $kgCO_2/kWh_{el}$;
- boiler: $\eta_{th,ref}$ = 85%, equivalent CO_2 emission = 0.200 $kgCO_2/kWh_p$; natural gas lower heating value = 9.59 kWh/Nm^3.

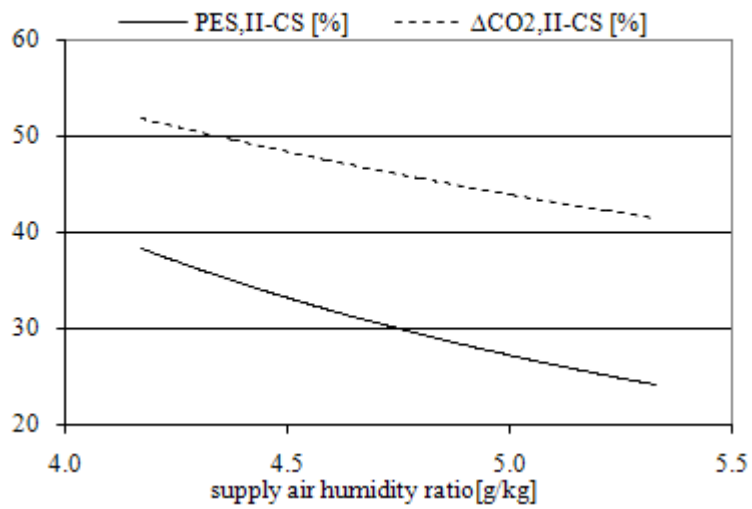

Fig. 3. 15: $PES_{II\text{-}CS}$ and $\Delta CO_{2,II\text{-}CS}$ versus supply air humidity ratio

3.3.3.2 Effect of outdoor air thermal-hygrometric conditions

In order to deepen the analysis, further tests have been carried out in order to evaluate the influence of outdoor air thermal-hygrometric conditions and electric grid efficiency on the global

performance of the hybrid AHU powered by the MCHP (AS, no distinction between the different alternative systems is done in this case) with respect to the conventional system, [116].

In particular, the effect of outdoor air thermal-hygrometric conditions on the performance of the chiller interacting with both the alternative and the conventional system has been evaluated by means of specific softwares, [112, 113]. Both full and part load operating conditions have been considered, in agreement with literature, [117].

In Fig. 3. 16, the full load COP of the chiller in alternative and conventional HVAC systems is shown as a function of t_{out} and for different ω_s values. The COP in the alternative system ("DW" line) obviously does not depend on ω_s, because the dehumidification is carried out by the desiccant wheel, not by the chiller. Contrariwise, the COP of the chiller interacting with the cooling/dehumidification coil strongly decreases when ω_s reduces, as the chilled water temperature decreases. For many operating conditions, the chiller interacting with the hybrid HVAC system performs better than the conventional one, that has also a "size" (cooling capacity) about twice.

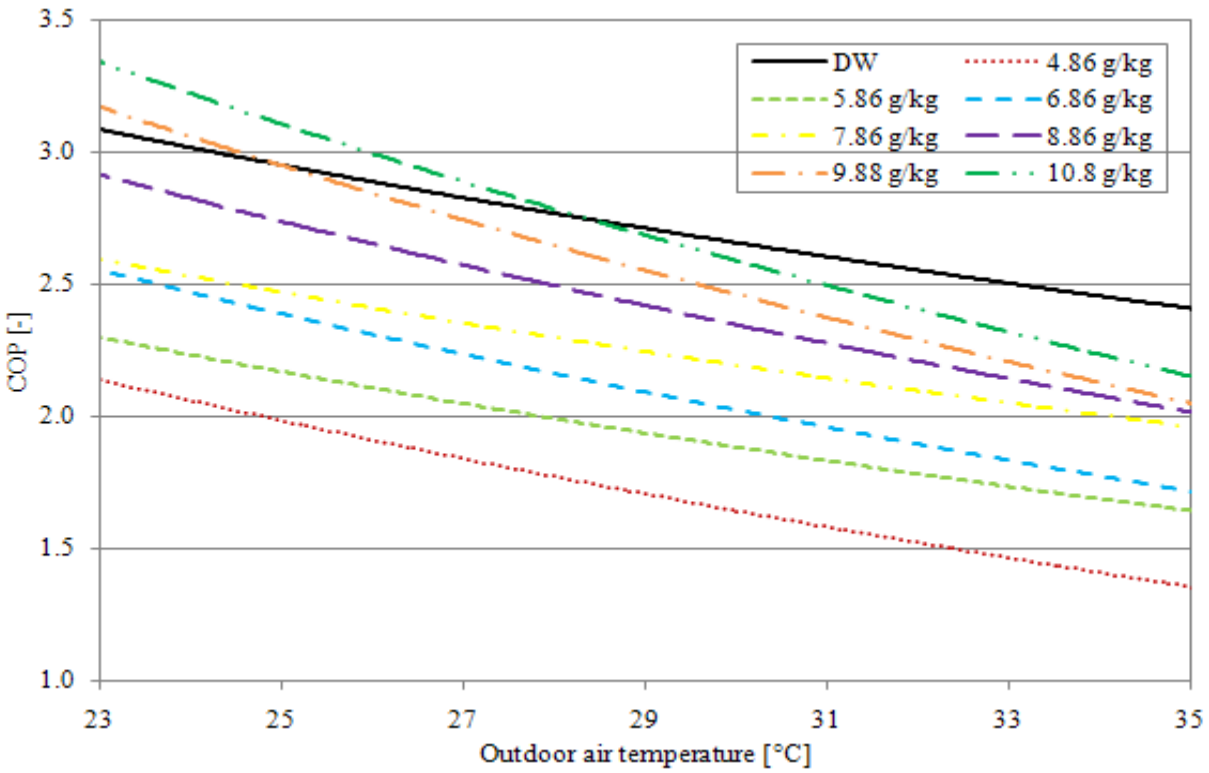

Fig. 3. 16: COP of the electric chiller in the conventional HVAC system (for different values of supply air humidity ratio) and in the desiccant-based HVAC system, as a function of the outdoor air temperature

Only for low outdoor temperature (< 29 °C) and high values of supply air humidity ratio (≥ 10.8 g/kg), the COP of the chiller interacting with the conventional AHU is greater than the alternative one.

To highlight the influence of outdoor air properties on the energy performances of AS and CS, in Fig. 3. 17 outdoor air thermal-hygrometric conditions that get a positive PES are shown. The hybrid HVAC system interacting with the MCHP requires less primary energy than the conventional system for ω_{out} lower than about 11.5 g/kg and t_{out} in the range 25-36 °C. For ω_{out} > 11.5 g/kg, the lower limit of the previous temperature range increases: for ω_{out} = 13.0 g/kg, AS is preferable only for t_{out} > 28 °C. Finally, for ω_{out} > 13.0 g/kg, AS is no more energetically suitable.

In Fig. 3. 18, the PES as a function of ω_{out} and for three different values of t_{out} is shown. PES increases when ω_{out} decreases, reaching a maximum value for ω_{out} = 8.00 g/kg (24 %, 31 % and 35 % for t_{out} equal to 25.0 °C, 29.0 °C and 33.5 °C, respectively). PES becomes positive when ω_{out} is lower than a certain value, depending on outdoor air temperature (11.4 g/kg, 12.6 g/kg and 13.0 g/kg for the three t_{out} values, respectively). Moreover, PES increases with t_{out}, as, when outdoor temperature increases, the COP of the chiller in the CS decreases more than the COP of the chiller interacting with the desiccant-based AHU (see also Fig. 3. 16).

In the range of operating conditions of Fig. 3. 18, the equivalent CO_2 avoided emissions show the same trend as PES, achieving a maximum value of 43%. The avoided emissions go to zero when ω_{out} is in the range 14.5-16 g/kg (depending on t_{out} value), while PES goes to zero when ω_{out} is in the range 11.4-13.0 g/kg. Therefore, the ambient convenience remains in a wider outdoor humidity ratio range compared to the energy convenience.

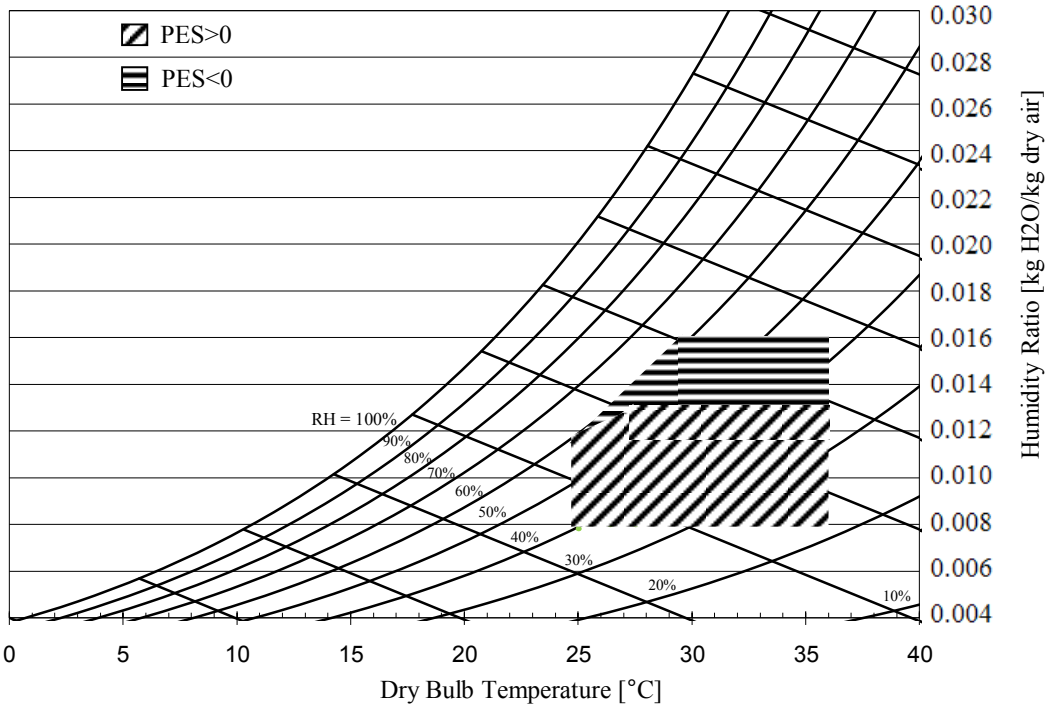

Fig. 3. 17: Psychrometric chart showing the area with PES <0 and that with PES >0

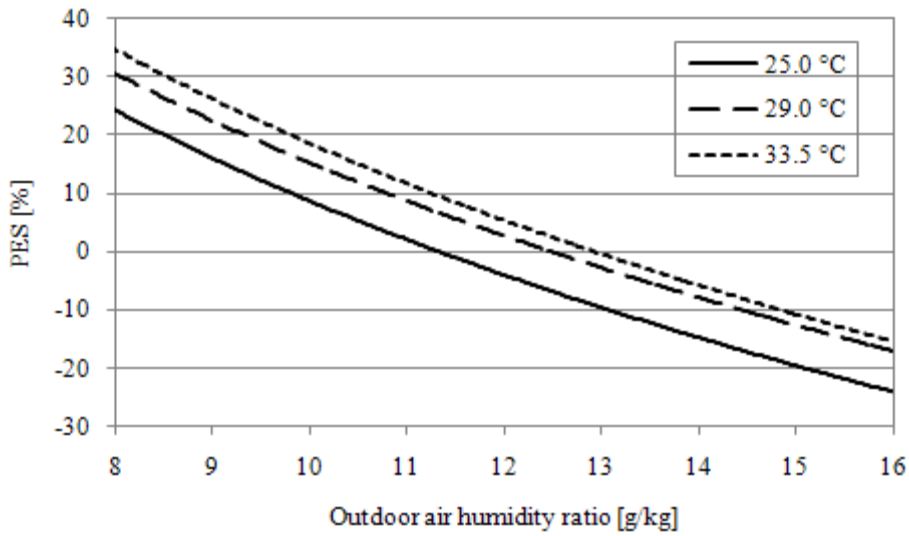

Fig. 3. 18: PES as a function of outdoor air humidity ratio for three different values of outdoor air temperature

3.3.3.3 Effect of MCHP partial load conditions

To point out the influence of MCHP partial load operation mode, Fig. 3. 19 shows $PES_{II\text{-}IIIb}$ and $\Delta CO_{2,II\text{-}IIIb}$ as a function of the electric power supplied by the MCHP (from 3 kW – chiller OFF, to 6 kW – chiller ON). It is possible to confirm that energy savings and avoided emissions of the

AS II, with respect to the desiccant based AHU with separate "production", AS IIIb, increase with electric power output of the MCHP itself.

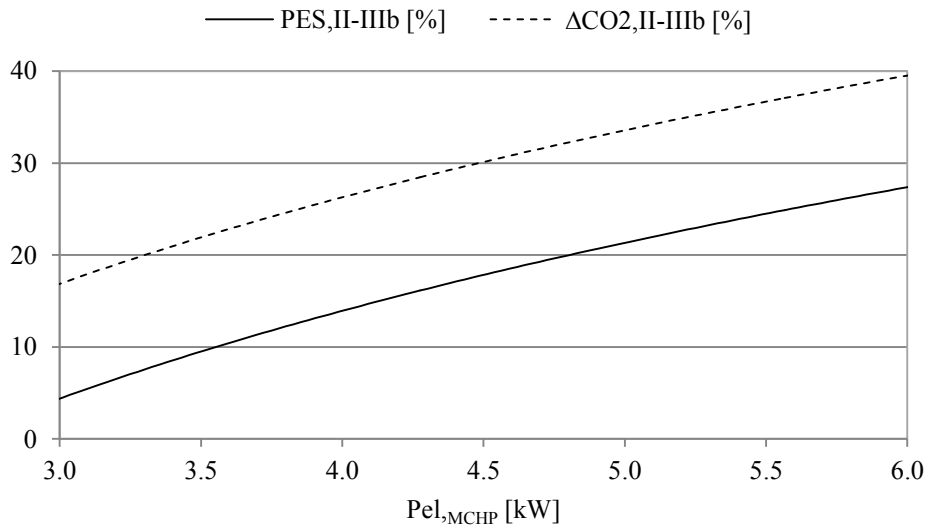

Fig. 3. 19: PES_{II-III} and $\Delta CO2_{,II-III}$ versus MCHP electric power

Further tests have been carried out to evaluate the influence of the partial load operation of the MCHP on the global energy performance in comparison with the conventional system. The net electric power for computers, lights, etc.., was gradually increased up to 1.5 kW to allow the full load of the cogenerator (for t_{out} = 29.5 °C and ω_{out} = 10.2 g/kg, the electric power supplied by the MCHP to the chiller and MCHP/AHU auxiliaries is about 4.5 kW).

Fig. 3. 20 shows that PES increases with the net electric power supplied to the final user, so it is convenient to operate the MCHP at full load for the maximum number of hours (PES of about 24%): this, in fact, causes an increase in the electric efficiency of the microcogenerator. Also in this case, the reduction in equivalent CO_2 emissions shows the same trend as PES; it achieves the maximum value (35%) at full load operation of the MCHP.

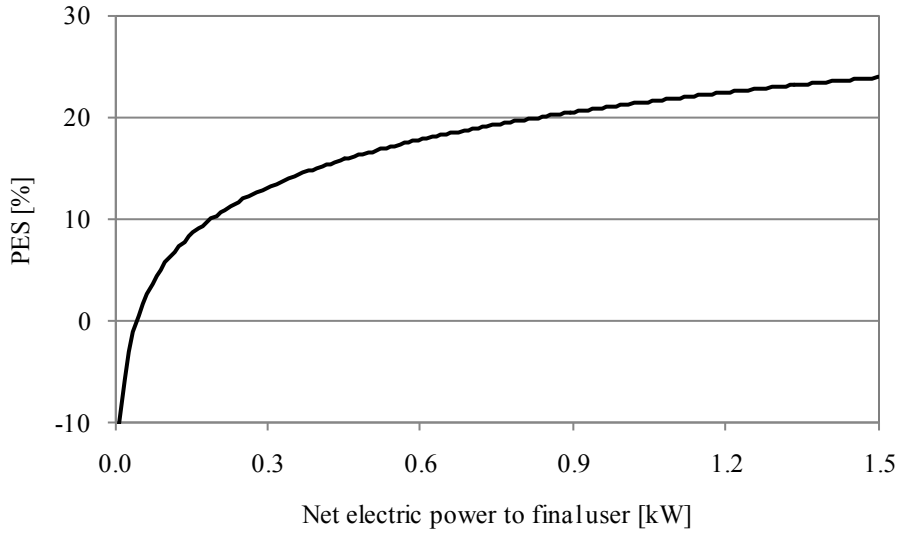

Fig. 3. 20: PES as a function of net electric power supplied to the final user

3.3.3.4 Effect of electric grid efficiency

As regards the influence of electric grid efficiency, in Fig. 3. 21, at constant operating conditions (reported in Tab. 3. 5), the influence of $\eta_{el,ref}$ on PES is reported. In the base case ($\eta_{el,ref}$ = 45.2%), PES is about 22%; then it increases with $\eta_{el,ref}$ reduction. Even if the electric energy "production" is based on the Best Available Technology (Gas Turbine Combined Cycle power plants, $\eta_{el,ref}$ = 0.58), PES remains positive (about 6%).

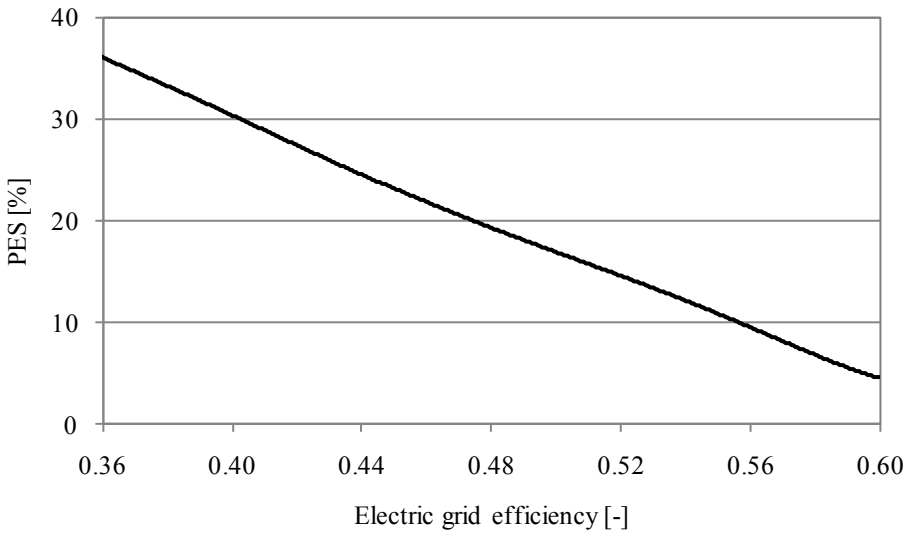

Fig. 3. 21: PES as a function of electric grid efficiency

Outdoor air temperature [°C]	Outdoor air humidity ratio [g/kg]	Supply air temperature [°C]	Supply air humidity ratio [g/kg]	Regeneration temperature [°C]
33.9	10.3	20.1	6.50	65.0

Tab. 3. 5: Operating conditions for the test of Fig. 3. 21

The PES values obtained in this work are in good agreement with quite similar polygeneration systems and operating conditions [43, 44].

3.3.3.5 The "POLILAB" application

In the framework of the project "Strumenti e tecnologie per l'efficienza energetica nel settore dei servizi", Università degli Studi del Sannio and Seconda Università di Napoli (SUN) cooperated with ENEA to the development of a Virtual Power Plant, aimed at the experimental analysis and the centralized remote control and thermo-economic optimization of the small scale polygeneration systems installed in the test facilities of the two mentioned universities, [118, 119].

To this aim, the software *POLILAB* has been developed.

In distributed energy systems, fuelled with both fossil and renewable energies, a central management unit (Energy Management System), with the aims of operating costs minimization, primary energy saving and reduction of climate-changing emissions, coordinates the operation of numerous distributed devices, interacting in a bidirectional way with different types of network (district heating and cooling, electric grid), according to a Virtual Power Plant (VPP) approach.

This approach has several advantages; in fact, linking distributed energy resources to a VPP makes their electricity output more predictable and controllable, favours the integration of renewable-based systems as well as CHPs, reducing grid losses due to transmission and distribution of energy over long distances.

Furthermore, it opens energy markets that could not be joined by individual devices. This could be the case of an Energy Service Company (ESCo), that may achieve significant primary energy savings from the centralized operation of distributed MCHPs, receiving energy efficiency credits (also known as white certificates) as well.

The optimal management of distributed generators from a unique central operator, particularly in residential and light commercial applications, is strictly bound to the following factors:

- an ESCo can draw its economic return by supplying and managing these systems;
- the design of a MCCHP system is very complex, due to the very large number of available technological combinations between direct and inverse machines;
- the difficulty in serving small scale users, characterized by uncertain and floating loads, as well as the interaction of polygeneration systems with external grids, make the optimization of such systems a very challenging task for the final user, in particular in residential and light commercial applications;

Furthermore, the remote control of distributed microgeneration systems will turn out necessary in the next future, in order to guarantee:

- optimal operating conditions for transmission and distribution electric grids, that would be highly vulnerable in a very probable and desirable scenario of a widespread diffusion of distributed generation technologies;
- the effective achievement of the community goals in terms of energy saving and emission reduction, on which the mechanisms for economic support of MG systems, that can at the moment allow to face the higher investment cost of such systems, are based.

The *POLILAB* software has the following features:

- it is possible to share among different operators (the researchers of ENEA, Università del Sannio and Seconda Università di Napoli, for the case of the ongoing project) the results of experimental tests, carried out to highlight the performances of single components or the whole system;
- it allows to remotely check if the systems are working in ranges of operating conditions that allow to obtain primary energy savings, emissions and energy costs reductions;
- it allows to remotely operate on MCCHPs to achieve the thermo-economic optimization of the distributed systems.

Due to the different type of equipments, devices and data acquisition softwares that in the next future will need a remote monitoring and control, in the first part of this project a widely diffused software for remote desktop has been used to access the local acquisition systems of the two test facilities.

This type of software has several advantages, e.g. it is widely diffuse, reliable and easy to use and it allows to access to the different data acquisition systems used in the two laboratories.

The last characteristic is very important in small scale applications, in which acquisition and monitoring softwares are based on different types of source code and cannot mutually interact.

In particular, at Università degli Studi del Sannio, the following three data acquisition softwares are currently installed in the test facility:

- the software *GecMon*, that allows to monitor and control the MCHP;
- the software *EcsWin*, that allows to monitor the electric consumption of the chiller and the auxiliaries and the electric power supplied by the cogenerator, [120];
- the *Labview*-based software *PoliLab_Unisannio*, that allows to monitor the thermal-dynamic properties in the MCHP/HVAC-DW system and to carry out energy balances on the main components, [121].

As regards the *GecMon* software, one of its most important feature allows to remotely control the operation of the microcogenerator; the central operator can start and stop the device, depending on boundary conditions, such as user's electric and thermal load, electric energy and fuel costs and so on.

As regards the *PoliLab_Unisannio* software, by means of several buttons in the main menu (Fig. 3. 22), it is possible to:

- view the thermodynamic and thermal-hygrometric properties of the fluids (air, water and natural gas) interacting with the MCHP/HVAC-DW system;
- evaluate energy performances of the main components: desiccant wheel, heating and cooling coils, MCHP, boiler and chiller;
- carry out a 3-E analysis, comparing the microcogeneration system with a user-defined reference system (it is possible to select the values of efficiencies, emission factors and energy costs).

Concerning this last feature, for example, by clicking on the button relating to the desiccant wheel, a new mask, referring to this component only, opens (Fig. 3. 23).

Fig. 3. 22: The main menu of the "PoliLab_Unisannio" software

Temperature, relative humidity and humidity ratio of process and regeneration air, upstream and downstream of the desiccant wheel, are shown in it, both as instant values and time trend. The dehumidification effectiveness is also shown.

The central or the local operator, thanks to these information, may modify the operating conditions of the desiccant wheel (e.g., varying the regeneration air temperature or flow rate and/or the rotational speed), in order to adequate the system to a change in the boundary conditions (e.g., a change in outdoor air conditions or in ventilation or internal latent loads).

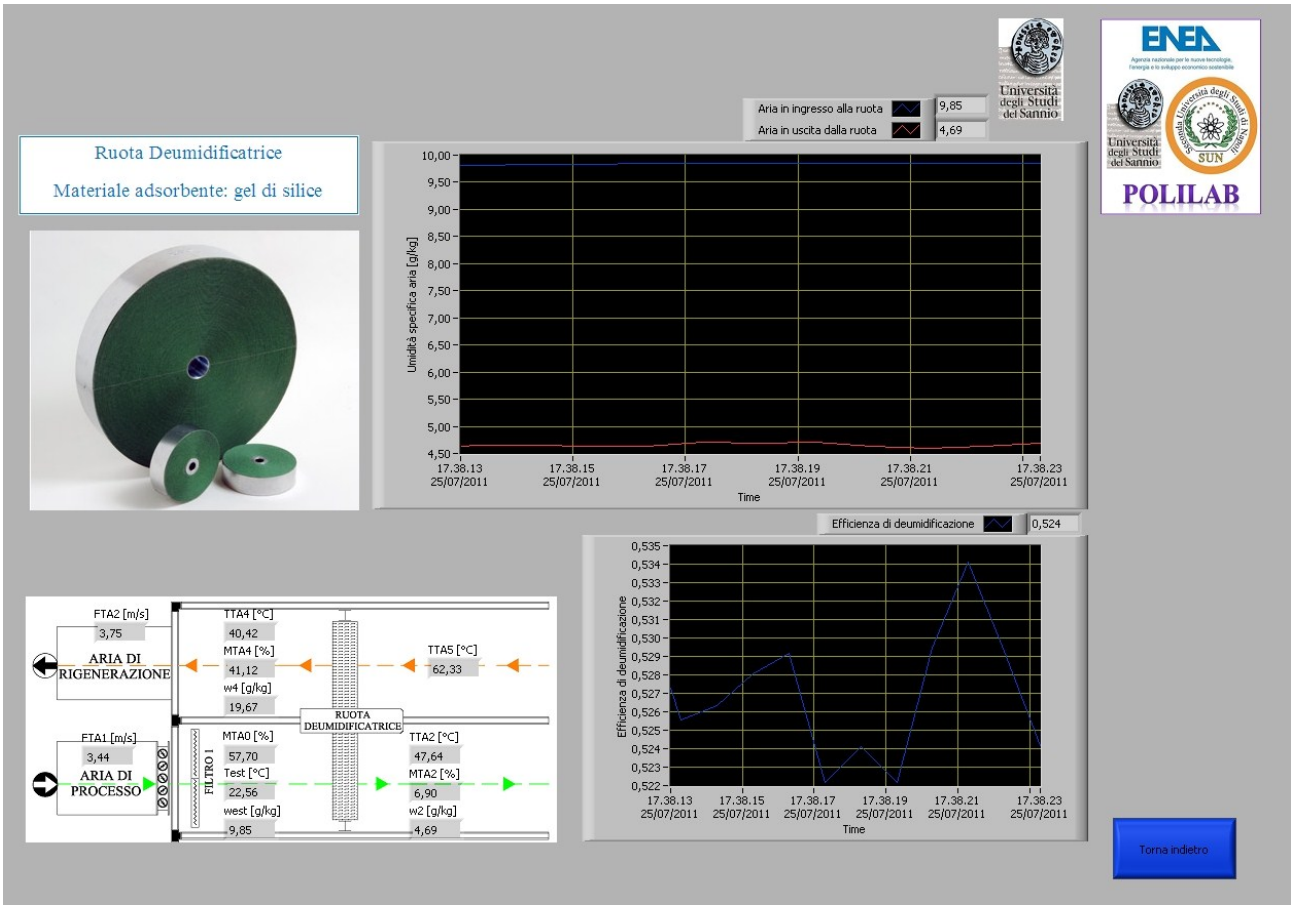

Fig. 3. 23: The desiccant wheel mask

Similar features are also integrated in the mask referring to the MCHP control volume, that for example allow to verify whether the cogenerator is working with satisfactory values of electric and thermal efficiency (Fig. 3. 24). In fact, as the analyzed MCHP is managed with an electric following approach and the electric efficiency strongly depends on the partial load ratio, it is necessary to operate the system so that it works at full load for most of the time.

In the MCHP mask, a button that allows to carry out a 3-E analysis is also present (see Fig. 3. 24). The 3-E mask is shown in Fig. 3. 25. There are several sliders, that allow to set the main energy parameters for the reference system (electric grid and boiler efficiency), the specific emission factors as well as the specific cost of energy carriers (natural gas and electricity).

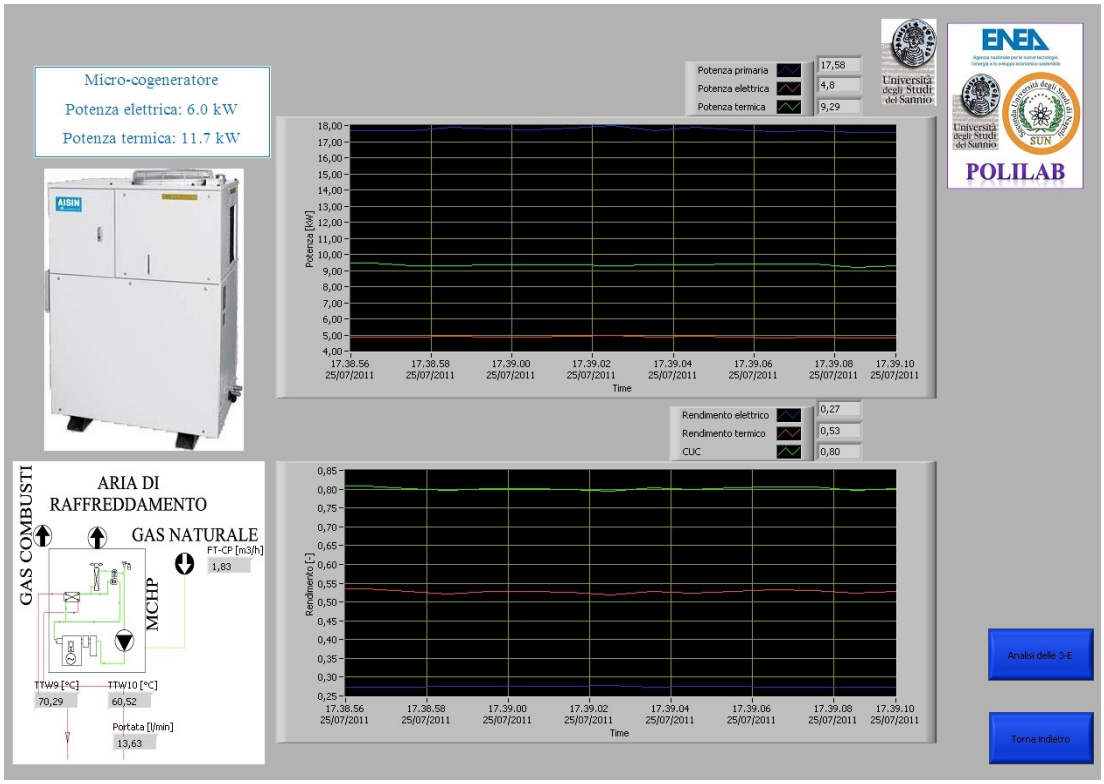

Fig. 3. 24: The MCHP mask

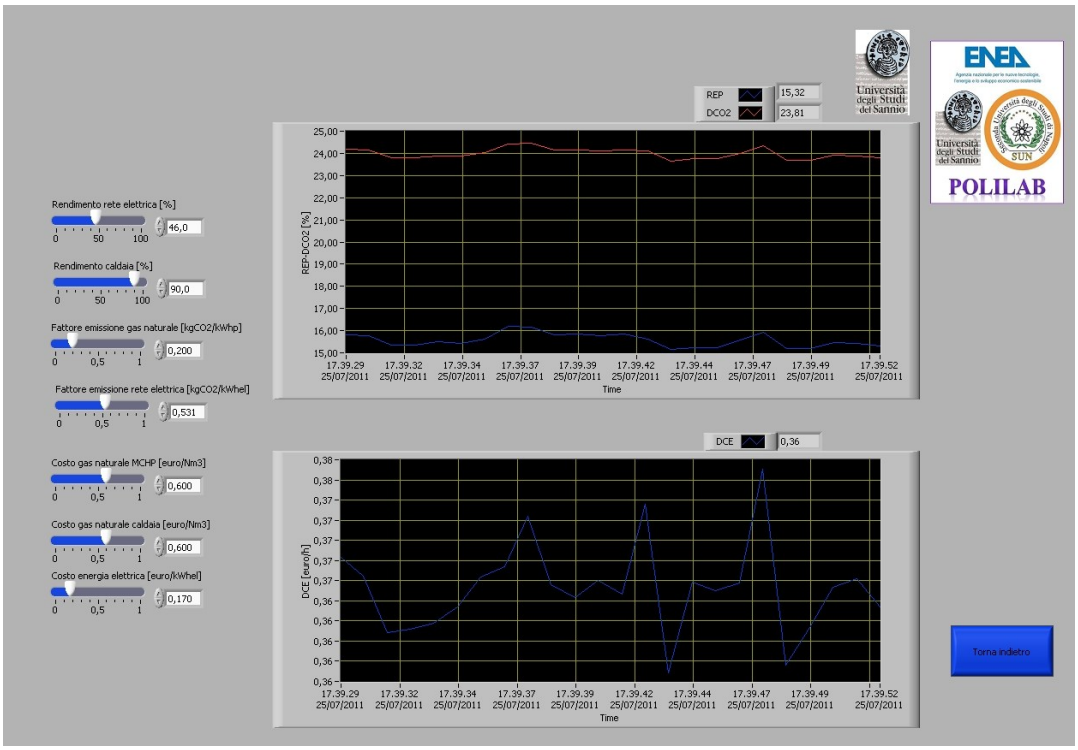

Fig. 3. 25: The 3-E analysis mask for the MCHP

The software elaborates in real-time the acquired data and provides the instant value and the time trend of the REP – Risparmio di Energia Primaria, that is the Italian equivalent of PES – the ΔCO_2 and the hourly difference in operating cost between MCHP and the separate "production" system.

3.4 Experimental analysis of a MCHP system at TUM

On April 2010, University of Sannio and Technische Universität München, in the framework of the Annex 54 project, started a cooperation on laboratory tests of small scale cogeneration systems.

The author of the present thesis worked on the following issues, [122]:

- getting familiar with the test facility, its hydraulic scheme, the *LabView* software for controlling the test bench and data acquisition;
- preparing the input data for the test bench measurements. Typical Italian demand profiles for space heating and Domestic Hot Water (DHW) were produced. They define type days for cold, cool and intermediate weather conditions;
- performing the measurements for the type days and the analysis of the experimental results.

3.4.1 The test facility

The Research Institute for Energy Economy (FfE e.V.) in cooperation with the Institute for Energy Economy and Application Technology (IfE) of TU Munich carried out a project to perform a comparison among residential small scale cogeneration systems. To this aim, a test facility, that allows to simulate space heating and DHW requirements of a residential user, represented by a Multi Family House (MFH), was realized. The test facility is equipped with different type of sensors (temperatures, flow rates, electric powers…) to evaluate the energy flows of the energy conversion systems.

Fig. 3. 26 shows the layout of the test facility and the control volumes (VC) that were considered to carry out energy balances.

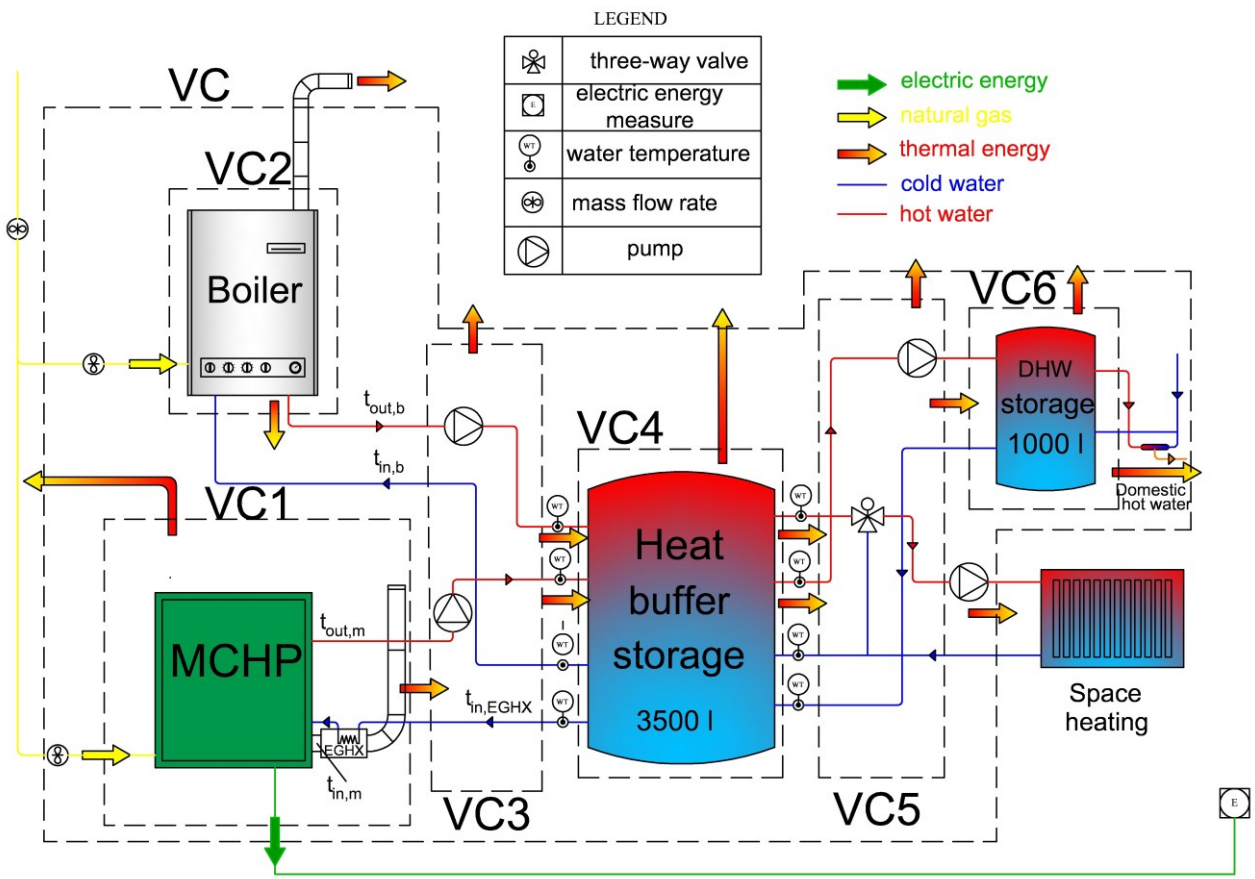

Fig. 3. 26: The test facility layout

The test facility has the following main components:

- an MCHP, VC1;
- an auxiliary boiler, VC2;
- a 3500 l thermal storage, VC4;
- a 1000 l thermal storage, VC6;
- a building simulation system, to simulate thermal energy requirements for space heating;

- a system for the simulation of thermal energy requirements for domestic hot water preparation;
- thermal energy distribution system and auxiliaries (pumps, three-way valves,…);
- air, natural gas and water sensors.

The control volume VC3 contains the pipes connecting the generation systems (MCHP and boiler) and the thermal storage in VC4, while the control volume VC5 contains the pipes connecting VC4 with VC6 and the space heating system. Finally, the overall control volume VC contains the whole test facility.

In accordance with Fig. 3. 26, both the MCHP and the boiler directly interact with the main thermal storage (VC4), from which thermal energy for the heating system and the 1000 l thermal storage is drawn. Finally, from VC6, thermal energy for the domestic hot water system is drawn.

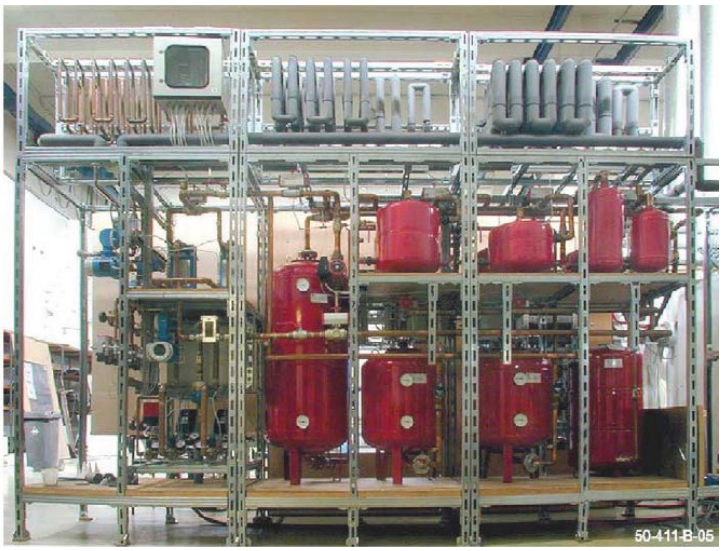

Fig. 3. 27: Building thermal load simulation system

The space heating thermal load simulation system is composed of several vessels, with different capacity, that simulate the thermal effects (thermal loads, inertia, thermal losses…) of the radiators and the distribution system (Fig. 3. 27). In particular, thermal energy related to thermal loads and losses is simulated by means of heat exchangers, that dissipate the heat interacting with a cooling circuit.

Thermal energy for DHW is instead simulated by means of pipes of different length and thermal insulation level, that simulate the distribution system of domestic hot water in the building; then, there are several taps, that draw hot water from the 1000 l thermal storage (Fig. 3. 28).

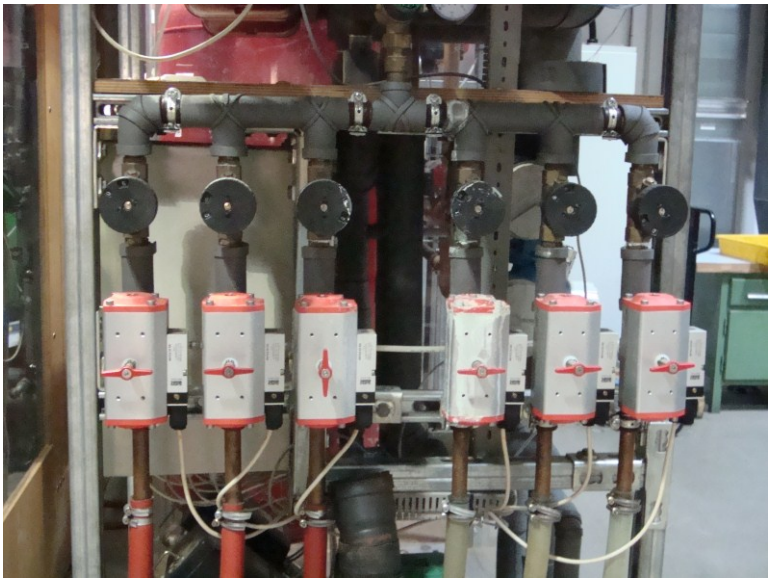

Fig. 3. 28: The taps for DHW requirements simulation

3.4.2 The SENERTEC DACHS Microcogenerator

The German manufacturer Senertec produces a cogeneration unit with 5.5 kW electric and 12.5 kW thermal power called Dachs (Fig. 3. 29), of which until now over 25,000 units has been installed in Europe, [123, 124]. The unit is based on a one-cylinder four-stroke Sachs engine; it has a displacement of 579 cm^3 and can be fuelled by natural gas, LPG, fuel oil or biodiesel.

The total efficiency at full load is about 90%. With an optional exhaust gas heat exchanger, the thermal output can be raised up to 14.8 kW, with a total efficiency almost unitary.

In particular, the tested model is the Dachs HKA G 5.5, fuelled with natural gas. The device is equipped with the optional exhaust gas heat exchanger (EGHX in Fig. 3. 26) that allows, with an inlet water temperature of 35 °C and an inlet exhaust gas temperature of 150 °C, to cool the exhaust gas down to about 55 °C, and to condense about the half of the water vapour contained, similarly to a condensing boiler.

Fig. 3. 29: Senertec Dachs HKA G 5.5

The analysed MCHP is designed for on-off operation, hence it cannot modulate the load. In Tab. 3. 6, technical characteristics of the Dachs are reported.

The MCHP is managed with a heat-led control system, while electricity can be locally consumed or exported to the grid; however, the management of the cogenerated electric energy does not affect the energy and emissions balances, but the economic analysis only, that is outside the aims of the current analysis.

As regards the thermal following control system of the MCHP, when the thermal storage temperature is below a set-point value, the microcogenerator starts and supplies thermal energy to VC4; when the storage temperature is above the set-point value, the MCHP stops.

A critical value for the thermal management of the system is the water temperature exiting the exhaust gas heat exchanger: if it is above 65°C, the MCHP automatically stops, as a so high return temperature denotes a poor thermal energy requirement of the user, and it is a common knowledge that energy and environmental benefits of cogeneration are strictly related to an

effective use of the recovered thermal energy. For this reason, the Senertec cogenerators are not equipped with an emergency radiator, differently from the AISIN.

Electrical power [kW]	5.5
Output voltage [V]	230
Thermal power [kW]	14.8
In/Out water temperature [°C]	70 – 83
Fuel	Natural gas
Power input [kW]	20.5
Engine type	Water cooled, 1 cylinder, 4 strokes
Engine displacement [cm^3]	579
Rated engine speed [rpm]	2530
Generator type	2 pole asynchronous generator
Depth [cm]	107
Width [cm]	72
Height [cm]	100
Weight [kg]	530
Electrical efficiency [%]	27.0
Thermal efficiency [%]	72.0
Overall efficiency [%]	99.0
Operating sound at 1 m distance [dB(A)]	52 – 56

Tab. 3. 6: Dachs microcogenerator characteristics

When thermal energy stored in VC4 is not sufficient to cover thermal energy needs for space heating and DHW and the MCHP is already working, the auxiliary boiler starts.

3.4.3 Building thermal energy requirements

It was assumed that the cogeneration plant is installed in a MFH with ten apartments, located in Naples.

In Tab. 3. 7 the characteristics of the final user are shown, while in Tab. 3. 8 the characteristics of the building envelope (area, U-value and solar gain g) are shown.

Heated living space [m^2]	1216
Heated building volume [m^3]	3176
Mean headroom [m]	2.61
Number of full storeys [-]	4
A/V ratio [-]	0.447
Period of construction	1961-1975
Number of occupants [-]	30
Space heating thermal energy requirement [kWh/m^2/year]	46.5
DHW demand [kWh/day]	42.9

Tab. 3. 7: User's characteristics

The reference year of operation was modeled by means of four type days, that represent the different climatic conditions that occur in Naples. The energy and emissions balances were then extended on an annual basis taking into account the number of days/year for each type day.

The following type days were identified:

- type day 1: winter (January and February);
- type day 2: intermediate with space heating needs (from 15 November to 31 December and March);
- type day 3: intermediate without space heating needs (April, May and from 16 September to 14 November);

- type day 4: summer (from 1 June to 15 September).

	Opaque devices			**Transparent devices**		
	Roof	*External walls*	*Cellar*	*N*	*S*	*E/O*
Area [m^2]	304	637	304	69	76	14
U [W/m^2K]	2.30	1.20	0.297	2.83	2.83	2.83
g [-]	-	-	-	0.76	0.76	0.76

Tab. 3. 8: Building envelope characteristics

In particular, the subdivision of the days of the year in the four type days was carried out taking into account the admissible heating period, [125], and the hourly temperature Meteonorm values, [126].

Thermal load profiles for the two type days in which there is a space heating requirement (type days 1 and 2, Fig. 3. 30) were obtained by simulating the building with the building interface (TRNBuild) of TRNSYS 17, [127].

The typical early-rising thermal power peak, when the temperature inside the building is increased to the desired value (20 °C), can be noted.

Afterwards, the thermal load decreases, reaching the minimum value in the central hours of the day, when solar radiation and outdoor temperature are at their maximum value.

To evaluate thermal energy requirement for DHW (shown in Fig. 3. 31 for type days 2 and 3), a consumption of 40 l/day per person and the load profiles in [128] were assumed.

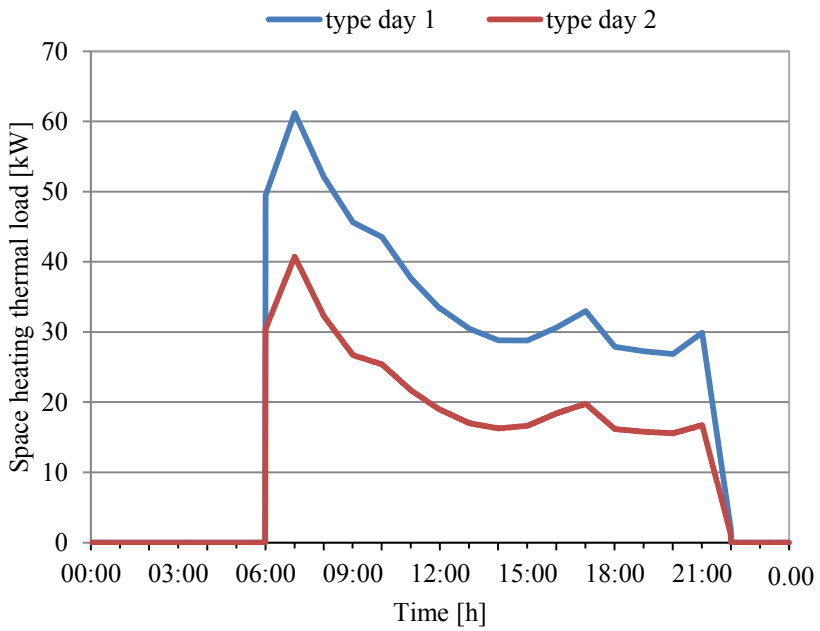

Fig. 3. 30: Thermal load profiles

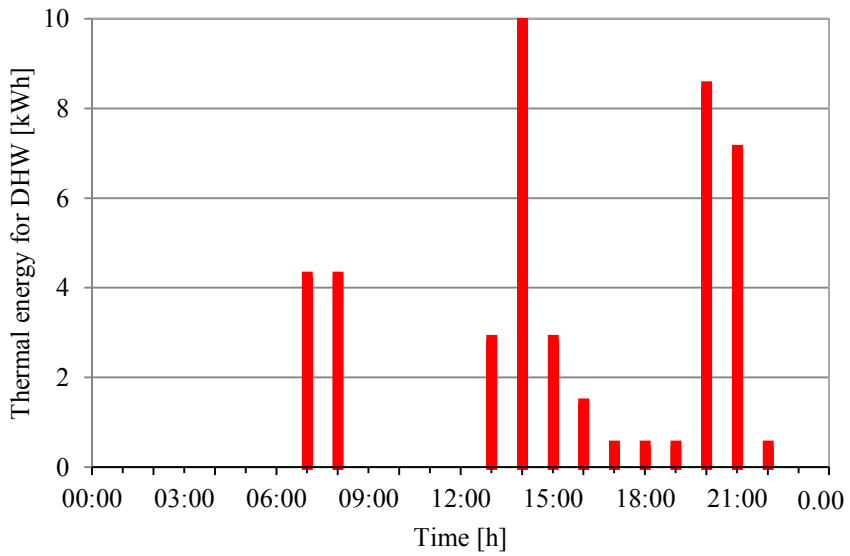

Fig. 3. 31: Thermal energy for DHW (type days 2 and 3)

3.4.4 Energy and environmental analysis

The National Instruments software *DIADEM*, [129], was used to elaborate the data acquired during the experimental tests.

In Fig. 3. 32a, thermal power supplied by the MCHP (with and without the heat recovery from exhaust gas, $Q_{th,m+EGHX}$ and $Q_{th,m}$, respectively) and by the boiler ($Q_{th,b}$), as well as primary and electric power of the cogenerator ($P_{p,m}$ and $P_{el,m}$, respectively) are shown for the type day 1.

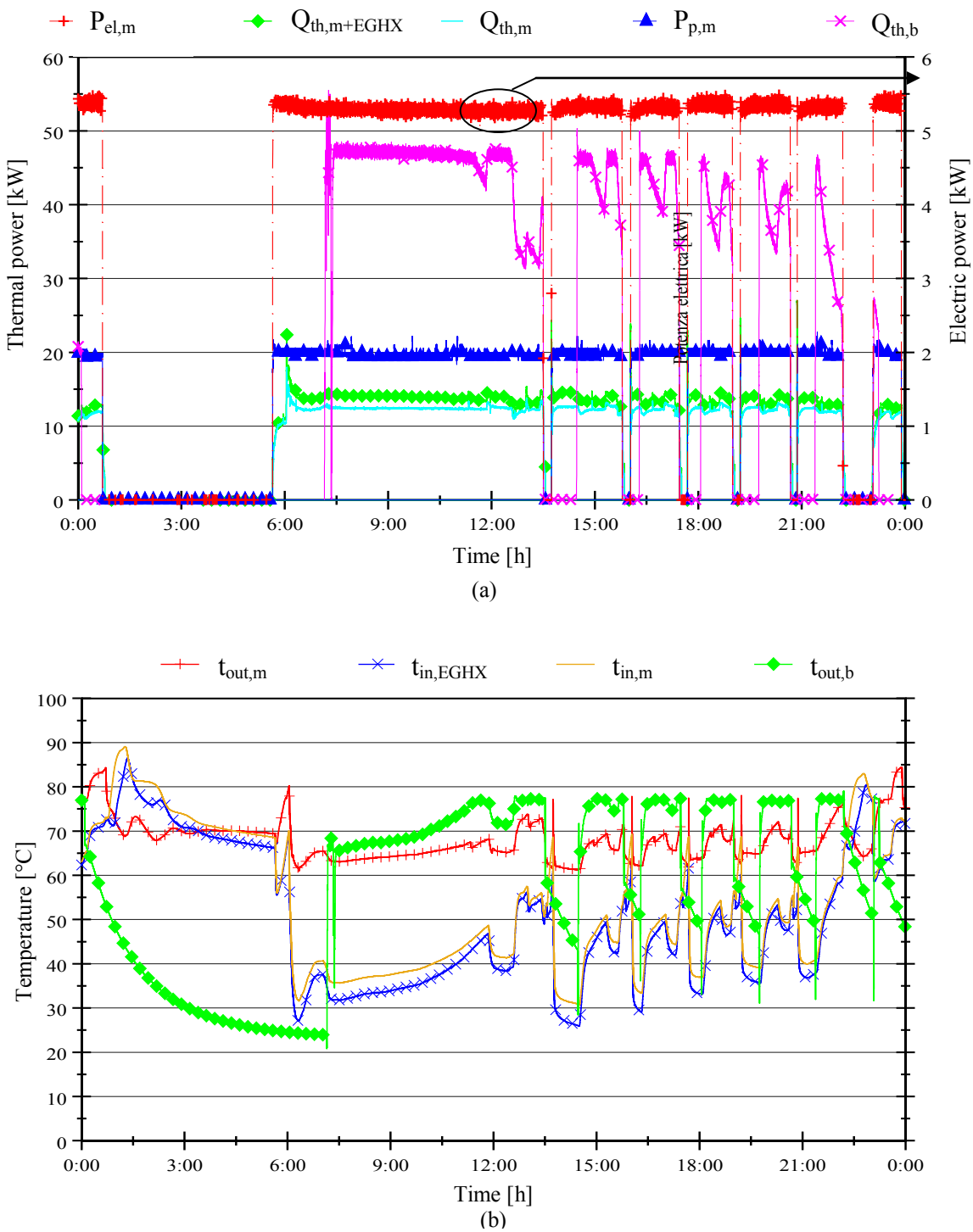

Fig. 3. 32: Power (a) and temperature (b) of MCHP and boiler for type day 1

The considerable contribution of the boiler, especially during the morning when there is a large need of thermal energy for space heating and DHW, should be noted.

The MCHP supplied an electric power steadily equal to about 5.3 kW; therefore, auxiliaries electric consumption can be estimated in about 200 W.

In Fig. 3. 32b, MCHP outlet and inlet temperatures ($t_{out,m}$ and $t_{in,m}$, respectively), boiler supply temperature ($t_{out,b}$), as well as water temperature entering the exhaust gas heat exchanger ($t_{in,EGHX}$) are shown, in this case also with respect to type day 1. The cogenerator provides, by means of the optional heat exchanger, an additional maximum rate of thermal power equal to 2 kW; moreover, this rate increases when $t_{in,EGHX}$ reduces, as the water condensation is favoured.

In Fig. 3. 33, the contribution of the two energy conversion devices (MCHP and boiler) to the overall thermal energy requirement for the four type days is shown. The boiler significantly contributes to the thermal need of the building during the type day 1, due to the large amount of thermal energy required for space heating purposes, while during type days 3 and 4 the boiler is inactive, as thermal energy is required for DHW only.

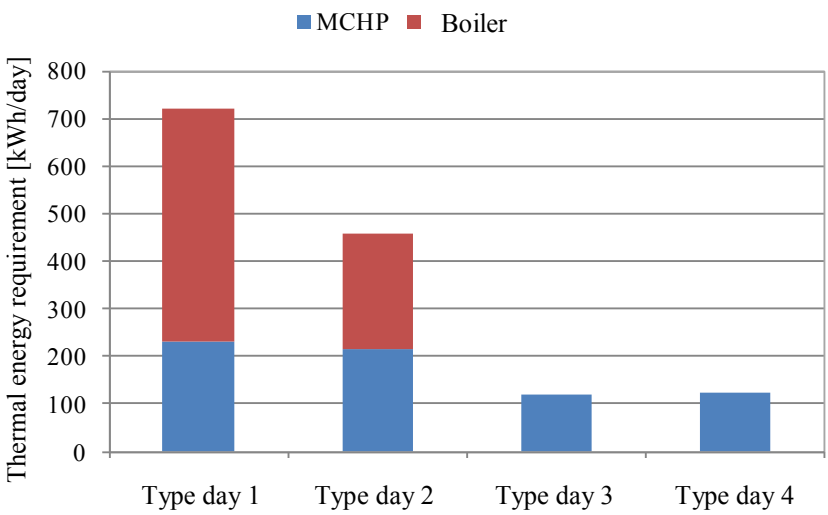

Fig. 3. 33: Contribution of the MCHP and the boiler to the overall thermal energy requirement

In Tab. 3. 9, energy balances with respect to a control volume including the MCHP only (VC1), are reported for each type day. The MCHP is able to achieve electrical, thermal and overall (PER) efficiency values quite comparable with the nominal ones; this is particularly true during

type days 1 and 2, in which the space heating thermal load implies a quite high number of operating hours (τ) in continuous and stationary conditions. Conversely, operating hours reduce during type day 3 and 4.

On an annual basis, PER is equal to 0.949.

	Type day 1	**Type day 2**	**Type day3**	**Type day 4**
E_p [kWh/day]	336	300	185	190
E_{el} [kWh/day]	89.8	82.0	50.0	51.5
E_{th} [kWh/day]	233	215	121	124
τ [h/day]	16.9	15.2	9.36	9.62
η_{el} [-]	0.267	0.273	0.270	0.271
η_{th} [-]	0.693	0.717	0.654	0.653
PER [-]	0.960	0.990	0.924	0.924

Tab. 3. 9: MCHP energy balance for the 4 type days

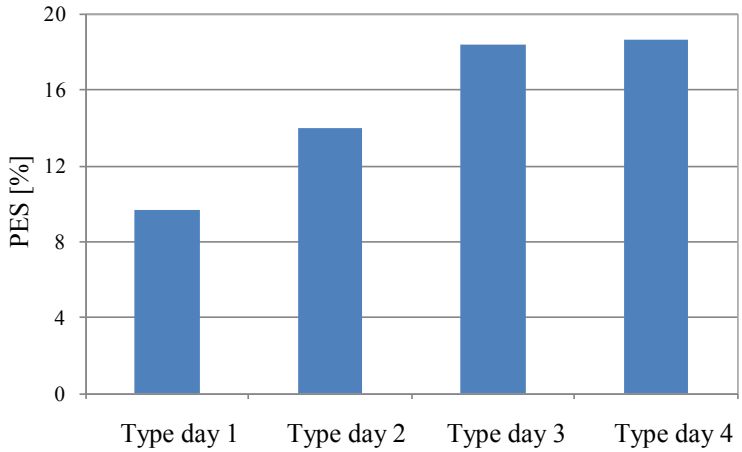

Fig. 3. 34: PES for the 4 type days

On the basis of the experimental results, the microcogeneration plant (that represents the alternative system, AS) was compared, in terms of energy and environmental performance, with a conventional reference system (CS). In the latter, a condensing natural gas boiler ($\eta_{th,ref}$ = 102%, equivalent CO_2 emission = 0.200 $kgCO_2/kWh_p$) is used for space heating and DHW purposes, while electric energy is drawn from the grid ($\eta_{el,ref}$ = 46.0%, [105], equivalent CO_2 emission = 0.531 $kgCO_2/kWh_{el}$, [108]).

In Fig. 3. 34, the PES for each type day is shown. It is positive for all type days and varies form 9.6% for type day 1 (winter) to 18.6% for type day 4 (summer). In particular, the PES has the minimum value for type day 1 due to the considerable contribution, in terms of thermal energy, of the boiler in the alternative system and to the high primary energy consumption of both AS and CS. On the contrary, during type days 3 and 4, the auxiliary boiler in the alternative system is inactive, and this allows to maximize the energy benefits of cogeneration. On an annual basis, PES is equal to 14.0%.

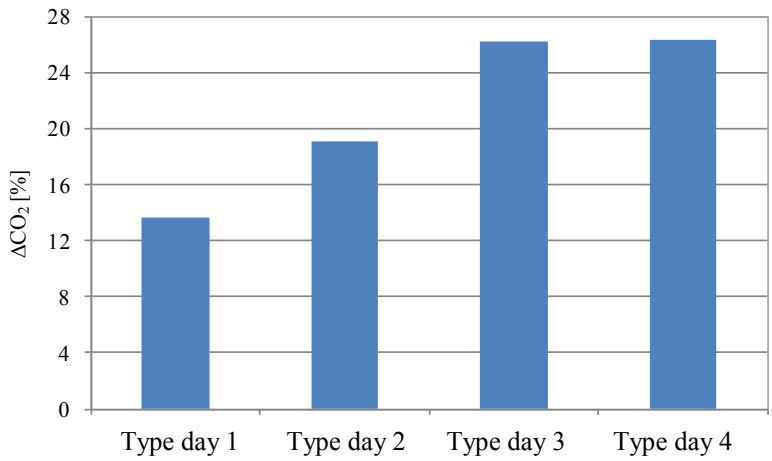

Fig. 3. 35: ΔCO_2 for the 4 type days

In Fig. 3. 35, the ΔCO_2 for each type day is shown. Considerations similar to Fig. 3. 34 can be made. The equivalent CO_2 avoided emissions range from 13.6% (type day 1) to 26.4% (type day 4) and achieve an annual value of 19.8%.

These results justify the European Union interest towards small scale cogeneration, in particular in residential applications, as it could significantly contribute in achieving the EU emissions reductions goals towards 2020.

In order to promote cogeneration, [69], the European Commission specifies, in [89], a method to calculate reference efficiencies values for the separate "production" of electric and thermal energy. In particular, $\eta_{el,ref}$ depends on the installation year of the MCHP, the burned fuel, the climatic conditions (average temperature of the country) as well as the avoided electric grid losses. Regarding the last parameter, correction factors, that depend on the voltage level and the ratio between self-consumed and exported rates of electric energy, are introduced.

The analysed MCHP uses natural gas as input fuel, it is assumed to be installed in 2011 and connected to the low voltage grid (< 400 V). Average temperature for Italy is 18 °C.

Concerning $\eta_{th,ref}$, it depends on the type of fuel and heat recovery (direct use of exhaust gas or hot water/steam production). For the analysed case, $\eta_{th,ref} = 0.90$.

The European Directive also uses PES in order to evaluate whether a CHP device can be classified as a high efficiency cogenerator; this qualification allows it to comply with several incentive mechanisms, such as the net metering, a very profitable method to manage the eventual electricity surplus.

The PES introduced by the Directive is defined as:

$$PES = 1 - \frac{E_{p,m}}{\frac{E_{el,m}}{\eta_{el,ref}} + \frac{E_{th,m}}{\eta_{th,ref}}} \tag{3.20}$$

Unlike the PES shown in Fig. 3. 34, in this case energy flows related to the MCHP are only involved in the calculation; the auxiliary boiler is not considered.

Regarding the amount of electric energy to introduce in the PES calculation ($E_{el,m}$), it does not necessarily correspond with the overall production, but this only happens if the annual PER of the system is above a threshold value (75% for RIC engine based cogenerators). The analysed MCHP achieves an annual PER of about 95%, therefore the whole electric energy produced (23.3 MWh) is produced in cogeneration.

In Fig. 3. 36, the PES as a function of the ratio between self-consumed and overall electric energy produced by the MCHP is shown.

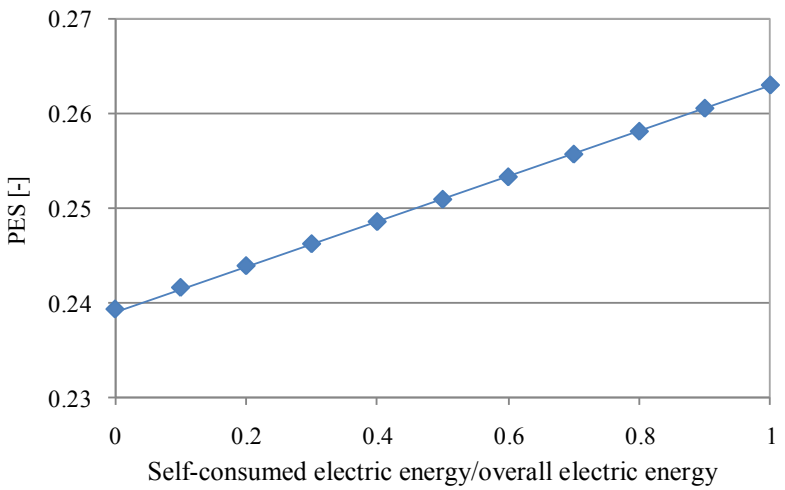

Fig. 3. 36: Primary Energy Saving as a function of the ratio between self-consumed and overall electric energy

The Directive establishes that CHPs with an electric power lower than 1 MW can be considered as high efficiency cogenerators if PES > 0. This condition is widely achieved for the considered system, as the Primary Energy Saving is higher than 24%. Furthermore, it increases when the rate of self-consumed electricity rises, as the correction factors for $\eta_{el,ref}$ are lower when the cogenerated electric energy is utilized on-site, instead of exported to the grid, in order to take into account the energy losses on the electric network, due to electric energy transmission.

In conclusion, the MCHP system considered, as the PES is positive, can comply with several advantages (tax exemption, net metering, energy efficiency credits, priority distribution) that can favour it also from an economic point of view, besides energy and environmental benefits.

CHAPTER 4: MODELLING AND SIMULATION ACTIVITY

The development of a simple and reliable model for the analysis of a desiccant-based AHU and its main components can lead to useful conclusions as regards the effect of the various operating parameters, namely, regeneration temperature, outdoor air temperature and humidity ratio, partial load ratio of the MHCP and so on. Moreover, such models can be used in whole-building simulation software, e.g. TRNSYS, in order to estimate annual energy and environmental performance of desiccant-based AHU, thermally activated by different energy sources (solar energy, thermal wastes…). This simulation activity is the main topic of the International Energy Agency Annex 54, in which the author is involved.

In this chapter, an overview of the TRNSYS software, used to simulate the polygeneration system, is provided; therefore, models for the main components of the MCHP/HVAC-DW system, drawn from the literature or used by the software itself, are calibrated and validated, starting from experimental tests and/or manufacturer's data, [130].

Finally, the operation and performance of a solar desiccant cooling system and the MCHP/HVAC-DW one were simulated.

4.1 TRNSYS overview

TRNSYS is a component-based, transient simulation software originally developed by the University of Wisconsin's Solar Energy Lab and the University of Colorado's Solar Energy Applications Lab in the 1970s, [127]. It is used by engineers and researchers around the world to validate new energy concepts, from simple domestic hot water systems to the design and simulation of buildings and their equipments, including control strategies, occupant behavior, alternative energy systems (wind, solar, photovoltaic, hydrogen systems), etc.

The program calls FORTRAN subroutines to represent each modeled component. The process is iterative, with components called in a predetermined sequence for a set number of iterations or until the convergence tolerance is met. The Simulation Studio allows to build the model, automating the process of linking component outputs and inputs.

TRNSYS features an internal standard library of components for different applications, such as outputs (printers and plotters), links to various external program (e.g., Matlab, EES and Excel) as

well as models of HVAC components, electronics, hydronics and many more. In addition to this default library, the distributor Thermal Energy System Specialists (TESS, [131]) has an extensive library of improved, modified and additional components.

Finally, the user can develop new components or modify existing ones. In fact, one of the key factors in TRNSYS success is its open, modular structure. The source code of the kernel as well as the component models is delivered to the end users. This simplifies extending existing models to make them fit the user's specific needs. Therefore, the architecture allows users and developers to easily add custom component models.

TRNSYS allows to model the building too. The building software bundled with TRNSYS is called TRNBuild, that links with the Simulation Studio through the Type 56 component. The TRNBuild software, that was used in section 3.4.3 to derive building thermal energy requirements, models buildings as a collection of zones. Each one has a volume, a thermal capacitance and boundary conditions (wall materials, adjacencies, ventilation and infiltration rates, orientation). Furthermore, zones can be given gains, scheduled or constant, to simulate the thermal gains caused by occupancy and use.

In any simulation requiring weather data, TRNSYS has a component to read a TMY (Typical Meteorological Year) file, with Meteonorm climate data provided by the US National Renewable Energy Lab (NREL) and derived from data collected between 1961-1990. Therefore, simulations can be performed using the typical weather patterns of various international locations for which data has been collected.

4.2 Models of desiccant-based AHU components

In several papers, available existing models are used in order to estimate the performance of desiccant-based air conditioning systems, in which the operation of each subsystem is described by a specific efficiency factor. However, few of them carry out an experimental calibration and validation of these models, and with reference to conventional layouts only, i.e. with two air flows (process and regeneration) crossing the AHU.

For example, in [132], a theoretical model is presented for the operation of a conventional desiccant air-conditioning system, developed on the basis of existing approaches for the main

subsystems of such a device. The model is experimentally validated on a real scale system, through a significant number of measurements.

In [133], a model of a desiccant air handling unit is presented and experimentally validated, with respect to conventional and recirculation configuration.

In other papers, modeling activity is focused only on main components, e.g. the desiccant wheel and the air-to-air heat exchanger. For example, in [35], an experimental validation of a simplified approach for a desiccant wheel model, based on the concept of the analogy method and the formulation proposed by Jurinak, is presented.

In [134], a model of the sensible heat regenerator and the desiccant wheel, inserted in a desiccant evaporative cooling system, is presented and experimentally validated. The approach of Kays and London and Maclaine-Cross and Banks is used.

In other papers, nominal or typical constant efficiency factors are a priori assumed for the aforementioned models.

In [135], a methodology is proposed for the definition of a solid desiccant air-conditioning system achievable working range, under a specific set of comfort requirements. Steady typical values are assumed for the desiccant wheel and rotary heat exchanger effectiveness.

In [136], a heat pump incorporating an active desiccant wheel and evaporative cooler is presented. An hour-by-hour energy comparison with a conventional mechanical dehumidification system is performed. Typical values for cooling and heating coils, sensible heat exchanger and evaporative cooler effectiveness are assumed; effectiveness of the wheel are pre-determined by detailed finite difference equations.

In [137], the performances of a solar assisted heating and desiccant cooling system for a domestic residence located in Baghdad are evaluated by means of a computer simulation. Typical values for the effectiveness of heat exchanger and evaporative cooler are used; as regards the desiccant wheel, three effectiveness values are selected, referring to good, medium and poor dehumidification performances.

In [138], a desiccant cooling system, in combination with chilled ceiling panels, is presented. Primary energy consumptions are calculated with a building energy simulation code. Psychrometric processes are calculated with constant effectiveness assumptions for various

equipments. A constant effectiveness is selected for sensible heat wheel and evaporative coolers. For desiccant wheels, effectiveness values at the optimum rotary speed are used.

In this section, well known models, drawn from the literature, for all components of an unconventional desiccant-based AHU, are calibrated and validated, starting from several experimental tests; furthermore, the validity of the assumption for efficiency factors presenting constant values was experimentally investigated, for a range of typical conditions for the air-conditioning applications. The validated models are then used to investigate the performance of both the desiccant wheel and the whole AHU.

During the experimental calibration, the following operating variables were regulated:

- the regeneration temperature of the desiccant wheel, t_{reg};
- the temperature of water entering the coils interacting with the MCHP, the boiler and the chiller, t_{w1}, t_{w3} and t_{w5}, respectively (see Fig. 2. 2).

The variation range of the above operating variables and outdoor air temperature, t_{out}, and humidity ratio, ω_{out}, are shown in Tab. 4. 1. The process, regeneration and cooling air flow rates are equal to their nominal value in each test (balanced flow rates = 800 m^3/h).

	t_{out} [°C]	ω_{out} [g/kg]	t_{reg} [°C]	t_{w1} [°C]	t_{w3} [°C]	t_{w5} [°C]
Min	23.8	8.16	51.0	59.9	7.44	59.7
Max	35.6	16.0	70.2	73.2	18.8	72.0

Tab. 4. 1: Range of the experimental test

The subsystems of the AHU for which a constant efficiency model has been experimentally validated are: the Direct Evaporative Cooler (DEC), the cross-flow air-to-air heat exchanger, the cooling coil, the heating coils and the desiccant wheel.

4.2.1 The Direct Evaporative Cooler

The Direct Evaporative Cooler of the hybrid AHU is a humidifier in which humidification is obtained by the evaporation of the water that is circulated within static elements of alveolar carton

material through which the air is blown. The air flowing through the humidifier supplies the required energy for water evaporation, such that it comes out cooled and humidified.

If there are no thermal losses to the environment, the process can be considered adiabatic and the wet bulb temperature of air remains steady. In this case, a useful quantity for expressing the performance of the evaporative cooler is its efficiency in terms of temperature, [50] (see also equation 3.6):

$$\eta_{dec} = \frac{t_1 - t_8}{t_1 - t_{1,wb}} \tag{4.1}$$

4.2.2 The cross-flow air-to-air heat exchanger

For the description of the operation of the cross-flow air-to-air heat exchanger, the NTU-effectiveness method has been used, [139] (see also equation 3.7):

$$\varepsilon_{cf} = \frac{Q_{th}}{Q_{th,max}} = \frac{C_{proc}\left(t_2 - t_3\right)}{C_{min}\left(t_2 - t_8\right)} \tag{4.2}$$

where C_{proc} is the capacity rate of process air flowing through the heat exchanger, while C_{min} is the minimum between C_{proc} and C_{cool}, the latter being the capacity rate of cooling air flowing through the heat exchanger.

Capacity rates have been calculated assuming constant value for the specific heat of air and water (1.01 and 4.19 kJ/kgK, respectively).

According to NTU-effectiveness approach, it could be noted that, within the analyzed range of operating conditions, the effectiveness should remain constant.

4.2.3 The cooling coil

A cooling coil is a device that dehumidifies and cools the air that flows in the vicinity of the tubes containing a colder liquid. Energy is transferred from the former to the latter; water vapour is removed as it condenses from the air stream and flows out of the coil. A common method for

modeling a cooling coil is to split the air stream that passes across the coil in two parts. One part of the air stream comes in perfect contact with the coils themselves and exits in a saturated condition at the temperature, supposedly uniform, of the surface of the cooling coil (t_{sur}). The other part of the air stream (the "bypass fraction") does not come in contact with the coil but bypasses it and mixes with the fraction of the air stream that effectively passes through the coil. The bypass fraction is therefore:

$$F_{bp} = \frac{h_4 - h_{sur}}{h_3 - h_{sur}} \tag{4.3}$$

where h_{sur} is the enthalpy of humid air, in a saturated condition, at the temperature t_{sur}.

For the actual desiccant-based AHU, the cooling coil only cools the process air, while it does not modify the humidity ratio of incoming air; for this case, F_{bp} can be expressed by:

$$F_{bp} = \frac{t_4 - t_{sur}}{t_3 - t_{sur}} \tag{4.4}$$

As regards t_{sur}, it has been assumed equal to the logarithmic mean temperature of chilled water flowing through the cooling coil, therefore the conductive resistance of the tubes has been neglected.

4.2.4 The desiccant wheel

Detailed models of the desiccant wheel, accounting for heat and mass transfer transport phenomena, have been investigated by many researchers over the years [23, 140]. In this work, both the approaches of Maclaine-Cross and Banks and Beccali et al. (Psychrometric model) have been used.

4.2.4.1 Maclaine-Cross and Banks model

This approach models the dehumidification process, a combined heat and mass transfer process, in analogy with a simple heat transfer process, [141]. Equations for coupled heat and mass transfer are reduced to two uncoupled differential equations of two independent variables called characteristic potentials, F_1 and F_2.

The discussion about the nature of these potentials is quite difficult and it is out of the scope of this work, but it can be stated that constant F_1 lines coincide with constant enthalpy lines, while constant F_2 lines coincide with constant relative humidity lines in the psychrometric chart, [142].

The potential functions depend on thermal-hygrometric properties of air and thermo-physical properties of the wheel, especially the desiccant material, [143].

Jurinak, in [142], has expressed such a relation for the working pair air-silica gel, defining the model presented below:

$$F_{1,i} = \frac{-2865}{(t_i + 273.15)^{1.49}} + 4.344(\omega_i/1000)^{0.8624} \tag{4.5}$$

$$F_{2,i} = \frac{(t_i + 273.15)^{1.49}}{6360} - 1.127(\omega_i/1000)^{0.07969} \tag{4.6}$$

The intersection of constant potential lines gives the outlet conditions of process air in the ideal case, i.e. assuming that both the adsorption and the desorption process are isenthalpic.

Then actual outlet conditions are estimated using two effectiveness indices of the wheel, η_{F_1} and η_{F_2}, calculated in analogy to the efficiency of a heat exchanger:

$$\eta_{F_1} = \frac{F_{1,2} - F_{1,1}}{F_{1,6} - F_{1,1}} \tag{4.7}$$

$$\eta_{F_2} = \frac{F_{2,2} - F_{2,1}}{F_{2,6} - F_{2,1}} \tag{4.8}$$

In particular, η_{F_1} represents the degree to which the process approximates the adiabatic one, while η_{F_2} represents the degree of dehumidification, [142]. If η_{F_1} = 0 and η_{F_2} = 1, the dehumidification process is ideal, i.e. it is adiabatic and there is a maximum dehumidification level for the assigned geometry and flow conditions.

If the values of η_{F_1} and η_{F_2} are known, then temperature and humidity ratio of the processed air exiting the wheel can be evaluated.

4.2.4.2 Psychrometric model

Psychrometric model, developed by Beccali et al., [31, 32], is based on the observation that RH and enthalpy can be expressed through a linear correlation of the following type:

$$\Delta RH = (RH_1 - RH_2) = m(RH_1 - RH_6) + q \tag{4.9}$$

$$\Delta h = (h_2 - h_1) = m'(h_6 - h_1) + q' \tag{4.10}$$

where RH is measured with relative humidity sensors and enthalpy is evaluated by means of eq. 2.2.

Once the values of *m*, *m'*, *q* and *q'* have been determined, the system of equations 2.1, 2.2, 4.9 and 4.10 can be solved to calculate outlet absolute humidity (ω_2) and temperature (t_2).

4.2.5 The heating coil interacting with the MCHP

As for the cross-flow heat exchanger, the NTU-effectiveness method has been used, [139]:

$$\varepsilon_{hc,m} = \frac{Q_{th}}{Q_{th,max}} = \frac{C_{reg}(t_5 - t_1)}{C_{min}(t_{w1} - t_1)} \tag{4.11}$$

where C_{min} = min (C_{reg}; C_w), C_{reg} is the capacity rate of regeneration air flowing through the heat exchanger and C_w is the water heat capacity.

4.2.6 The heating coil interacting with the boiler

Also for the description of the operation of the heating coil interacting with the boiler, the NTU-effectiveness method has been used, [139]:

$$\varepsilon_{hc,b} = \frac{Q_{th}}{Q_{th,max}} = \frac{C_{reg}(t_6 - t_5)}{C_{min}(t_{w5} - t_5)} \tag{4.12}$$

where C_{reg} and C_{min} are the same as in the heating coil interacting with the MCHP model.

Two different values of the boiler heating coil efficiency have been considered, $\varepsilon_{hc,b1}$ and $\varepsilon_{hc,b2}$. The former is valid when the MCHP is off, the latter when the MCHP is on. In fact, as will be shown in the results section, the boiler heating coil efficiency obtains a different value whether or not the microcogenerator works.

4.3 Calibration and validation of subsystems and complete AHU models

To calibrate and validate the presented above models, the whole data set has been divided in two equal subsets: the former has been used for the calibration, the latter for the validation of the models.

The present section experimentally investigates the assumption of constant efficiency factors for the above described models within the range of operating conditions that covers the available experimental data.

In the model calibration effort, for each subsystem, the average value of the selected efficiency factor is calculated, [132], for each test included in the calibration data subset. Efficiency average values, together with the standard deviation, are presented in Tab. 4. 2 for all analyzed subsystems.

The values of standard deviations are rather low, suggesting the plausibility of the constant efficiency hypothesis.

In particular, other studies experimentally validated the constant efficiency model for a DEC [132, 144]: in the former, a value of η_{dec} (0.65) comparable to the one obtained in the present study is presented, while in the latter, the efficiency of an evaporative cooler during a whole day of test is shown. Fluctuations are evident only in transient conditions.

In [35, 132], the constant efficiency model for a DW is experimentally validated. In this case also, the values of η_{F_1} (0.15) and η_{F_2} (0.69) are in agreement with the ones obtained in this work.

Component		Average Value	Standard deviation
Direct evaporative cooler	η_{dec} [-]	0.551	0.0917
Cross-flow heat exchanger	ε_{cf} [-]	0.446	0.0325
Cooling coil	F_{bp} [-]	0.177	0.0140
Desiccant wheel	η_{F_1} [-]	0.207	0.0460
	η_{F_2} [-]	0.717	0.0478
MCHP heating coil	$\varepsilon_{hc,M}$ [-]	0.868	0.0119
Boiler heating coil	$\varepsilon_{hc,B1}$ [-]	0.842	0.00572
	$\varepsilon_{hc,B2}$ [-]	0.582	0.0462

Tab. 4. 2: Average value and standard deviation for the subsystems efficiency factors

Moreover, in [132, 134, 144, 145], the validity of the constant efficiency model for an air-to-air heat exchanger (even for the rotary type) is also confirmed, but higher values of ε_{cf} are obtained, probably because return air, which is cooler than outdoor air, is used to pre-cool the process air.

As regards the psychrometric model of the desiccant wheel, the available experimental data have been used to determine the parameter *m*, *m'*, *q* and *q'* introduced with eqs. 4.9 and 4.10.

In Fig. 4. 1 the measured values of (RH_1-RH_2) and (RH_1-RH_6) are shown, while in Fig. 4. 2 the measured values of (h_2-h_1) and (h_6-h_1) are reported. From these two figures, the following values of the parameters introduced by the psychrometric model can be derived: m = 0.942, q = -1.859, m' = 0.335, q' = -4.024.

It should be noted, however, that in this case the linear model is not a very good approximation of the enthalpy change through the DW, as shown by the quite low value of the determination coefficient in Fig. 4. 2.

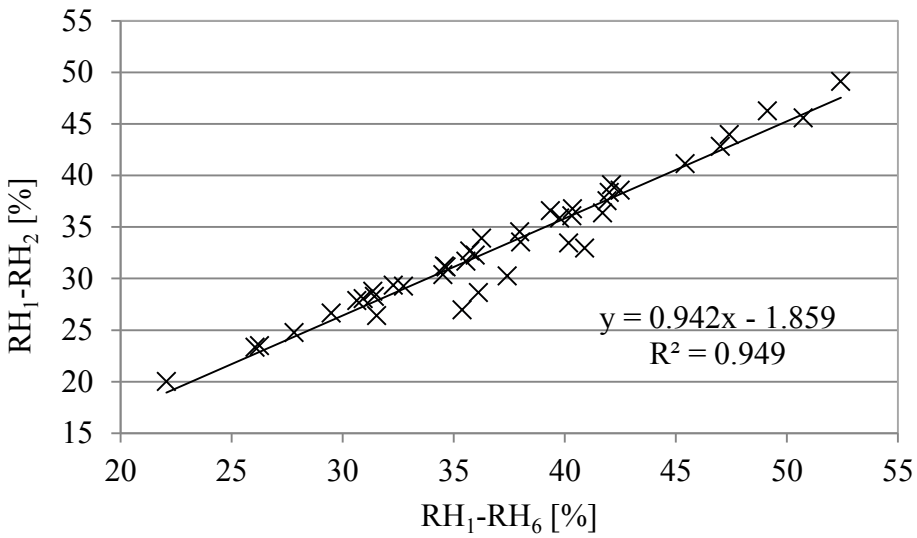

Fig. 4. 1: Measured values of (RH_1-RH_2) and (RH_1-RH_6)

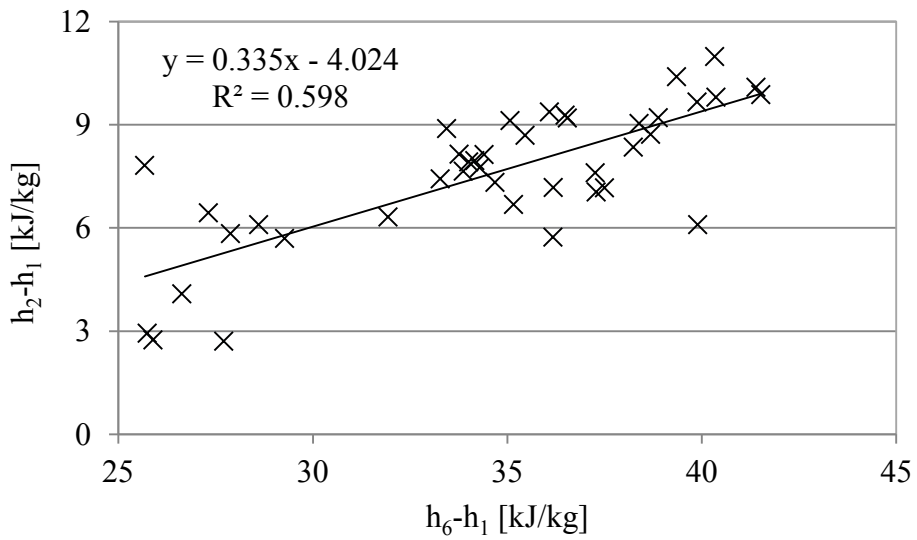

Fig. 4. 2: Measured values of (h_2-h_1) and (h_6-h_1)

Validation of the subsystem models has been carried out by comparing the measured air thermal-hygrometric properties at the outlet of each subsystem with the corresponding values calculated by the models, while the remaining thermal-hygrometric properties that are contained in each model equation are treated as inputs to the model itself. In fact, according to the efficiency factors determined, the temperature, in the case of all subsystems, and the absolute humidity, in the case of the desiccant wheel, at the outlet of the examined subsystem can be simulated, in the operating conditions of the measurements included in the validation data subset. Thus, *n* pairs of

measured and simulated values of temperature and/or absolute humidity are available, where *n* denotes the number of these measurements.

The validity of the assumed models can be confirmed by the evaluation of the Root Mean Standard Error between experimental and simulated values, by means of equation 2.15, in which experimental results are compared with simulated ones, instead of manufacturer's data.

In Tab. 4. 3, the RMSE value for each component specific property, for which the comparison between measured and simulated values has been carried out, is reported. For $RMSE_t$, the comparison is based on temperature values while for $RMSE_\omega$, on humidity ratio values.

Concerning the two analyzed DW models, while $RMSE_t$ have similar values, the Maclaine-Cross and Banks model has a much lower $RMSE_\omega$.

It can be noted that $RMSE_t$ for both the desiccant wheel models is quite higher than for the other subsystems.

Component	**Variable**	**$RMSE_t$ [°C]**	**$RMSE_\omega$ [g/kg]**
Desiccant wheel	t_2	1.28	-
(Maclaine-Cross and Banks)	ω_2	-	0.301
Desiccant wheel	t_2	1.45	-
(Psychrometric model)	ω_2	-	1.02
Cross-flow heat exchanger	t_3	0.713	-
Cooling coil	t_4	0.309	-
Direct evaporative cooler	t_8	0.764	-
MCHP heating coil	t_5	0.461	-
Boiler heating coil	t_6 with MCHP off	0.165	-
	t_6 with MCHP on	0.267	-

Tab. 4. 3: RMSE for the subsystems models

Moreover, $RMSE_\omega$ for the Maclaine-Cross and Banks model is in very good agreement with [132], while $RMSE_t$ for the heat exchanger, [132, 134], and the DEC, [132], are slightly higher.

Considering the uncertainties of the measuring instruments, it can be stated that the above results demonstrate the adequacy of the constant efficiency models.

The previous analysis is confirmed by Fig. 4. 3 and Fig. 4. 4. In the former, the measured and simulated values for regeneration air temperature, exiting the heating coil interacting with the MCHP, t_5, are shown; ±2.5% and ±5% error bands have been also plotted. No simulated values are outside the ±5% error band while only two values are outside the ±2.5% error band.

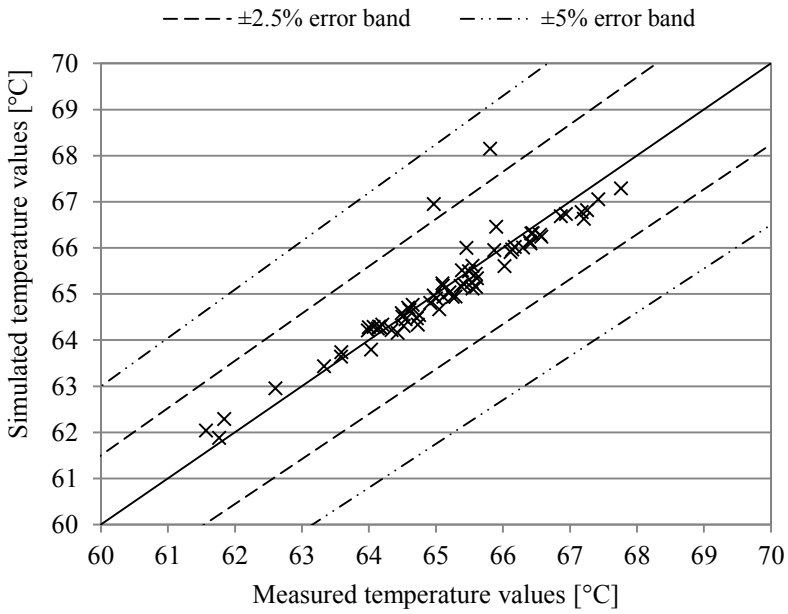

Fig. 4. 3: Measured and simulated values of t_5

In Fig. 4. 4 the measured and simulated values for process air humidity ratio, exiting the desiccant wheel, ω_2, are shown, together with the ±2.5% and ±5% error bands (Maclaine-Cross and Banks model is used). In particular Fig. 4. 4 has been divided in Fig. 4. 4a and Fig. 4. 4b in order to improve its readability. In the former, ω_2 ranges from 4 to 9 g/kg, in the latter from 9 to 13 g/kg. Only few values are outside the ±5% error band.

The agreement between measured and simulated values is quite good for both cases.

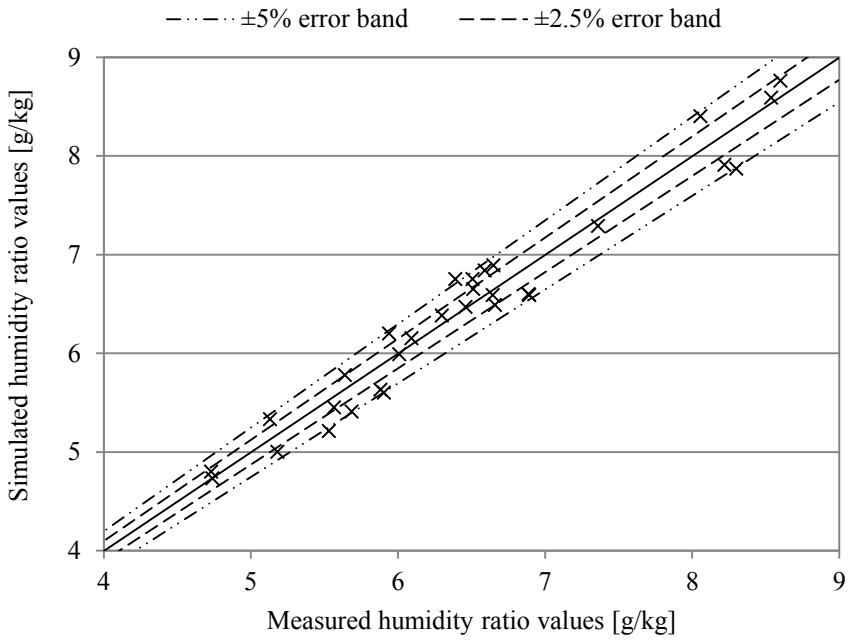

(a)

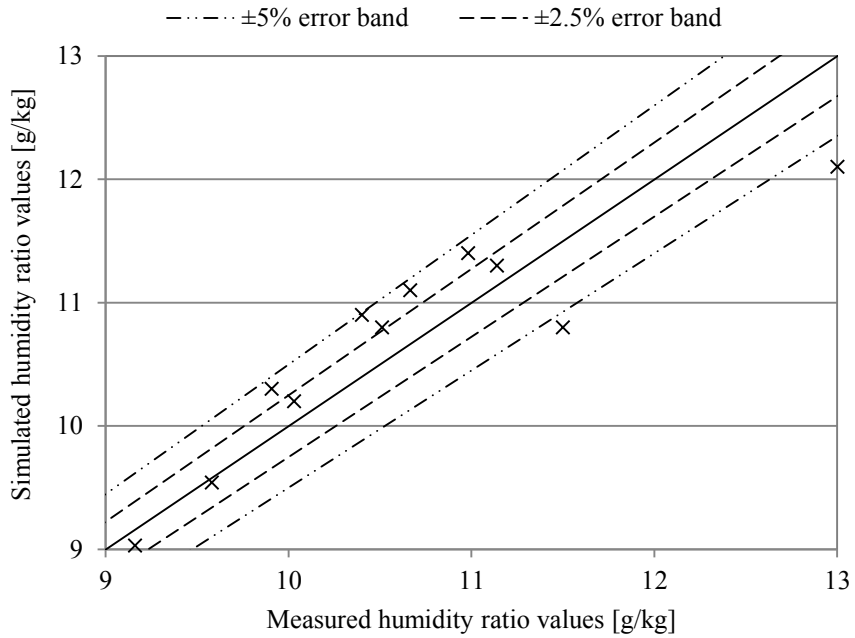

(b)

Fig. 4. 4: Measured and simulated values of ω_2

Similarly to Fig. 4. 4, in Fig. 4. 5 the measured and simulated values for ω_2 are shown, together with the ±2.5% and ±5% error bands, by using the psychrometric model. All values are

outside the ±5% error band; particularly, the model generally provides an underestimation of outlet humidity ratio.

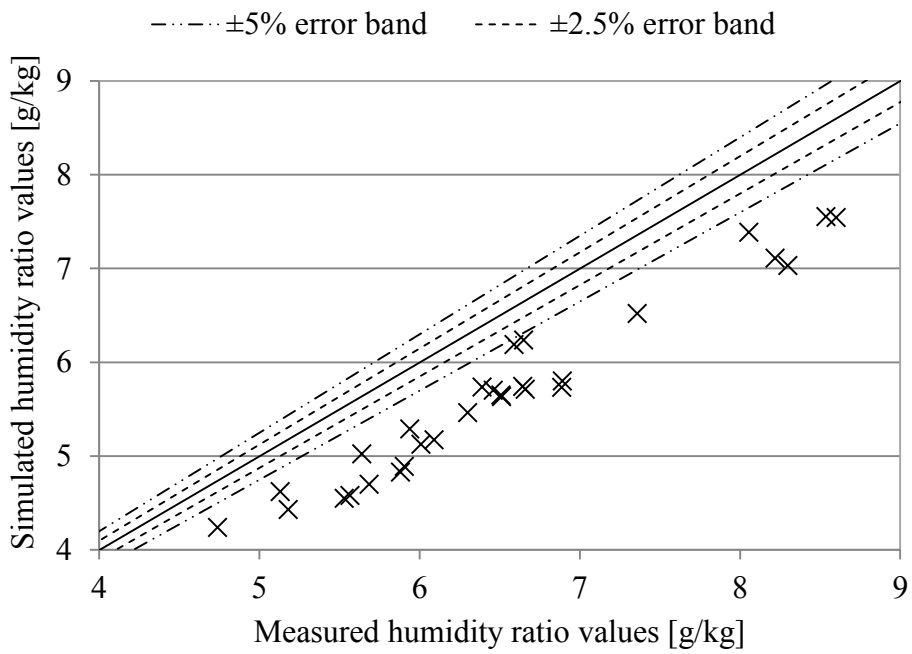

(a)

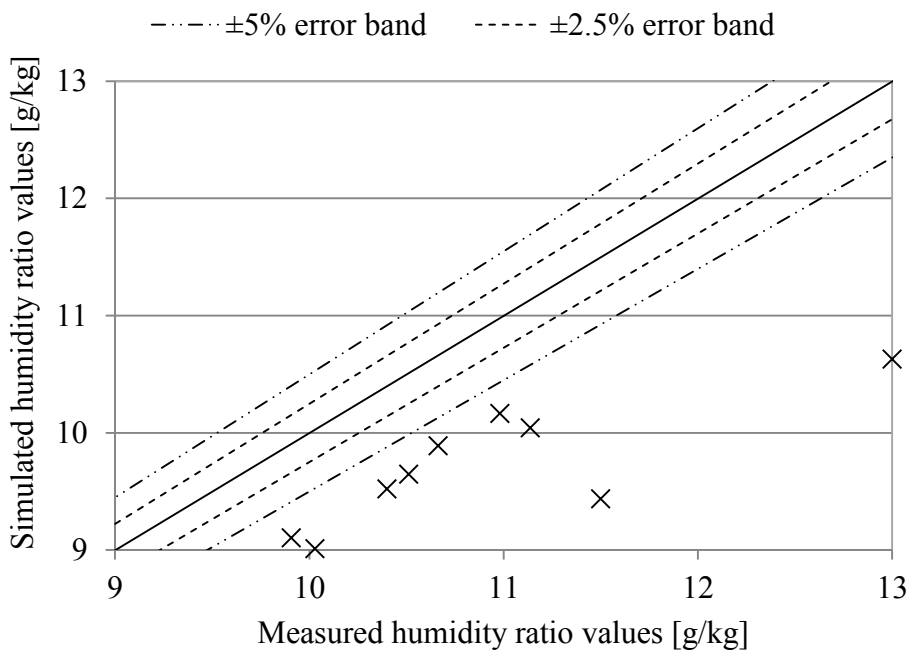

(b)

Fig. 4. 5: Measured and simulated values of ω_2 (Psychrometric model)

In Fig. 4. 6, the measured and simulated values for process air temperature at the outlet of the desiccant wheel, t_2, are shown. Few values are outside the ±5% error band, while the major part are within the ±2.5% error band.

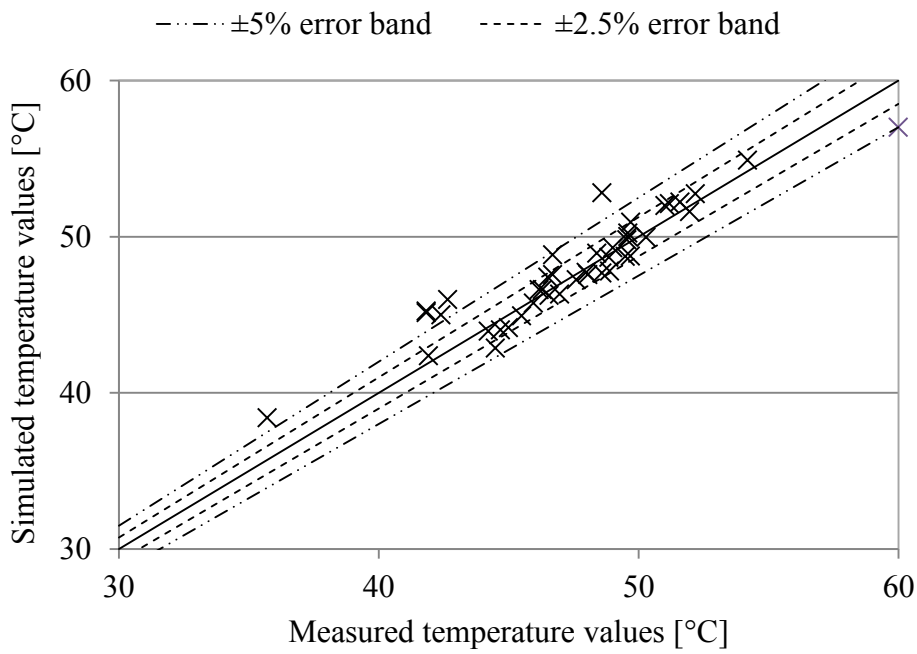

Fig. 4. 6: Measured and simulated values of t_2 (Psychrometric model)

These considerations lead to affirm that the Maclaine-Cross and Banks model better represents the performance of the analyzed desiccant wheel. Therefore, this model is used afterwards.

Regarding the validation of the complete system model, the simulation of the overall AHU must obviously consider that the components analysed in the previous paragraphs are physically linked. Moreover, the simulation algorithm must allow for an evaluation of the properties, temperature and humidity ratio, of the three air flows in particular key points, such as inlet room conditions, starting by outdoor air state.

Therefore the overall AHU model was validated by comparing experimental and simulated values of the most important temperature values in the AHU, namely, the process air supply temperature, t_4, and the regeneration temperature, t_6. Obviously, also the process air supply humidity ratio, ω_4, is a key value in air conditioning applications but the only component that

modifies humidity ratio in the process air flow is the desiccant wheel, hence the validation of the complete system model in terms of ω_4 coincides with that of the desiccant wheel (Tab. 4. 3).

For example, in Fig. 4. 7, the measured and simulated values of t_4, for the complete system model are shown, with the ±2.5% and ±5% error bands and only two values are outside the ±5% error band.

$RMSE_t$ for t_4 and t_6, considering the complete system model, are 0.507 and 0.939 °C, respectively. Once again, these results are in good agreement with [132].

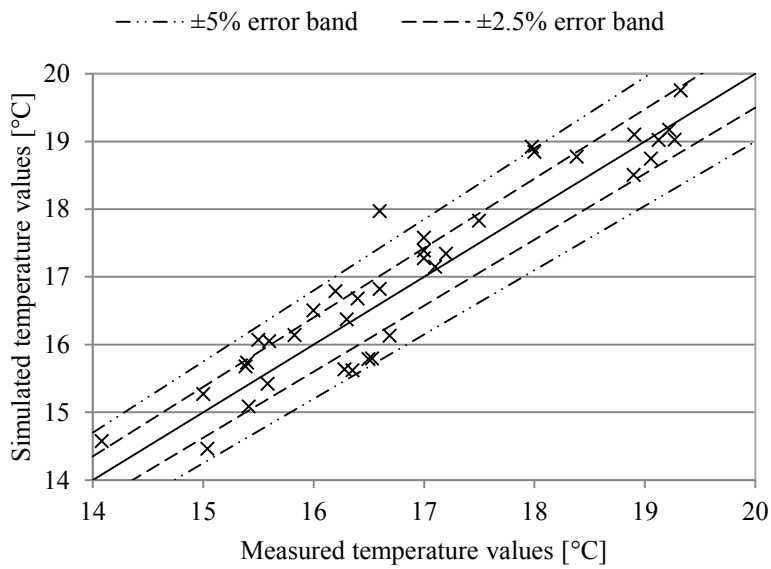

Fig. 4. 7: Measured and simulated values of t_4 for the complete system model

4.4 Simulation of the performance of the desiccant-based AHU

The models of the complete system and its main subsystems allow for an evaluation of several performance figure of merit, as the MRC, defined in equation 2.7.

In Fig. 4. 8a, MRC as a function of outdoor air humidity ratio is shown ($\dot{V}_{proc} = \dot{V}_{reg} = 800$ m^3/h, $t_{reg} = 64$ °C, $t_{out} = 30$ °C). Both simulative curves and experimental data have been reported. MRC increases when outdoor air humidity ratio increases. In fact, the higher the water vapour content in outdoor air, the higher the difference of vapour partial pressure between outdoor air and

desiccant material surface. Consequently, diffusion of the water vapour droplets from the former to the latter is higher and the dehumidification capability of the DW, Δω, increases.

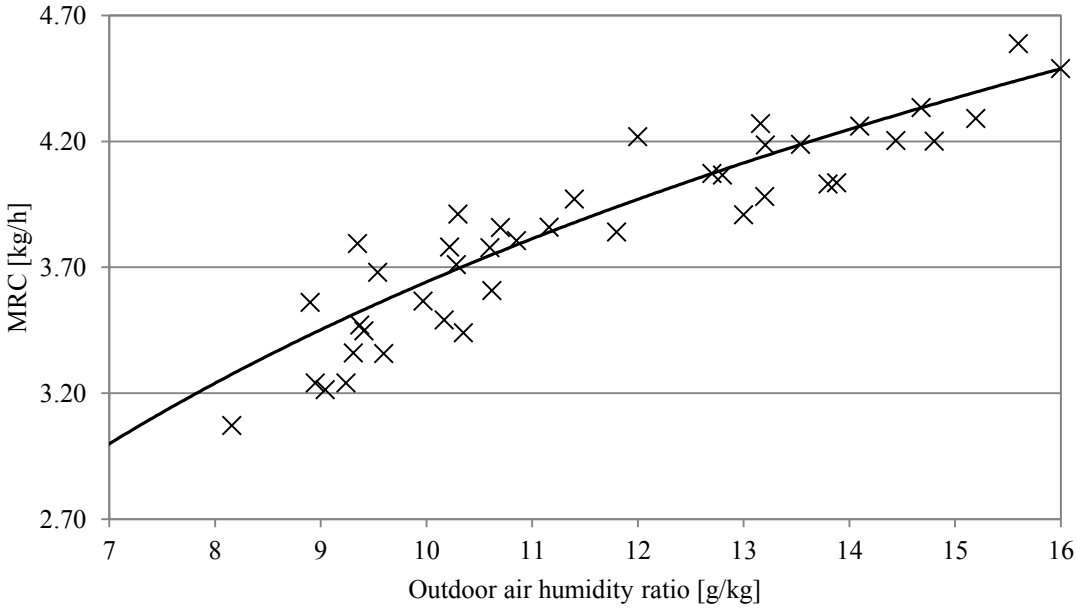

(a)

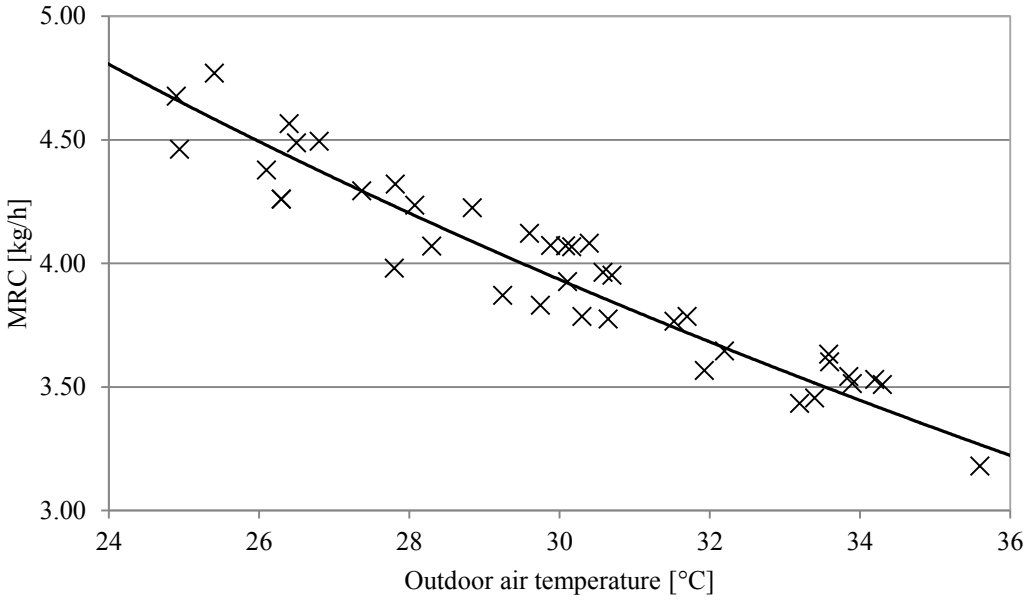

(b)

Fig. 4. 8: MRC as a function of outdoor humidity ratio (a) and outdoor temperature (b)

In Fig. 4. 8b, MRC as a function of outdoor air temperature is shown ($\dot{V}_{proc} = \dot{V}_{reg} = 800$ m^3/h, $t_{reg} = 64$ °C, $\omega_{out} = 12$ g/kg). MRC reduces when outdoor air temperature increases, because the adsorption process is exothermic, hence favored by low temperatures.

RMSE between measured and simulated values of MRC is 0.352.

These results are quantitatively and qualitatively in good agreement with literature, [24, 26, 146].

The validation was also based on an energy balance approach and to this aim the thermal Coefficient of Performance, COP_{th}, was used, as defined in [147]:

$$COP_{th} = \frac{\dot{m}_{proc}\left(h_1 - h_4\right)}{\dot{m}_{reg}\left(h_6 - h_1\right)} \tag{4.13}$$

Assuming that the thermal power is supplied by the MCHP only and that the regeneration air temperature, cogenerator and chiller supply water temperatures are 64.0 °C, 70.3 °C and 12.6 °C respectively (mean experimental values), the simulation model allows to evaluate the COP_{th} as a function of outdoor air humidity ratio or temperature.

In Fig. 4. 9a, COP_{th} as a function of outdoor air humidity ratio is shown ($\dot{V}_{proc} = \dot{V}_{reg} = 800$ m^3/h, $t_{out} = 29$ °C), while in Fig. 4. 9b, COP_{th} as a function of outdoor air humidity ratio is shown ($\dot{V}_{proc} = \dot{V}_{reg} = 800$ m^3/h, $\omega_{out} = 10$ g/kg).

COP_{th} increases with outdoor air temperature and humidity ratio, according to [46], and its values are coherent with those found in the literature, [46, 99, 148]. Higher values of thermal COP were instead found in [149], in which a high efficiency one-rotor two-stage desiccant cooling system is investigated.

RMSE between measured and simulated COP_{th} is 0.0328, confirming the validity of the overall AHU model. The average value of the uncertainty for COP_{th}, evaluated by means of the root sum square method proposed in [54], is 15.3 %.

Results are considered satisfactory, for both the subsystems and the complete system models, given the fact that the validated models aim to present a simple tool for the analysis of the performance of the described system.

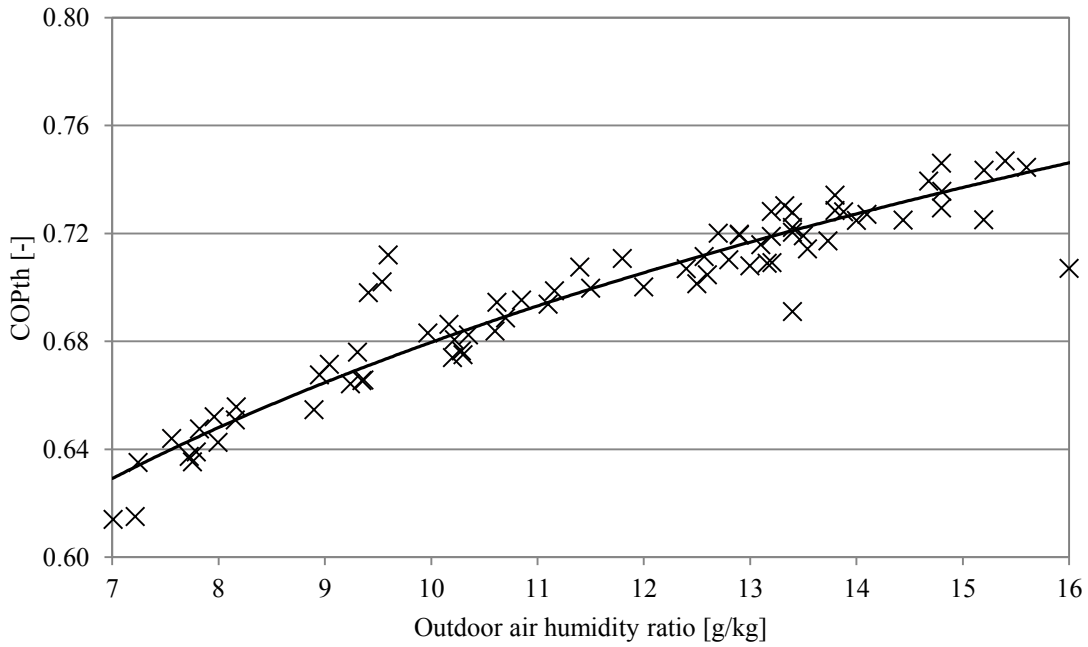

(a)

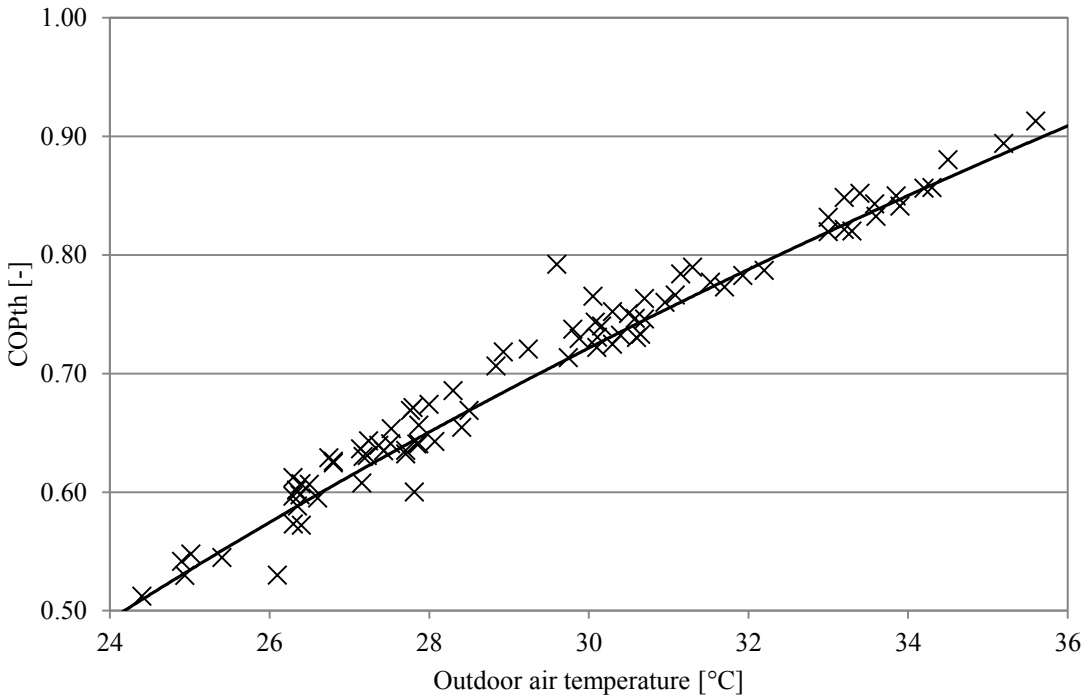

(b)

Fig. 4. 9: Thermal COP of the desiccant cooling system as a function of outdoor humidity ratio (a) and outdoor air temperature (b)

4.5 Model of the microcogenerator

MCHP has been dealt by several researchers for its potential savings, particularly in distributed energy systems, especially to determine suitable applications and evaluate the financial feasibilities of such devices in comparison with other generation options.

Therefore, several techniques for modelling the performance of both CHP and MCHP technologies have been developed, based on a variety of basic modelling aims, [150]. Modelling methods range from simple calculations using thermal and electric energy demand (several computer design tools are commercially available), to multiple-objective optimization approaches. In particular with reference to building-integrated MCHP systems, there are a wide range of levels in modelling detail and temporal resolution.

The analysis of MCHP utilization in buildings is complicated by the strong matching between the cogeneration unit, other HVAC components, and the user's thermal and electrical demands.

The literature is rich with examples of ICE models developed for general analysis of combustion-based stationary engines, but with few exceptions, these models focus on engine phenomena occurring over very short time-scales, which are several orders of magnitude smaller than the time scales used in building simulation.

This issue leads to the development of models for whole-building simulation programs, to facilitate the analysis of residential application. One of the aim of Annex 42 of the International Energy Agency's Energy Conservation in Buildings and Community Systems Programme was to develop simulation models, calibrated and validated by results from laboratory and field tests, and to apply these models to assess the technical, environmental, and economic performance of MCHP technologies in buildings.

The International Energy Agency published a series of reports from the Annex 42 project; in these, fuel cell and combustion based (RIC and Stirling) MCHP devices are modeled and tested, [151-153]. The modeling efforts included TRNSYS, EnergyPlus and ESP-r, [154].

In [155], an analysis of energy demand profiles of a 120 m^2 house and a simulation, based on a spreadsheet, of a microcogeneration system consisting of a 6 kW_{el} gas fired internal combustion engine was performed. A 3-E analysis was carried out varying some parameters, such

as number of dwellings, operating mode and reference systems. The introduction of a microcogeneration system allows primary energy savings ranging between 6% and 13%, equivalent CO_2 avoided emissions from 8 to 18% and a payback-period lower than 5 years.

In [156], several MCHP systems were analysed, comprising two systems based on internal combustion engine, one with Stirling engine and the last one with a PEMFC. Starting by experimental data available from the above mentioned units and considering typical daily profiles and characteristics of the heating period, daily energy balances of the MCHP systems were evaluated. A projection to annual values was done and the energy performance parameters were evaluated. Two building loads were considered: a MFH with 10 apartments for the ICE and the PEMFC units, and a MFH with 20 apartments for the Stirling unit.

Kelly et al. modeled a 0.75 kW Stirling cycle CHP unit, a 5 kW Senertec internal combustion engine and a building as final user. Then, they ran one-week simulations to evaluate CHP cogenerators performance in a residential application, [157].

De Paepe et al. carried out a comparison between several CHP systems, applied to a reference house model, to compare energy savings. Their work showed financial feasibility of all the CHP systems modeled, [158].

In [159], a comparison between two different energy supply systems for a student housing building, located in Coimbra (Portugal), from both an energy and exergy point of view, was performed. The analysed systems are the conventional one, based on separate "production" of heat and power, and a 12 kW_{el} MCHP system, internal combustion engine based. A model of the building was implemented in TRNSYS, while electric and DHW load profiles were determined by statistical analysis, based on gas and electricity bills. The results showed that the MCHP system performs better than the conventional one on the basis of energy and exergy analysis.

The study reported in [160] analysed the potential for residential cogeneration in Italy, carried out with the microcogenerator model developed within IEA/ECBCS Annex 42. The aim of the study was the 3-E analysis related to the use of a RIC-based MCHP in a meaningful sample of Italian residential buildings stock, accordingly to different climate zones, and the comparison with traditional energy supply systems for residential buildings. Performance assessment of cogeneration plant was carried out in terms of the IEA Annex 42 selected criteria: primary energy demand, CO_2 emissions, costs.

In [161], a performance assessment study for different MCHP units serving residential buildings in Switzerland was carried out. Energy and environmental analysis for different cogenerations technologies, such as SOFC, PEMFC, Stirling and internal combustion engines was performed, using the Annex 42 model when possible. The cogeneration units were integrated in Single-Family Houses (SFH) and MFH with different energy standards. The simulations were conducted for one Swiss location (Zurich) using TRNSYS.

The Annex 42 is a very complete but quite complex model, as it needs over than one hundred parameters to model the different operating modes of MCHP (warm-up, stand-by, cool-down and normal operation). Furthermore, with the actual configuration of the test facility at University of Sannio, the determination of some of these parameters is not possible. Therefore in the following, a simplified MCHP model (TESS model in TRNSYS), suited for whole-building simulation softwares, is described, calibrated and validated by means of the available experimental data on the AISIN Toyota device.

4.5.1 MCHP TESS model (Type 907)

To simulate the microcogenerator operation, the TRNSYS RIC engine model has been used.

The internal combustion engine is modeled using the Type 907 TESS component. It uses a table of performance data to determine the outputs of the engine, given a set of input conditions. Thermal power can be recovered from the oil cooler, the exhaust gas heat exchanger, the aftercooler and the engine jacket.

The model relies on an external data file which contains efficiency (both mechanical and electrical), air flow rate (fraction of rated flow rate) and heat transfer data (fraction of total thermal power recovered from the generator, the oil cooler, the exhaust gas heat exchanger and the engine jacket and the fraction dissipated to the environment) as a function of the intake temperature and the part load ratio (actual power over rated power).

As already said, the tested microcogenerator is not equipped with invasive temperature and flow rate sensors to separately measure the thermal power recovered from the exhaust gas and the engine jacket; hence it has been assumed that, in the TRNSYS engine model, all the thermal power is recovered by the engine jacket. Moreover, it is not possible to measure the mechanical power

transferred from the engine to the electric generator; therefore, a constant value of 0.95 has been assumed for the electrical efficiency of the generator.

The MHCP is modeled by three components, as shown in Fig. 4. 10, that are the IC engine, a plate heat exchanger, used to transfer the recovered thermal power to a secondary fluid (i.e. water), and a three-way valve. The latter mixes the part of solution flow rate that passes through the plate heat exchanger and the one that is bypassed toward the engine. A control system that manages the thermal recovery circuit of the microcogenerator is also modeled.

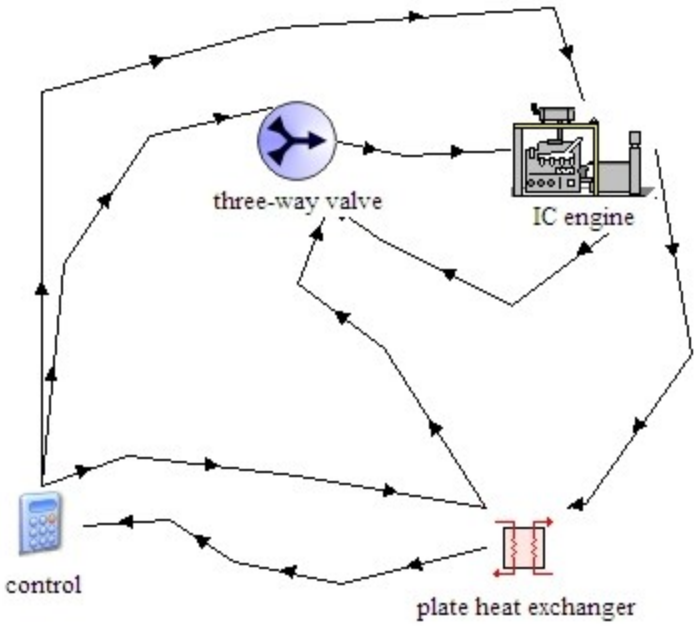

Fig. 4. 10: The MCHP model in TRNSYS

Some tests were carried out to evaluate the mass flow rate of solution that indeed crosses the plate heat exchanger, $\dot{m}_{sol,pl}$, as a function of its temperature at the outlet of the heat exchanger itself, $t_{sol,out,pl}$ (Fig. 4. 11). Results show that $\dot{m}_{sol,pl}$ increases with a 2nd-order curve when $t_{sol,out,pl}$ is lower than 55 °C (the equation is shown in Fig. 4. 11); for higher outlet temperatures, a constant mass flow rate of solution (about 0.3 kg/s) passes through the plate heat exchanger.

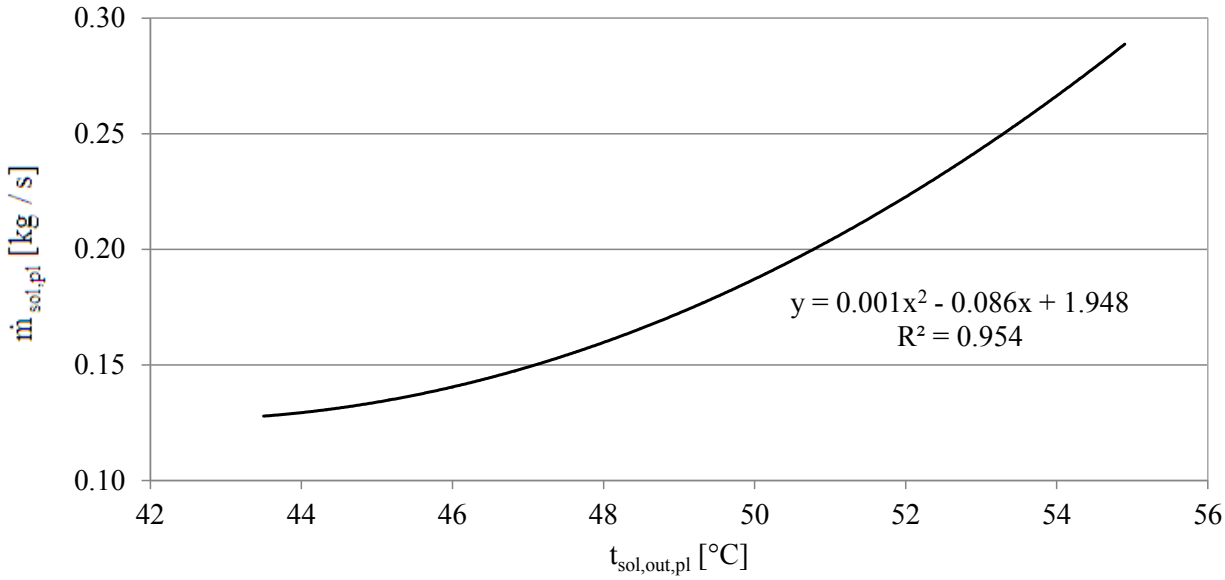

Fig. 4. 11: Solution mass flow rate passing through the plate heat exchanger as a function of its outlet temperature

Concerning the parameters of the RIC engine, only the specific heat of jacket water fluid (3.72 kJ/kgK, [162]) and maximum power output (5.73 kW, considering an average consumption of MCHP auxiliaries of 270 W, with fan off) are effectively used, while the other parameters (specific heat of oil cooler fluid, exhaust air, aftercooler fluid and rated exhaust air flow rate) are not used.

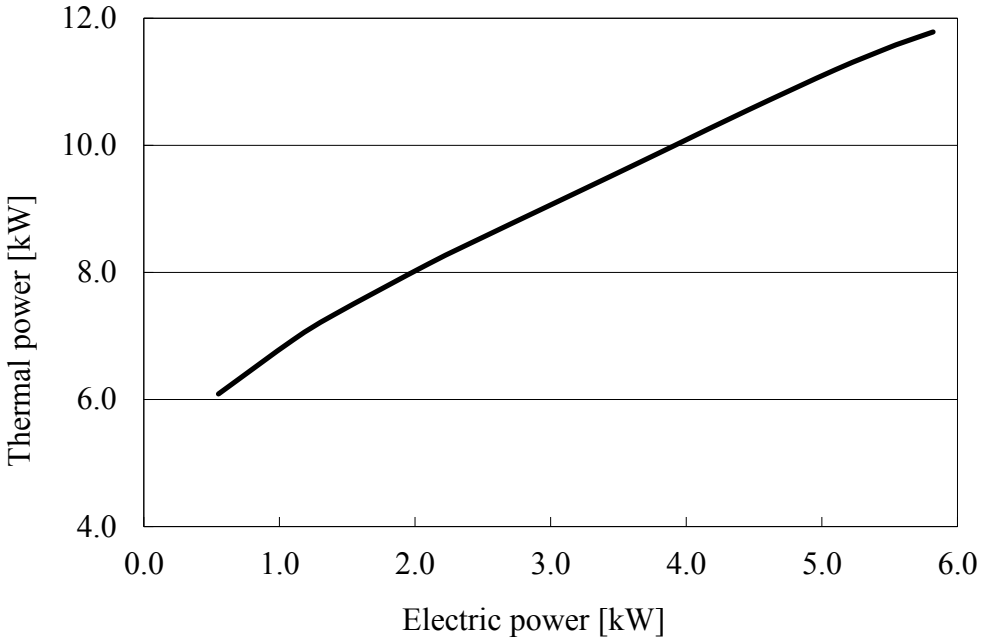

Fig. 4. 12: Thermal power as a function of electric power for the AISIN MCHP

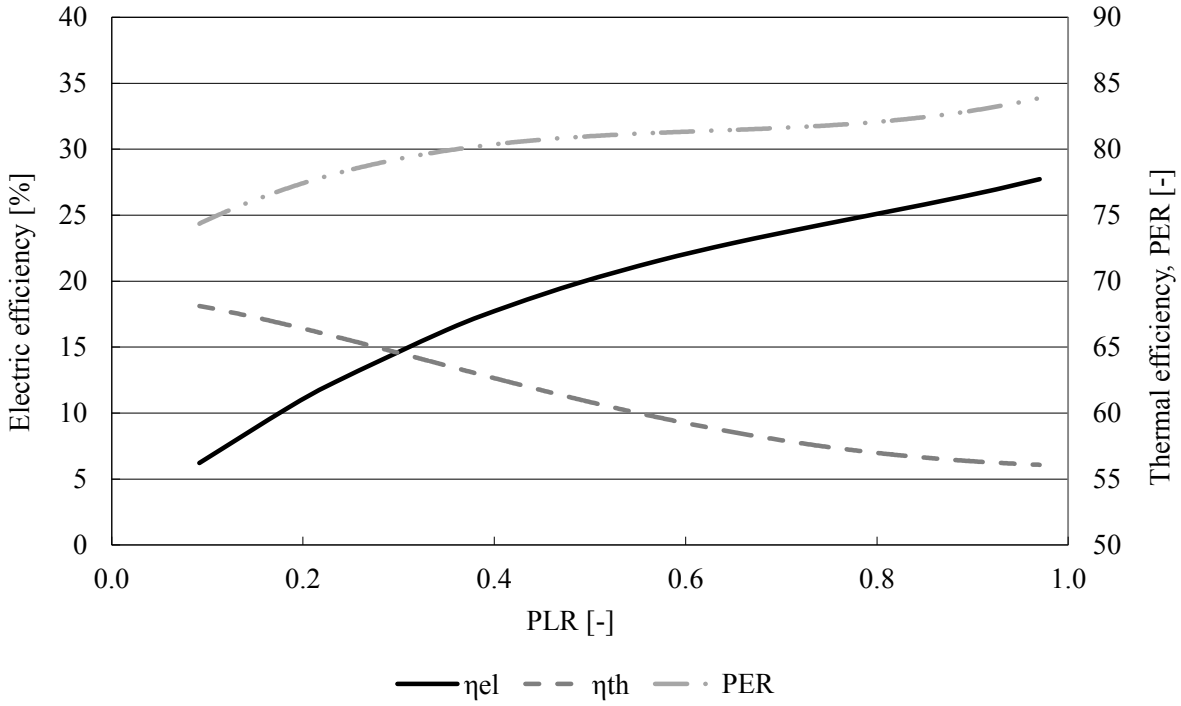

Fig. 4. 13: η_{el}, η_{th} and PER of the AISIN as a function of PLR

The desired output, that is an input of the model, is converted to a part load ratio value and then used to refer to a performance map which contains information on efficiency, exhaust flow and heat distribution. From this performance map, the fuel use and thermal output can be derived, [163].

Regarding the characterization of the MCHP performance, the recovered thermal power as a function of electric power supplied by the MCHP is shown in Fig. 4. 12.

In Fig. 4. 13, electric, thermal and overall (PER) efficiency of AISIN as a function of PLR are shown. Experimental tests established that electric efficiency increases with PLR, as expected.

Even if thermal power increases with PLR (see Fig. 4. 12), thermal efficiency reduces as the primary power input increases more than thermal power itself. Finally, the increase in η_{el} prevails over the reduction in η_{th}; hence PER rises with PLR.

For the description of the operation of the plate heat exchanger, the NTU-effectiveness method, [139], applied to a counter flow heat exchanger, has been used:

$$\varepsilon_{pl} = \frac{1 - exp\left[-\frac{UA}{C_{min}}\left(1 - \frac{C_{min}}{C_{max}}\right)\right]}{1 - \frac{C_{min}}{C_{max}} exp\left[-\frac{UA}{C_{min}}\left(1 - \frac{C_{min}}{C_{max}}\right)\right]} \tag{4.14}$$

where $C_{min} = \min(C_{sol}; C_w)$ and $C_{max} = \max(C_{sol}; C_w)$, where C_{sol} is the capacity rate of the glycol-ethylene mixture through the heat exchanger and UA is its overall heat transfer coefficient.

Experimental data were used to evaluate the overall heat transfer coefficient as a function of $\dot{m}_{sol,pl}$ (Fig. 4. 14); the 2-nd order equation shown in the figure is used to model the plate heat exchanger.

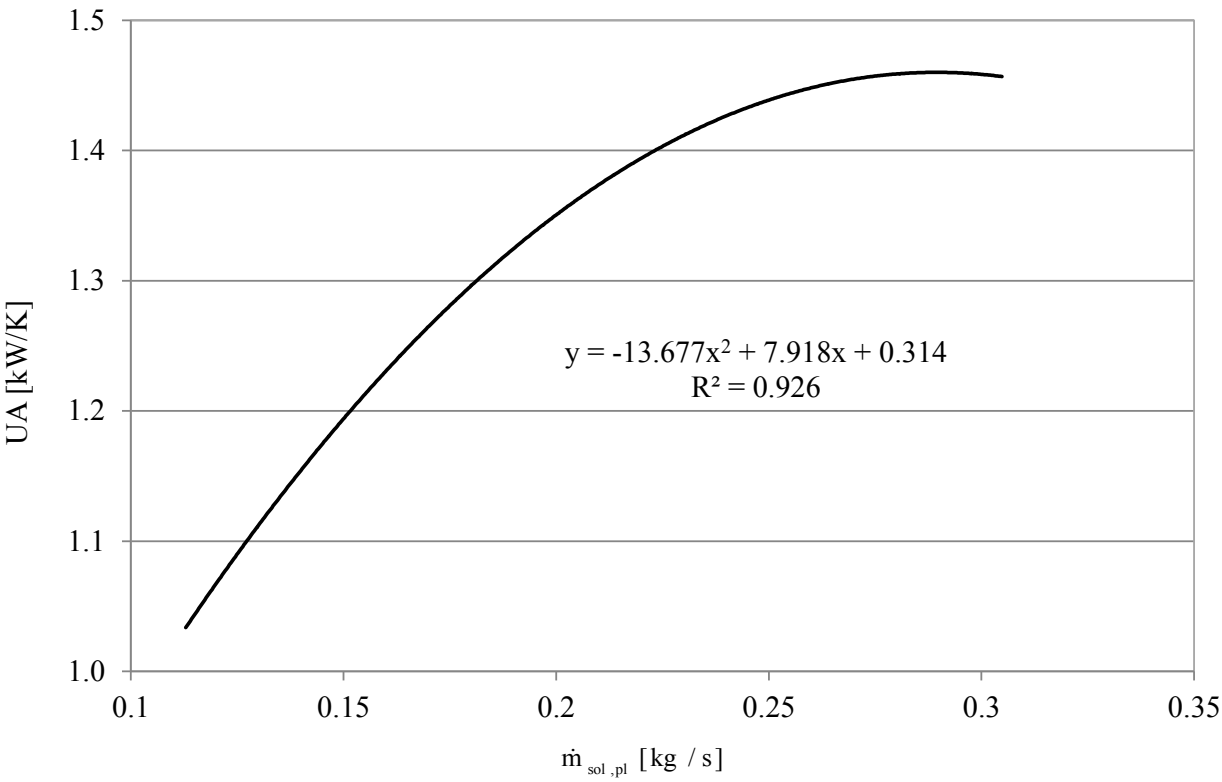

Fig. 4. 14: UA of the plate heat exchanger as a function of the solution mass flow rate passing through it

To validate the MCHP model (RIC engine and plate heat exchanger), a comparison between measured and experimental values of water temperature at the outlet of the heat exchanger (t_{w8} in Fig. 2. 2) was performed, Fig. 4. 15.

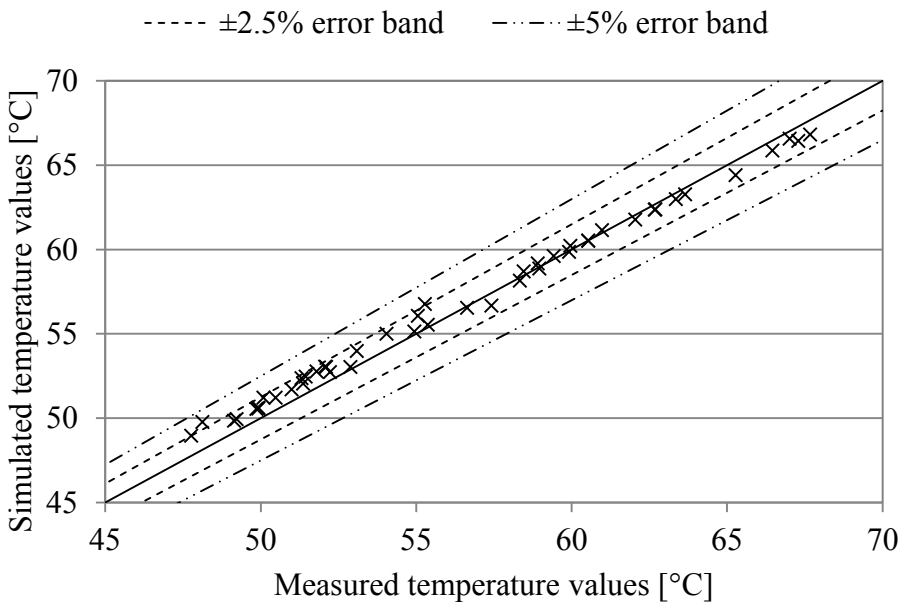

Fig. 4. 15: Measured and simulated values of t_{w8} for the MCHP model

No values are outside the ±5% error band and only two values are outside the ±2.5% error band. Furthermore, a RMSE of 0.714 °C, comparable to the values obtained for the AHU subsystems models (see Tab. 4. 3), was obtained.

The validation was also based on an energy balance approach and to this aim a specific test was carried out. It had a duration of 75 minutes, during which the electrical power output of the microcogenerator was increased from 2 to 6 kW with steps of 1 kW. Simultaneously, the temperature of water entering the plate heat exchanger was linearly increased from 40 to 56 °C.

The same forcing functions were also applied in a TRNSYS simulation of the MCHP; the error between measured and simulated values are 4.71% and 3.98%, in terms of overall thermal energy produced and overall primary energy required, respectively.

Results are considered satisfactory in this case also, especially considering that the analyzed model does not take into account transient effects.

4.6 Air-cooled chiller TESS model (Type 655)

Type655 models a vapor compression air cooled chiller. It relies on catalog data, provided as external text files, to predict the performance of a vapor compression air cooled chiller.

These devices are in essence, air conditioners that cool a fluid stream on the evaporator side while rejecting heat to an air stream on the condenser side.

To set up the model, the user must provide two text based data files in the standard TRNSYS data file format. The first of these files provides the chiller capacity ratio (actual nominal capacity over rated capacity, Fig. 4. 16) and the chiller COP ratio (actual nominal COP over rated COP, Fig. 4. 17) for different values of chilled water set point temperature, and for different outdoor ambient temperatures. Manufacturer's data were used to obtain Fig. 4. 16 and Fig. 4. 17.

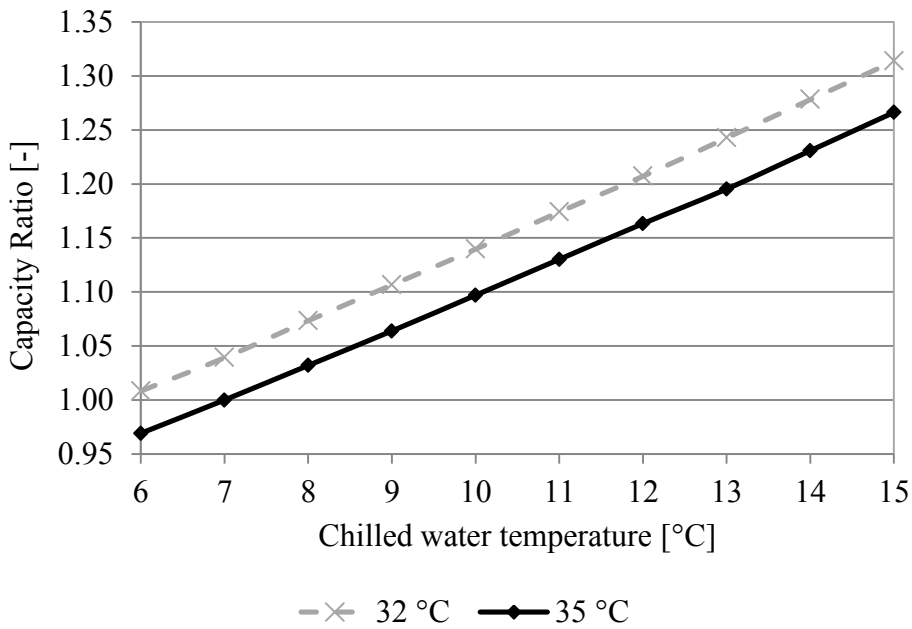

Fig. 4. 16: Capacity ratio as a function of chilled water temperature for two different outside air temperature

The nominal COP is evaluated by means of the following equation:

$$COP_{nom} = COP_{rated} \cdot COP_{ratio} \tag{4.15}$$

while the nominal capacity is given by:

$$Capacity_{nom} = Capacity_{rated} \cdot Capacity_{ratio} \tag{4.16}$$

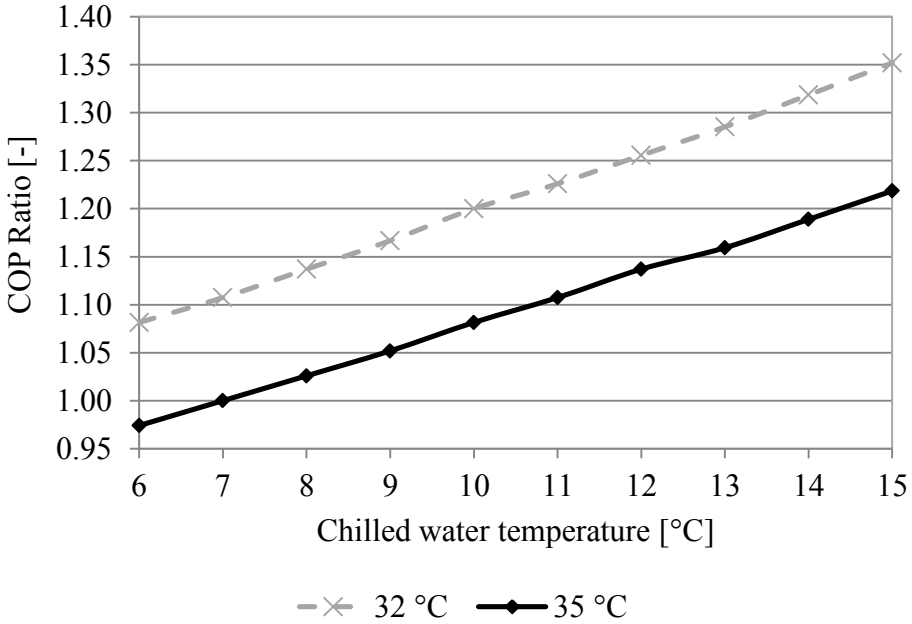

Fig. 4. 17: COP ratio as a function of chilled water temperature for two different outside air temperature

The chiller PLR is evaluated as the ratio between the actual cooling power and the nominal capacity:

$$PLR = \frac{Q_{cool}}{Capacity} \tag{4.17}$$

If the calculated PLR is greater than unity, the component automatically limits the load met by the chiller to the capacity of the machine. With a valid PLR calculated (between 0 and 1), the software accesses the second data file, that provides values of the chiller Fraction of Full Load electric Power (FFLP) for different values of part load ratio.

Experimental data and specific softwares, [112, 113], were used to obtain the trend of FFLP shown in Fig. 4. 18.

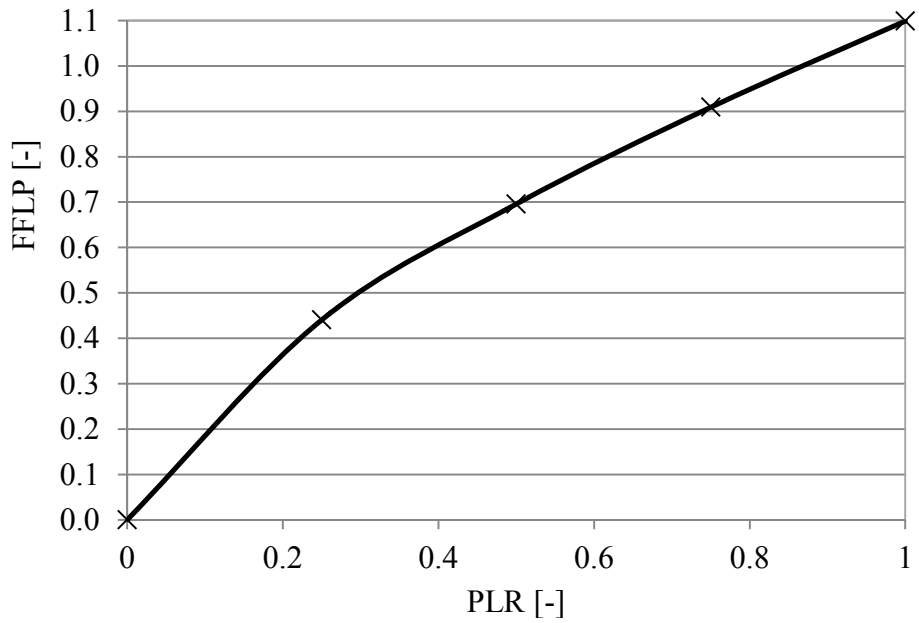

Fig. 4. 18: FFLP as a function of PLR

The chiller's power draw is given by:

$$P_{el} = \frac{Capacity}{COP_{nom}} \cdot FFLP \tag{4.18}$$

The actual COP is then calculated as:

$$COP = \frac{Q_{cool}}{P_{el}} \tag{4.19}$$

4.7 Simulation of a solar desiccant-based Air Handling Unit

As already noted, desiccant cooling systems are an interesting technology for sustainable building air conditioning, as the main energy required is low temperature heat, which can be supplied by solar thermal energy or waste heat. The use of solar energy, being a renewable energy source, has several advantages, e.g.:

- reduction of fossil fuel demand;

- energy source differentiation;

- reduction of the environmental impact.

In particular, the use of solar energy for space cooling requirements (solar cooling) is highly desirable, because its availability coincides with the need for cooling; therefore the summer peak demand of electricity due to extensive use of electric air conditioners, that matches with the peak solar irradiance, can be lowered, [37].

The aim of this simulation activity is to design a Solar Collectors (SC) system that provides the required regeneration thermal energy, [164]. The designed solar assisted desiccant cooling system is successively simulated by means of the TRNSYS software, in order to evaluate operational data and performance parameters of the system in a typical week of operation, e.g. thermal-hygrometric conditions of air in the mean sections of the AHU and Solar Fraction (SF).

As regards the solar collector system, it has been designed, by means of a commercial software, considering the typical operating requirements of the regeneration coil, as reported in Tab. 4. 4.

Considering the quite low needed temperature, flat plate collectors have been chosen; the characteristic of the solar field and collectors have been summarized in Tab. 4. 5.

Moreover, it is assumed that the collectors are positioned on the roof of the four-storey building that hosts the test facility.

Regeneration thermal power [kW]	12.0
Regeneration temperature [°C]	65.0
Regeneration mass flow rate [kg/s]	0.262
Outdoor air temperature [°C]	25.0

Tab. 4. 4: Typical operating requirements of the regeneration coil

Number of collectors	7
Collectors area [m^2]	14
Azimuth [°]	0
Slope [°]	20

Tab. 4. 5: Characteristics of the solar field and collectors

Component	Type no.	Library	Main parameters	Value	Unit
Desiccant Wheel	1716	TESS	F1 Effectiveness	0.207	-
			F2 Effectiveness	0.717	-
Solar Collectors	1b	Standard	Tested Flow Rate	0.0306	$kg/(m^2s)$
			Intercept Efficiency	0.712	-
			Efficiency Slope	3.56	$W/(m^2K)$
			Efficiency Curvature	0.0086	$W/(m^2K^2)$
Thermal Storage	60d	Standard	Tank Volume	0.855	m^3
			Tank Height	2.18	m
			Tank Loss Coefficient	2.30	$W/(m^2K)$
			Number of Internal Heat Exchanger	2	-
Cross Flow Heat Exchanger	91	Standard	Effectiveness	0.446	-
DEC	506c	TESS	Parasitic Power	40 W	W
			Saturation Efficiency	0.551	-
Cooling Coil	508f	TESS	Coil Bypass Fraction	0.177	-
Heating Coil	670	TESS	Effectiveness	0.868	-
Process Air Fan	744	TESS	Rated Flow Rate	0.226	kg/s
			Rated Power	310	W
			Power Coefficients	See eq. 4.21	-
			Motor Efficiency	0.80	-
Boiler	6	Standard	Maximum Heating Rate	26.7	kW
			Efficiency	0.902	-
Air-Cooled Chiller	655	TESS	Rated Capacity	8.45	kW
			Rated COP	2.93	-
			Performance Data	Manufacturer and experimental data	-

Tab. 4. 6: Main models used for the simulation and their main parameters

In order to simulate the solar assisted desiccant-based AHU, a simulation model was built by using TRNSYS 17 and the component library TESS. A list of the main models used in the simulations is reported in Tab. 4. 6.

The model of the thermal solar collectors is described by the following equation:

$$\eta = \eta_0 - a_1 \frac{(t - t_{amb})}{G} - a_2 \frac{(t - t_{amb})^2}{G} \tag{4.20}$$

where the parameters η_0 (Intercept Efficiency), a_1 (Efficiency Slope) and a_2 (Efficiency Curvature) are the characteristics performance coefficients of flat plate collectors, t_{amb} is the ambient temperature and G is the total radiation per unit area on the plane of the solar collector.

The electric power drawn by the fan is given by:

$$\frac{P_{el}}{P_{el,rated}} = b_0 + \sum_{i=1}^{6} b_i \left(\dot{m}/\dot{m}_{rated}\right)^i \tag{4.21}$$

where the coefficients in equation 4.21 were experimentally evaluated; their values are: $b_0 = 8.08$, $b_1 = -68.0$, $b_2 = 253.1$, $b_3 = -488.2$, $b_4 = 518.2$, $b_5 = -287.4$, $b_6 = 65.3$.

Manufacturer data have been used for the performance of solar collectors, thermal storage, and boiler.

A view of the complete simulation studio project is shown in Fig. 4. 19.

The simulation was run for a time period of one week, from the 1st to the 7th of August, assuming the Meteonorm climatic conditions for Naples.

Moreover, it was assumed that the AHU provides conditioned air to an office, whose working hours are from 9.00 a.m. to 6 p.m., from Monday to Friday.

It was assumed that the AHU is controlled in order to obtain a supply humidity ratio (point 4 in Fig. 2. 2) of 9 g/kg; to this aim, the solar collectors and the boiler interact with the thermal storage in order to supply hot water at the regeneration temperature required by the DW.

Finally, the chiller is controlled to provide chilled water to the cooling coil in order to obtain a supply temperature of 18 °C.

In Fig. 4. 20, the temperature of process air at various section of the AHU and the required regeneration temperature are shown, while in Fig. 4. 21 humidity ratio of outdoor air and process and regeneration air exiting the desiccant wheel are shown.

Obviously, the higher the outdoor air humidity ratio, the higher are both the regeneration temperature required to obtain the fixed value of supply humidity and the temperature of process air exiting the DW.

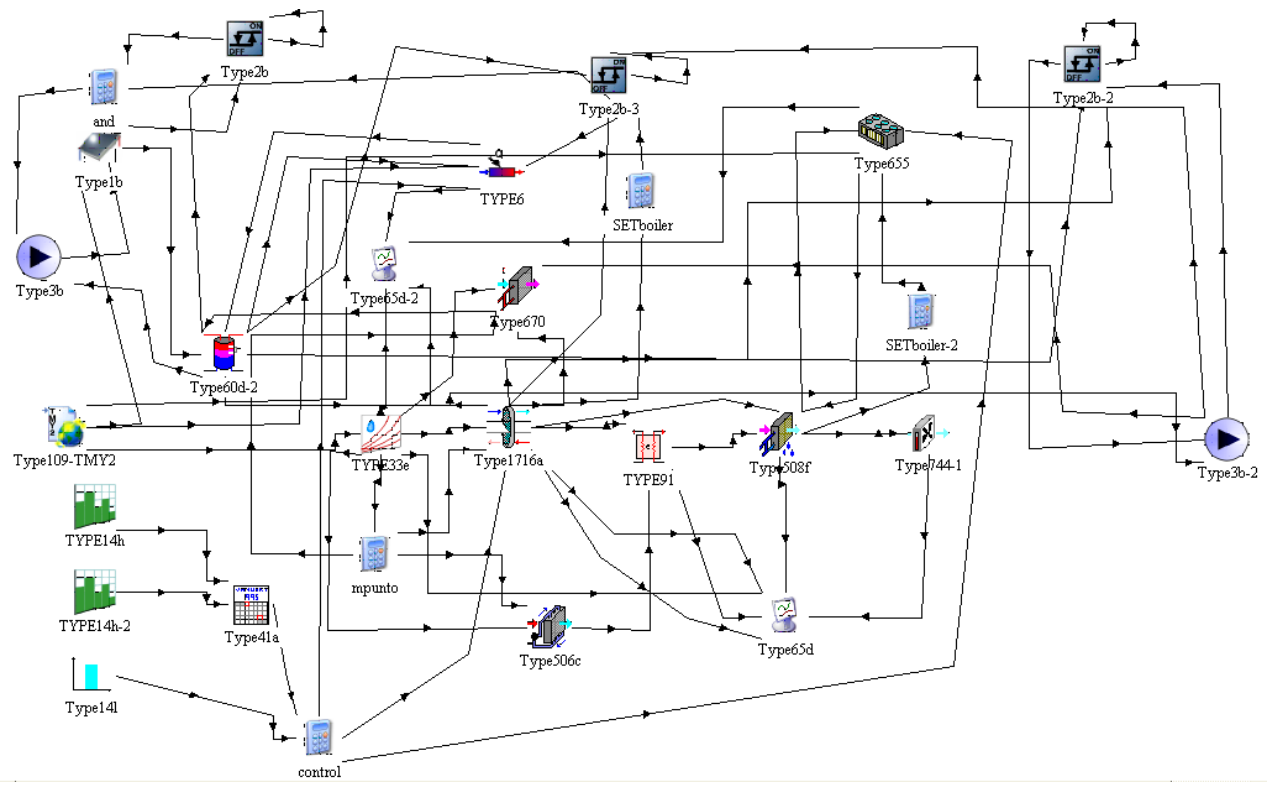

Fig. 4. 19: TRNSYS simulation studio project of solar assisted desiccant-based AHU showing components and their connections

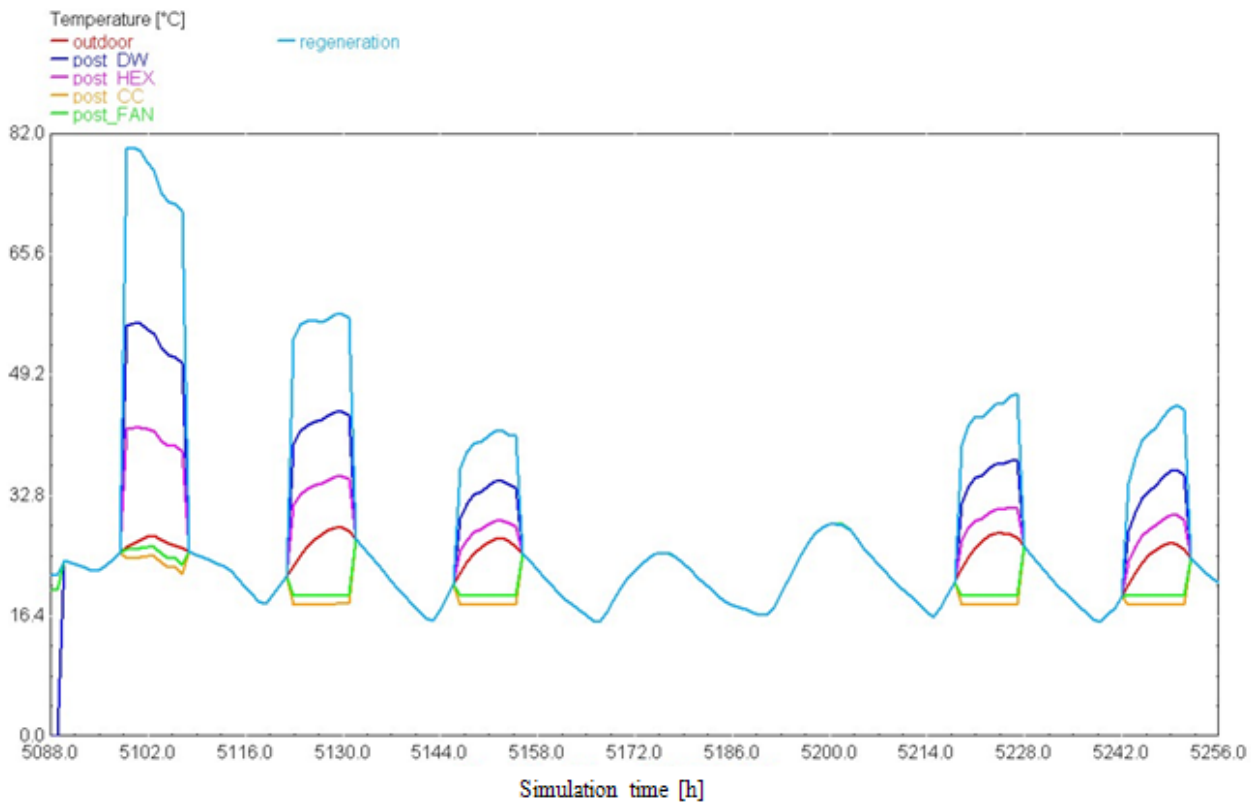

Fig. 4. 20: Temperatures of process air at various section of the AHU and required regeneration temperature

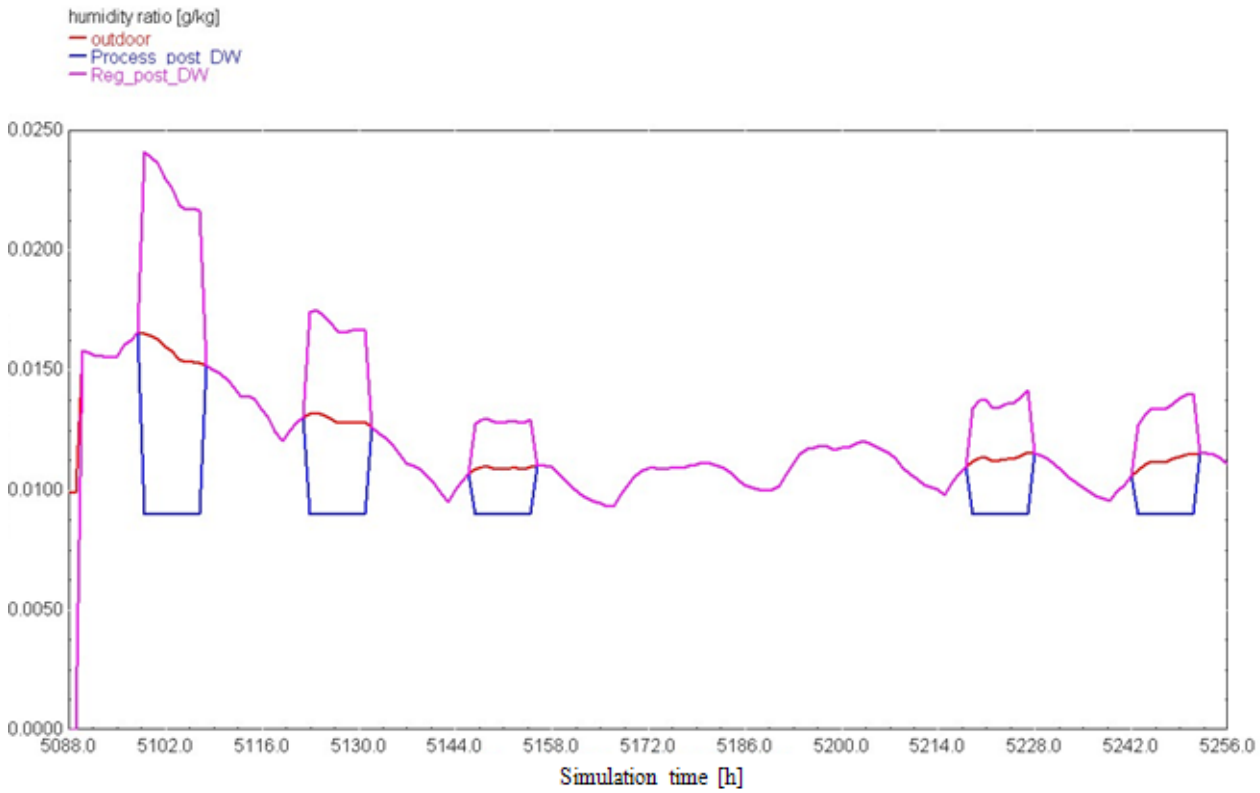

Fig. 4. 21: Humidity ratio of outdoor air and of process air and regeneration air exiting the DW

Furthermore, during the first day of simulation, the chiller cooling power is less than required and it is not able to guarantee the desired supply temperature; in fact, process air temperature exiting the cooling coil is higher than 18 °C.

Finally, the fan determines an increase of process air temperature of about 1 °C.

TRNSYS simulation also allows to evaluate typical performance parameters of a single component or the whole system.

For example, the efficiency of the solar collectors can be evaluated. It is defined as, [165]:

$$\eta_{SC} = \frac{\int Q_{th,SC}\, d\tau}{\int GAd\,\tau} \tag{4.22}$$

where $Q_{th,SC}$ is thermal energy provided by the solar collector system for regeneration, G is the solar radiation, A is collectors area and the integration is carried out for the hours of operation of the AHU.

For the week of simulation, the efficiency of the solar collectors is 0.48.

Another critical parameter for solar cooling systems is the Solar Fraction, [166], that shows the contribution of thermal energy from solar collectors within the total heat input for regeneration. It is defined as:

$$SF = \frac{\int Q_{th,SC}\, d\tau}{\int Q_{th,SC}\, d\tau + \int Q_{th,b}\, d\tau} \tag{4. 23}$$

where $Q_{th,b}$ is thermal energy for regeneration provided by the boiler. The simulation provides on a weekly basis a SF = 0.603, therefore a large amount of thermal energy for the regeneration of the Desiccant Wheel is effectively provided by the solar collectors.

4.8 Simulation of the MCHP/HVAC-DW system

The models of the AHU components and energy conversion devices, experimentally calibrated and validated in the previous sections, were also used to simulate the MCCHP system.

Besides the components represented in Fig. 4. 19 and listed in Tab. 4. 6 (with the exception of the solar collectors model), the microcogenerator model (type 907), as described in section 4.5.2 was also used to simulate the MCHP/HVAC-DW system.

It was assumed that the MCHP always works at full load; thermal energy from the cogenerator is used to regenerate the desiccant wheel, while electric energy is partially used to activate the electric chiller and auxiliaries and partially provided to the final user.

A regeneration temperature of 65 °C and a supply air temperature of 18 °C were set.

The trigeneration system is compared to the conventional one, in which thermal, cooling and electric energies are provided by separate "production" systems (energy and environmental performance indices of CS are the same of section 3.2.2). In particular, it was assumed that the conventional Air Handling Unit operates in order to obtain the same values of t_s and ω_s provided by the desiccant-based AHU. The supply air humidity ratio for both the alternative and conventional systems obviously depend on outdoor air thermal-hygrometric conditions and t_{reg}.

Furthermore, for the air conditioning system, the same final user and time schedule as in section 4.7 were used.

In Fig. 4. 22, the PES and the ΔCO_2 is shown as a function of time.

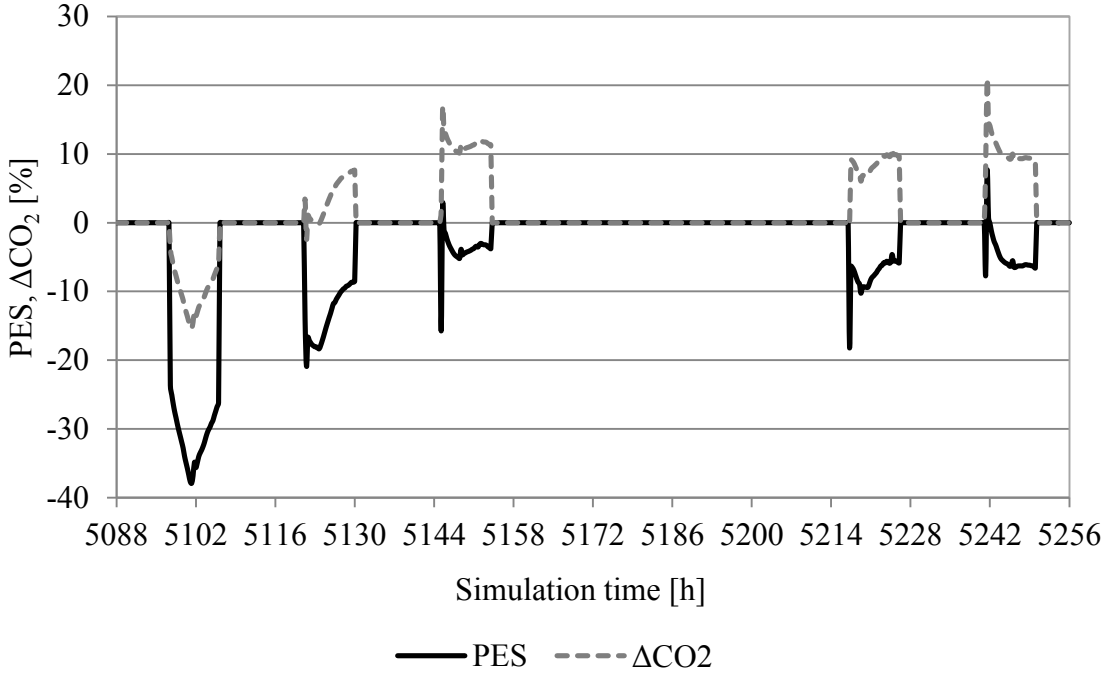

Fig. 4. 22: Simulative PES and ΔCO_2 of the MCCHP system

Simulation results show that, for the analyzed simulation period, the AS has a higher primary energy consumption with respect to the CS in each day; on the contrary, it has a lower carbon dioxide equivalent emissions, except than the first day of simulation.

As shown in section 3.3.3.2, energy and environmental performance of both MCCHP and reference systems obviously depend on outdoor air thermal-hygrometric conditions. Results of Fig. 4. 22 are in good agreement with experimental results reported in Fig. 3. 17 and Fig. 3. 18, considering the value of outside temperature and humidity ratio shown in Fig. 4. 20 and Fig. 4. 21, respectively. For the overall simulation period considered, PES = -12.4% and ΔCO_2 = 4.60%.

CONCLUSIONS

The transition from conventional centralized energy systems, based on separate "production", to decentralized ones is currently in progress. This is due to the market availability of a wide variety of small scale energy conversion systems, allowing for the satisfaction of different energy requirements (electricity, cooling and heating) with a great potential of primary energy saving, greenhouse gas emission and operating costs reduction.

In this work, a microtrigeneration system, consisting of a desiccant-based Air Handling Unit, interacting with an electric chiller, a boiler and a microcogenerator, was presented.

The desiccant wheel is regenerated by mainly using thermal energy from a microcogenerator, therefore at low temperature (lower than 70 °C); this range of regeneration temperature is poorly investigated in literature.

First of all, an experimental analysis on dehumidification and thermal performances of the silica-gel desiccant wheel, contained in the Air Handling Unit, was presented. Useful performance curves were obtained, as regards the difference between process air inlet and outlet humidity ratio (i.e. the moisture removal capability of the wheel) and temperature, as a function of regeneration temperature and process air inlet humidity ratio and temperature. The performance curves considering an ideal isoenthalpic adsorption dehumidification process were presented too.

Furthermore, the trends of various types of performance figures of merit (MRC, DCOP, regeneration, dehumidification, thermal and adiabatic effectiveness, SER) were also analyzed, as a function of five operating parameters: outdoor air temperature and humidity ratio, regeneration temperature, the ratio between regeneration and process air flow rates and desiccant wheel rotational speed.

Results show that the thermal-hygrometric properties of the process air entering the wheel (outdoor air, in this case) and the regeneration temperature strongly influence the performance of the desiccant wheel; furthermore the process air humidity ratio and regeneration temperature have a higher influence on the desiccant wheel performance compared to the process air temperature.

However, one of the most innovative results is related to the effect of the ratio between the regeneration and process air flow rates; in fact, in case of fixed regeneration temperature, the

dehumidification effectiveness increases with the ratio of flow rates, as well as the moisture removal capacity; on the contrary, they decrease in the case of fixed regeneration thermal power. This means that the dehumidification performance of the desiccant wheel is more influenced by the regeneration temperature than by the regeneration air flow rate.

Experimental results on the performance of the desiccant wheel were compared with data provided by the manufacturer: a very good agreement was obtained; in particular, the average and maximum difference as well as the root mean square error, for each performance index and operating variable, are satisfactorily low.

Furthermore, an analysis to evaluate the desiccant wheel performance in handling the ventilation and internal latent load for various cities around the world was presented. The results showed that the selected outdoor thermal-hygrometric design data strongly affect the possibility for the desiccant wheel to completely balance the latent load. When using ASHRAE design dehumidification data (characterized by high dew point temperature) for the analyzed cities, the desiccant wheel is often not able to entirely handle even the ventilation latent load (due also to the low regeneration temperature, equal to about 65 °C). On the contrary, when using ASHRAE design cooling data, the wheel always allows at least the covering of the ventilation latent load.

Then, the results obtained for given cities were generalized for any climatic condition. Useful diagrams were obtained to evaluate the specific latent load that the desiccant wheel can handle as a function of outdoor humidity ratio, for different outdoor temperatures. The results showed that, for outdoor humidity ratio higher than about 15.5 g/kg, the desiccant wheel can balance at least the ventilation latent load only for low outdoor temperatures. This confirms that the process air inlet temperature also strongly affects the dehumidification capability of the rotor. Moreover, the specific internal latent load that can be handled by the desiccant wheel versus outdoor humidity ratio for different outdoor temperatures was evaluated. A simple chart to identify the required specific internal latent load as a function of the Sensible Heat Ratio was obtained. In this way, the designer can easily evaluate the specific internal latent load for the analyzed indoor ambient (characterized by a given SHR) and check if the silica-gel desiccant wheel with low regeneration temperature is able to balance it; otherwise, higher regeneration temperatures are necessary and the waste heat from the microcogenerator could be not sufficient for the desiccant regeneration.

As regards the global system, a desiccant based AHU powered by separate "production" (thermal power for regeneration from a natural gas boiler and electric power from the grid) can guarantee sensible savings in terms of primary energy consumption (6.5%) and greenhouse-gas emissions (14.6%) with respect to a conventional system (*"cooling dehumidification"* + re-heating of the supply air) in which electric, thermal and cooling energy is provided by the electric grid, a natural gas-fired boiler and an air-cooled water chiller, respectively. Primary Energy Saving and equivalent CO_2 avoided emissions increase (9.0% and 28.6% respectively) when the regeneration of the desiccant wheel is obtained by the waste heat recovered from a microcogenerator, which also supplies electrical energy to power the chiller and the AHU self-consumptions.

The best energetic and environmental results (PES and ΔCO_2 respectively equal to 21.2% and 38.6%) are obtained when the MCHP supplies its maximum electric and thermal power, and when the AHU has to dehumidify very humid outdoor air or when a very low humidity ratio of the supply air is required.

The performances of both the MCHP/HVAC-DW and the conventional system are strongly influenced by outdoor thermal-hygrometric conditions: the alternative system can guarantee a Primary Energy Saving when outdoor air humidity ratio is lower than 11.5 g/kg and outdoor air temperature is in the range 25 – 36 °C. Moreover, PES increases with outdoor temperature and when outdoor humidity decreases. The equivalent CO_2 avoided emissions show the same trend as PES.

Obviously, PES decreases when electric grid efficiency increases; however, even if the electric energy "production" is based on the Best Available Technology, PES remains positive (6%).

Therefore, desiccant-based AHUs are especially indicated in hot and humid climates, such as in Mediterranean countries, and can lead to sensible energy savings and equivalent CO_2 emission reductions with respect to conventional air conditioning systems, especially when it is matched to a small scale cogeneration system operating at full load.

Energy savings often give rise to economic savings. To that way, before installing such a system, a careful economic analysis has to be realized, in order to establish if a reasonable value of the pay-back period can be obtained, usually between three and five years for this type of investment. Presently, the first cost of both MCHP and desiccant wheel does not allow to obtain an

acceptable pay-back period. Anyway, there are several subjects involved in the definition of the economic variables concerning this type of energy conversion system, including the institutional sector and the private one (gas utilities, manufacturers,…). For example, government grants along with attractive rates for electricity export to the grid may significantly encourage MCHP and DW market penetration [167].

As it is also well known, legislative initiatives play a basic role in supporting very efficient technologies; for example EU introduced directives that can strongly contribute to the diffusion of small scale cogeneration and/or polygeneration systems, such as the directives on emission trading, electricity and gas markets as well as energy performance of building.

Further policies could be introduced by governments, such as low tax rates on gas, carbon tax exemption, dispatch priority in the transmission grid and economic instruments to support high energy efficiency systems.

In order to deepen the benefits of distributed generation systems, an experimental analysis of a MCHP, carried out at Technical University of Munich, was presented. Experimental tests were conducted in a test facility, that allows to simulate the space heating and domestic hot water requirements of a residential user, represented by a "Multi Family House", and to evaluate the energy flows of the energy conversion systems.

The MCHP was tested in four type days, that represent the different climatic conditions during the year. Experimental results show that the MCHP is able to achieve efficiencies and Primary Energy Ratio values quite comparable with the nominal ones.

Subsequently, the microcogeneration plant was compared, in terms of energy and environmental analysis, with a conventional reference system based on separate "production". On an annual basis, PES is equal to 14.0%, while ΔCO_2 is equal to 19.8%.

Finally, the PES calculation, as defined by the European Directive 2004/8/CE, was carried out. The qualification condition established by EU is widely achieved, as the Primary Energy Saving is higher than 24%. Therefore, the considered system can comply with several advantages (tax exemption, net metering, energy efficiency credits, priority distribution) that can favour it from an ecomomic point of view.

In distributed energy systems, a central management unit, with the aims of operating costs minimization, primary energy saving and reduction of climate-changing emissions, coordinates the

operation of numerous distributed devices, according to a Virtual Power Plant approach. This has several advantages, such as a more predictable and controllable electricity output of distributed energy resources, the integration of renewable-based systems as well as CHPs, the reduction of grid losses, the possibility to gain energy efficiency credits.

Università degli Studi del Sannio and Seconda Università di Napoli (SUN) cooperated with ENEA to the development of a Virtual Power Plant, aimed at the experimental analysis and the centralized remote control and thermo-economic optimization of the small scale polygeneration systems. To this aim, the software *POLILAB* was developed. It allows to: share among different operators the results of experimental tests; remotely check if the systems are working in ranges of operating conditions that allow to obtain primary energy savings, emissions and energy costs reductions; remotely operate on the MCCHP system to achieve the thermo-economic optimization of the distributed systems.

Due to the different type of equipments, devices and data acquisition softwares, a widely diffused software for remote desktop has been used to access the local acquisition system of the test facility. In particular, the *Labview*-based software *PoliLab_Unisannio* allows to monitor the thermal-dynamic properties in the MCHP/HVAC-DW system and to carry out energy balances on the main components. Furthermore, it is possible to evaluate energy performances of the main components (desiccant wheel, heating and cooling coils, MCHP, boiler and chiller) and carry out a 3-E analysis, comparing the microcogeneration system with a user-defined reference system.

The central operator, thanks to these information, may modify the operating conditions of one or more subsystems, in order to adequate the whole system as a consequence of a change in the boundary conditions.

Available experimental tests, as well as manufacturers' data, allowed to calibrate and validate models for the components of the MCHP/HVAC-DW system (AHU component, MCHP and chiller). The model of each subsystem in the desiccant-based AHU is based on the description of the operation through specific efficiency factors. In particular, the validity of the assumption for efficiency factors presenting constant values was experimentally investigated. The values of standard deviations deriving from the calibration effort are rather low, suggesting that the constant efficiency hypothesis is reasonable within the range of the analyzed operating conditions. Experimental validation was based on the RMSE and energy balance approaches. Both confirmed the validity of the assumed models, for each subsystem and for the complete system models.

Reliability of such models enables the simulation of the performance, considering both the single component (Moisture Removal Capacity of the desiccant wheel in the range 2.6 – 4.8 kg/h) and the complete system (thermal COP in the range 0.50 – 0.92), for example as a function of outdoor air thermal-hygrometric properties.

Simulation activity also aimed to investigate the technical feasibility of a solar collector system that provides regeneration thermal energy replacing the MCHP.

To this aim, a commercial software was used to design the solar collector system.

Afterwards, the simulation software TRNSYS was used in order to simulate the operation of the whole system, in which the solar collectors and the boiler interact with a tank, in which thermal energy for regeneration is stored.

Both Standard and TESS libraries were used to model the main components of the solar assisted desiccant-based AHU, that provides conditioned air to an office in Naples.

Results show that the solar collectors achieve a reasonable efficiency and can provide a significant amount (about 60%) of the thermal energy required for the regeneration of the desiccant wheel.

TRNSYS software was also used to model the current MCCHP system, simulating the energy and environmental performance of the trigeneration system with respect to the reference separate "production" one; simulative results agree with experimental ones, particularly concerning the effect of outdoor air thermal-hygrometric conditions on PES and ΔCO_2.

To conclude, the key factors that can sustain the diffusion of a microtrigeneration systems are:

- primary energy savings,
- reduction of greenhouse gas emissions,
- transition to gas cooling technologies, that shifts energy demand in summer from electricity to gas,
- shift from centralized to distributed energy "production" systems to avoid distribution losses, thus assuring high quality power supply and finally increasing the network availability.

The energy and environmental benefits of small-scale on-site trigeneration systems are undisputed, but some obstacles, such as high initial cost are still very prominent. In fact a support action is necessary which allows for an adequately short payback period.

NOMENCLATURE

A	collectors area, m^2
a1	solar collector efficiency slope, W/m^2K
a2	solar collector efficiency curvature, W/m^2K^2
AFUE	Annual Fuel Utilization Efficiency, dimensionless
AOC	Annual Operating Cost, k€/y
$b_0,b_1\ldots b_6$	fan power coefficient, dimensionless
C	Capacity rate, kW/K
CO_2	carbon dioxide equivalent emissions, kg/h
COP	Coefficient Of Performance, dimensionless
DCOP	Dehumidification Coefficient Of Performance, dimensionless
E	Energy, kJ or kWh
EER	Energy Efficiency Ratio, dimensionless
EF	Energy Factor, dimensionless
ESEER	European Seasonal Energy Efficiency Ratio, dimensionless
F_{bp}	Bypass factor, dimensionless
FFLP	Fraction of Full Load Power, dimensionless
G	total incident radiation per unit area, W/m^2
g	solar gain, dimensionless
GWP	Global Warming Potential, kg
h	enthalpy, kJ/kg
HHV	Higher Heating Value, kWh/Nm^3

HSPF	Heating Season Performance Factor, dimensionless
L	specific ventilation latent load, W/(m^3/h)
LHV	Lower Heating Value, kWh/Nm^3
$\dot{m}$	mass flow rate, kg/s
MRC	Moisture Removal Capacity, kg/h
N	Operating Hours, h
p	pressure, kPa
PEF	Primary Energy Factor, dimensionless
P_{el}	Electric power, kW
PER	Primary Energy Ratio, dimensionless
PES	Primary Energy Saving, dimensionless
PLR	Partial Load Ratio, dimensionless
P_p	Primary power, kW
Q_{cool}	Cooling power, kW
Q_{th}	Thermal power, kW
R^2	Determination coefficient, dimensionless
r_e	electric energy share provided to the chiller, dimensionless
RH	Relative Humidity, dimensionless
r_t	thermal energy share provided to the DW, dimensionless
SC	Specific Cost, €/kWh or €/Nm^3
SEER	Seasonal Energy Efficiency Ratio, dimensionless
SER	Sensible Energy Ratio, dimensionless

SF	Solar Fraction, dimensionless
SHR	Sensible Heat Ratio, dimensionless
SPB	Simple Payback Period, y
t	temperature, °C
U	thermal transmittance, W/m^2K
UA	Overall heat transfer coefficient, W/K
$\dot{V}$	volumetric flow rate, m^3/h

Greek symbols

Δ	difference
ΔCO_2	equivalent CO_2 avoided emissions, dimensionless
Δh_{vs}	latent heat of vaporization of water, kJ/kg
ΔIC	Investment Cost difference, k€
Φ	Desiccant wheel rotational speed, RPH
ε	effectiveness, dimensionless
η	efficiency or effectiveness, dimensionless
η_0	solar collector intercept efficiency, dimensionless
ρ	air density, kg/m^3
τ	time, s or hours
ω	air humidity ratio, g/kg

Acronyms

ABHP	Absorption Heat Pump
AHU	Air Handling Unit

AS	Alternative System
BAT	Best Available Technology
CB	Condensing Boiler
CCHP	Combined Cooling Heating and Power
CHP	Combined Heat and Power
CS	Conventional System
DB-MCWB	Dry Bulb – Mean Coincident Wet Bulb
DCHP	Domestic Combined Heat and Power
DEC	Direct Evaporative Cooler
DG	Distributed Generation
DHW	Domestic Hot Water
DP	Distributed Polygeneration
DP-MCDB	Dew Point – Mean Coincident Dry Bulb
DW	Desiccant Wheel
EGHX	Exhaust Gas Heat Exchanger
EHP	Electric Heat Pump
F1, F2	Characteristics potentials of Maclaine-Cross and Banks desiccant wheel model
G	electricity generator
GCT	Gas Cooling Technologies
GHG	Green House Gas
GHP	Gas engine driven Heat Pump

HVAC	Heating, Ventilation and Air Conditioning
IAQ	Indoor Air Quality
IC	Internal Combustion
LCA	Life Cycle Analysis
MCCHP	Micro Combined Cool, Heat and Power
MCHP	Micro Combined Heat and Power
MFH	Multi Family House
MG	Micro Generation
PM	Prime Mover
RIC	Reciprocating Internal Combustion
RPH	Revolutions Per Hour
RMSE	Root Mean Standard Error
SB	Standard Boiler
SC	Solar Collector
SFH	Single Family House
T&D	Transmission and Distribution
THP	Thermally activated Heat Pump
VC	Control Volume

Subscripts

ad	adiabatic
amb	ambient
aux	auxiliaries

b	boiler
cc	cooling coil
cf	cross flow
cool	cooling
dec	direct evaporative cooler
deh	dehumidification
dhw	domestic hot water
EGHX	Exhaust Gas Heat Exchanger
el	electric
F1, F2	Characteristics potentials of Maclaine-Cross and Banks desiccant wheel model
hc	heating coil
in	inlet
M	relative to the MCCHP system
m	relative to the MCHP system
max	maximum
min	minimum
n	net
NG	Natural Gas
nom	nominal
opt	optimal
out	outdoor or outlet

p	primary
pl	plate heat exchanger
proc	process
r	indoor thermal-hygrometric conditions
ref	reference system
reg	regeneration
s	supply thermal-hygrometric condition
sat	saturation
sol	solution
sum	summer
sur	surface
SC	Solar Collectors
t	temperature
th	thermal
v	vapour
w	water
win	winter
wb	wet bulb
wh	water heater
ω	humidity ratio

Superscripts

AS	Alternative System

B	Boiler
CH	Chiller
CS	Conventional System
EG	Electric Grid
SP	Separate Production
US	User

REFERENCES

[1] Munters Cargocaire, The Dehumidification Handbook, 2nd ed., Amesbury, MA, USA, 1990;

[2] L.G. Harriman, The basics of commercial desiccant systems, *Heating, Piping and Air Conditioning* 66 (1994) 77-85;

[3] ASHRAE, 2008 ASHRAE Handbook – HVAC Systems and Equipment, American Society of Heating, Refrigerating and Air-Conditioning Engineers, Atlanta, GA, USA, chapter 23 (Desiccant Dehumidification and Pressure-Drying Equipment), 2008;

[4] M. Kubota, T. Hanada, S. Yabe, D. Kuchar, H. Matsuda, Water desorption behavior of desiccant rotor under microwave irradiation, *Applied Thermal Engineering* 31 (2011) 1842-1846;

[5] R.F. Babus'Haq, H. Olsen, S.D. Probert, Feasibility of using an Integrated Small-Scale CHP Unit plus Desiccant Wheel in a Leisure Complex, *Applied Energy* 53 (1996) 179-192;

[6] H.M. Henning, T. Erpenbeck, C. Hindenburg, I.S. Santamaria, The potential of solar energy use in desiccant cooling cycles, *International Journal of Refrigeration* 24 (2001) 220-229;

[7] A. Capozzoli, P. Mazzei, F. Minichiello, D. Palma, Hybrid HVAC systems with chemical dehumidification for supermarket applications, *Applied Thermal Engineering* 26 (2006) 795-805;

[8] P. Mazzei, F. Minichiello, D. Palma, HVAC dehumidification systems for thermal comfort: a critical review, *Applied Thermal Engineering* 25 (2005) 677-707;

[9] K.J. Chua, S.K. Chou, W.M. Yang, Advances in heat pump systems: A review, *Applied Energy* 87 (2010) 3611-3624;

[10] B. Kovak, P.R. Heimann, J. Hammel, The sanitizing effects of desiccant based cooling, *ASHRAE Journal* 39 (1997) 60-64;

[11] M. Meckler, Desiccant-assisted air conditioner improves IAQ and comfort, *Heating, Piping and Air Conditioning* 66 (1994) 75-84;

[12] R.M. Lazzarin, F. Castellotti, A new heat pump desiccant dehumidifier for supermarket application, *Energy and Buildings* 39 (2007) 59–65;

[13] T.N. Aynur, Y. Hwang, R. Radermacher, Field performance measurements of a heat pump desiccant unit in dehumidification mode, *Energy and Buildings* 40 (2008) 2141-2147;

[14] G. Angrisani, C. Roselli, M. Sasso, Experimental tests on a polygeneration system with a desiccant-based AHU, 2nd International Conference on Microgeneration and Related Technologies, University of Strathclyde, Glasgow, UK, April 4 – 6, 2011;

[15] G. Angrisani, Analisi sperimentale di impianti di climatizzazione ibridi ad elevata efficienza energetica, Master's degree in Energy Engineering, Faculty of Engineering, University of Sannio, 2008;

[16] S.J. Slayzak, J.P. Ryan, Desiccant Dehumidification Wheel Test Guide, NREL Technical report, NREL/TP-550-26131, 2000;

[17] R. Mastrullo, P. Mazzei, R. Vanoli, Termodinamica per ingegneri – Applicazioni, Liguori Editore, 1996;

[18] D. La, Y.J. Dai, Y. Li, R.Z. Wang, T.S. Ge, Technical development of rotary desiccant dehumidification and air conditioning: A review, *Renewable and Sustainable Energy Reviews* 14 (2010) 130-147;

[19] F. Esfandiari Nia, D. Van Paassen, M.H. Saidi, Modeling and simulation of desiccant wheel for air conditioning, *Energy and Buildings* 38 (2006) 1230-1239;

[20] P. Stabat, D. Marchio, Heat and mass transfer modeling in rotary desiccant dehumidifiers, *Applied Energy* 86 (2009) 762-771;

[21] C.X. Jia, Y.J. Dai, J.Y. Wu, R.Z. Wang, Experimental comparison of two honeycombed desiccant wheels fabricated with silica gel and composite desiccant material, *Energy Conversion and Management* 47 (2006) 2523-2534;

[22] C.X. Jia, Y.J. Dai, J.Y. Wu, R.Z. Wang, Use of compound desiccant to develop high performance desiccant cooling system, *International Journal of Refrigeration* 30 (2007) 345-353;

[23] T.S. Ge, F. Ziegler, R.Z. Wang, A mathematical model for predicting the performance of a compound desiccant wheel (A model of compound desiccant wheel), *Applied Thermal Engineering* 30 (2010) 1005-1015;

[24] N. Enteria, H. Yoshino, A. Satake, A. Mochida, R. Takaki, R. Yoshie, T. Mitamura, S. Baba, Experimental heat and mass transfer of the separated and coupled rotating desiccant wheel and heat wheel, *Experimental Thermal and Fluid Sciences* 34 (2010) 603-615;

[25] D. Rossington, S. White, A. Weigand, R. Sire, R. Reece, P. Kohlenbach, Comparison of silica gel and zeolite desiccant wheel performance, 3rd Solar Air Conditioning, Palermo, Italy, September 30 – October 2, 2009, 230-235;

[26] N. Subramanyam, M.P. Maiya, S. Srinivasa Murthy, Parametric studies on a desiccant assisted air-conditioner, *Applied Thermal Engineering* 24 (2004) 2679-2688;

[27] P. Stabat, D. Marchio, Heat-and-mass transfers modelled for rotary desiccant dehumidifiers, *Applied Energy* 85 (2008) 128-142;

[28] M. Hamed Ahmed, A. Khalil, A.E. Kabeel, M.M. Bassuoni, A.M. Elzahaby, Performance analysis of dehumidification rotating wheel using liquid desiccant, *Renewable Energy* 30 (2005) 1689-1712;

[29] Z.Q. Xiong, Y.J. Dai, R.Z. Wang, Development of a novel two-stage liquid desiccant dehumidification system assisted by $CaCl_2$ solution using exergy analysis method, *Applied Energy* 87 (2010) 1495-1504;

[30] Z. Gao, V.C. Mei, J.J. Tomlinson, Theoretical analysis of dehumidification process in a desiccant wheel, *Heat and Mass Transfer* 41 (2005) 1033-1042;

[31] M. Beccali, F. Butera, R. Guanella, R.S. Adhikari, Simplified models for the performance evaluation of desiccant wheel dehumidification, *International Journal of Energy Research* 27 (2003) 17-29;

[32] M. Beccali, F. Butera, V. Franzitta, R.S. Adhikari, Update on desiccant wheel model, *International Journal of Energy Research* 28 (2004) 1043-1049;

[33] M.A. Mandegari, H. Pahlavanzadeh, Introduction of a new definition for effectiveness of desiccant wheels, *Energy* 34 (2009) 797-803;

[34] Y. Yao, W. Zhang, S. Liu, Feasibility study on power ultrasound for regeneration of silica gel – A potential desiccant used in air-conditioning system, *Applied Energy* 86 (2009) 2394-2400;

[35] G. Panaras, E. Mathioulakis, V. Belessiotis, N. Kyriakis, Experimental validation of a simplified approach for a desiccant wheel model, *Energy and Buildings* 42 (2010) 1719-1725;

[36] M.H. Ahmed, N.M. Kattab, M. Fouad, Evaluation and optimization of solar desiccant wheel performance, *Renewable Energy* 30 (2005) 305-325;

[37] T. Vitte, J. Brau, N. Chatagnon, M. Woloszyn, Proposal for a new hybrid control strategy of a solar desiccant evaporative cooling air handling unit, *Energy and Buildings* 40 (2008) 896–905;

[38] A. Khalid, M. Mahmood, M. Asif, T. Muneer, Solar assisted, pre-cooled hybrid desiccant cooling system for Pakistan, *Renewable Energy* 34 (2009) 151-157;

[39] N. Enteria, H. Yoshino, A. Satake, A. Mochida, R. Takaki, R. Yoshie, S. Baba, Development and construction of the novel solar thermal desiccant cooling system incorporating hot water production, *Applied Energy* 87 (2010) 478-486;

[40] N. Enteria, H. Yoshino, A. Mochida, R. Takaki, A. Satake, R. Yoshie, T. Mitamura, S. Baba, Construction and initial operation of the combined solar thermal and electric desiccant cooling system, *Solar Energy* 83 (2009) 1300-1311;

[41] U. Eicker, D. Schneider, J. Schumacher, T. Ge, Y. Dai, Operational experiences with solar air collector driven desiccant cooling systems, *Applied Energy* 87 (2010) 3735-3747;

[42] H.M. Henning, T. Pagano, S. Mola, E. Wiemken, Micro tri-generation system for indoor air conditioning in the Mediterranean climate, *Applied Thermal Engineering* 27 (2007) 2188-2194;

[43] G. Schmitz, W. Casas, Experiences with a gas driven, desiccant assisted air conditioning system with geothermal energy for an office building, *Energy and Buildings* 37 (2005) 493-501;

[44] G. Schmitz, W. Casas, Experiences with a small gas engine driven desiccant HVAC-System, International Gas Research Conference, Amsterdam, Netherlands, November 5 – 8, 2001;

[45] G. Schmitz, C.K. Qin, Engine driven desiccant-assisted hybrid air-conditioning system, 23rd World Gas Conference, Amsterdam, Nederlands, June 5 – 9, 2006;

[46] A. Jalalzadeh-Azar, S. Slayzak, R. Judkoff, T. Schaffhauser, R. DeBlasio, Performance assessment of a desiccant cooling system in a CHP application incorporating an IC engine, *International Journal of Distributed Energy Resources* 1 (2005) 163-184;

[47] G. Angrisani, A. Capozzoli, F. Minichiello, C. Roselli, M. Sasso, Desiccant wheel regenerated by thermal energy from a microcogenerator: Experimental assessment of the performances, *Applied Energy* 88 (2011) 1354–1365;

[48] G. Angrisani, F. Minichiello, C. Roselli, M. Sasso, Experimental analysis on the performances of a desiccant wheel regenerated by low grade thermal energy, International Sorption Heat Pump Conference, Padua, Italy, April 6 – 8, 2011, ISBN 978-1-61782-952-9;

[49] G. Angrisani, C. Roselli, M. Sasso, F. Minichiello, Experimental analysis on the dehumidification and thermal performances of a desiccant wheel, accepted for publication by the international journal *Applied Energy*, 2011;

[50] K. Daou, R.Z. Wang, Z.Z. Xia, Desiccant cooling air conditioning: a review, *Renewable and Sustainable Energy Reviews* 10 (2006) 55-77;

[51] M. Kanoğlu, M. Özdinç Çarpınlıoğlu, M. Yıldırım, Energy and exergy analyses of an experimental open-cycle desiccant cooling system, *Applied Thermal Engineering* 24 (2004) 919-932;

[52] E. Van Den Bulck, S.A Klein, J.W. Mitchell, Second law analysis of solid desiccant rotary dehumidifiers, *ASME Journal of Heat Transfer* 110 (1988) 2-9;

[53] R.R. Rogers, M.K. Yau, A Short Course in Cloud Physics, Pergamon, 1989;

[54] S.J. Kline, F.A. McClintock, Describing uncertainties in single-sample experiment, *Mechanical Engineering* 75 (1953) 3-8;

[55] S.J. Slayzak, J.P Ryan, Instrument uncertainty effect on calculation of absolute humidity using dewpoint, wet-bulb, and relative humidity sensors, International Solar Energy Conference, Albuquerque, New Mexico, USA, June 14 – 17, 1998, 473-479;

[56] J.R. Camargo, E. Godoy Jr., N. de Paula da Silva, Performance analysis of a rotary wheel dehumidifier applied to air conditioning, *Journal of Engineering and Applied Sciences* 2 (2007) 186-190;

[57] S. De Antonellis, C.M. Joppolo, A. Pasini, F. Romano, Effect of desiccant wheel revolution speed control on performances of solar desiccant cooling systems, 3rd Solar Air Conditioning, Palermo, Italy, September 30 – October 2, 2009;

[58] J. D. Chung, D.Y. Lee, S. M. Yoon, Optimization of desiccant wheel speed and area ratio of regeneration to dehumidification as a function of regeneration temperature, *Solar Energy* 83 (2009) 625–635;

[59] A. Kodama, T. Hirayama, M. Goto, T. Hirose, R.E. Critoph, The use psychrometric charts for the optimisation of a thermal swing desiccant wheel, *Applied Thermal Engineering* 21 (2001) 1657-1674;

[60] C.R. Ruivo, J.J. Costa, A.R. Figueiredo, A. Kodama, Effectiveness parameters for the prediction of the global performance of desiccant wheels - An assessment based on experimental data, *Renewable Energy* 38 (2012) 181-187;

[61] American Society of Heating, Refrigerating and Air-Conditioning Engineers, 2009 ASHRAE Handbook – Fundamentals, Atlanta, GA, USA, chapter 14 (Climatic design information), 2009;

[62] L. Harriman, G. Brundrett, R. Kittler, Humidity Control Design Guide for Commercial and Institutional Buildings, American Society of Heating, Refrigerating and Air-Conditioning Engineers, Atlanta, GA, USA, chapter 31 (Weather data for design), 2001;

[63] D. Favrat, La conversion d'énergie primaire en électricité: En quête de performances, *Revue Suisse de l'Énergie* 23 (1994) 16-23;

[64] H.L. Willis, W.G. Scott, Distributed power generation: planning and evaluation, Marcel Dekker Inc., New York (ISBN 0-8247-0336-7), 2000;

[65] R. Possidente, C. Roselli, M. Sasso, S. Sibilio, Small scale decentralized polygeneration systems, ECOS 2009, 22nd International Conference on Efficiency, Cost, Optimization,

Simulation and Environmental Impact of Energy Systems, Foz do Iguaçu, Paraná, Brazil, August 31 – September 3, 2009;

[66] M. Sasso, V. Scuto, G.P. Vanoli, Miniaturization of energy conversion systems: Energetic analysis, IMECE International Mechanical Engineering Congress & Exposition, The Winter Annual Meeting of ASME (WAM), Orlando, USA, 2005;

[67] M. Sasso, V. Scuto, G.P. Vanoli, Energetic Analysis of miniaturization in cooling devices, IRHACE - Innovative Equipment and Systems for Comfort and Food Preservation, Auckland, New Zealand, 2006;

[68] J.A. Orlando, Cogeneration design guide, American Society of Heating, Refrigerating and Air-Conditioning Engineers, Atlanta, GA, USA, 1996;

[69] Directive 2004/8/EC of the European Parliament and of the Council of the 11 February 2004 on the promotion of cogeneration based on the useful heat demand in the internal energy market and amending Directive 92/42/ EEC, Official Journal of the European Union, 21.02.2004;

[70] G. Angrisani, C. Roselli, M. Sasso, Distributed microtrigeneration systems, under review by the international journal *Progress in Energy and Combustion Science*, 2011;

[71] M. Dentice d'Accadia, M. Sasso, S. Sibilio, L. Vanoli, Micro-combined heat and power in residential and light commercial applications, *Applied Thermal Engineering* 23 (2003) 1247-1259;

[72] G. Angrisani, C. Roselli, M. Sasso, M. Citterio, Creazione di un database di sistemi di microcogenerazione, Report RSE/2009/118, ENEA – MSE, 2009, http://old.enea.it/attivita_ricerca/energia/sistema_elettrico/Governance/RSE118.pdf;

[73] A. Piacentino, F. Cardona, An original multi-objective criterion for the design of small-scale polygeneration systems based on realistic operating conditions, *Applied Thermal Engineering* 28 (2008) 2391-2404;

[74] G. Angrisani, C. Roselli, M. Sasso, S. Sibilio, Analisi sperimentale di impianti di poligenerazione di piccola taglia basati su un motore a combustione interna alimentato a gas naturale, 65° Congresso Nazionale ATI – Domus de Maria (CA), 13 – 17 settembre 2010;

[75] G.R. Simader, R. Krawinkler, G. Trnka, Micro CHP systems: state-of-the-art, A technical report of Green Lodges Project (EIE/04/252/S07.38608), 2006, http://www.polysmart.org/cms/upload/publications/WP_final_reports/WP2_Market_Study_Final_Report_v10_Final.pdf;

[76] I. Knight, I. Ugursal, Residential cogeneration systems: a review of the current technologies, Technical report of Subtask A FC+COGEN-SIM, IEA Annex 42, 2005,

http://www.ecbcs.org/docs/Annex_42_Review_Residential_Cogen_Technologies.pdf;

[77] D.W. Wu, R.Z. Wang, Combined cooling, heating and power: a review, *Progress in energy and combustion science* 32 (2006) 459-495;

[78] G. Angrisani, A. Rosato, C. Roselli, M. Sasso, S. Sibilio, Trial results of domestic CHP & solar cooling technologies use in an office application, 2nd International Conference on Microgeneration and Related Technologies, University of Strathclyde, Glasgow, UK, April 4 – 6, 2011;

[79] G. Angrisani, C. Roselli, M. Sasso, S. Sibilio, A. Rosato, Experimental results of a micro-trigeneration installation, under review by the international journal *Applied Thermal Engineering*, 2011;

[80] PolySMART, POLYgeneration with advanced Small and Medium scale thermally driven Air-conditioning and Refrigeration Technology, 2010, www.polysmart.org;

[81] G. Angrisani, C. Roselli, M. Sasso, Review of existing Micro-Generation performance assessments studies and experimental activity, a draft report of Subtask B of IEA/ECBCS Annex 54, Integration of Micro-Generation and Related Energy Technologies in Buildings, 2011;

[82] G. Angrisani, C. Roselli, M. Sasso, Methodologies for the Performance Assessment of Micro Hybrid Poligeneration Systems, a draft report of Subtask B of IEA/ECBCS Annex 54, Integration of Micro-Generation and Related Energy Technologies in Buildings, 2011;

[83] P. Mancarella, G. Chicco, Global and local emission impact assessment of distributed cogeneration systems with partial-load models, *Applied Energy* 86 (2009) 2096-2106;

[84] M.F. Torchio, G. Genon, A. Poggio, M. Poggio, Merging of energy and environmental analyses for district heating systems, *Energy* 34 (2009) 220-227;

[85] G. Genon, M.F. Torchio, A. Poggio, M. Poggio, Energy and environmental assessment of small district heating systems: Global and local effects in two case-studies, *Energy Conversion and Management* 50 (2009) 522-529;

[86] A. Canova, G. Chicco, G. Genon, P. Mancarella, Emission characterization and evaluation of natural gas-fueled cogeneration microturbines and internal combustion engines, *Energy Conversion and Management* 49 (2008) 2900-2909;

[87] W.M. Ellis, M.B. Gunes, Status of fuel cell systems for combined heat and power applications in buildings, *ASHRAE Transactions* (2002) 108-11;

[88] H.I. Onovwiona, V.I. Ugursal, Residential cogeneration systems: review of the current technology, *Renewable and Sustainable Energy Reviews* 10 (2006) 389-431;

[89] European Commission Decision of 21st December 2006, Official Journal of the European Union, 06.02.2007;

[90] V. Dorer, A. Weber, Methodologies for the Performance Assessment of Residential Cogeneration Systems, A Report of Subtask C of FC+COGEN-SIM The Simulation of Building-Integrated Fuel Cell and Other Cogeneration Systems, Annex 42, IEA, 2007, http://www.ecbcs.org/docs/Annex_42_STC_PAM.pdf;

[91] A.D. Hawkes, Estimating marginal CO_2 emissions rates for national electricity systems, *Energy Policy* 38 (2010) 5977-5987;

[92] H. Hondo, Life cycle GHG emission analysis of power generation systems: Japanese case, *Energy* 30 (2005) 2042-2056;

[93] Covenant of Mayors, How to develop a Sustainable Energy Action Plan (SEAP) – Guidebook, 2010, http://www.eumayors.eu/IMG/pdf/seap_guidelines_en.pdf;

[94] X.H. Liu, K.C. Geng, B.R. Lin, Y. Jiang, Combined cogeneration and liquid-desiccant system applied in a demonstration building, *Energy and Buildings* 36 (2004) 945-953;

[95] M. Badami, A. Portoraro, Performance analysis of an innovative small-scale trigeneration plant with liquid desiccant cooling system, *Energy and Buildings* 41 (2009) 1195-1204;

[96] R.M. Lazzarin, A. Gasparella, New ideas for energy utilisation in combined heat and power with cooling: I. Principles, *Applied Thermal Engineering* 4 (1997) 369-384;

[97] R.M. Lazzarin, A. Gasparella, New ideas for energy utilisation in combined heat and power with cooling: II. Applications, *Applied Thermal Engineering* 5 (1997) 479-500;

[98] T. Katejanekarn, S. Kumar, Performance of a solar-regenerated liquid desiccant ventilation pre-conditioning system, *Energy and Buildings* 40 (2008) 1252-1267;

[99] L. Mei, D. Infield, U. Eicker, D. Loveday, V. Fux, Cooling potential of ventilated PV façade and solar air heaters combined with a desiccant cooling machine, *Renewable Energy* 31 (2006) 1265-1278;

[100] Y. Sukamongkol, S. Chungpaibulpatana, B. Limmeechokchai, P. Sripadungtham, Condenser heat recovery with a PV/T air heating collector to regenerate desiccant for reducing energy use of an air conditioning room, *Energy and Buildings* 42 (2010) 315-325;

[101] G. Angrisani, F. Minichiello, C. Roselli, M. Sasso, Desiccant HVAC system driven by a micro-CHP: Experimental analysis, *Energy and Buildings* 42 (2010) 2028–2035;

[102] R. Possidente, C. Roselli, M. Sasso, S. Sibilio, Analysis of small scale decentralized cogeneration in Southern Italy, 1st International Conference & Workshop on Micro-Cogeneration Technologies & Applications, Micro-Cogen 2008, Ottawa, Canada, 2008;

[103] http://www.aisin.com;

[104] R. Possidente, C. Roselli, M. Sasso, S. Sibilio, Experimental analysis of micro-cogeneration units based on reciprocating internal combustion engine, *Energy and Buildings* 38 (2006) 1417-1422;

[105] C. Roselli, M. Sasso, S. Sibilio, P. Tzscheutschler, Experimental analysis of microcogenerators based on different prime movers, *Energy and buildings* 43 (2011) 796-804;

[106] G. Angrisani, C. Roselli, M. Sasso, Numerical analysis of a Small Scale Polygeneration Plant with a Desiccant-Based Air Handling Unit, 23rd International Conference on Efficiency, Cost, Optimization Simulation and Environmental Impact of Energy Systems, Lausanne, Switzerland, June 14 – 17, 2010, ISBN/EAN13 1456303201 / 9781456303204;

[107] G. Chicco, P. Mancarella, Trigeneration primary energy saving evaluation for energy planning and policy development, *Energy Policy* 35 (2007) 6132-6144;

[108] Italian Environmental Ministry, www.minambiente.it;

[109] National Italian Organization for Unification, norm UNI 10339:1995;

[110] N. Rossi, Manuale del Termotecnico, Ulrico Hoepli, Milano, 2003;

[111] A. Briganti, Manuale della Climatizzazione, Tecniche Nuove, Milano, 2001;

[112] CoolPack Software Package, Ver. 1.46, Department of Mechanical Engineering, Technical University of Denmark, Lyngby, Denmark, 2000;

[113] IMST-ART Software Package, Ver. 3.20.02, Instituto de Ingeniería Energética, Universidad Politécnica de Valencia, Valencia, Spain, 2009;

[114] H. Li, L. Fu, K. Geng, Y. Jiang, Energy utilization evaluation of CCHP systems, *Energy and Buildings* 38 (2006) 253-257;

[115] G. Angrisani, F. Minichiello, C. Roselli, M. Sasso, G. P. Vanoli, Experimental analysis of a small scale polygeneration system based on a natural gas-fired micro-CHP and a hybrid HVAC system equipped with a desiccant wheel, ECOS 2009, 22nd International Conference on Efficiency, Cost, Optimization, Simulation and Environmental Impact of Energy Systems, Foz do Iguaçu, Paraná, Brazil, August 31 – September 3, 2009, ISSN 2175-5426;

[116] G. Angrisani, F. Minichiello, C. Roselli, M. Sasso, Experimental investigation to optimise a desiccant HVAC system coupled to a small size cogenerator, *Applied Thermal Engineering* 31 (2011) 506-512;

[117] E. Bettanini, A. Gastaldello, L. Schibuola, Simplified models to simulate part load performances of air conditioning equipments, IBPSA 2003, 8th International Conference of International Building Performance Simulation Association, Eindhoven, The Netherlands, August 11 – 14, 2003;

[118] G. Angrisani, C. Roselli, M. Sasso, in collaboration with con A. Rosato, S. Sibilio, Sviluppo di un ambiente di monitoraggio, controllo e gestione remota di una rete di micro_poligeneratori distribuiti, Report RdS/2011/131, ENEA – MSE, 2011, http://editors.enea.it/it/Ricerca_sviluppo/documenti/ricerca-di-sistema-elettrico/efficienza-energetica-servizi/rds-131.pdf;

[119] G. Angrisani, C. Roselli, M. Sasso, in collaboration with con A. Rosato, S. Sibilio, Report RdS/2011/130, ENEA – MSE, 2011, http://editors.enea.it/it/Ricerca_sviluppo/documenti/ricerca-di-sistema-elettrico/efficienza-energetica-servizi/rds-130.pdf;

[120] http://www.gossenmetrawatt.com/english/produkte/ecswin.htm;

[121] http://www.ni.com/labview/;

[122] G. Angrisani, C. Roselli, M. Sasso, S. Sibilio, A. Rosato, Analisi sperimentale di un sistema di microcogenerazione per utenze residenziali, 66° Congresso Nazionale ATI – Università della Calabria, Rende (CS), 5 – 9 settembre 2011;

[123] http://www.senertec.de/;

[124] P. Tzscheutschler, H. Muehlbacher, Results of experimental measurement of residential cogeneration systems, 1st International Conference & Workshop on Micro-Cogeneration & Applications, Ottawa, Canada, 2008;

[125] D.P.R. 26 agosto 1993, n. 412. Regolamento recante norme per la progettazione, l'installazione, l'esercizio e la manutenzione degli impianti termici degli edifici ai fini del contenimento dei consumi di energia;

[126] www.meteonorm.com;

[127] TRNSYS 17, a TRaNsient SYstem Simulation program, Solar Energy Laboratory, University of Wisconsin-Madison, 2010;

[128] M. Oliva, Analisi energetica di utenze domestiche e valutazione dell'impiego di sistemi di microcogenerazione, Tesi di Laurea, Facoltà di Ingegneria, Università degli Studi di Napoli Federico II, 2005;

[129] http://www.ni.com/diadem/;

[130] G. Angrisani, C. Roselli, M. Sasso, Experimental validation of constant efficiency models for the subsystems of an unconventional desiccant-based Air Handling Unit and investigation of its performance, *Applied Thermal Engineering* 33-34 (2012) 100-108;

[131] T.E.S.S. Component Libraries v.17.01 for TRNSYS v17.0 and the TRNSYS Simulation Studio, Parameter/Input/Output Reference Manual, Thermal Energy System Specialists, LLC, 2004;

[132] G. Panaras, E. Mathioulakis, V. Belessiotis, N. Kyriakis, Theoretical and experimental investigation of the performance of a desiccant air-conditioning system, *Renewable Energy* 35 (2010) 1368-1375;

[133] P. Bourdoukan, E. Wurtz, P. Joubert, Comparison between the conventional and recirculation modes in desiccant cooling cycles and deriving critical efficiencies of components, *Energy* 35 (2010) 1057-1067;

[134] P. Bourdoukan, E. Wurtz, P. Joubert, M. Spérandio, Critical efficiencies of components in desiccant cooling cycles and a comparison between the conventional mode and the recirculation mode, 21st International Conference on Efficiency, Cost, Optimization, Simulation and Environmental Impact of Energy Systems, Cracow-Gliwice, Poland, June 24 – 27, 2008;

[135] G. Panaras, E. Mathioulakis, V. Belessiotis, Achievable working range for solid all-desiccant air-conditioning systems under specific space comfort requirements, *Energy and Buildings* 39 (2007) 1055-1060;

[136] L.Z. Zhang, Energy performance of independent air dehumidification systems with energy recovery measures, *Energy* 31 (2006) 1228-1242;

[137] K.A. Joudi, N.S. Dhaidan, Application of solar assisted heating and desiccant cooling systems for a domestic building, *Energy Conversion and Management* 42 (2001) 995-1022;

[138] L.Z. Zhang, J.L. Niu, Indoor humidity behaviors associated with decoupled cooling in hot and humid climates, *Building and Environment* 38 (2003) 99-107;

[139] W.M. Kays, A.L. London, Compact Heat Exchangers, McGraw-Hill Book Co., New York, 1964;

[140] R. Narayanan, W.Y. Saman, S.D. White, M. Goldsworthy, Comparative study of different desiccant wheel designs, *Applied Thermal Engineering* 31 (2011) 1613-1620;

[141] I.L. Maclaine-Cross, P.J. Banks, Coupled heat and mass transfer in regenerators – predictions using an analogy with heat transfer, *International Journal of Heat and Mass Transfer* 15 (1972) 1225-1242;

[142] J.J. Jurinak, Open cycle solid desiccant cooling: component models and system Simulations, Ph.D. Thesis, Univ. of Wisconsin-Madison, 1982;

[143] P.J. Banks, Prediction of Heat and Mass Regenerator performance using nonlinear analogy method: part 1 – basis, *Journal of Heat Transfer* 107 (1985) 222-229;

[144] E. Hürdoğan, O. Büyükalaca, T. Yılmaz, A. Hepbaşlı, Experimental investigation of a novel desiccant cooling system, *Energy and Buildings* 42 (2010) 2049-2060;

[145] P. Bourdoukan, E. Wurtz, P. Joubert, Experimental investigation of a solar desiccant cooling installation, *Solar Energy* 83 (2009) 2059-2073;

[146] N. Subramanyam, M.P. Maiya, S. Srinivasa Murthy, Application of desiccant wheel to control humidity in air-conditioning systems, *Applied Thermal Engineering* 24 (2004) 2777-2788;

[147] D. La, et al., Use of regenerative evaporative cooling to improve the performance of a novel one-rotor two-stage solar desiccant dehumidification unit, *Applied Thermal Engineering* (2011), doi:10.1016/j.applthermaleng.2011.01.010;

[148] A. Preisler, T. Selke, Experience report on two different solar driven air-conditioning systems in Vienna/Austria based on monitoring data of summer 2008/2009, 3rd Solar Air Conditioning International Conference, Palermo, Italy, September 31 – October 2, 2009;

[149] T.S Ge, Y.J. Dai, R.Z. Wang, Y. Li, Experimental investigation on a one-rotor two-stage rotary desiccant cooling system, *Energy* 33 (2008) 1807-1815;

[150] V. Dorer, A. Weber, Energy and CO_2 emissions performance assessment of residential micro-cogeneration systems with dynamic whole-building simulation programs, *Energy Conversion and Management* 50 (2009) 648-657;

[151] I. Beausoleil-Morrison, Specifications for Modelling Fuel Cell and Combustion-Based Residential Cogeneration Devices within Whole-Building Simulation Programs, A Report of Subtask B of FC+COGEN-SIM The Simulation of Building-Integrated Fuel Cell and Other Cogeneration Systems, Annex 42, IEA, 2007, http://www.ecbcs.org/docs/Annex_42_Cogen_Model_Specifications.pdf;

[152] I. Beausoleil-Morrison, A. Ferguson, Inter-model Comparative Testing and Empirical Validation of Annex 42 Models for Residential Cogeneration Devices, A Report of Subtask B of FC+COGEN-SIM The Simulation of Building-Integrated Fuel Cell and Other Cogeneration Systems, Annex 42, IEA, 2007, http://www.ecbcs.org/docs/Annex_42_Comparative_Testing_&_Empirical_Validation.pdf

[153] I. Beausoleil-Morrison et al., Experimental Investigation of Residential Cogeneration Devices and Calibration of Annex 42 Models, A Report of Subtask B of FC+COGEN-SIM The Simulation of Building-Integrated Fuel Cell and Other Cogeneration Systems, Annex 42, IEA, 2007,

http://www.ecbcs.org/docs/Annex_42_Experiments_&_Model_Calibration.pdf;

[154] A. Ferguson, N. Kelly, A. Weber, B. Griffith, Modelling Residential-scale Combustion-based Cogeneration in Building Simulation, *Journal of Building Performance Simulation*, 2 (2009) 1-14;

[155] R. Possidente, C. Roselli, M. Sasso, S. Sibilio, Performance assessment of residential cogeneration systems in southern Italy, A Report of Subtask C of FC+COGEN-SIM The Simulation of Building-Integrated Fuel Cell and Other Cogeneration Systems, Annex 42, IEA, 2007,

http://www.ecbcs.org/docs/Annex_42_Performance_Assessment_of_Residential_Cogeneration_Systems_in_Southern_Italy.pdf;

[156] U. Arndt, W. Mauch, H. Mühlbacher, P. Tzscheutschler, B. Geiger B, Performance of residential cogeneration systems in Germany, A Report of Subtask C of FC+COGEN-SIM

The Simulation of Building-Integrated Fuel Cell and Other Cogeneration Systems, Annex 42, IEA, 2007,

http://www.ecbcs.org/docs/Annex_42_Performance_of_Residential_Cogeneration_Systems_in_Germany.pdf;

[157] N.J. Kelly, J. A. Clarke, A. Ferguson, G. Burt, Developing and Testing a Generic Micro-combined Heat and Power Model for Simulations of Dwellings and Highly Distributed Power Systems, *Power and Energy* 222 (2008) 685-695;

[158] M. De Paepe, P. D'Herdt, D. Mertens, Micro-CHP systems for residential applications, *Energy Conversion and Management* 47 (2005) 3435-3446;

[159] P. Gonçalves, A. Gaspar, M. Gameiro da Silva, Comparative exergy and energy performance analysis of a separated and combined heat and power system for a student housing building, Microgen II – 2nd International Conference on Microgeneration and related Technologies, April 4 – 6, Glasgow, UK, 2011;

[160] B. Di Pietra, Performance assessment of residential cogeneration systems in different Italian climatic zones, Report of Subtask C of FC+COGEN-SIM The Simulation of Building-Integrated Fuel Cell and Other Cogeneration Systems, Annex 42, IEA, 2007,

http://www.ecbcs.org/docs/Annex_42_Performance_Assessment_of_Residential_Cogeneration_Systems_in_Different_Italian_Climatic_Zones.pdf;

[161] V. Dorer, A. Weber, Performance assessment of residential cogeneration systems in Switzerland, A Report of Subtask C of FC+COGEN-SIM The Simulation of Building-Integrated Fuel Cell and Other Cogeneration Systems, Annex 42, IEA, 2007, http://www.ecbcs.org/docs/Annex_42_Switzerland_Empa_Study.pdf;

[162] G.O. Curme Jr., F. Johnston, Glycols, Reinhold Publishing Corp., New York, 1952;

[163] J. Bush, Modeling of a combined heat and power unit and evaluation of system performance in building applications, Masters of Science, 2010;

[164] G. Angrisani, C. Roselli, M. Sasso, C. Stellato, Design and simulation of a solar assisted desiccant-based air handling unit, HEFAT 2011, 8th International Conference on Heat

Transfer, Fluid Mechanics and Thermodynamics, Pointe Aux Piments, Mauritius, July 11 – 13, 2011, ISBN 978-1-86854-948-1;

[165] H. Li, Y.J. Dai, Y. Li, D. La, R.Z. Wang, Experimental investigation on a one-rotor two-stage desiccant cooling/heating system driven by solar air collectors, *Applied Thermal Engineering* 31 (2011) 3677-3683;

[166] K.F. Fong, T.T. Chow, Z. Lin, L.S. Chan, Simulation-optimization of solar-assisted desiccant cooling system for subtropical Hong Kong, *Applied Thermal Engineering* 30 (2010) 220-228;

[167] R. Possidente, C. Roselli,, M. Sasso, S. Sibilio, Microcogeneration and polygeneration for building in mild climate, 1st International Conference & Workshop on Micro-Cogeneration Technologies & Applications, Micro-Cogen 2008, Ottawa, Canada, 2008.

LIST OF TABLES

LIST OF FIGURES